Universiteit Antwerpen

Faculteit Wetenschappen

Departement Bio-ingenieurswetenschappen

Injecteerbare Fe-houdende deeltjes voor de in-situ sanering van vervuild grondwater

Proefschrift voorgelegd tot het behalen van de graad van doctor in de bio-ingenieurswetenschappen aan de Universiteit Antwerpen te verdedigen door

Milica Velimirovic

Promotoren
Prof. dr. ir. Piet Seuntjens (UA, VITO, UGent)
Prof. dr. Roeland Samson (UA)
Copromotor
Dr. ir. Leen Bastiaens (VITO)

Antwerpen, 2013

ISBN: 9789057284243
Wettelijk depotnummer: D/2013/12.293/17

Universiteit Antwerpen

Faculteit Wetenschappen

Departement Bio-ingenieurswetenschappen

Use of injectable Fe-based particles for in-situ treatment of contaminated groundwater

Milica Velimirovic

Members of the jury
Prof. dr. S. Lenaerts (UA)
Prof. dr. B. Van de Steene (UA)
Prof. dr. E. Smolders (KULeuven)
Prof. dr. R. Sethi (POLITO)
Dr. ir. G. Schoups (TUDelft)

Antwerpen, 2013

“Life is and will ever remain an equation incapable of solution, but it contains certain known factors.”

Nikola Tesla
“A Machine to End War”
(Liberty, February, 1935)

“That is the trouble with many inventors; they lack patience. They lack the willingness to work a thing out slowly and clearly and sharply in their mind, so that they can actually 'feel it work'. They want to try their first idea right off; and the result is they use up lots of money and lots of good material, only to find eventually that they are working in the wrong direction. We all make mistakes, and it is better to make them before we begin.”

Nikola Tesla
“Tesla, Man and Inventor”
(New York Times, March 31, 1895)

“The scientific man does not aim at an immediate result. He does not expect that his advanced ideas will be readily taken up. His work is like that of a planter -- for the future. His duty is to lay foundation of those who are to come and point the way.”

Nikola Tesla
“The Problem of Increasing Human Energy”
(The Century Magazine, June, 1900)

SAMENVATTING

Gedurende de afgelopen decennia is er veel onderzoek verricht naar het reinigen van grondwater dat vervuild is met vluchtige alifatische chloorkoolwaterstoffen (VOCl's). Het gebruik van granulair (0.3 – 3 mm) nulwaardig of zero-valent ijzer (ZVI) is intussen goed ingeburgerd voor de ondergrondse behandeling van zulke grondwaters (de zogenaamde pluimbehandeling) in permeabele reactieve barrières (PRBs). Hierbij wordt een sleuf gegraven in de ondergrond die hervuld wordt met ZVI. De VOCl's in het doorstromende water worden door the ZVI gereduceerd tot schadeloze producten waarbij ijzer precipitate op het ZVI worden gevormd. PRBs zijn echter niet geschikt voor het behandelen van bronzones, verontreinigingen op grote diepte (> 20 m) en moeilijk bereikbare zones in grondwater. Een alternatief is om ZVI in de ondergrond te injecteren en zodoende een reactieve zone te creëren. Aangezien granulair ijzer niet injecteerbaar is, wordt de laatste jaren meer onderzoek gedaan naar fijnere ZVI deeltjes (< 100 µm). In eerste instantie richtte men zich op nanoschaal-ZVI (nZVI, 20-100 nm) deeltjes die zeer reactief zijn. Zowel het snelle verbruik van nZVI's na reactie met water, alsook de agglomeratie van deeltjes tijdens de injectie blijven echter een grote uitdaging. Vanwege de hoge kosten, de korte levensduur na in-situ toepassingen en mogelijke toxische effecten van nZVI's, zou het gebruik van microschaal-ZVI (mZVI) als alternatief voor nZVI een belangrijke rol kunnen spelen in toekomstige toepassingen.

In dit doctoraatsonderzoek werden deze mZVI-deeltjes bestudeerd als mogelijke oplossing ter vervanging van nZVI-deeltjes voor de in-situ sanering van grondwater verontreinigd met VOCls. Daarbij werd de reactiviteit en de levensduur van mZVI-deeltjes bestudeerd en werden de mogelijkheden en gebruiksvoorwaarden van gestabiliseerde mZVI-deeltjes voor de in-situ sanering van VOCl's nagegaan.

Ten eerste werd een reactiviteit studie uitgevoerd (batch testen) voor zowel nieuw ontwikkelde mZVI-deeltjes, als voor commercieel verkrijgbare nZVI's en mZVI's. Uit de testen werden afbraaksnelheden voor verschillende VOCl's afgeleid en vergeleken onder gestandaardiseerde experimentele condities. De experimentele resultaten tonen aan dat bepaalde nieuw ontwikkelde mZVI-deeltjes een groot potentieel hebben bij het saneren van VOCl's.

Vervolgens werd de impact van de samenstelling van ZVI partikels op hun reactiviteit bestudeerd via VOCl-afbraaktesten in een gesloten

batch-systeem. Meer specifiek werd de correlatie tussen de reactiviteit van mZVI-deeltjes en hun koolstof-, zuurstof- en zwavelgehalte bekeken. De bevindingen tonen aan dat het meest reactieve mZVI's minder zuurstof bevatten. Een hoog koolstofgehalte leidde aan de andere kant tot sorptie van de vervuiling op de mZVI-deeltjes. De impact van het zwavelgehalte op de reactiviteit van mZVI-deeltjes is minder uitgesproken dan dat van het koolstof- en zuurstofgehalte.

Corrosie van het ZVI bepaalt de reactiviteit van het ZVI op lange termijn. Om tot een schatting te komen van de duurzaamheid van mZVI-deeltjes na in-situ toepassing, werd de hoeveelheid gevormde waterstof bestudeerd als indicator voor anaerobe corrosie van ZVI in batch-degradatie-experimenten zonder aquifermateriaal. Experimentele metingen tonen aan dat mZVI-deeltjes een corrosiesnelheid vertonen die ongeveer 30 keer lager ligt dan nZVI-deeltjes, waardoor ze een langere werking hebben dan nZVI's. Voorts hangt de corrosiesnelheid van ZVI's af van de grootte van de deeltjes en hun specifiek oppervlak. De gegevens van de batch-degradatie-experimenten zonder aquifermateriaal werden bevestigd aan de hand van de productie van waterstof in batch-experimenten met aquifermateriaal en vervuild grondwater. Hierbij werd een hogere corrosiesnelheid vastgesteld in aanwezigheid van aquifermateriaal, wat mogelijk verklaard wordt door de lager pH in dit aquifermateriaal en zijn die de pH op een lager peil houdt. Om dit aan te tonen, werd een corrosiesnelheidsmodel gekalibreerd aan de hand van de batch-experimenten waarbij rekening werd gehouden met de remmende effecten van de corrosieproducten op de ijzercorrosiesnelheid.

Een belangrijke uitdaging bij het plaatsen van mZVI-deeltjes onder de oppervlakte wordt gevormd door hun sedimentatie-eigenschappen tijdens de injectie. Om de mobiliteit te bevorderen en sedimentatie van mZVI-deeltjes tijdens de injectie te voorkomen, is het gebruik van stabiliserende middelen noodzakelijk. Gezien de relatief lage kosten, het schadeloos karakter en de biodegradeerbaarheid, werd guargom als stabilisator voor deze studie geselecteerd. De aanwezigheid van guargom had een positieve uitwerking op de stabilisering van mZVI, maar leidde wel tot een behoorlijke afname van de verwijdering van de VOCL's door mZVI in kunstmatig vervuild grondwater. De reactiviteit voor VOCls werd hersteld door het intensief spoelen van de ijzerdeeltjes, waardoor het inhiberen de resten van guargom verwijderd werden van de deeltjes. Batch onderzoeken toonden m.a.w. aan dat de guargom leidde tot een tijdelijke maar volledig omkeerbare afname in de reactiviteit van de mZVI.

In een volgende stap werd een kolomtest uitgevoerd onder in-situ condities om te evalueren in welke mate de inactiviteit van mZVI door de guargom plaats vond onder voortdurende grondwaterstroming. Vijf kolommen met daarin bodem werden onder verschillende condities opgezet. Stabilisatie van de mZVI met guargom leidde tot een iets lagere reactiviteit. Een nog lagere reactiviteit in de toxische kolom, die met guargom gestabiliseerde mZVI bevatte, bevestigde dat micro-organismen in de grond de guargom afbreken. Door daarna de oligosachariden te verwijderen door middel van de grondwaterstroming (flushing effect) kon het mZVI gereactiveerd worden. DNA-gebaseerde qPCR-analyse toonde aan dat mZVI geen significante invloed heeft op de bacteriële gemeenschap, terwijl met guargom gestabiliseerde mZVI-deeltjes zelfs bacteriële groei stimuleren. Deze studie toont aan dat (1) guargom de performantie van mZVI niet significant beïnvloedt, rekening houdend met de levensduur van mZVI en de sanering, en (2) dat de iets gereduceerde reactiviteit van mZVI voor VOCls ook gepaard gaat met een lagere corrosiesnelheid, en dus met een langere levensduur van de partikels.

Tenslotte werd een veld test in een industrieel gebied uitgevoerd om de injectie-eigenschappen van de mZVI-deeltjes aan te tonen en vast te stellen wat de verticale en horizontale verspreiding was van mZVI-deeltjes in de ondergrond na injectie in de aquifers. Ook werd de impact van de met guargom gestabiliseerd mZVI op de VOCl-concentraties in het grondwater onderzocht. De onderzoeksresultaten laten zien dat met guargom gestabiliseerd mZVI aangemaakt kan worden op pilot-schaal, en met meer gespecialiseerd materiaal naar verwachting ook op grote schaal. De injectie van het gestabiliseerd mZVI via direct push methodes bij verhoogde druk, matige stroom en relatief grote injectievolumes bleken mogelijk. Er werden duidelijke voorkeursbanen gecreëerd in de ondergrond met een heterogene verspreiding van ijzerdeeltjes in de ondergrond als gevolg. Tot 2,5 m van het injectiepunt werd mZVI gedetecteerd. Bewijzen werden verzameld voor afbraak van 1,1,1-TCA in zones waar met guargom gestabiliseerde mZVI-deeltjes werden aangetroffen. Bijkomende bewijzen dat deze technologie werkt op verontreinigde terreinen is essentieel om schaalvergroting en courant gebruik van de technologie te realiseren.

ABSTRACT

Over the last decades, remediation of groundwater polluted with chlorinated aliphatic hydrocarbons (CAHs) has been studied intensively. The use of zerovalent iron (ZVI) as a nontoxic material was found to be efficient in degrading various CAHs like chlorinated ethenes and ethanes. In the presence of ZVI, CAHs are directly dechlorinated due to the redox reactions on the ZVI surface where Fe(II) and Fe(III) precipitates are formed. Meanwhile, it is widely accepted that granular ZVIs can be used for in-situ remediation of different CAHs (plume treatment) in so-called permeable reactive barriers (PRBs). Nevertheless, PRBs are not suitable for contaminant source treatment, deeper aquifers (> 20 m) and places that are hard to access. Injection of small ZVI particles in the contaminated zone offers an alternative. Granular ZVI has typical particle size of 0.3 to 3 mm and cannot be injected. Nanoscale ZVI (nZVI, typically between 20 to 100 nm) is highly reactive towards CAHs. Smaller sized ZVI particles offer opportunities for further development of the injectable ZVI technology for contaminant plume treatment and contaminant treatment closer to the source zone. However, agglomeration of nZVI and the fast consumption of nZVIs by reaction with water remain a big challenge for future research. Due to the high costs, short life-time after in-situ application and possible toxical effects of nZVIs, the use of microscale ZVI (mZVI, particle size of 1-100 µm) for degradation of CAHs may play important role in future applications. In comparison with nZVI, mZVI are less expensive, have a longer life-time and pose less risk for human health. On the other hand, mZVI particles remove CAHs slower than the same mass of well suspended nZVIs.

In this PhD research, injectable mZVI particles of about 50 µm were evaluated as a possible substitute of nZVI particles for in-situ remediation of groundwater heavily polluted by CAHs. Moreover, assessment of the reactivity and, consequently, life-time of mZVI particles was elaborated with possibilities and boundary conditions of stabilized mZVI particles for in-situ remediation of CAHs.

First, a batch degradation study was performed to compare the disappearance kinetics of different CAHs under standardized experimental conditions for newly designed mZVI particles, as well as for commercially available nZVIs and mZVIs within reasonable time and effort frame. Reactivity of the particles was based on observed (k_{obs}) and mass normalized (k_M) pseudo-first-order degradation rate constants, as well as specific surface area normalized reaction rate constants (k_{SA}).

Among the new mZVIs, significant differences in reactivity were observed and the most reactive particles were identified. Based on k_M data, nZVI degraded the examined contaminants one to two orders of magnitude faster than the mZVIs. On the other hand, comparison of k_{SA} data revealed that the reactivity of some newly designed mZVIs was similar to highly reactive nZVIs, and even up to one order of magnitude higher.

Next, the impact of the chemical composition of the bare mZVI particles on its reactivity towards CAHs was studied. More specifically, correlations between the mZVI particles reactivity and their carbon, oxygen and sulfur content were evaluated. Particles containing oxygen content lower than 0.01 % were the most reactive particles. High carbon content, on the other hand, induced nonreactive sorption of the contaminants on the mZVI particles. The impact of sulfur content on the reactivity of mZVI particles is less pronounced than that of the carbon and oxygen content.

To estimate the aging behavior of mZVI particles after in-situ application the production of hydrogen (H_2) generated by anaerobic corrosion of ZVI in batch degradation experiments was measured. Experimental data show that mZVI particles have approximately a 30 times lower corrosion rate than nZVI particles, making them beneficial for a longer term performance. In addition, the corrosion rate of ZVIs depends on the particle size and the specific surface area of the particles. To confirm the data obtained during batch degradation experiments in aquifer-free conditions, H_2 production was also monitored during batch tests in the presence of aquifer material and real polluted groundwater. As an outcome, higher corrosion rate of particles in the natural environment was observed compared to the one in the standardized batch tests, which were related to the lower pH in these systems and the buffer capacity of the aquifer. A corrosion rate model was calibrated on the batch experiments to take into account the inhibitory effects of the iron corrosion reactivity products on the corrosion rate.

A key challenge to place the mZVI particles in the subsurface is their sedimentation properties during the injection. To enhance the mobility and prevent sedimentation of mZVIs during injection, the use of stabilizing agents is necessary. Considering its relatively low cost and high biodegradability, guar gum was identified as a promising stabilizer in lab-scale experiments. However, the starting hypothesis was that high guar gum concentration necessary to stabilize the significant concentration of mZVIs preventing particle aggregation and sedimentation required for field application might impact contaminants degradation in the subsurface. The present study focused on the reactivity of guar gum stabilized mZVI towards CAHs for use in reactive

zones. The presence of the guar gum had a positive impact on the mZVI stability, but significantly decreased the removal of chlorinated ethenes (PCE, TCE, cDCE) from artificially polluted groundwater by the mZVI particles. It was proved that the reactivity towards CAHs could be restored by intensive rinsing of the iron particles, simulating groundwater movement in the injection zone in the field, hereby removing the guar gum fragments from the particles.

Batch tests showed that the guar gum reduces the reactivity of mZVI temporarily and in a reversible way. In a next step, a column study was performed under in-situ conditions to evaluate to which extent the inactivation of the mZVI by the guar gum occurs under continuous flow conditions. Five aquifer containing columns were set-up under different conditions. Stabilization of the mZVI with guar gum led to a slightly reduced reactivity. Poisoned column with guar gum stabilized mZVI had lower reactivity to CAHs than unpoisoned ones confirming that soil microorganisms actually degraded the guar gum and that the subsequent removal of the oligosaccharides by the groundwater flow (flushing effect) may reactivate the mZVI. DNA-based qPCR analysis revealed that mZVI does not significantly affect the bacterial community, while guar gum stabilized mZVI particles even induce bacterial growth. Overall, this study suggests that the temporary decreased mZVI reactivity due to guar gum, has only a very limited impact on the performance of in-situ reactive zone. The presence of guar gum slightly reduced the reactivity of iron, but also slowed down the iron corrosion rate which prolongs the life time of reactive zone.

Finally, a field test in an industrial area was performed to demonstrate the injection characteristics of the mZVI particles and determine the vertical and horizontal distribution of mZVI particles in the subsurface after injection into aquifers. The efficiency of mZVI in reducing contaminant fluxes such as chlorinated ethenes and chlorinated ethanes was examined as well. The results of this study demonstrate that mZVI slurries stabilized with guar gum can be prepared at pilot scale and can be delivered in the subsurface via a direct push injection using high pressures, medium flow rates and large injection volumes; under these conditions, heterogeneous distribution of the iron particles via preferential flow paths was found, with a maximum delivery distance of 2.5 m from the injection point. Moreover, once guar gum stabilized mZVI particles are injected at desired depths, 1,1,1-TCA can be degraded. Via a batch degradation using 2 month old mZVI from the reactive zone, it was proved that the guar gum stabilized mZVI is reactive (reactivated) within 2 months after the injection. An additional proof of this technology in zones with different CAH-pollutants and with more controlled delivery of the particles is essential for further up scaling and technology use.

ACKNOWLEDGEMENTS

Three and a half years of journey is coming to the end summarizing all in one book. When I look behind, all what I can say is that working on PhD was an unforgettable experience.

First of all, I am very grateful to my supervisor Dr. ir. Leen Bastiaens. Thank you for giving me opportunity to work in VITO environment and Aquarehab project. I appreciate your contributions of time (plenty of time), ideas, knowledge, patience, support in writing and encouragement. You guided me always in the right direction and you were the key to finish this research successfully. I could not have imagined having better supervisor for my PhD research. It has also been a real pleasure to work within Soil group.

Besides my advisor, I would like to thank the rest of my thesis committee: Prof. dr. ir. Piet Seuntjens, Prof. dr. Roeland Samson, Prof. dr. Silivia Lenaerts, Prof. dr. Boudewijn Van de Steene, Prof. dr. Erik Smolders, Prof. dr. Rajandrea Sethi and Dr. ir. Gerrit Schoups for their encouragement, insightful comments, and some hard questions as well.

This research was carried out in the framework of FP7 AQUAREHAB project (Development of the rehabilitation technologies and approaches for multi-pressured degraded waters and the integration of their impact on river basin management) under contract number 226565. My dearest thanks to the people with whom I had very close collaboration, the enjoyable discussions and for all the fun we have had: Tiziana Tosco, Francesca Gastone, Michela Luna, Cjestmir de Boer, Hans Sapion and Luca Carniato. I have greatly enjoyed working with you guys! Moreover, all my work would not be possible without mZVI particles provided by Höganäs, with special thanks to Per-Olof Larsson. Your theoretical reasoning gave other dimension to this research.

In my work with guar gum stabilized mZVI, I am particularly indebted to Prof. dr. Rajandrea Sethi and his group at Politecnico di Torino. I had the most interesting interaction with the members of yours research group. The good advices, support and unsurpassed knowledge has been invaluable for my research.

I also want to thank Dr. Heinrich Eisenmann. My work has benefited from your ‘artistic’ knowledge on specific stable isotope analysis.

Back to VITO, I have been privileged to work with Queenie, Leen S., Carine, Nicole and Miranda. Thank you for your willingness to teach me all what I will bring from the VITO labs and showing me how to tackle with the problems and what are the possibilities to solve them. The pleasant working atmosphere you provided was very productive and stimulating.

Furthermore, I would like to thank Tom, Jean-Pierre, Rob, Danny, Hans, Guy and Jef for all technical support and help. Was also nice having Silvia and Christof around. Griet, Sofie and Katrien, thank you for all administrative and no administrative help.

My time at VITO was also made enjoyable in large part due to the students I was working and/or sharing office with. Peter, Siavash, Celine, Pieter Jan, Eylem, Doga, Naresh, Vinay, and Yamini you helped to make my time in Vito more fun and interesting. I am also indebted to Winnie and Maarten for all their useful suggestions.

I also thank to my friends from home for their sincere friendship. At my arrival in Boeretang, Gabriella, Davide, Sebastien and Luca made me to feel welcome far away from home. Thank you for being there!

I am very grateful to Sofija, Boris, Filip and a new born baby boy Stefan for their honest friendship and lovely time we have spent (and we will) together.

Heartfelt thanks to Vesna and Maarten. It is amazing having you as friends. Maarten, thank you for reading all my articles. Vesna, thank you for an unending encouragement and support.

I would like to thank my family for their love and unlimited support through everything. Tata, Živka, Stevo, Tea i Krisi hvala vam što postojite i uvek ste tu kada ste mi potrebni!

Baćko... my soul mate, my friend, my love. Thank you for taking this ride with me. You were very supporting in all crazy ideas born here. Your love meant to me and made me to overcome all challenges! I owe my every achievement to you. Thank you with all my heart!

Mol, June 2013 *Milica Velimirović*

TABLE OF CONTENTS

LIST OF FIGURES

LIST OF TABLES

LIST OF ABBREVIATIONS

1,1,1-TCA	1,1,1-Trichloroethane
1,1-DCA	1,1-Dichlroethane
1,1-DCE	1,1-Dichlroethene
AA	Annual average
CAHs	Chlorinated aliphatic hydrocarbons
cDCE	cis-Dichloroethene
DNAPL	Dense non-aqueous phase liquid
EEA	European Environmental Agency
EPA	Environmental Protection Agency
GG	Guar gum
GG-mZVI	Guar gum stabilized mZVI
MAC	Maximum allowable concentrations
mZVI	Microscale zerovalent iron
nZVI	Nanoscale zerovalent iron
PCE	Tetrachloroethene
PRB	Permeable reactive barrier
qPCR	Quantitative PCR
TCE	Trichloroethene
ZVI	Zerovalent iron
VC	Vinyl chloride
WFD	Water Framework Directive
WHO	World Health Organization

CHAPTER 1 GENERAL INTRODUCTION AND THESIS OUTLINE

Freshwater resources consist of surface water and groundwater. Water utilization is influenced by water quality, whether it is for drinking, industrial, recreational or irrigation purposes. The overall quality status of freshwater resources is determined by (1) the kind and quantity of contaminants that are released in the water system by a variety of inputs, being either diffuse or point sources and (2) the migration of the pollutants (via groundwater and run-off) towards different rivers, lakes, and seas. The migration of pollutants towards vulnerable receptors (drinking water reserves in the subsurface, surface waters, water wells) is of particular concern.

The European Parliament and the Council adopted the Water Framework Directive (WFD) (EC/2000/60) in 2000 in order to integrate existing legislation on water resources management and to introduce new technologies for water rehabilitation. The WFD establishes a legal framework within which to protect surface and ground waters using a common management approach and following common objectives, principles and basic measures.

The two main objectives of the WFD are (1) to restore good ecological and chemical status for all water bodies (or good ecological potential for heavily modified water bodies) across the Community by 2015 and (2) to integrate water management activities at the river basin level. This means that technologies to rehabilitate degraded waters need to be able to restore good ecological and chemical status by 2015 and be integrated into water management activities at the river basin level. In general the quality of river water, lakes and ground water across Europe has improved thanks to a range of EU environmental directives since the 1970s, but there still remain significant "hot spots" of degraded waters from both point and diffuse sources. In 2007, it was estimated that potentially polluting activities have been taken place at nearly three million sites across European Environment Agency (EEA) member countries and remediation of at least 250000 sites is required. There are in addition approximately 20000 contaminated sites (Prokop et al., 2000). If current investigation trends continue, the number of sites needing remediation will increase by more than 50% by 2025 (EEA, 2007). However, according to the EEA data, remediation progress is relatively slow and only 80000 sites have been cleaned-up in the countries where the data on remediation processes exist.

1.1. CAHS AND THEIR FATE IN SOIL AND GROUNDWATER

Chlorinated aliphatic hydrocarbons (CAHs) represent the most frequently detected groundwater contaminants in industrialized countries (Squillace et al., 2004; Prommer et al., 2008). As most of the CAHs are known to have indefinite life span, and potentially carcinogenic and toxic effect on humans and environment (Henschler, 1994; Doherty, 2000a,b), annual average (AA) and maximum allowable concentrations (MAC) of certain CAHs in surface and drinking waters are regulated in Europe by the WFD (Table 1). CAHs intervention values are also regulated by European Union countries. Intervention values of CAHs in Flanders, Belgium are reported in the Soil Remediation Decree Vlarebo (2009) (Table 1). Guidelines on CAHs concentrations in drinking water are established by the World Health Organization (WHO) and by the Environmental Protection Agency (EPA) in the USA as presented in Table 1.

Chlorinated aliphatic hydrocarbons (chlorinated ethanes and ethenes) such as tetrachloroethene (PCE), trichloroethene (TCE), cis-dichloroethene (cDCE) and 1,1,1-trichloroethane (1,1,1-TCA) are being used as dry cleaning and metal degreasing agents, paint removers and industrial solvents, as well as in the production of pesticides, electronic components and polymers (Doherty, 2000a,b; Tobiszewski and Namieśnik, 2012). Inappropriate use of CAHs and their inadequate disposal lead to accidental releases to the soil and groundwater environment as dense nonaqueous phase liquids (DNAPLs), as shown in Figure 1. These DNAPLs migrate in the subsurface and dissolve slowly into the passing groundwater, leading to groundwater contamination plumes for decades.

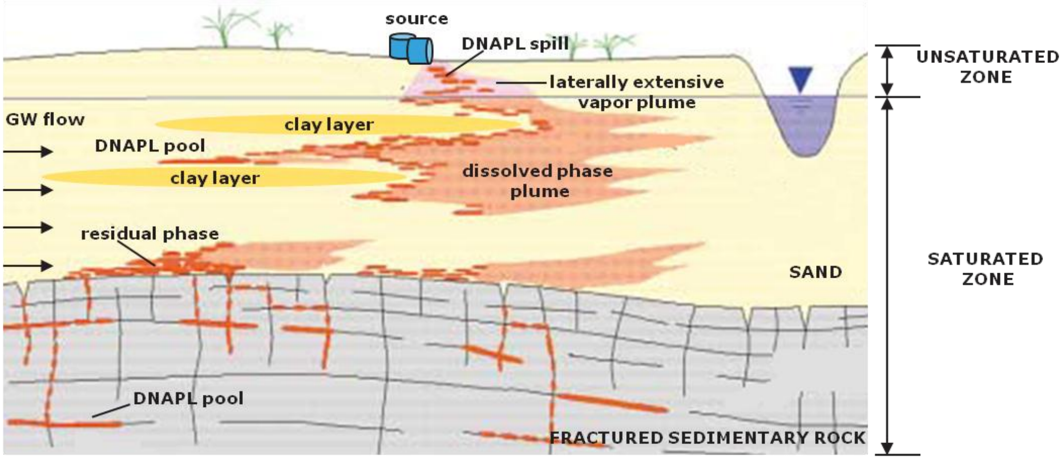

Figure 1 - Conceptual model of a dense non aqueous phase liquid (DNAPL) distribution in the soil and ground water (GW) environment (modified from Pankow and Cherry, 1996).

Table 1 : Selected physical and chemical properties of selected chlorinated aliphatic hydrocarbons.

Compound	Formula weight (g mol $^{-1}$)	Boiling point (°C)	Density at 25°C (g mL^{-1})[a]	Solubility in water at 25°C (mg L^{-1})[a]	WFD AA-EQS (µg L^{-1})[b]	WFD MAC-EQS (µg L^{-1})[c]	EPA MCLs (µg L^{-1})[d]	WHO guideline values (µg L^{-1})[e]	Flanders 80% intervention values (µg L^{-1})[f]
Chlorinated ethanes									
1,1,1,2-Tetrachloroethane	167.9	130.2	1.54	1,100	nr	nr	nr	nr	nr
1,1,2,2-Tetrachloroethane	167.9	145.2	1.60	2,962	nr	nr	nr	nr	nr
1,1,1-Trichloroethane	133.4	74.0	1.35	1,495	nr	nr	200	nr	400
1,1,2-Trichloroethane	133.4	113.8	1.44	4,394	nr	nr	5	nr	9.6
1,1-Dichloroethane	99.0	57.3	1.17	4,676	nr	nr	nr	nr	264
1,2-Dichloroethane	99.0	85.3	1.25	8,606	10	na*	5	30	24
Chlorinated ethenes									
Tetrachloroethene	165.8	121.3	1.63	150	10	na*	5	40	32
Trichloroethene	131.4	88.0	1.46	1,100	10	na*	5	70	56
1,1-dichloroethene	96.9	31.6	1.22	3,344	nr	nr	7	30	nr
Trans- dichloroethene	96.9	48.7	1.26	6,260	nr	nr	100	50	nr
Cis- dichloroethene	96.9	60.1	1.28	3,500	nr	nr	70	50	nr
Vinyl chloride	62.5	-13.9	0.91	2,763	nr	nr	2	0.3	4

[a]Mackay et al. (1993); [b]Water Framework Directive (WFD) annual average environmental quality standards (AA-EQS) for priority substances and certain other pollutants for inland and other surface water (2008); [c]WFD maximum allowable concentration (MAC-EQS) for priority substances and certain other pollutants for inland and other surface waters (2008); [d]United States Environmental Protection Agency (EPA) maximum contaminant levels (MCLs) (2004); [e]World Health Organization (WHO) drinking water guidelines (2004); [f]Vlarebo (2009) – groundwater intervention values; *WFD priority substances in the field of water policy; nr – not regulated; na – not applicable.

1.2. DNAPLS REMEDIATION TECHNIQUES

Remediation of DNAPLs is both difficult and expensive. The main difficulty is the localization of the DNAPL spots that are distributed heterogeneously in the subsurface. As a result, besides conventional groundwater remediation technologies, several innovative remediation techniques were introduced in the past decade (Table 2).

Over the past two decades ex-situ conventional groundwater remediation technologies, such as pump-and-treat, were sufficient for treatment of the dissolved phase plume which migrates down-gradient of the DNAPL source zone. However, US EPA (2001) studies at more than 30 sites estimated the annual average operating costs of pump and treat systems of approximately 600.000 € per site including ongoing monitoring which increase the costs.

Therefore, research and development of technologies for remediation of CAHs was more directed towards other in-situ technologies such as thermal treatment, chemical oxidation, surfactant cosolvent flushing and bioremediation. Strengths and weaknesses of the abovementioned methods are displayed in Table 2.

The use of in-situ remediation technologies, which allow for treatment in the subsurface without exhaustive energy input, increased tremendously over recent years. As an example of passive in-situ remediation technology, permeable reactive barriers (PRBs) were developed in the US and used over past two decades for remediation of contaminant plumes. PRBs represent a treatment zone which is composed of materials that efficiently degrade or immobilize contaminants present in the groundwater that passes through the barrier (Karn et al., 2009). The first field-scale PRB has been introduced in the US containing granular zerovalent iron (ZVI) as a medium for transformation of CAHs (Gillham and O’Hannesin, 1994). However, PRBs as well as pump and treat technology cannot efficiently cope with DNAPL source zones and heterogeneous plumes. Moreover, challenges such as a high costs associated with installation in deep aquifers and lack of flexibility after installation may limit application of PRBs (Li et al., 2006).

As an alternative or extension to the conventional PRBs, injectable ZVI technology emerged for the remediation of a DNAPL source. Moreover, injectable ZVI technology might be chosen for the sites where bioremediation is not efficient due to the site conditions (high contaminant concentration, toxic metabolites, type of soil, pH, temperature, oxygen and nutrients content).

Table 2 : Summary of DNAPL remediation technologies, conventional or under development.

DNAPL remediation technology	Strengths	Weakness
Ex-situ		
- *Pump-and-treat*	Suitable for all types of groundwater contaminants.	Length of operation period. Depended on hydrogeological factors. Residuals trapped by soil cannot be extracted.
In-situ		
- *Permeable reactive barriers*	Ground water plume treatment ideal for shallow depths and easily accessible sites.	Do not address DNAPLs or contaminated ground-water beyond the barrier and hard-to-access places.
- *Thermal treatment*	Remediation of DNAPLs consolidated within lower permeability zones. No depth limitations.	Not cost effective approach for source zone treatment. Uniformity of heating. Requires more basic research.
- *Chemical oxidation*	Relatively rapid treatment of contaminants. No depth limitations.	Very sensitive and nonselective. Depends on natural organic matter and other reduced species.
- *Chemical reduction*	Source zone treatment using highly reactive **nanoscale and microscale ZVIs**. Possible injection at deeper depths.	**Depends on iron delivery techniques.** **Longevity of nanoscale ZVIs.**
- *Bioremediation*	Less invasive injection of electron donor solutions (lactate, molasses) stimulating anaerobic dechlorination with microorganisms.	Highly dependent on site-specific conditions and extended treatment time.
References	*Yin and Allen, 1999; US EPA, 2003a; US EPA, 2006.*	

1.3. USE OF ZVI FOR REMEDIATION OF CAHS

The use of ZVI as a nontoxic material has been shown as one of the most promising remediation techniques for in-situ passive removal of CAHs via abiotic reductive dehalogenation (Gillham and O'Hannesin, 1992, 1994; Mathenson and Traynek, 1994). Since the early 1990s zerovalent iron has been used for site remediation in permeable reactive barriers because of its low cost, availability, and high ability to dehalogenate chlorinated organic compounds over a wide concentration range (US EPA, 1999). ZVI particles have been found attractive not only for remediation of chlorinated organic solvents, but also for remediation of organochlorine pesticides, polychlorinated biphenyls and organic dyes (Zhang, 2003). ZVI particles are also effective in treatment of heavy metals such as chromium and lead (Zhang et al., 1998).

In contrast to the established permeable reactive barriers (Figure 2a), where millimeter size ZVI is installed in the subsurface under the form of a reactive wall in a trench that need to be excavated, injectable ZVI particles (from 15 nm to 100 µm) are directly applied in the subsurface as aqueous suspensions. These particles can be injected in the subsurface under pressure conditions or/and gravity flow (Li et al., 2006) creating an in-situ reactive zone (Figure 2b).

The use of injectable ZVI particles reduces the costs and efforts for constructions in deep aquifers drastically. In addition, the particles can be applied directly in the source zone of the contamination, which potentially leads to a large reduction of the time necessary for remediation.

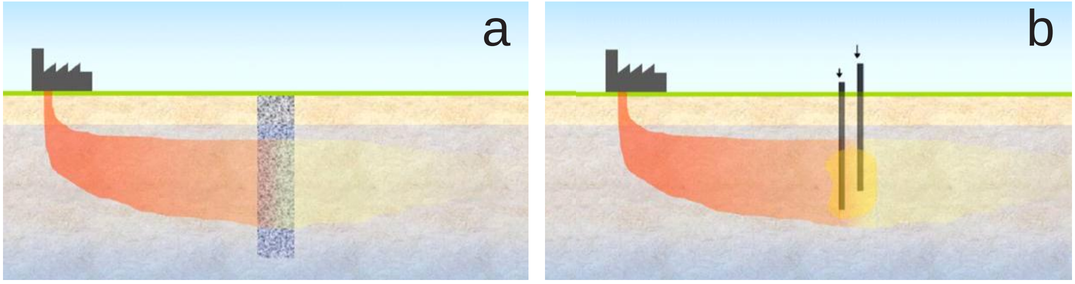

Figure 2 – Permeable reactive barrier (a) vs. In-situ reactive zone (b).

The reduction of chlorinated solvents into less toxic compounds is determined by elemental iron, ferrous iron and hydrogen that results from iron corrosion (Matheson and Tratnyek 1994) with three possible degradation mechanisms.

The first reduction pathway involves an oxidation (corrosion) of zerovalent iron surface, causing a direct electron transfer from the surface to the chlorinated compound:

$Fe^0 + RCl + H^+ \text{ ----> } Fe^{2+} + RH + Cl^-$ (1).

The second pathway involves reductive dehalogenation of CAHs by surface bound ferrous iron (Fe^{2+}) formed during iron corrosion with water:

$2Fe^{2+} + RCl + H^+ \text{ ----> } 2Fe^{3+} + RH + Cl^-$ (2).

The reaction causing anaerobic corrosion of zerovalent iron according to reaction:

$Fe^0 + 2H_2O \text{ ----> } Fe^{2+} + H_2 + 2OH^-$ (3).

Finally, the hydrogen fromed during this anaerobic corrosion of Fe^0 can also serve as electron donor for abiotic reductive halogenation of CAHs:

$H_2 + RCl \text{ ----> } RH + H^+ + Cl^-$ (4).

Moreover, under anaerobic conditions the corrosion of iron presented in eq. 3 decreases the redox potential and an increase in pH. This reaction causes precipitation of the generated Fe^{2+} on the iron grain surface. Depending on the geochemical conditions (groundwater composition, pH, redox potential, alkalinity and dissolved oxygen) the present Fe^{2+} can be converted to oxidized precipitates (Odziemkowski et al. 1998). The precipitation of ferrous hydroxide will be consequence of the limited buffer capacity of groundwater and strongly increased pH (Liang et al., 2000):

$Fe^{2+} + 2OH^- \text{ ----> } Fe(OH)_2\ (s)$ (5).

Finally, thermodynamically unstable ferrous hydroxide can be further oxidized to magnetite (Odziemkowski et al. 1998, Farrell et al. 2000, Roh et al. 2000):

$3Fe(OH)_2 \text{ ----> } Fe_3O_4\ (s) + H_2\ (g) + 2H_2O$ (6).

Interestingly, mixed valent Fe(II)-Fe(III) salts (green rusts) can be also formed and further oxidized to passivating precipitates such as magnetite, maghemite (Fe_2O_3), goethite (α-FeOOH) and lepidocrocite (γ-FeOOH) (Farrell et al. 2000, Roh et al. 2000, Kohn et al., 2005). However, Lee and Batchelor (2002) reported that green rusts are capable in reducing chlorinated ethenes more efficiently than Fe^0.

Finally, the rapid iron corrosion in the presence of dissolved O_2 or highly corrosive contaminants such as Cr(VI) and nitrate will have a major impact on iron reactivity (Kohn et al., 2005).

In the presence of zerovalent iron, reductive dechlorination of chloroethenes and chloroethanes occurs through different pathways involving dihaloelimination (β-elimination or α-elimination) and/or hydrogenolysis (Arnold and Roberts, 2000).

Dihaloelimination is elimination of two chlorine atoms involving a two-electron transfer to the molecule:

$$RCCl - CClR + 2e^- \text{---->} \; RC = CR + 2Cl^- \qquad (7).$$

In the hydrogenolysis reactions, each chlorine atom is replaced by a hydrogen atom, with the simultaneous addition of two electrons to the molecule (Mohn and Tiedje, 1992):

$$RCl + H^+ + 2e^- \text{---->} \; RH + Cl^- \qquad (8).$$

The main degradation pathways of CAHs are presented in Figure 3.

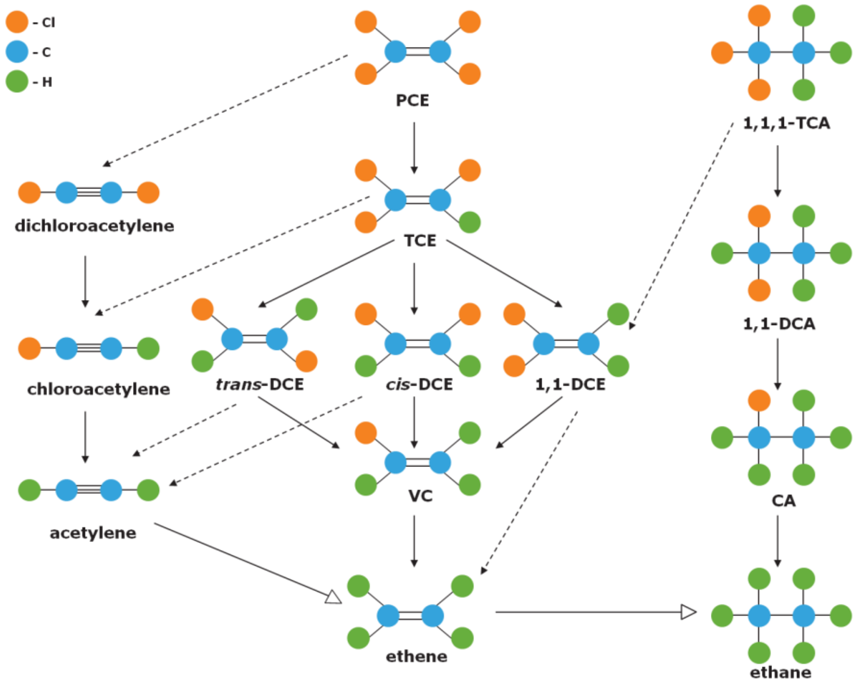

Figure 3 – Hypothesized transformation pathways of selected chlorinated ethenes and ethanes by ZVI (adapted from Arnold and Roberts 2000; Tobiszewski and Namieśnik, 2012). Solid arrows represent hydrogenolysis reactions, while dashed arrows indicate reductive β-elimination reactions. Open arrowheads indicate reductions not involving dehalogenation.

Table 3 : The first-order decay constant k_{obs} (h^{-1}), half-life times $t_{1/2}$ (h) and surface area normalized reaction rate constants k_{SA} ($L\ m^{-2}\ h^{-1}$) for reaction of different chlorinated compounds with ZVI particles, adapted from Gillham and O'Hannesin (1994) and Song and Carraway (2005).

Compound	***Treatment***	***Specific surface area*** **($m^2\ g^{-1}$)**	***Treatment concentration*** **($g\ L^{-1}$)**	k_{obs} **(h^{-1})**	$t_{1/2}$ **(h)**	k_{SA} **($L\ m^{-2}\ h^{-1}$)**	***Reference***
Chlorinated ethanes							
1,1,2,2-tetrachloroethane	*Fisher electrolytic*	0.287	250 $g\ L^{-1}$	3.61×10^{-2}	19.2	5.03×10^{-4}	Gillham and O'Hannesin, 1994
	Nanosized iron	27.9 ± 1.7	0.08 – 0.16	6.82×10^{-2}	10.16	3.03×10^{-2}	Song and Carraway, 2005
1,1,1,2-tetrachloroethane	*Fisher electrolytic*	0.287	250	1.57×10^{-1}	4.4	2.19×10^{-3}	Gillham and O'Hannesin, 1994
	Nanosized iron	27.9 ± 1.7	0.08 – 0.16	1.21×10^{0}	0.57	5.38×10^{-1}	Song and Carraway, 2005
1,1,1-trichloroethane	*Fisher electrolytic*	0.287	250	1.31×10^{-1}	5.3	1.82×10^{-3}	Gillham and O'Hannesin, 1994
	Nanosized iron	27.9 ± 1.7	0.08 – 0.16	3.40×10^{-1}	2.04	1.51×10^{-1}	Song and Carraway, 2005
1,1-dichloroethane	*Nanosized iron*	27.9 ± 1.7	0.08 – 0.16	2.41×10^{-4}	2875	1.99×10^{-5}	Song and Carraway, 2005
Chlorinated ethenes							
Tetrachloroethene	*Fisher electrolytic*	0.287	250	3.87×10^{-2}	17.9	5.39×10^{-4}	Gillham and O'Hannesin, 1994
	Nanoscale Pd/Fe	35	5	2.13×10^{0}	0.32	12.2×10^{-3}	Lien and Zhang, 2001
	Iron filings		100	1.6×10^{-1}			Dries et al., 2005
Trichloroethene	*Fisher electrolytic*	0.287	250	5.1×10^{-2}	13.6	7.1×10^{-4}	Gillham and O'Hannesin, 1994
	Fisher electrolytic	1.635	200	4.25×10^{-1}	1.63	1.30×10^{-3}	Johnson et al., 1996
	Nanoscale Pd/Fe	33.5	20	6.70×10^{1}	0.01	1.0×10^{-1}	Wang and Zhang, 1997
	Nanoscale Pd/Fe	35	5	3.18×10^{0}	0.22	18.2×10^{-3}	Lien and Zhang, 2001
	Fisher Fe^{0}	1.1	143	7.5×10^{-3}	92.4	6.8×10^{-5}	Tratnyek et al., 2001
	nano	18	2.5	1.98×10^{0}	0.35	4.4×10^{-2}	Schrick et al., 2002
	nine types of granular ZVI*	n.a.	100	n.a.	n.a.	2.24×10^{-3}**	Miehr et al., 2004
	ZVI powder	0.71	n.a.	7.6×10^{-2}	9.1	n.a.	Lookman et al., 2004
	Microscale iron	1.8	20	8.0×10^{-2}	8.7	2.37×10^{-3}	Lin and Lo, 2005
	Fe/B nanoscale	36.5	0.2	1.02×10^{-1}	0.68	1.4×10^{-2}	Liu et al., 2005
	RNIP Toda	23	0.5	3.45×10^{-2}	20.08	3.0×10^{-3}	Liu et al., 2005
	Iron filings	n.a.	100	2.7×10^{-1}	n.a.	n.a.	Dries et al., 2005

1,1-dichloroethene	*Fisher electrolytic*	0.287	250	1.73×10^{-2}	40.0	2.41×10^{-4}	Gillham and O'Hannesin, 1994
	Nanoscale Pd/Fe	35	5	2.01×10^{0}	0.34	11.5×10^{-3}	Lien and Zhang, 2001
Trans-dichloroethene	*Fisher electrolytic*	0.287	250	1.26×10^{-2}	55.0	1.76×10^{-4}	Gillham and O'Hannesin, 1994
	Nanoscale Pd/Fe	33.5	20	0.7×10^{-1}	0.1	1.0×10^{-2}	Zhang et al., 1998
	Microscale Fe (Aldrich)	0.9	20	1.8×10^{-3}	385	1.0×10^{-4}	Zhang et al., 1998
	Nanoscale Pd/Fe	35	5	2.64×10^{0}	0.26	15.1×10^{-3}	Lien and Zhang, 2001
Cis-dichloroethene	*Fisher electrolytic*	0.287	250	1.60×10^{-3}	432.0	2.23×10^{-5}	Gillham and O'Hannesin, 1994
	Nanoscale Pd/Fe	35	5	3.08×10^{0}	0.22	17.6×10^{-3}	Lien and Zhang, 2001
Vinyl chloride	*Fisher electrolytic*	0.287	250	1.85×10^{-3}	374.0	2.58×10^{-5}	Gillham and O'Hannesin, 1994

* Aldrich powder (Milwaukee, WI, 97%), Fisher electrolytic powder (Pittsburgh, PA, 99%), EM Science degreased filings (Cherry Hill, NJ), Fluka filings (Milwaukee, WI, 99+%), Baker chips (Phillipsburg, PA, 99.9%), Fisher filings (Pittsburgh, PA, >97%), Master Builders (Cleveland, OH), Peerless Powders and Abrasives (Detroit, MI, "PMP Traditional" Size 8/50, >90%), and Connelly (Chicago, IL, ETI CC-1004, 90%). ** the average k_{SA}'s

Table 4 : Overview of literature data concerning successful mZVI and nZVI pilot tests applications, adapted from Karn et al. (2009) and from Mueller et al. (2012).

Site	Year	Target compounds	Iron particles	Injection technology	Iron efficiency	Reference
Trenton	2001	PCE, TCE, cis-DCE, vinyl chloride, chloroform, carbon tetrachloride, 1,1-DCE	BNP	Gravity + recirculation	Contaminant concentrations reduced by 1.5% to 96.5%	a)
Launch complex 34, Cape Canaveral (FL) – U.S.A.	2002	TCE and corresponding daughters products	EZVI*	Pressure Pulse Technology	Contaminant concentrations reduced by 99%	b)
Research Triangle Park (NC) – U.S.A.	2002	TCE, cis-DCE	BNP	Gravity + recirculation	90 percent reduction of total CAHs concentrations	c)
Klockner Road Site, Hamilton (NJ) – U.S.A.	2004	TCE, DCE, TCA, DCA	nZVI	Direct push	Contaminant concentrations reduced up to 99%	d)
NAS Jacksonville (FL) – U.S.A.	2005	TCE, TCA, DCE, vinyl chloride	BNP	Direct push + recirculation	Rapid reductions by 65% to 99%	e)
NAES Lakehurst – U.S.A.	2005	Soil: PCE, TCE, 1,1,1-TCA Groundwater: PCE, TCE, cis-DCE	BNP	Direct push	The average decrease in total CAHs concentrations was 74%.	e)
Marshall Space Flight Center, Huntsville (AL) – U.S.A.	2000	TCE	mZVI	Pneumatic fracturing	90% of TCE reduction, increase in cis-1,2-DCE	f)
Hunter Point Shipyard (CA) – U.S.	2002	TCE	mZVI	Pneumatic fracturing	99% of reduction	e)
DuPont's Kinston Plant, Ontario, CAN	1999	TCE	Granular ZVI	Clay-soil mixing	95% of reduction	g)

Camp Lejeune (NC) – U.S.A.	2005	PCE (soil & groundwater)	Granular ZVI	Clay-soil mixing	Significant decrease of 67-90%	h)
Goodyear (AZ) – U.S.A.	2007	TCE, PCE, Perchlorate	nZVI	Jetting	n.a.	i)
Marine Corp Logistic Base, Albany (GA) – U.S.A.	2002	TCE, PCE, DCE, TCA, and VC	ZVI Ferrox	Pneumatic fracturing	n.a.	j)
Palo Alto (CA) – U.S.A.	2006	PCE, TCE, Freon	nZVI	Push Pull	n.a.	k)
Bornheim, Germany	2007	PCE	nZVI + mZVI	Sleeve pipe injection	Approximately 90% reduction of the concentration of total chlorinated compounds.	l)
Horice, Czech Republic	2008	PCE, TCE, DCE	nZVI	Direct Push	Reductions of 60–75% of the original contaminant concentration were achieved	l)
Pisecna, Czech Republic	2009	Chlorinated ethenes	nZVI	n.a.	Significant decrease of 40-80%	l)
Biella, Italy	2005	TCE & cDCE	nZVI	Gravity infiltration	20-50% reductions in total chlorinated solvent concentrations after one month	m)
Former USAF ““Atlas 12”” Missile Site, Colorado, USA	2009	TCE	Micro iron/carbon (Adventus EHC) - “EHC-G”	Fracturing	TCE reduction with first 90 days cis-DCE increased Ethene detected at low levels	n)

n.a. information not available,

a) Elliot and Zhang, 2001, b) Quinn et al., 2005, c) Zhang and Elliot, 2006, d) Varadhi et al., 2005, e) Gavaskar et al., 2005, f) US EPA, 2003b, g) Kavanaugh and Rao, 2003, h) Olson et al., 2012, i) Chang, 2010, j) Sprinkle, 2004, k) Bennett, 2010, l) Mueller et al., 2012, m) *http://www.nanotechproject.org/inventories/remediation_map*, n) North Wind Inc., 2010

BNP: bimetallic nanoscale particles with palladium shell
EZVI: emulsified zerovalent iron
mZVI: microscale zerovalent iron
nZVI: nanoscale zerovalent iron
ZVI Ferox: microscale iron particles (commercial product, ARS Technologies)

From a remediation perspective, β-elimination represents the preferable pathway in reductive dechlorination of chloroethenes and chloroethanes as the reaction products are non-toxic.

In laboratory batch scale studies a rapid reaction of ZVI with the different CAHs was generally observed. Dissolved contaminants are usually destroyed within hours or a few days as presented in Table 3. Reported data show that the highest removal rate of different CAHs is obtained by nanoscale zerovalent iron (nZVI) particles due to the small particle size and, as a consequence, a high specific surface area. In contrast, granular and microscale zerovalent iron (mZVI) particles show lower contaminant reduction rates. Looking more closely the first order decay constant for TCE, surface area of the particles might affect TCE reduction. It is evident that nanoscale particles, with the highest specific surface area, degrade TCE fastest. On the other hand, compared to the nZVIs, Fisher electrolytic fillings and microscale particles degraded TCE slower as a consequence of the low specific surface area.

According to the literature data presented in Table 4, field case studies identified nZVI particles as promising agents for treatment of CAHs because of their extreme reactivity. However, limited mobility due to rapid aggregation and limited longevity of the particles due to high reactivity are critical issues that deserve further attention. According to experiences in field case studies, multiple successive treatments are required for a successful clean-up of the contaminated site by injection of nZVI particles (Elliott and Zhang, 2001).

Attraction among nZVI particles will induce aggregation and reduce the mobility of the particles within the porous medium (Kanel et al., 2007; Schrick et al., 2004). Due to aggregation, the surface area of the particles, and thus consequently particles’ reactivity, is reduced. To decrease aggregation of nZVI particles and to enhance their mobility in the porous medium, extensive research on surface modification of nZVI particles is performed by different research groups. Different polymers such as guar gum (Tiraferri et al., 2008), xanthan gum (Comba and Sethi, 2009; Vecchia et al., 2009), carboxymethyl cellulose (He et al., 2007), starch (He and Zhao, 2005; Tiraferri et al., 2008) were used to improve technological and environmental performance of nZVI particles with a minimal impact on reactivity. However, lab scale experiments proved that efficient stabilization of the nZVI particles by these coatings leads to a higher mobility, but a reduced reactivity is possible (Phenrat et al., 2007). In addition, the potential risk of nZVI particles to impair human health is still not sufficiently studied.

In comparison with nZVI particles, mZVI particles are less expensive, show a longer life-time after application and are believed to pose less risk to human health (Lee et al., 2008). On the other hand, mZVI particles are less reactive than nZVI particles, as shown in Table 3. Due to the relevant mass and high density, sedimentation of mZVI particles in tubes and injection wells will reduce the radius of influence as well as the contact with contaminants. To be used in the field applications mZVI particles must be stabilized against sedimentation. To prevent sedimentation of mZVI particles, the use of a stabilizing agent is necessary to increase viscosity of the mZVI suspension and enhance its mobility (Comba and Braun, 2012).

From recent studies (Tiraferri et al., 2008; Tiraferri and Sethi, 2009; Xue and Sethi, 2012) it is known that guar gum as a biodegradable polymer stabilizes both nZVIs and mZVIs slurries by adsorbing to the surface of the iron and providing steric repulsion. Moreover, nZVI and mZVI particles can be stabilized by viscous (kinetic) stabilization mechanism, increasing the viscosity of the suspension by guar gum and consequently slowing the aggregation processes (Comba and Sethi, 2009; Tiraferri et al., 2008; Xue and Sethi, 2012).

Finally, close to the ZVI-PRBs, iron sulfide (FeS) precipitates are formed under sulfate reducing conditions. The reductive dechlorination of several CAHs by FeS under anoxic conditions was previously reported (Butler and Hayes, 2000; 2001; Gander et al., 2002; He et al., 2010; Jeong et al., 2007)and may play significant role in future reductive dechlorination of several CAHs.

1.4. PROBLEM STATEMENT AND RESEARCH OBJECTIVE

The presented research aims to develop and to optimize the injectable zerovalent iron (ZVI) technology for in-situ remediation of groundwater contaminated with chlorinated compounds. The project contributes to more reliable, ecologically engineered and cost-effective technological solutions.

Granular ZVI particles (mm-range) have been studied extensively for in-situ abiotic degradation of chlorinated compounds. Common practice nowadays is to implement granular reactive particles (millimeter size) in PRB for in-situ plume treatment. To this purpose, soil material has to be excavated and replaced by the reactive particles. The excavation and refilling operation is invasive and is not flexible, nor cost-effective for deep aquifers. Injectable iron-based micro- (100 nm < d < 100 μm) and nano-scale particles (< 100 nm) are smaller sized reactive particles and can be injected in the subsurface, creating a reactive zone, and are as such less invasive and potentially economically more attractive (Zhang, 2003). In addition, smaller particles have a higher specific surface area and are more reactive. Not only higher degradation rates are observed in previous studies, but also a wider range of pollutants can be abated (Bastiaens et al., 2005).

Although applications of injectable ZVI particles are already available on the market, there are still major uncertainties about the application. Moreover, based on previous lab scale and the pilot scale studies, the application of both nZVIs and mZVIs was found challenging due to the colloidal instability of particles and the lack of data considering particles distribution and consequently reactivity after in-situ application. Fundamental parameters for a successful application of mZVIs as a substitution to highly reactive nZVIs that have not been investigated so far comprise (1) the reactivity and consequently life-time of the mZVI particles, (2) the stability and reactivity of mZVI particles in the suspension and consequently their mobility and effectiveness in the porous medium, and (3) the direct and non-intrusive measurement of the (reactive) mZVI particles in the subsurface.

The general objective of this PhD research therefore is to study injectable microscale ZVI particles as a substitution to nZVI particles used for in-situ reactive zone treatment of groundwater heavily polluted by chlorinated aliphatic hydrocarbons (chlorinated ethenes and ethanes). This research should give a more accurate assessment of the reactivity and life-time of microscale ZVI particles, possibilities and limitations of stabilized microscale ZVI particles for in-situ remediation of CAHs.

This research was performed in the framework of European project AQUAREHAB (Development of rehabilitation technologies and approaches for multi-pressured degraded waters and the integration of their impact on river basin management, FP7 contract n° 226565). Within this project, different innovative rehabilitation technologies for soil, groundwater and surface water were developed to cope with a number of priority contaminants (nitrates, pesticides, chlorinated compounds, aromatic compounds and mixed pollutions) within heavily degraded water systems.

1.5. THESIS OUTLINE

Figure 4 illustrates more specifically the scientific objectives and the link between the chapters of the present work.

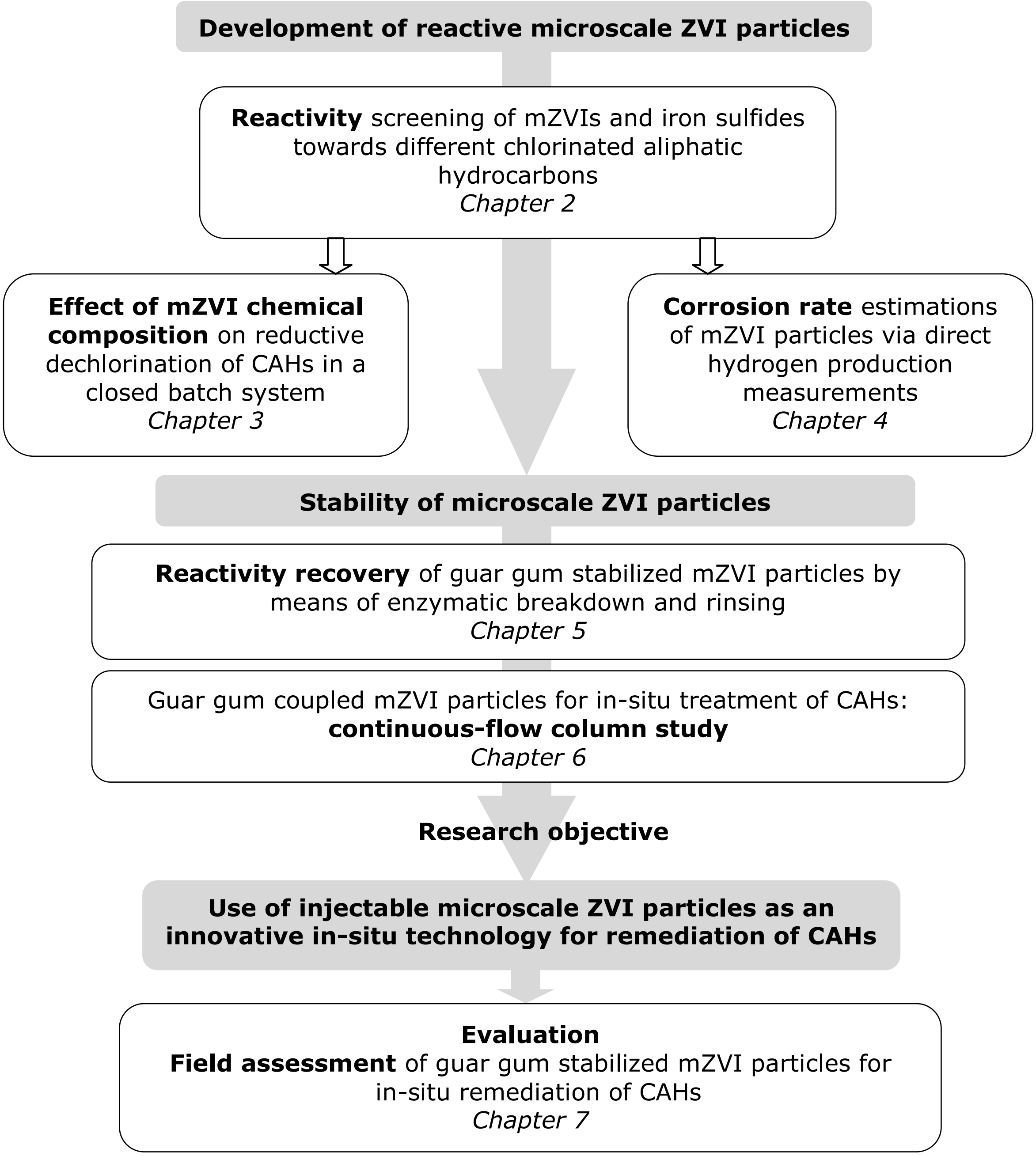

Figure 4 - Interaction diagram of the research approach and thesis outline.

In **Chapter 2**, a standardized lab-scale batch test procedure is used to evaluate and compare the reactivity of newly designed mZVIs and biogenic iron sulfides towards a mixture of different CAHs and their breakdown products. The mixture contained CAHs being tetrachloroethene (PCE), trichloroethene (TCE), cis-dichloroethene (cDCE) and 1,1,1-trichloroethane (1,1,1-TCA). For comparison, commercially available mZVIs, nZVIs, iron sulfides (FeS) and granular ZVI were also tested. Reactivity of the particles was based on observed (k_{obs}) and mass normalized (k_M) pseudo-first-order degradation rate constants, as well as specific surface area normalized reaction rate constants (k_{SA}). Sorption characteristics of the particles were based on mass balance data. Among the new mZVI particles, significant differences in reactivity were observed and the most reactive mZVI particles were selected for a more detailed study.

The fast degradation of CAHs by mZVI particles depends on the specific surface area of the mZVI particles as well as the iron composition. In **Chapter 3**, the knowledge gained from Chapter 2 was extended to show effect of microscale zerovalent iron chemical composition on reductive dechlorination of CAHs in a closed batch system. mZVI reactivity was correlated with the carbon, oxygen and sulfur content on the surface of mZVI particles, as well as specific surface area. In this chapter the optimal composition of mZVI particles for efficient remediation of CAHs was determined.

The long-term performance of mZVI particles to serve as an electron donor in reducing CAHs and consequently site cleanup time was investigated in **Chapter 4**. The aging behavior of mZVI particles was obtained by measuring the evolution of hydrogen as a consequence of anaerobic corrosion during the lab-scale batch degradation test explained in Chapter 2. Granular iron, commercially available mZVI and nZVI particles were included in this study as controls. In addition, the correlation between the surface area normalized corrosion rate (R_{SA}) and the reaction rate constants (k_{SA}) of PCE, TCE, cDCE and 1,1,1-TCA was evaluated. To confirm the data obtained during batch degradation experiments in aquifer free conditions, hydrogen evolution was monitored during the batch tests in the presence of aquifer material and polluted ground water. Finally, a corrosion rate numerical model was calibrated on the batch experiments to take into account the inhibitory effects of the iron corrosion reaction products on the corrosion rates.

mZVI transfers chlorinated aliphatic hydrocarbons (CAHs) to harmless compounds, but the sedimentation of the mZVI particles in the injection fluid limits the mobility of the particles during field applications. To prevent sedimentation of selected mZVI particles during injections, the use of a stabilizing agent is necessary. In **Chapter 5**, an elaborate literature research on stabilizing agents that have already been studied to improve technological and environmental performance of ZVI was reported. Promising stabilizer being guar gum required for mZVI particles to prevent sedimentation in the tubing and injection wells was selected according to the data obtained in sedimentation tests. Furthermore, batch degradation experiments were performed to examine the impact of the stabilizer on the reactivity of mZVI particles towards different CAHs. The use of commercial enzymes for guar gum degradation was also investigated. To conclude on the pertinent mZVI stabilization mechanism, scanning electron microscopy (SEM) analyses and Fourier transform infrared spectroscopy (FTIR) were conducted.

Subsequently, in **Chapter 6**, five aquifer containing columns were set up under different conditions to validate and discuss the application of guar gum stabilized mZVI particles for in-situ treatment of CAHs. After more than six months of continuous operation columns were dismantled and DNA-based qPCR analysis of aquifer material was performed to evaluate the effect of mZVI and guar gum stabilized mZVI on present bacterial community.

In **Chapter 7**, field-scale assessment of guar gum stabilized mZVI particles for in-situ remediation of CAHs in an industrial area is presented. One spot injection at high pressure via direct push was performed to demonstrate that mZVI slurries stabilized with guar gum can be prepared at pilot scale and delivered in the subsurface. The vertical and horizontal distribution of mZVI particles in the subsurface after injection is presented, as well as significant dechlorination of some CAHs. In order to distinguish between a reduction in concentration due to mixing with the injected fluid and a reduction due to degradation, carbon stable isotope analyses were conducted.

Finally, a general discussion of the research and some future perspectives are given in **Chapter 8**.

CHAPTER 2 REACTIVITY SCREENING OF MICROSCALE ZEROVALENT IRONS AND IRON SULFIDES TOWARDS DIFFERENT CHLORINATED ALIPHATIC HYDROCARBONS UNDER STANDARDIZED EXPERIMENTAL CONDITIONS

Based on: Velimirovic, M., Larsson, P.-O., Simons, Q., Bastiaens, L. Reactivity screening of microscale zerovalent irons and iron sulfides towards different chlorinated aliphatic hydrocarbons. Journal of Hazardous Materials 252-253 (2013) 204-212.

2.1. INTRODUCTION

As previously mentioned, zerovalent iron (ZVI) has been widely used for site remediation by permeable reactive barriers (PRBs) because of its passive character, low cost, availability and high ability to dehalogenate chlorinated aliphatic hydrocarbons (CAHs) over wide concentration ranges (Gavaskar 1999; Gillham and O’Hannesin, 1994; Tratnyek et al., 1997). Mostly, granular sized ZVIs have been used in PRBs (Lai et al., 2005). In respect to fine injectable ZVI particles for in-situ remediation of CAHs, mainly nanoscale zerovalent iron (nZVI) particles were studied because of their extreme reactivity, although their efficiency in the field is not completely clear (Noubactep, 2010; Noubactep et al., 2012). Loss in reactivity and decreased mobility of uncoated nZVIs is explained by rapid aggregation and agglomeration forming micron sized aggregates (Phenrat et al., 2007). In comparison with the nanoscale ones, microscale zerovalent iron (mZVI) particles are less expensive, have a longer life-time and pose less risk for human health (Lee et al., 2008; Li et al., 2009; Phenrat et al., 2009). The capacity of soil mineral iron sulfide (FeS) to transform several CAHs has been reported by several research groups (Butler and Hayes, 2000; 2001; Gander et al., 2002; He et al., 2010; Jeong et al., 2007). At least one study compared the reactivity of FeS with granular ZVIs (Butler and Hayes, 2001). However, no detailed study on comparison of FeS, mZVIs and nZVIs has been reported.

Comparison of mZVIs and nZVIs in respect to their efficiency for degrading chlorinated ethenes has been extensively reported (Barnes et al., 2010; Schrick et al., 2002; Xu and Zhang, 2000; Zhang et al., 1998). Generally, mZVI particles remove CAHs slower than the same mass of well suspended nZVIs. The higher reactivity of nZVIs is explained by the greater specific surface area (Zhang et al., 1998; Zhang, 2003). On the other hand, when focusing on surface area normalized reaction rate constants, similar reactivity is obtained for nZVIs and mZVIs (Nurmi et al., 2005). Following the research of Mace (2006), conducted to prove advantages of nZVIs over microscale and bimetallic nanoscale iron particles, Comba et al. (2011) collected 112 field case studies available in the literature where fine ZVIs were used for in-situ remediation of CAHs. According to statistical analysis, a higher degree of CAHs degradation was observed for mZVIs than for nZVIs when the ZVI material is not combined with other technologies (e.g. addition of organic component, presence of a catalyst) (Comba et al., 2012).

A number of papers have been published focusing on the reactivity of different ZVI particles deduced from batch studies (Barnes et al., 2010; Johnson et al., 1996; Hara et al., 2009; Liu et al., 2005; Ma and Wu, 2008; Miehr et al., 2004; Scherer et al., 1998; Zhang et al., 1998). This resulted in a wide range of reactivity within ZVIs towards various CAHs. The characteristics of the iron material are an explanation, but also different experimental conditions (pH, buffer, temperature etc.), iron pretreatment kinetic and type of organic pollutants (Farrell et al., 2000). Additionally, many of these batch studies were limited to a single CAH-compound. Degradation of a mixture of contaminants has been generally reported in numerical experiments (Bayer and Finkel, 2005). Consequently, large reactivity data sets using consistent experimental conditions for different iron based particles including iron sulfides and mixtures of different pollutants are limited.

The primary objective of the present study was to evaluate the reactivity of 23 different iron based fine particles towards a mixture of chlorinated ethenes and ethanes, using consistent experimental conditions to exclude the impact of experimental conditions on the evaluation of the iron reactivity. This paper focuses mainly on mZVI particles (17 materials, from which 12 newly designed) and biogenic iron sulfides (2 materials). One granular ZVI, one commercial FeS and two nZVIs were included as reference materials. In contrast to other studies, where batch and column experiments were mainly performed for one chlorinated aliphatic hydrocarbon (Cheng and Wu, 2000; Cho and Choi, 2010; Johnson et al., 1996; Lie et al., 2005; Song and Carraway, 2005; Zhang et al., 1998), the study reported herein evaluates the reactivity of different iron based particles towards an environmentally relevant mixture of four chlorinated compounds: tetrachloroethene (PCE), trichloroethene (TCE), cis-dichloroethene (cDCE) and 1,1,1-trichloroethane (1,1,1-TCA) under standardized batch test conditions.

The motivation behind using the selected standardized degradation procedure for a mixture of CAHs, was to compare the CAH-removal kinetics of newly designed mZVIs as well as biogenic iron sulfides with commercially available ZVI materials within a reasonable time frame and with a reasonable amount of effort. Mixtures of pollutants are also representative for most contaminated sites. The formation and degradation of breakdown products of the tested CAHs (i.e. 1,1-dichloroethane) was also considered, rendering information about the reactivity towards these compounds.

2.2. MATERIALS AND METHODS

2.2.1. MEDIA

Artificial groundwater used for the batch tests consisted of anaerobic autoclaved MilliQ water supplemented with 0.5 mM $CaCl_2.2H_2O$, 0.5 mM $MgCl_2.6H_2O$, 0.5 mM $NaHCO_3$ and 0.5 mM $KHCO_3$ (Dries et al., 2005). Under anaerobic conditions, the pH was adjusted to neutral by adding 1M HCl and the artificial groundwater was spiked aiming at a final concentration of approximately 5 mg L^{-1} of PCE, TCE, cDCE and 1,1,1-TCA each. The chemicals PCE (> 99 % purity), TCE (> 99 %) and cDCE (97 %) were supplied by Acros Organics (Belgium). 1,1,1-TCA (97 %) was purchased from JT Baker Chemicals (The Netherlands).

2.2.2. IRON BASED PARTICLES

The reducing iron based particles included in the test comprise zerovalent irons (micron, nano and granular size) and iron sulfides. Details on size, specific surface area, supplier, production process of all the studied iron based particles are given in Table 5 and were obtained before batch experiments were started.

Twelve mZVI types with different particle size distributions, morphologies and slightly different chemical compositions were prepared by iron powder manufacturer Höganäs (Sweden) using two different production methods.

The two biogenic iron sulfides were freshly produced at small scale by growing two different mixed enrichment cultures of sulfate-reducing bacteria in Postgate’s medium B (Postgate, 1984). Biogenic iron sulfides were harvested by centrifugation at 4000 rpm for 10 min. at room temperature. The supernatant was discarded and the precipitates were used in degradation experiments. The final concentration of biogenic iron sulfides included in the tests was calculated via dry weight measurement and precipitation of organic matter.

Table 5 : Properties of studied iron based particles.

Iron name	PSD [D_{10}, D_{50}, D_{90}][a] [µm]	BET[b] [m^2 g^{-1}]	Production process	Supplied by	Form
FeA4 [C]	300-1300 mm[c]	1.15	Granulated grey cast iron	Gotthart Maier (DE)	Iron Filings
FeH1 [N]	8, 26, 50	0.27	Iron oxides*	Höganäs (SE) [N]	Powder
FeH3 [N]	36, 84, 168	0.06	Atomization		
FeH4 [N]	22, 41, 62	0.09	Atomization		
FeH6 [N]	41, 98, 162	0.09	Iron oxides		
FeH7 [N]	44, 96, 158	0.12	Iron oxides		
FeH8 [N]	34, 63, 97	0.35	Iron oxides		
FeH9 [N]	3, 7, 16	0.50	Iron oxides		
FeH10 [N]	9, 22, 42	1.21	Iron oxides		
FeH11 [N]	6, 19, 38	3.98	Iron oxides		
FeH12 [N]	6, 17, 32	3.62	Iron oxides		
FeH13 [N]	7, 18, 34	1.50	Iron oxides		
FeH14 [N]	21, 79, 162	11.40	Iron oxides		
FeQ2 [C]	8, 26, 44	0.40	Iron oxides	Höganäs (SE)	Powder
MS200 [C]	2.1, 4.2, 7.2	0.36	Carbonyl irons**	BASF (DE)	Powder
MS200+ [C]	1.7, 3.7, 7.1	0.47	Carbonyl irons		
SM [C]	1.4, 2.5, 4.1	0.48	Carbonyl irons		
HQ [C]	0.6, 1.2, 2.4	0.82	Carbonyl irons		
Nanofer25s [C]	D_{50} < 0.05[c]	25.0[c]	Surface modified nanoscale iron	NANOIRON (CZ)	Suspension
RNIP[C]	D_{50} < 0.07[c]	4.97	Fe^0/Fe_3O_4 core-shell nZVI particles	TODA (JP)	Suspension
FeS Aldrich [C]	12, 89, 268	0.90	Iron sulfides	Aldrich	Powder
FeS BIO1[N]	0.002-001[d]	3.40	Biogenic iron sulfides	VITO [N]	Suspension
FeS BIO2 [N]	0.002-001[d]	3.40	Biogenic iron sulfides		

[a] Particle Size Distribution measured by laser diffraction with a Sympatec Helos/Rodos dry particle size analyzer;
[b] BET : Specific Surface Area analyzed with a Micromeritics Flowsorb II according to the Brunauer-Emmett-Teller (Single point measurement);
[c] Producers data;
[d] According to Ohfuji and Rickard (2006);
[N] Newly prepared for this study;
[C] Commercially available;
*Particles production process starts from iron oxide, which is further reduced by carbon and/or hydrogen in different continuous reduction processes;
**Chemical decomposition of purified iron pentacarbonyl.

2.2.3. DEGRADATION EXPERIMENTS

Batch experiments were performed to study degradation of a mixture of CAHs by different iron based particles. Glass vials contained 50 g L^{-1} of granular or microscale ZVI, FeS, approximately 40 g L^{-1} of biogenic iron sulfides or 5 g L^{-1} of nZVI. Lower concentrations of nanoscale particles were used due to their high reactivity. Subsequently, 100 ml of anaerobic, artificially contaminated groundwater was added to the vials in an anaerobic glove box (nitrogen), leaving a 60 ml headspace. The bottles were capped with butyl/PFTE grey septa. The experiments were carried out in triplicates and at a groundwater temperature of 12±1 0C. As the role of mass transport processes in determining degradation kinetics is very important, all vials were placed on an Edmund Bühler SM 30-control shaker (125 rpm min^{-1}). Each series included a control set without iron particles to identify losses of CAHs (e.g. photo degradation, adsorption, leakage, samplings). In the control sets, no formation of metabolites was observed and losses of the examined CAHs were ~ 10-15%. Mass transfer resistance at the vapor/liquid interface was not considered as these phases are assumed to be in equilibrium with each other (Burris et al., 1999). As a function of time, the concentration of CAHs was followed along with pH and ORP values. For nanoscale particles, samples were taken 0, 3, 6, 8 and 22 days after the start of the test, for the other particles after 0, 14, 28, 49 and 105 days.

The concentrations of CAHs, intermediate- and end-products were determined via direct headspace measurements using a Varian GC-FID (CP-3800 with CTC-auto sampler) equipped with a Rt-U plot column for the detection of ethene, ethane and acetylene or a split-splitless injector followed by a Rt-X column (Restek) and a DB-1 column (J&W Scientific) for analysis of CAHs. At each sampling time 1.5 ml of sample was removed for measurements of the oxidation-reduction potential (ORP) and pH using a redox/pH meter (Radiometer). Mass recoveries were made on molar basis (PCE + TCE + cDCE + VC + 1,1,1-TCA + 1,1-dichloroethane (1,1-DCA) + acetylene + ethene + ethane) to determine if sorption occurred. To determine acetic acid, diethyl ether extraction was used. Samples were analyzed by a Focus GC-FID, while the quantification was done according to the internal standard method. Based on triplicate analysis of samples, analytical errors were typically ~ 5%.

2.2.4. DATA ANALYSIS

A pseudo-first-order model was applied to describe the reductive dechlorination of a parent compound by the reactive materials (Johnson et al., 1996):

$$C = C_0 \, e^{-k_{obs} t} \tag{9}$$

where C is the concentration at any time and C_0 is the initial concentration of parent compound (mg L^{-1}), k_{obs} is the pseudo-first-order rate constant (h^{-1}) and t (h) is the reaction time. The natural logarithmic transformation of eq. 9 yields a linear equation with the first-order rate constant k_{obs} as slope:

$$\ln (C / C_0) = - k_{obs} \, t \tag{10}$$

Mass normalized rate constants (k_M, L g^{-1} h^{-1}) and specific surface area normalized rate constants (k_{SA}, L m^{-2} h^{-1}) were calculated using the following relationship (Johnson et al., 1996; Nurmi et al., 2005):

$$k_{obs} = k_M \rho_M = k_{SA} a_s \rho_M = k_{SA} \rho_a \quad (11)$$

with a_s as the specific surface area of iron based particles (m^2 g^{-1}), ρ_M as the mass concentration of the iron based particles (g L^{-1}) and ρ_a as the surface area concentration of iron based particles (m^2 L^{-1} of solution).

Pseudo-first-order model was also used to calculate the reduction of the maximal observed amount of 1,1-DCA formed during 1,1,1-TCA degradation.

Finally, a one-way ANOVA analysis was used to compare differences between mass normalized (k_M) and specific surface area normalized rate constants (k_{SA}) for selected pollutants (PCE, TCE, cDCE and 1,1,1-TCA), as well as specific surface area at a significance level of 0.05.

2.3. RESULTS AND DISCUSSION

Comparison of the CAH removal kinetics of different reactive iron based particles was based on observed (k_{obs}) and mass normalized (k_M) pseudo-first-order degradation rate constants, as well as specific surface area normalized reaction rate constants (k_{SA}) under similar experimental conditions. Disappearance rate curves of parent compound by the reactive materials are presented in Figure 5. k_{obs} was determined via linear regression of ln-transformed data (eq. 10). The slope of the degradation rate curves represents k_{obs}. This is a commonly used approach to determine first order degradation rate constants, where it is known that low concentration data may have overestimated impact on the result. Generally, all measured data points were used to determine the curves. However, low concentration data were omitted when already proceeding by low concentration data (e.g. FeH3, FeH4, FeH6). For a number of iron particles the CAH-concentration decrease stopped after the second data point with no appearance of degradation products, indicating the sorption effects were dominant. The sorption effects are later explained by chemical composition of particles (Chapter 3) and no significant iron corrosion deduced from H_2 production rates followed in the same batches (Chapter 4). In these cases, the sorption rates were calculated. For irons with a mixed removal mechanisms (degradation and sorption), the first order degradation rates were calculated and the lower correlation coefficient indicated the mixed effect.

Most of the examined iron based materials reduced 1,1,1-TCA rapidly, and gave first-order disappearance rate for PCE, TCE and cDCE.

However, five of all tested mZVI materials (FeH3, FeH4, FeH6, FeH7 and FeQ2) gave first-order disappearance rate of TCE with tailing after 105 days of experiment that might be due to the accumulation of reaction products as previously reported by Miehr et al. (2004). For these irons, the last data point was omitted. For FeH1 and FeH9 slow or no reduction was observed and these data were assumed to be first-order rate. Rapid initial loss of PCE, TCE, cDCE and 1,1,1-TCA with no further reduction for FeH11 and FeH12 is due to the sorption properties as deduced from no detection of degradation products and no pressure build-up as a consequence of iron corrosion in batch reactors. To obtain disappearance rate constants, only first data were fitted and reported as a sorption. Similar was observed for FeH10 and FeH13 (PCE and TCE reduction), HQ (PCE reduction), FeS Aldrich (TCE reduction), FeS BIO1 (PCE, TCE, cDCE). FeS BIO2 showed slow degradation of PCE and 1,1,1-TCA with tailing of TCE as a possible byproduct of PCE degradation and cDCE as a byproduct of TCE degradation. For this iron only first data for TCE and cDCE were fitted.

The evolution of pH and redox potential during the test are summarized in Figure 6. On average, the pH increased rapidly above pH 9.9 ± 0.7 due to the iron corrosion (Su and Puls, 1999), and remained constant afterwards.

2.3.1. CAH-REMOVAL EFFICIENCIES BY DIFFERENT IRON BASED PARTICLES

Data on selected pollutant removal efficiencies are given in Table 6. After 105 days, the granular iron (FeA4), used as a reference material in this study, degraded > 95% of PCE, TCE and 1,1,1-TCA and > 40% of cDCE. Nanofer25s, the most efficient iron among all examined iron based particles, removed 100% of the pollutants mixture within a 22 days reaction period. The most reactive mZVIs capable of PCE, TCE, cDCE and 1,1,1-TCA removal of > 98% within the test period (105 days) are: FeH4, FeH8, FeH14 and FeQ2. In contrast, the least reactive mZVI particles were FeH1 and FeH9. The observed fast pH increase from pH 7.20 to approximately 11 with no observed change in the redox potential shows the low reduction capacity of these particles. Possible explanations for this comprise inhibition of reactivity due to the high pH or passive film of iron oxides and/or iron-oxyhydroxides on the surface. pH values above 11 may be an indication for less reactive mZVI particles. The lowest pH (9.33) was observed for FeH3 and FeH4 which are both produced via atomization process where low amount of iron oxides on the iron surface is expected. At the end of the test period, FeS Aldrich removed 95% of TCE and 20% of cDCE, while complete degradation of PCE and 1,1,1-TCA was observed. Biogenic FeS BIO1 realized a slow degradation of PCE (37%) and 1,1,1-TCA (62%) after 105 days. However, FeS BIO2 was not reactive towards the examined

CAHs. Moreover, 70% of all studied irons were capable of efficient removal of 1,1,1-TCA. Despite the high percentage of tested pollutants removal, the microscale particles FeH11 and FeH12 showed mainly sorption tendencies which was concluded from calculated mass recoveries (26-27%) and no increase of the degradation products (ethene and ethane) and no pressure build-up. Low calculated mass recoveries were also obtained for highly reactive materials such as nZVIs, HQ, FeH4 and FeH14, where high production of ethene and ethane and high pressure build-up were observed (data not shown). A loss of volatile reactants and products during the sampling process due to the high pressure build-up in batch reactors has also been observed by other researchers (Tratnyek et al, 1997). In addition, incomplete mass recoveries can be explained by the fast transformation of 1,1,1-TCA and formation of acetic acid as degradation end-product.

The PCE, TCE, cDCE and 1,1,1-TCA observed degradation rate constants (k_{obs}) are summarized in Table 6. The range in reported k_{obs} corresponds to half life time ($t_{1/2}$) from 6 h to 866 days, depending on the type of iron based particles used and the specific pollutant. Considering kobs data, Nanofer25s, the iron with the highest surface area and tested in ten times lower concentration, is the most reactive iron used in this study. A significantly high degradation capacity was also observed for the newly designed FeH14 iron.

Table 6 : Summary of results for PCE, TCE, cDCE and 1,1,1-TCA removal efficiency by studied iron based particles.

	Mass recovery	**PCE**	**TCE**	**cDCE**	**1,1,1-TCA**
		(5 mg L^{-1})[a]	**(5 mg L^{-1})**[a]	**(5 mg L^{-1})**[a]	**(5 mg L^{-1})**[a]
Treatment (concentration)	%	% reduced	% reduced	% reduced	% reduced
FeA4 (50 g L^{-1})	67	97	100	42	100
FeH1 (50 g L^{-1})	93	31	25	16	19
FeH3 (50 g L^{-1})	60	98	98	51	100
FeH4 (50 g L^{-1})	43	100	98	98	100
FeH6 (50 g L^{-1})	68	91	99	65	100
FeH7 (50 g L^{-1})	68	96	99	42	100
FeH8 (50 g L^{-1})	54	98	100	100	100
FeH9 (50 g L^{-1})	97	9	5	3	4
FeH10 (50 g L^{-1})	69	88	51	30	46
FeH11 (50 g L^{-1})	29	100*	100*	100*	100*
FeH12 (50 g L^{-1})	31	100*	99*	87*	98*
FeH13 (50 g L^{-1})	66	95	100	45	100
FeH14 (50 g L^{-1})	44	100	100	99	100
FeQ2 (50 g L^{-1})	44	100	100	100	100
MS200 (50 g L^{-1})	108	69	8	1	100
MS200+ (50 g L^{-1})	75	79	61	34	100
SM (50 g L^{-1})	83	30	24	21	100
HQ (50 g L^{-1})	51	99	100	88	100
Nanofer25s (5 g L^{-1})	11	100	100	100	100
RNIP (5 g L^{-1})	32	97	99	33	100
FeS Aldrich (50 g L^{-1})	65	100	98	20	100
FeS BIO1 (40 g L^{-1})[b]	74	37	26	16	62
FeS BIO2 (40 g L^{-1})[b]	91	25	16	6	28

[a] Initial concentration or concentration range;

[b] Concentration calculated according to dry weight measurement and precipitation of organic matter;

*Sorption.

Table 7 : Summary of kinetic data for dehalogenation of PCE, TCE, cDCE and 1,1,1-TCA by studied iron based particles.

	PCE (5 mg L^{-1})[a]			**TCE (5 mg L^{-1})**[a]			**cDCE (5 mg L^{-1})**[a]			**1,1,1-TCA (5 mg L^{-1})**[a]		
Treatment (concentration)	**k_{ob} (h^{-1})**[b]	**SD***	**k_{SA} (L m $^{-2}$ h^{-1})**[c]	**k_{ob} (h^{-1})**[b]	**SD**	**k_{SA} (L m $^{-2}$ h^{-1})**[c]	**k_{ob} (h^{-1})**[b]	**SD**	**k_{SA} (L m $^{-2}$ h^{-1})**[c]	**k_{ob} (h^{-1})**[b]	**SD**	**k_{SA} (L m $^{-2}$ h^{-1})**[c]
FeA4 (50 g L^{-1})	1.6x10^{-3}	5.8x10^{-5}	2.8x10^{-5}	2.4x10^{-3}	2.6x10^{-4}	4.2x10^{-5}	2.0x10^{-4}	2.2x10^{-5}	3.4x10^{-6}	1.9x10^{-2}	5.1x10^{-8}	3.4x10^{-4}
FeH1 (50 g L^{-1})	3.9x10^{-4}	2.3x10^{-5}	2.9x10^{-5}	3.8x10^{-4}	3.0x10^{-5}	2.8x10^{-5}	2.6x10^{-4}	7.9x10^{-5}	1.9x10^{-5}	2.7x10^{-4}	7.9x10^{-11}	2.0x10^{-5}
FeH3 (50 g L^{-1})	1.5x10^{-3}	5.8x10^{-5}	4.9x10^{-4}	2.8x10^{-3}	1.2x10^{-4}	8.8x10^{-4}	2.5x10^{-4}	1.3x10^{-5}	8.1x10^{-5}	4.4x10^{-3}	5.1x10^{-9}	1.4x10^{-3}
FeH4 (50 g L^{-1})	1.7x10^{-3}	2.3x10^{-5}	3.7x10^{-4}	3.1x10^{-3}	1.5x10^{-4}	6.5x10^{-4}	1.2x10^{-3}	1.2x10^{-4}	2.6x10^{-4}	6.2x10^{-3}	9.4x10^{-9}	1.3x10^{-3}
FeH6 (50 g L^{-1})	9.0x10^{-4}	1.4x10^{-4}	2.0x10^{-4}	2.9x10^{-3}	1.2x10^{-4}	6.4x10^{-4}	3.6x10^{-4}	4.4x10^{-5}	8.2x10^{-5}	6.3x10^{-3}	7.4x10^{-9}	1.4x10^{-3}
FeH7 (50 g L^{-1})	1.3x10^{-3}	6.9x10^{-5}	2.1x10^{-4}	3.9x10^{-3}	2.4x10^{-4}	6.2x10^{-4}	1.9x10^{-4}	3.2x10^{-5}	3.1x10^{-5}	5.9x10^{-3}	1.4x10^{-8}	9.4x10^{-4}
FeH8 (50 g L^{-1})	1.3x10^{-3}	9.9x10^{-5}	7.7x10^{-5}	2.2x10^{-3}	1.7x10^{-4}	1.3x10^{-4}	8.0x10^{-4}	8.9x10^{-5}	4.6x10^{-5}	1.6x10^{-2}	2.7x10^{-8}	9.2x10^{-4}
FeH9 (50 g L^{-1})	9.6x10^{-5}	5.0x10^{-5}	3.8x10^{-6}	4.2x10^{-5}	5.4x10^{-7}	1.7x10^{-6}	3.3x10^{-5}	1.4x10^{-5}	1.3x10^{-6}	3.3x10^{-5}	1.8x10^{-13}	1.3x10^{-6}
FeH10 (50 g L^{-1})	3.2x10^{-3}	1.8x10^{-4}	5.2x10^{-5}	7.0x10^{-4}	4.7x10^{-5}	1.1x10^{-5}	1.3x10^{-4}	3.5x10^{-5}	2.1x10^{-6}	2.5x10^{-4}	1.2x10^{-10}	4.1x10^{-6}
FeH11 (50 g L^{-1})	2.0x10^{-2}	5.3x10^{-6}	9.9x10^{-5}	1.2x10^{-2}	6.7x10^{-4}	5.9x10^{-5}	3.6x10^{-3}	7.8x10^{-5}	1.8x10^{-5}	8.8x10^{-3}	5.9x10^{-8}	4.4x10^{-5}
FeH12 (50 g L^{-1})	1.9x10^{-2}	1.4x10^{-5}	1.0x10^{-4}	1.1x10^{-2}	4.1x10^{-4}	5.9x10^{-5}	3.0x10^{-3}	6.9x10^{-4}	1.7x10^{-5}	7.8x10^{-3}	3.2x10^{-8}	4.3x10^{-5}
FeH13 (50 g L^{-1})	3.8x10^{-3}	1.1x10^{-4}	5.1x10^{-5}	7.1x10^{-3}	2.6x10^{-4}	9.5x10^{-5}	2.0x10^{-4}	2.2x10^{-5}	2.6x10^{-6}	1.8x10^{-2}	4.5x10^{-8}	2.3x10^{-4}
FeH14 (50 g L^{-1})	2.3x10^{-2}	2.9x10^{-4}	4.1x10^{-5}	9.8x10^{-3}	6.6x10^{-4}	1.7x10^{-5}	2.1x10^{-3}	3.9x10^{-5}	3.6x10^{-6}	2.0x10^{-2}	1.3x10^{-7}	3.5x10^{-5}
FeQ2 (50 g L^{-1})	2.1x10^{-3}	2.3x10^{-6}	1.0x10^{-4}	4.5x10^{-3}	4.9x10^{-4}	2.3x10^{-4}	1.4x10^{-3}	1.6x10^{-4}	6.9x10^{-5}	2.5x10^{-2}	1.2x10^{-7}	1.3x10^{-3}
MS200 (50 g L^{-1})	4.9x10^{-4}	5.2x10^{-5}	2.7x10^{-5}	4.1x10^{-4}	2.0x10^{-5}	2.3x10^{-5}	6.3x10^{-5}	4.1x10^{-6}	3.5x10^{-6}	1.3x10^{-2}	2.6x10^{-9}	7.3x10^{-4}
MS200+ (50 g L^{-1})	4.9x10^{-4}	2.7x10^{-5}	2.1x10^{-5}	3.8x10^{-4}	2.6x10^{-5}	1.6x10^{-5}	1.8x10^{-4}	1.3x10^{-5}	7.6x10^{-6}	2.5x10^{-2}	6.6x10^{-9}	1.1x10^{-3}
SM (50 g L^{-1})	1.3x10^{-4}	2.3x10^{-5}	5.2x10^{-6}	1.0x10^{-4}	1.3x10^{-5}	4.3x10^{-6}	9.2x10^{-5}	3.3x10^{-6}	3.8x10^{-6}	4.0x10^{-3}	5.2x10^{-10}	1.7x10^{-4}
HQ (50 g L^{-1})	7.0x10^{-3}	2.4x10^{-4}	1.7x10^{-4}	3.3x10^{-3}	2.2x10^{-4}	8.2x10^{-5}	9.8x10^{-4}	1.9x10^{-4}	2.4x10^{-5}	2.5x10^{-2}	5.4x10^{-8}	6.0x10^{-4}
Nanofer25s (5 g L^{-1})	1.4x10^{-2}	1.1x10^{-3}	1.1x10^{-4}	1.2x10^{-2}	4.5x10^{-4}	9.8x10^{-5}	1.0x10^{-2}	1.0x10^{-3}	8.2x10^{-5}	1.2x10^{-1}	5.3x10^{-7}	9.4x10^{-4}
RNIP (5 g L^{-1})	7.1x10^{-3}	4.4x10^{-4}	2.6x10^{-4}	9.6x10^{-3}	3.4x10^{-4}	3.5x10^{-4}	8.8x10^{-4}	3.1x10^{-5}	3.2x10^{-5}	1.5x10^{-2}	5.1x10^{-8}	5.6x10^{-4}
FeS Aldrich (50 g L^{-1})	4.2x10^{-3}	5.8x10^{-4}	9.3x10^{-5}	6.6x10^{-3}	7.0x10^{-4}	1.5x10^{-4}	5.8x10^{-5}	3.9x10^{-6}	1.3x10^{-6}	2.5x10^{-2}	1.7x10^{-7}	5.5x10^{-4}
FeS BIO1 (40 g L^{-1})	6.4x10^{-4}	3.2x10^{-5}	4.9x10^{-6}	4.2x10^{-4}	8.4x10^{-5}	3.2x10^{-6}	2.9x10^{-4}	3.8x10^{-5}	2.2x10^{-6}	4.3x10^{-4}	3.6x10^{-10}	3.2x10^{-6}
FeS BIO2 (40 g L^{-1})	1.4x10^{-4}	3.1x10^{-5}	1.1x10^{-6}	1.3x10^{-4}	2.8x10^{-5}	1.0x10^{-6}	1.8x10^{-4}	5.0x10^{-5}	1.4x10^{-6}	1.5x10^{-4}	4.1x10^{-11}	1.2x10^{-6}

[a] Initial concentration or concentration range;

[b] k_{ob} the first order decay constant (h^{-1});

[c] k_{SA} surface area normalized reaction rate constants (L m^{-2} h^{-1});

*Standard deviation from triplicates;

Underlined data present sorption rate constants.

In general, when comparing the reduction rates of the tested CAHs for the different irons (Table 8), 1,1,1-TCA is clearly degraded at the fastest rate (complete reduction was achieved within 14 days) by most of the studied irons. This might be explained by differences in bond strength between ethenes and ethanes (sp2 > sp3) (Scherer et al., 1998). cDCE was the least reactive examined pollutant as possible competition between cDCE and TCE can occur (Schafer, 2003). For the other pollutants, no fixed order of degradation was observed; it was dependent on the reaction mechanism (Arnold and Roberts, 2000; Ebert et al., 2006; Schafer, 2003) and in certain cases on the specific surface areas. Effect of iron surface area on the degradation kinetics was observed for irons produced from the same raw material (from FeH10 to FeH14). The iron with the lowest specific surface area (FeH10) had the slowest degradation rate of the examined chloroethenes, while the fastest degradation was observed for FeH14 iron (the highest specific surface area). A one-way analysis of variance (ANOVA) revealed that lower ORP values were responsible for significant reduction of PCE, TCE and cDCE ($p<0.01$). There was no correlation between k_{obs} and maximal observed pH values.

Table 8 : Comparison of the PCE, TCE, cDCE and 1,1,1-TCA reduction rates for each iron based particles.

Order of reduction rates	**Iron based particle**
1,1,1-TCA > TCE > PCE > cDCE	FeA4; RNIP; FeH3; FeH4; FeH6; FeH7; FeH8; FeH13; FeQ2; HQ
1,1,1-TCA > PCE > TCE > cDCE	FeS Aldrich; MS200; SM; MS 200+; Nanofer25s
PCE > TCE > 1,1,1-TCA > cDCE	FeH1; FeH10; FeH11; FeH12; FeH14
cDCE > PCE > 1,1,1-TCA > TCE	FeH9
PCE ≥ 1,1,1-TCA > TCE > cDCE	FeS BIO1, FeS BIO2

Furthermore, VC as an intermediate product did not increase significantly. Acetylene was detected in low concentrations indicating that the reductive β-elimination pathway was followed with further degradation of acetylene to ethene and ethane. This is in accordance with previous studies (Farrell et al., 2000; Roberts et al., 2006). In respect to iron sulfides, production of acetylene as an intermediate product was observed for both the commercial FeS and FeS BIO1, indicating on abiotic degradation of contaminants via the β-elimination pathway. This is consistent with conclusions from others research (He et al., 2010; Jeong et al., 2007; Zhang et al., 1998).

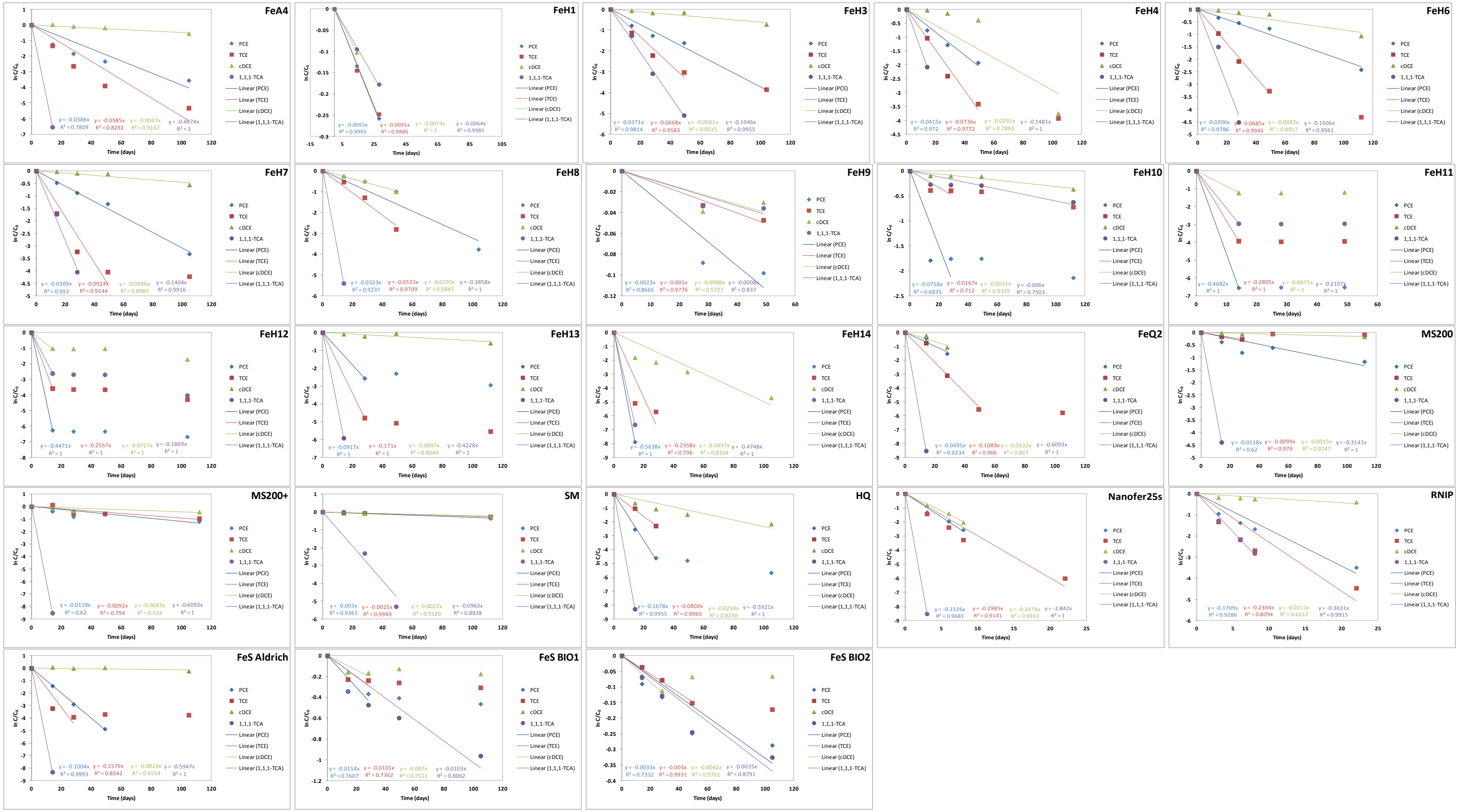

Figure 5 - PCE, TCE, cDCE and 1,1,1-TCA reaction rate constants for different iron based particles. Lines present pseudo-first-order fit of data. All data points represent average values from triplicates.

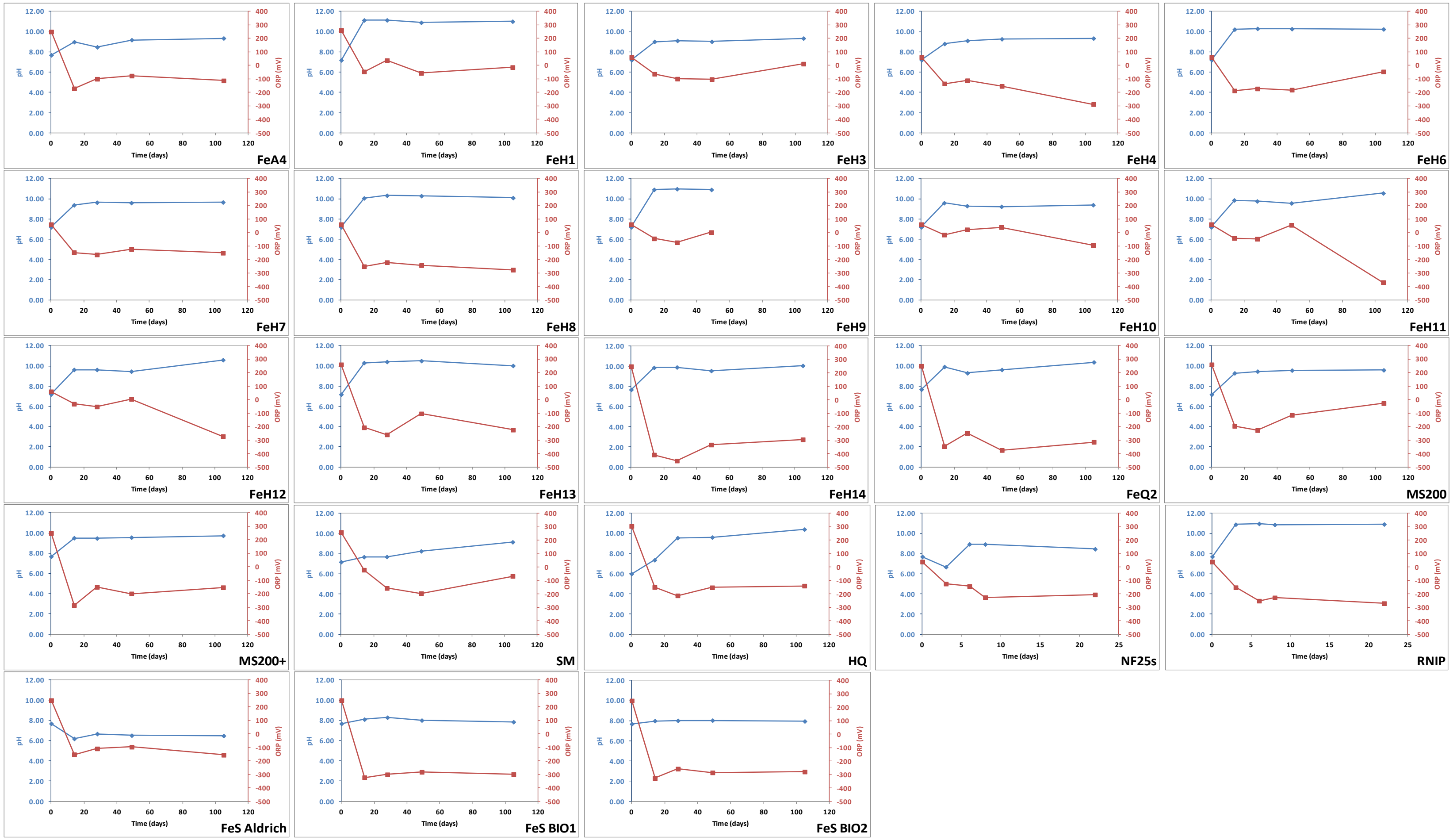

Figure 6 - Change of pH and ORP values in time (days). All data points represent average values from triplicates.

2.3.2. MASS NORMALIZED CAH-REMOVAL KINETICS FOR DIFFERENT IRON BASED PARTICLES

To obtain removal kinetic data that are independent of the mass of iron based particles, mass normalized degradation rate constants (k_M) were calculated and plotted for comparison in Figure 7. Focusing on mZVI, FeH14 was found to be the most reactive microscale iron among all other newly produced mZVIs. FeH3 and FeH4, which are both different size fractions of the same metal powder, had a similar reactivity. This observation suggests that there is no significant impact of particle size on iron efficiency in CAHs removal. Based on the data presented herein particle size and shape do not have a strong impact on observed mZVI reactivity. This was also suggested for nZVIs by another research group (Liu et al., 2005). Comparing the k_M values of the newly developed FeH14, FeH3 and FeH4 to the reactivity of the most reactive commercial microscale product (HQ), it is evidenced that these new irons have the similar or faster degradation rate for tested CAHs.

Calculated k_M values for PCE, TCE, cDCE and 1,1,1-TCA degradation by granular reference material (FeA4) and by mZVIs were similar. For Nanofer25s the k_M values were one to two orders of magnitude higher than the values for FeH14, FeH3, FeH4 and HQ. Nanofer25s is the most reactive among all studied iron based particles. FeS Aldrich gave kM values for PCE, TCE and 1,1,1-TCA similar to the k_M values of highly reactive mZVIs and FeA4 iron, but was the least reactive towards cDCE among all examined irons. After mass normalization, the reactivity of FeS BIO1 is one to two orders of magnitude lower than reference granular iron and similar to less reactive commercially available mZVIs (SM and MS200).

2.3.3. SURFACE AREA NORMALIZED KINETICS FOR IRON BASED MATERIALS

As reductive dehalogenation of CAHs by ZVI is a surface mediated process, the available ZVI surface is an important parameter. Several studies revealed that it is not just k_{obs} and k_M data that should be considered for examination of the zerovalent iron particles reactivity (Johnson et al., 1996; Scherer et al., 1998). Also specific surface area normalized data (k_{SA}) can serve as general descriptor of iron reactivity (Johnson et al., 1996; Miehr et al., 2004), especially due to the higher reactive surface area of nanoscale particles (4-25 m^2 g^{-1}) over microscale ones (0.1-4 m^2 g^{-1} for most of examined mZVIs).

k_{SA} data for all iron particles tested in this work are presented in Figure 8.

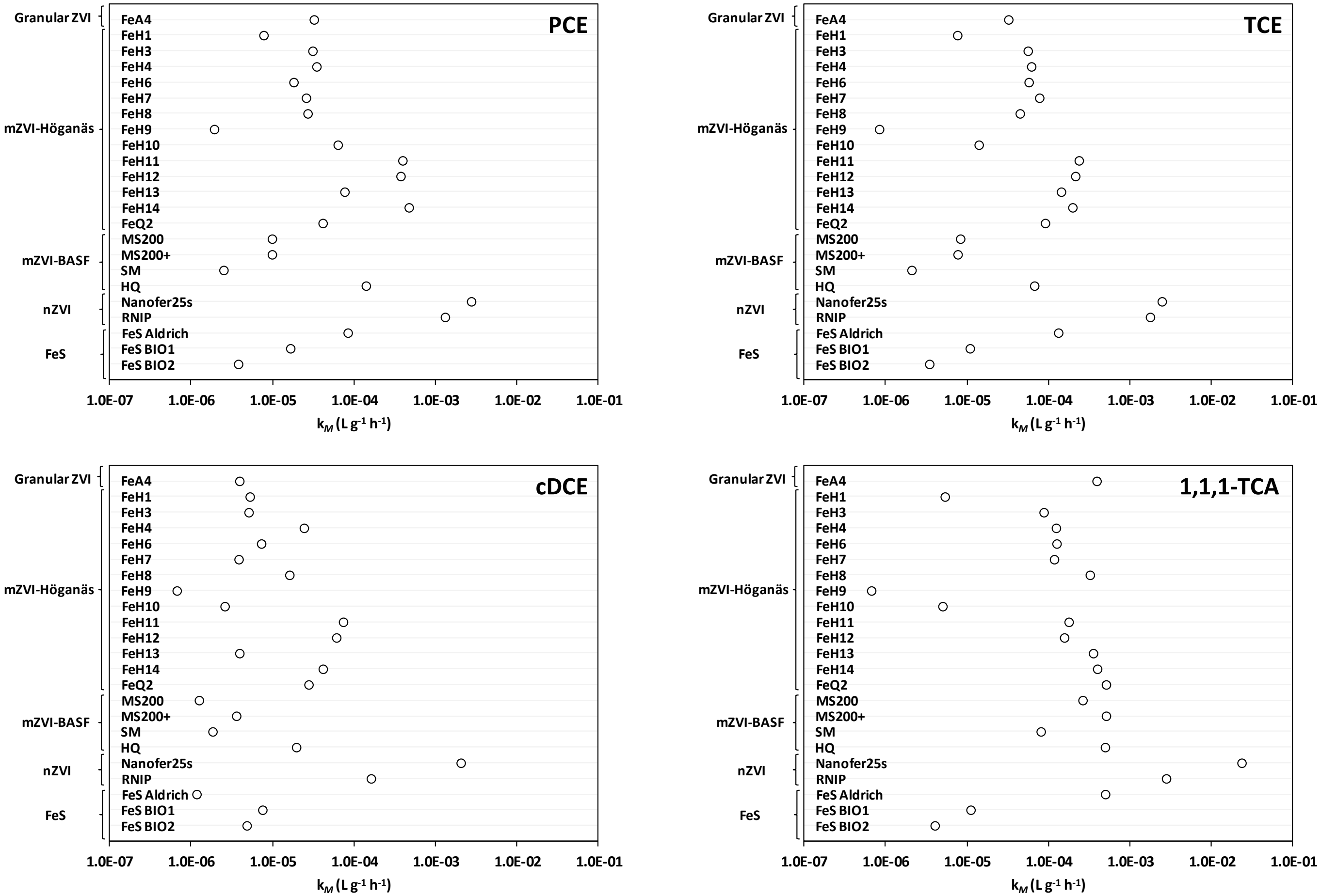

Figure 7 - Distribution of mass normalized rate constants for the reduction of PCE, TCE, cDCE and 1,1,1-TCA by different zerovalent iron particles and iron sulfides.

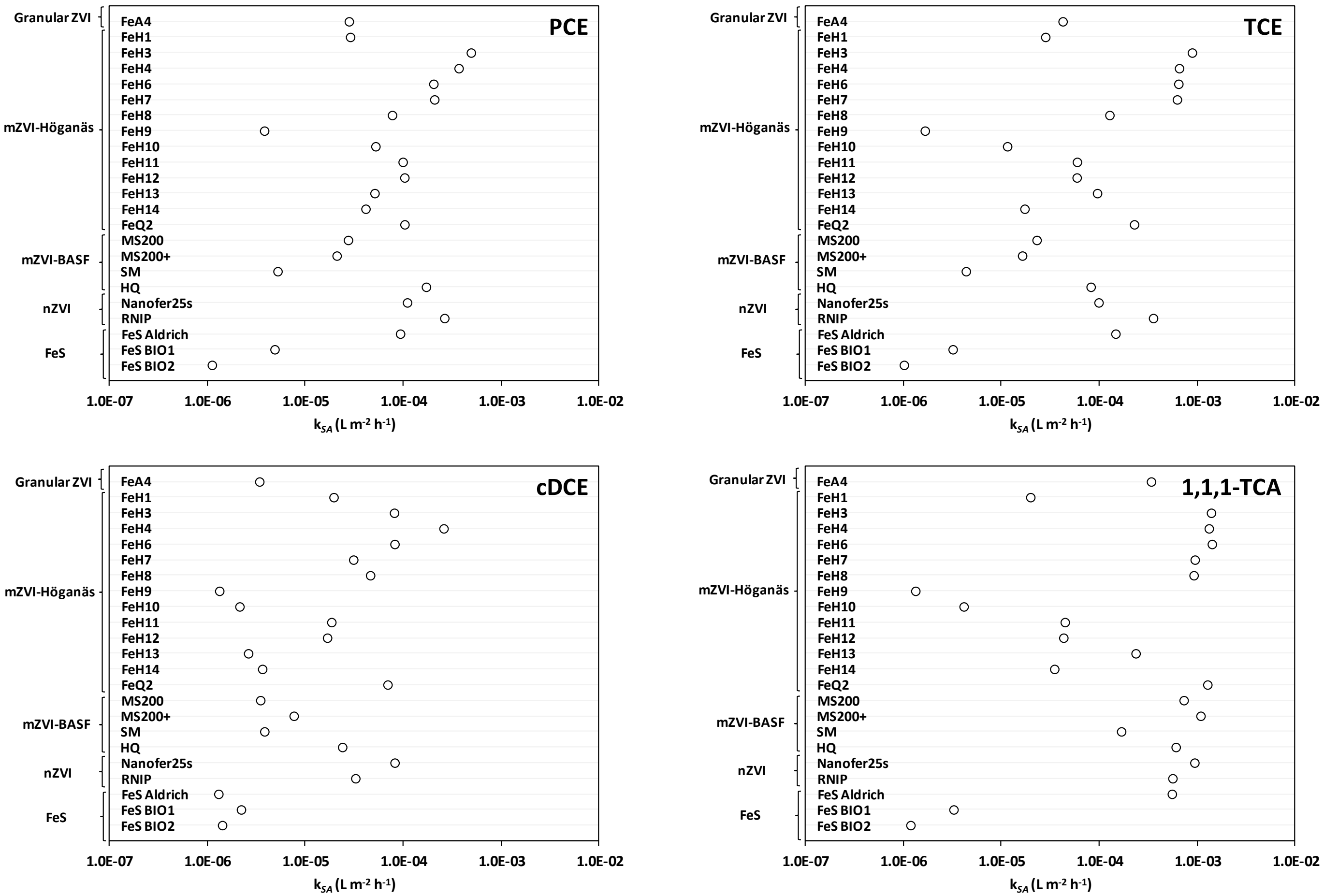

Figure 8 - Distribution of surface area normalized rate constants for the reduction of PCE, TCE, cDCE and 1,1,1-TCA by different iron particles and iron sulfides.

Figure 8 shows that differences in reactivity between iron particles are large (up to three orders of magnitude).

The obtained k_{SA} values for all tested mZVIs are similar or one to two orders of magnitude different than representative average literature k_{SA} values of 2.1 ± 2.7 x 10^{-3} L m^{-2} h^{-1} (PCE), 3.9 ± 3.6 x 10^{-4} L m^{-2} h^{-1} (TCE), 4.1 ± 1.7 x 10^{-5} L m^{-2} h^{-1} (cDCE) and 1.1 x 10^{-2} L m^{-2} h^{-1} (1,1,1-TCA) for commercial iron particles (Johnson et al., 1996). Based on k_{SA} data, FeH3 and FeH4 were the most reactive towards CAHs among other mZVIs. Interestingly, k_{SA} (PCE, TCE and cDCE) obtained with FeH3 and FeH4 were approximately 1 to 5 times higher than for Nanofer25s. The rate constants obtained for the granular reference material (FeA4) and commercially available mZVIs are in the same order of magnitude. The distribution of k_{SA} values shows that the reactivity of the commercially available FeS (Aldrich) and granular ZVI are in the same order of magnitude. Moreover, the k_{SA} values for biogenic iron sulfides are similar to the k_{SA} values of the least reactive mZVIs. This implies that biogenic iron sulfides are not highly reactive, but can contribute to slow reduction of CAHs in natural systems.

To investigate to what extent the reactivity of iron particles is impacted by specific surface area, the variability of k_M versus k_{SA} is summarized graphically in Figure 9. According to the presented data, k_M rates in general decrease with the decrease of k_{SA} indicating that the particle’s reactivity is dependent to a certain extent on specific surface area. However, looking more in detail at each pollutant separately, Figure 9 reveals that the change in k_M may also be due to other factors than surface area as evidenced by the scatter of the k_M values at a specific k_{SA} value for an individual substance. This is confirmed by the ANOVA analysis where probability of $p>0.4$ rejects the hypothesis that the reactivity of the iron particles is only impacted by the specific surface area. This is even more pronounced for the variability of k_M versus the specific surface area of iron based particles as can be seen in Figure 10.

Finally, presented data suggest that some newly designed microscale zerovalent iron particles, and especially FeH4, can be considered as promising particles for remediation of the studied CAHs. FeH4 was capable of removal of all pollutants, as well as slow degradation of intermediate product 1,1-dichloroethane (1,1-DCA) as shown in Figure 11.

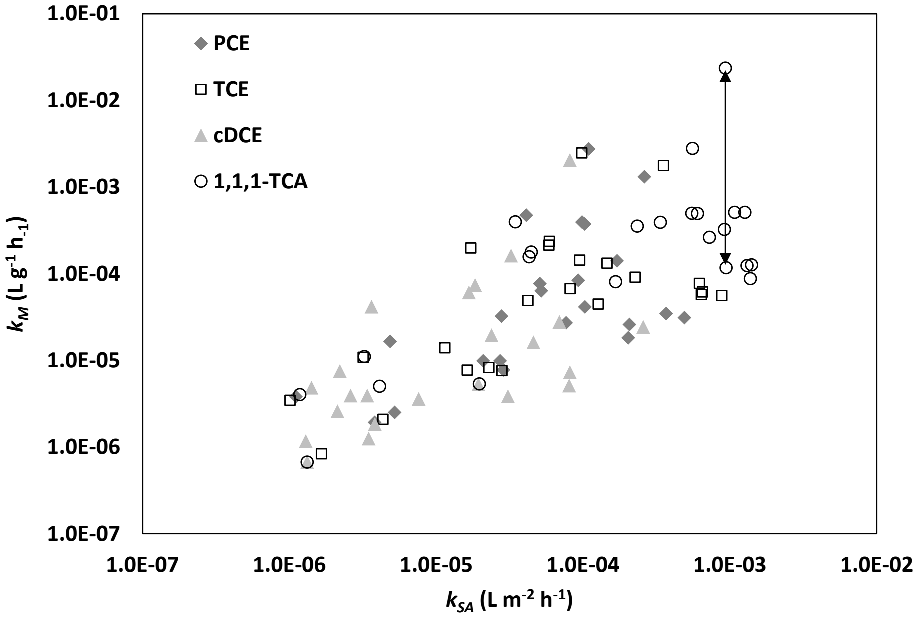

Figure 9 - Correlation between log k_M and log k_{SA} for the pollutants examined in the batch degradation study by different iron particles. Arrow in the vertical direction for a specific k_{SA} value indicates that other factors may influence k_M.

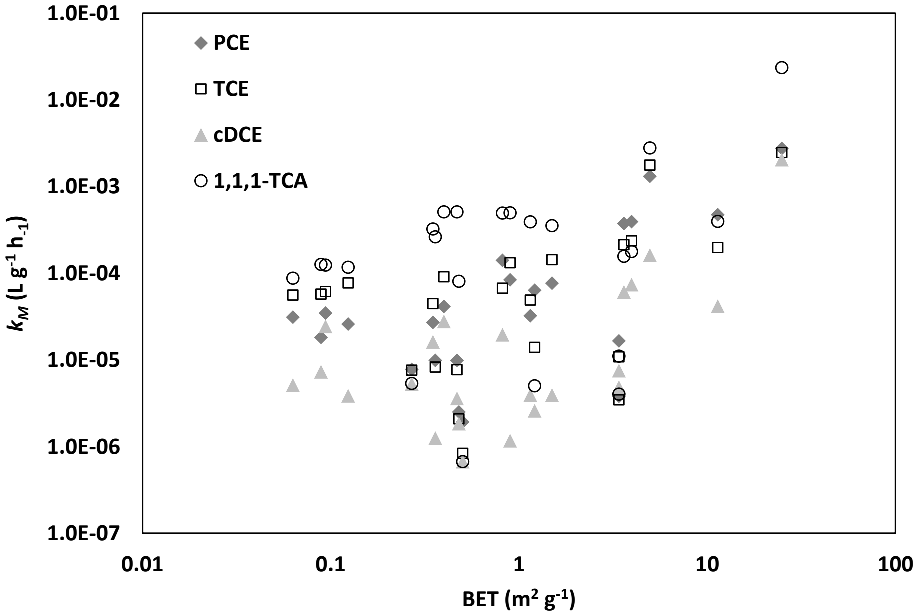

Figure 10 - Correlation between log k_M and log BET (the specific surface area of iron based particles) for the pollutants examined in the batch degradation study by different iron particles.

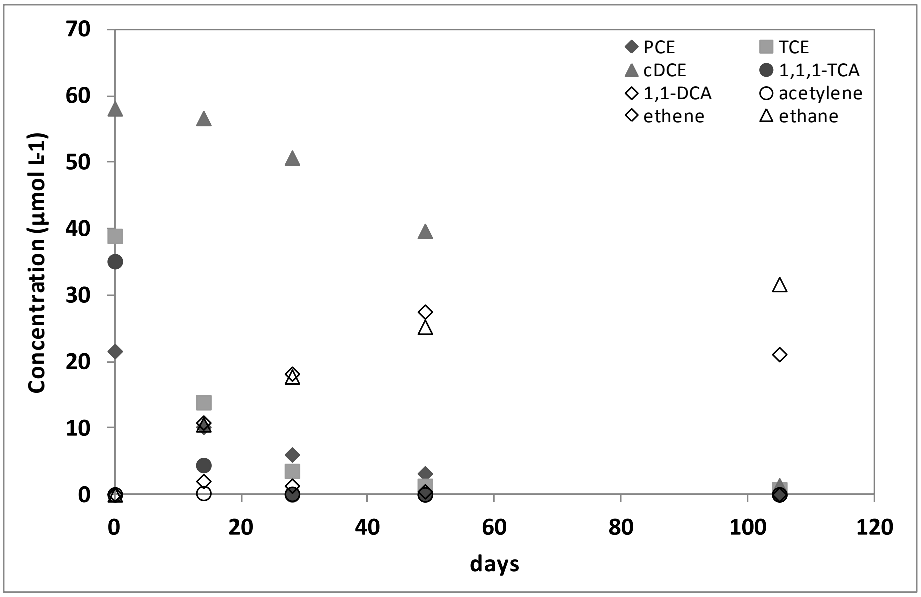

Figure 11 - Reduction of different CAHs by 50 g L-1 of FeH4 iron.

2.3.4. 1,1-DCA

1,1-DCA is a degradation product of 1,1,1-TCA that has been reported to be degradable by ZVI (Lookman et al., 2004; Song and Carraway, 2005). Degradation of this pollutant, however, is slow and a laboratory abiotic degradation half-life of 61 years has been reported (Jeffers, 1989). In this study, increased 1,1-DCA concentrations were observed for most tested iron based particles, but the maximal observed amount of 1,1-DCA produced during 1,1,1-TCA degradation was found to depend on the particles type (Table 5). The most pronounced production of 1,1-DCA was observed for FeA4, MS200, MS200+ and HQ (40-65%), while the lowest levels were measured for FeH1 and FeH9 (<0.4 %). In respect to 1,1-DCA degradation, the fastest degradation rates 2.4 x 10^{-3} h^{-1} and 1.2 x 10^{-3} h^{-1} were observed for FeH4 and Nanofer25s respectively.

An additional batch degradation experiment with 1,1,1-TCA as single pollutant was performed using FeH4 to examine 1,1,1-TCA degradation and 1,1-DCA formation/degradation more in detail. Approximately 70 % of the 1,1,1-TCA was found to be transformed to acetic acid by hydrolysis. The 1,1,1-TCA hydrolysis pathway has been reported before (McCarty, 1997). The remaining 28 percent obtained herein were transformed to ethane, while only 2 percent were transformed to 1,1-DCA by reductive dechlorination. The pronounced production of 1,1-DCA observed for several irons involved the *α*-elimination and hydrogenolysis pathway in degradation of 1,1,1-TCA. Chemical transformation of 1,1,1-TCA by these pathways has also been reported previously (Song and Carraway, 2005).

Table 9 : 1,1-DCA appearance after 1,1,1-TCA degradation with estimated 1,1-DCA degradation rates for studied iron based particles (values reported as a mean of triplicates) in the batch reactors.

		1,1-DCA	
Treatment	**(% produced)** [a]	**k_{ob} (h^{-1})**[b]	**R^2 (n)**[c]
FeA4 (50 g L^{-1})	40.7	7.5×10^{-5}	1.00 (2)
FeH1 (50 g L^{-1})	0.37	*	*
FeH3 (50 g L^{-1})	5.90	4.3×10^{-4}	0.99 (3)
FeH4 (50 g L^{-1})	5.71	2.4×10^{-3}	0.81 (3)
FeH6 (50 g L^{-1})	9.27	2.2×10^{-4}	0.96 (3)
FeH7 (50 g L^{-1})	8.73	2.7×10^{-4}	0.93 (3)
FeH8 (50 g L^{-1})	25.1	2.5×10^{-4}	0.93 (3)
FeH9 (50 g L^{-1})	0.19	*	*
FeH10 (50 g L^{-1})	1.87	*	*
FeH11 (50 g L^{-1})	1.38	*	*
FeH12 (50 g L^{-1})	2.26	*	*
FeH13 (50 g L^{-1})	26.9	2.2×10^{-4}	1.00 (2)
FeH14 (50 g L^{-1})	4.00	5.7×10^{-4}	0.98 (4)
FeQ2 (50 g L^{-1})	25.9	3.4×10^{-4}	0.87 (4)
MS200 (50 g L^{-1})	65.8	*	*
MS200+ (50 g L^{-1})	65.2	8.8×10^{-4}	0.99 (4)
SM (50 g L^{-1})	20.0	2.0×10^{-4}	1.00 (2)
HQ (50 g L^{-1})	42.4	2.3×10^{-4}	0.91 (4)
Nanofer25s (5 g L^{-1})	18.6	1.2×10^{-3}	0.99 (4)
RNIP (5 g L^{-1})	6.29	*	*
FeS Aldrich (50 g L^{-1})	26.1	4.0×10^{-4}	0.08 (4)
FeS BIO1 (40 g L^{-1})	3.25	*	*
FeS BIO2 (40 g L^{-1})	3.11	*	*

2.4. CONCLUSION

Reactivity data were collected for 23 reactive iron based particles via standardized test procedure allowing reactivity comparison between the different materials towards different pollutants within a reasonable amount of time. The reactivity of the particles was compared based on k_{obs} and k_M data, as well as k_{SA} values. As an appropriate descriptor of the overall surface reactivity of the particles and contaminants degradation kinetics, k_{SA} data were used for the selection of the most promising iron for in situ application.

The obtained k_{SA} values show that the microscale iron particles FeH3 and FeH4 perform mostly better than Nanofer25s and commercially available mZVIs. The k_{SA} values of commercial FeS were similar to that of the granular ZVI material selected as a reference material. The reactivity of commercial FeS and granular ZVI towards 1,1,1-TCA was in the same order of magnitude as Nanofer25s and some mZVIs. On the other hand, their PCE, TCE and cDCE degradation kinetics were one to two orders of magnitude slower than Nanofer25s and some mZVIs. This study also suggests that biogenic iron sulfides may contribute to the reductive degradation of mainly 1,1,1-TCA, although they were the least reactive among all studied irons. No correlation was found between reactivity of the examined particles and particle size or pH. Except for pH increase to approximately 11 where particles were found non-reactive. In general, significantly reduced ORP values were found good indicators for reactive particles.

The large data set resulting from this study, shows that some of the newly designed mZVI particles introduced in this study have promising reactive properties for in-situ remediation applications, also towards 1,1-DCA. These particles are relatively low-cost and easy to handle compared to nZVIs.

CHAPTER 3 IMPACT OF CARBON, OXYGEN AND SULFUR CONTENT OF MICROSCALE ZEROVALENT IRON PARTICLES ON ITS REACTIVITY TOWARDS CHLORINATED ALIPHATIC HYDROCARBONS

Based on: Velimirovic, M., Larsson, P.-O., Simons, Q., Bastiaens, L. Impact of carbon, oxygen and sulfur content of microscale zerovalent iron particles on its reactivity towards chlorinated aliphatic hydrocarbons. Submitted to Chemosphere.

3.1. INTRODUCTION

To select cost effective ZVI particles for the cleanup of CAHs contaminated sites, the reactivity of particles is considered crucial for the success of the remediation. Over time, ZVI particles with different properties and from different origin have been studied extensively (Barnes et al., 2010; Cheng and Wu, 2000; Johnson et al., 1996; Su and Puls, 1999). The high specific surface area of the ZVI particles has been identified as an important feature that contributes to the fast degradation of CAHs (Zhang, 2003). However, there are indications that other characteristics of the ZVI particles, such as the source, quality and content of impurities, influence the reactivity as well (Barnes et al., 2010; Burris et al., 1998; Johnson et al., 1996; Song and Carraway, 2005; Su and Puls, 1999; Wüst et al., 1999). For ZVIs produced from different raw materials, the reaction rates may differ up to three orders of magnitude (Cheng and Wu, 2000).

Some studies even emphasized that iron reactivity is more influenced by impurities than by the specific surface area of the ZVI (Cheng and Wu, 2000; Su and Puls, 1999). Impurities in the ZVI particles can either stimulate or inhibit CAHs degradation, or alter the degradation mechanism (Cheng and Wu, 2000; Su and Puls, 1999). To further enhance the degradation of CAHs by primarily nanoscale zerovalent iron (nZVI) particles, the alloying of particles with a noble metal (e.g. Cu, Ni, Pt, Pd or Ag) has been reported (Barnes et al., 2010; Cheng and Wu, 2000; Schrick et al., 2002; Zhang et al., 1998). The presence of the second metal that acts as a catalyst highly increases the reactivity of nZVIs (Barnes et al., 2010; Schrick et al., 2002; Zhang et al., 1998). Higher reactivity of nZVIs was also observed in the presence of sulfate (Moore et al., 2011).

The degradation of CAHs may further depend on high content of carbon and oxygen impurities by inhibiting iron reactivity and inducing sorption (Burris et al., 1998). The subsequently reduced iron reactivity has been associated with thin oxide coatings on the iron surface (Uludag-Demirer and Bowers, 2003; Wang and Zhang, 1997). On the other hand, significant non-reactive sorption of several CAHs on iron surface has been linked to the carbon impurities (Burris et al., 1995, 1998; Deng et al., 1999; Dries et al., 2004; Sherer et al., 1997). Besides, Jung and Lo (2005) reported that sorption of trichloroethene was proportionally associated with the carbon fraction on the surface of cast iron.

In chapter 2, more than 20 different iron particles reactivity data were collected using a standardized test procedure. Among the tested materials were a set of newly designed microscale zerovalent iron (mZVI) particles. Although the reactivity of ZVI is often only related to specific surface area, in this chapter the relevance of mZVI chemical composition in determining its reactivity (particularly carbon, oxygen and sulfur content) was studied.

Finally, this study determines the optimal composition of mZVI particles for efficient remediation of CAHs.

3.2. MATERIALS AND METHODS

3.2.1. MICROSCALE ZEROVALENT IRON PARTICLES

The newly developed mZVI particles supplied by Höganäs (Sweden) reported in Table 5 were studied more in detail in this chapter. Elemental analyses of carbon and sulfur were analyzed by combustion analysis with a CS-400 LECO. Elemental analyses of oxygen and nitrogen was analyzed by an inert gas fusion principle with a TC-436 LECO. The accuracy of analyses was +/- 0.01%. Further, the specific surface area has been analyzed by single point measurement with a Micromeritics Flowsorb II instrument according to the BET method (Brunauer-Emmett-Teller method) using adsorption of N_2 at the temperature of liquid N_2. All samples were degassed at 110°C for 30 minutes before analysis.

3.2.2. BATCH EXPERIMENTS

Reactivity tests were performed under consistent experimental conditions as described in Chapter 2.2.3. First order disappearance rate constants (k_{obs}, h^{-1}), and surface area normalized rate constants (k_{SA}, L m^{-2} h^{-1}) are input from Chapter 2.

3.3. RESULTS AND DISCUSSION

An overview of the mZVI particles considered in Table 10 the previously reported screening tests is given in along with their characterization and bulk content of C, O, S and N in the iron particles. Höganäs (Sweden) produced mZVI particles in a similar way with different particle sizes, different specific surface areas and different surface compositions. In this study, the reactivity of these particles towards a selection of CAHs, was correlated with the specific surface area of the iron particles, as well as their carbon, oxygen and sulfur content.

Table 10 : Characterization data of tested ZVI.

Iron name	Carbon content (wt%)[a]	Oxygen content (wt%)	Sulfur content (wt%)	Nitrogen content (wt%)
FeH1	0.01	1.48	0.00	0.00
FeH3	0.00	0.08	0.01	0.00
FeH4	0.00	0.09	0.01	0.00
FeH6	0.00	0.41	0.01	0.00
FeH7	0.00	0.43	0.83	0.00
FeH8	0.01	0.63	0.00	0.00
FeH9	0.03	1.38	0.00	0.00
FeH10	0.07	0.81	0.01	0.00
FeH11	0.74	0.97	0.01	0.01
FeH12	0.61	0.86	0.01	0.01
FeH13	0.12	1.07	1.10	0.00
FeH14	1.40	1.55	0.00	0.00
FeH17*	0.01	1.04	0.00	0.00

[a]The bulk concentration of C, O, S and N in the iron powder.
*New produced Höganäs mZVI particles.

3.3.1. EFFECT OF SURFACE AREA ON CAHS DEGRADATION IN BATCH MZVI SYSTEMS

For the mZVI particles, previously reported first order disappearance rate constants (Table 7) were correlated with the specific surface area of the particles (Figure 12). The highest surface area was observed for FeH14 iron (11.4 m^2 g^{-1}), which also showed the fastest disappearance rate for PCE and 1,1,1-TCA. Prior studies have also noted that the higher surface area results in a faster degradation of contaminants (Li et al., 2006; Lien and Zhang, 2001; Wang and Zhang, 1997). On the other hand, particles with the lowest specific surface area (FeH3, FeH4, FeH6 and FeH7), ranging from 0.04-0.12 m^2 g^{-1}, show similar disappearance rates for PCE, TCE and 1,1,1-TCA, which were up to one order of magnitude lower than the rates calculated for particles with higher specific surface areas. FeH11 and FeH12 irons have relatively high specific surface areas, 3.98 and 3.62 m^2 g^{-1} respectively, but showed mainly CAHs-removal via sorption as previously reported in Chapter 2. FeH1 and FeH9 irons showed limited or no reactivity despite 4-10 times higher surface area than FeH3, FeH4, FeH6 and FeH7 irons.

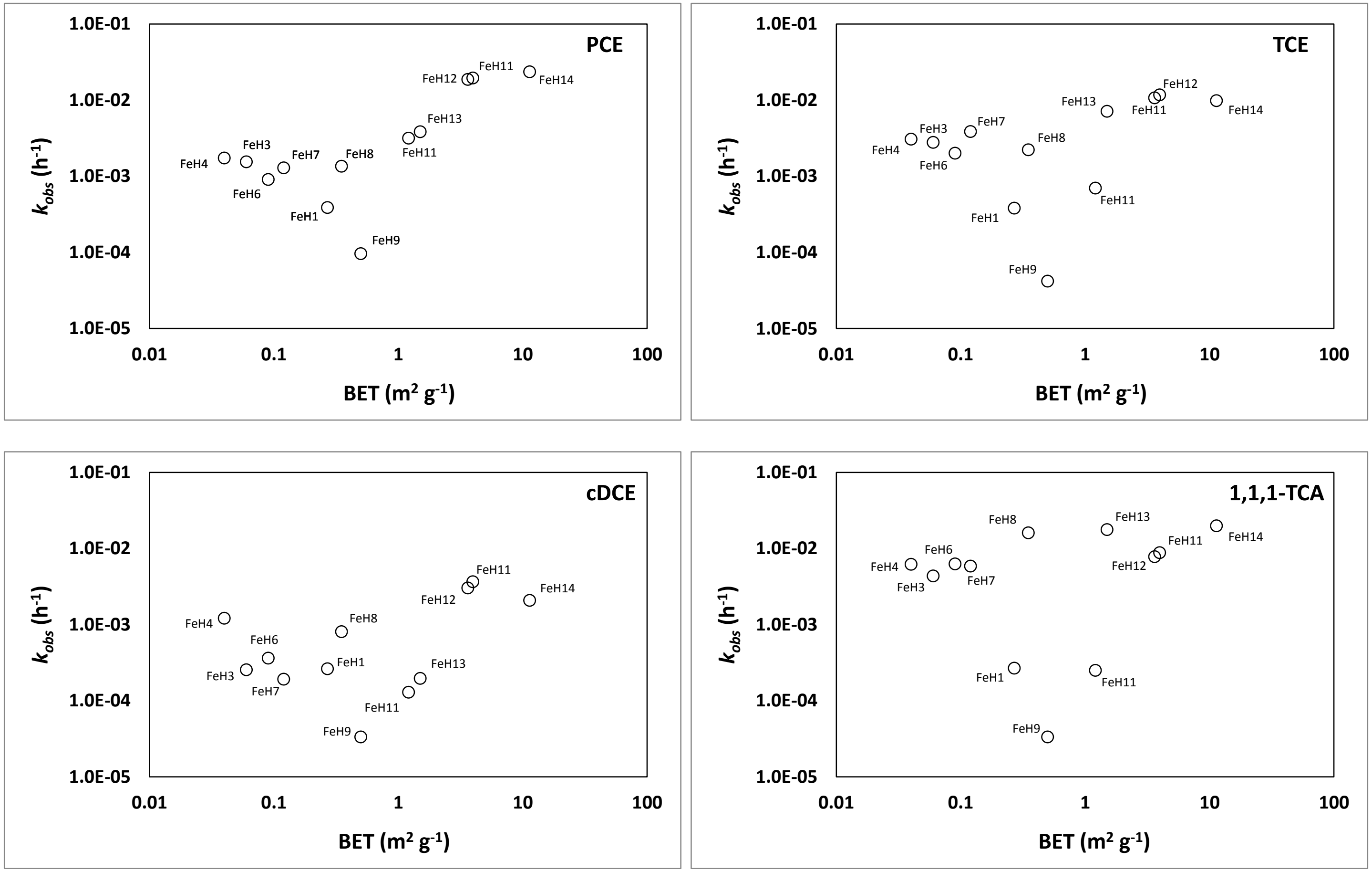

Figure 12 - Distribution of first order disappearance rate constants (k_{obs}) for PCE, TCE, cDCE and 1,1,1-TCA by different mZVIs with different specific surface areas (m^2 g^{-1}).

The presented data show that there is no particular correlation between disappearance rate constants and specific surface area. Earlier, a linear correlation between granular ZVI reactivity and specific surface area of the ZVI has been reported (Gillham and O’Hannesin, 1994; Su and Puls, 1999). Our study is in agreement with Johnson’s et al. (1996) findings, which showed that this correlation is not valid in general. Moreover, data presented in our study clearly imply that other factors may have had an impact on determining ZVI reactivity towards CAHs. These other factors may comprise ZVI impurity or morphology of the ZVI particles. A correlation between the high reactivity of the iron particles and the size of the ZVIs has not been observed (Chapter 2).

3.3.2. EFFECT OF CARBON CONTENT ON CAHS SORPTION IN BATCH MZVI SYSTEMS

The carbon content has been associated with removal of CAHs via sorption (Jung and Lo, 2005). To discriminate sorption from degradation, previously reported mass recoveries for the considered mZVIs were used (Table 6). Comparison of the mass recoveries with the carbon content on the surface of the mZVI particles (Figure 13) revealed that a higher carbon content of mZVI particles increases the probability for sorption of the contaminants on the particles and reduces the effective degradation of CAHs.

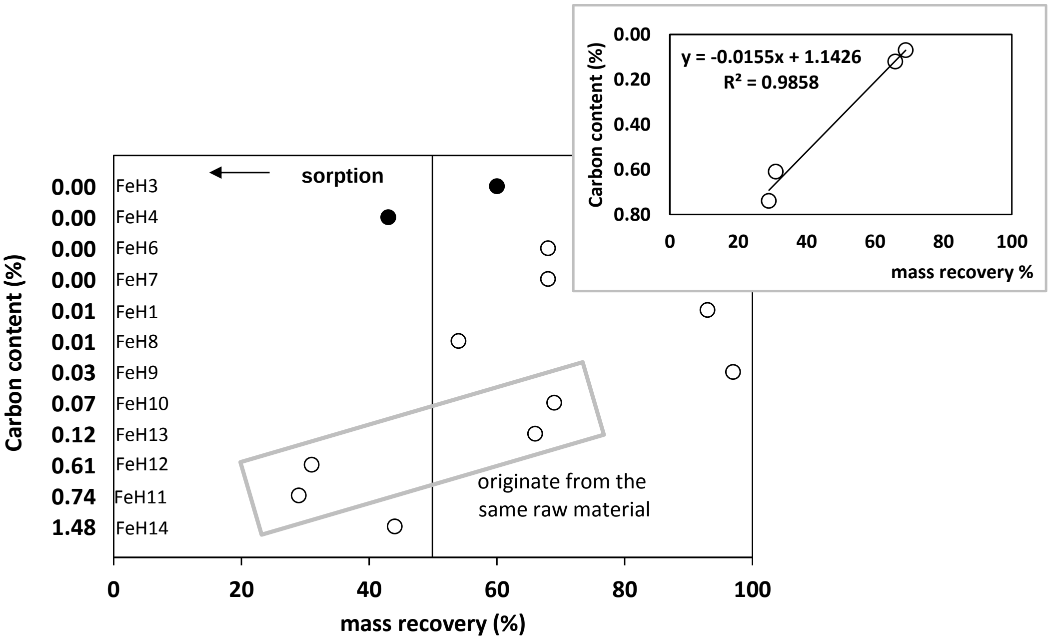

Figure 13 - Comparison of mass recovery (%) and carbon content (%) illustrating that sorption characteristic of the iron are dependent on the carbon content (particles originated from the same raw material). Low mass recovery was also observed for highly reactive mZVIs (•) with high production of ethene and ethane. This is explained by the loss of volatile reactants and degradation products during the sampling process.

This has been concluded from the data found for FeH10, FeH11, FeH12 and Fe13, which all originate from the same raw material and have been processed in a similar way, but differ in carbon content. FeH10 and FeH13 are produced with very low carbon content (0.07-0.12 %), while FeH11 and FeH12 have a 6 to 8 times higher carbon content (0.6-0.75 %). From the k_{obs} data (Table 7) it is evident that all irons have similar CAHs disappearance rate constants. However, a mass recovery of only 29 and 31 % for FeH11 and FeH12, respectively, indicated that the major part of the CAHs is removed by sorption. Further, FeH14 iron contained the highest carbon content (1.4 %), and a mass recovery of 44 % was reported, which points towards significant removal of CAHs by sorption onto the mZVI. The highest carbon content is dedicated to amorphous C that was added after heat treatment at the end of the FeH14 production process. The present findings show that sorption capacity has been increased by carbon content higher than 0.5 %. This carbon content of the iron particles is even lower than the 3 % previously reported for the cast irons (Deng et al., 1997). These results are consistent with previously reported sorption behavior of ZVI particles (Burris et al., 1995, 1998) and suggest that carbon content is very important for CAHs-removal mechanism.

Finally, a strong positive correlation was observed between the specific surface area and the carbon content (Figure 14).

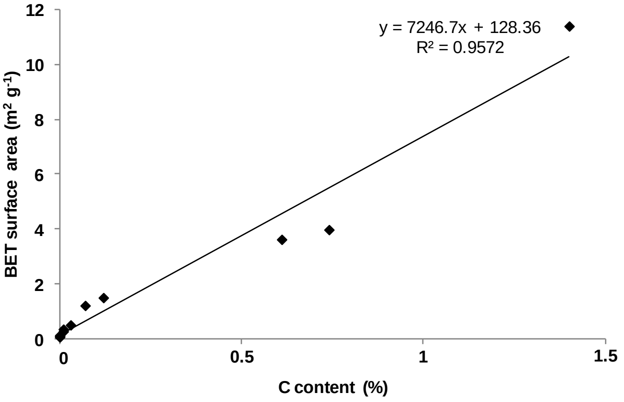

Figure 14 - Effect of carbon content (%) on measured specific surface areas (BET, m^2 g^{-1}) of the mZVIs.

It is evident that greater carbon mass of the iron particles corresponds to a higher surface area of the iron what is consistent with earlier observations by Jung and Lo (2005). Therefore, the carbon content can be an indicator in determining the surface area of iron particles and consequently present a more profound source of variability in further generalization of kinetic models published up to date.

3.3.3. EFFECT OF OXYGEN CONTENT ON CAHS DEGRADATION IN BATCH MZVI SYSTEMS

To investigate the effect of oxygen content of the mZVI particles on its reactivity towards different CAHs, the oxygen content (% O) of the examined mZVIs was compared with the k_{obs} data for PCE, TCE, cDCE and 1,1,1-TCA obtained from a Chapter 2 (Figure 15). To our knowledge, this is the first reported study where the reactivity of mZVI particles with different oxygen content (ranging between 0.08-1.55 %) has been evaluated. The most pronounced effect of oxygen content on mZVI particles reactivity was observed for FeH1 and FeH9. Reactivity of these particles is negatively affected by the high oxygen content (1.48 and 1.38 % O for FeH1 and FeH9 respectively). On the other hand, particles containing the lowest amount of oxygen FeH3 (0.08 % O) and FeH4 (0.09 % O) were the most reactive particles with no sorption properties among other examined irons. The difference in reactivity between iron containing no oxides and passivating oxide content could vary by up to two to four orders of magnitude. The exception is FeH14, where the high CAHs removal rate is significantly influenced by the sorption. This observation is explicable by the high carbon content (1.40 % C). Summarizing the data presented in Figure 15, a faster degradation rate of examined CAHs by approximately 40 % of mZVIs can be attributed to the lower oxygen content of the iron particles with no additional impact of carbon. A negative influence of oxide layers on ZVI has been reported before (Wang and Zhang, 1997). Further, the distribution of the oxide on the ZVI particles was shown to affect the reactivity (Agrawal and Tratnyek, 1996; Miehr et al., 2004).

Our study, in addition, led to a clear trend between the oxygen content ranging between 0.08 and 1 % in the iron particles and surface area normalized disappearance rates (Figure 16). To evaluate the effect of oxygen content on surface area normalized disappearance rates, one way analysis of variance (ANOVA) was performed. Results indicate that a high oxygen content is generally linked to lower disappearance rate constants (p-value below 0.01). Already an initial oxygen content of the mZVI particles of approximately 1 %, influence the reactivity. Finally, oxygen content higher than 1 % reduced the CAHs surface normalized disappearance rates significantly.

To increase the reactivity of ZVIs it is an option to remove the surface oxides from the iron powders in a pretreatment step before they are used in remediation applications (Wang and Zhang, 1997). Pretreatment methods such as acid-washing (Matheson and Tratnyek, 1994; Su and Puls, 1999) or H_2-reducing process (Lin and Lo, 2005) have been previously used.

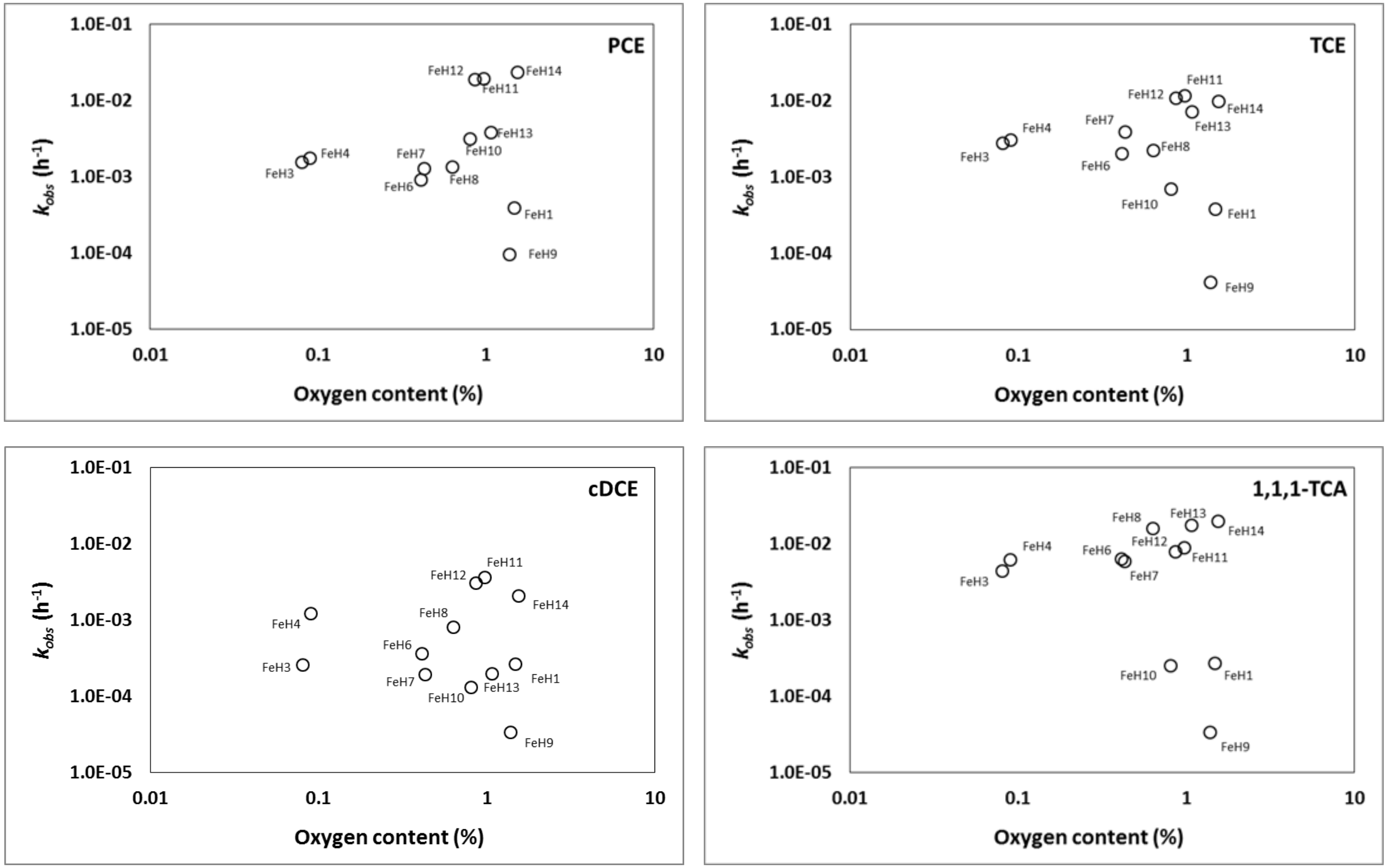

Figure 15 - Comparison of first order rate constants (k_{obs}) data for PCE, TCE, cDCE and 1,1,1-TCA obtained from previously reported batch study (Velimirovic et al., 2013) and oxygen content (% O) of examined mZVIs.

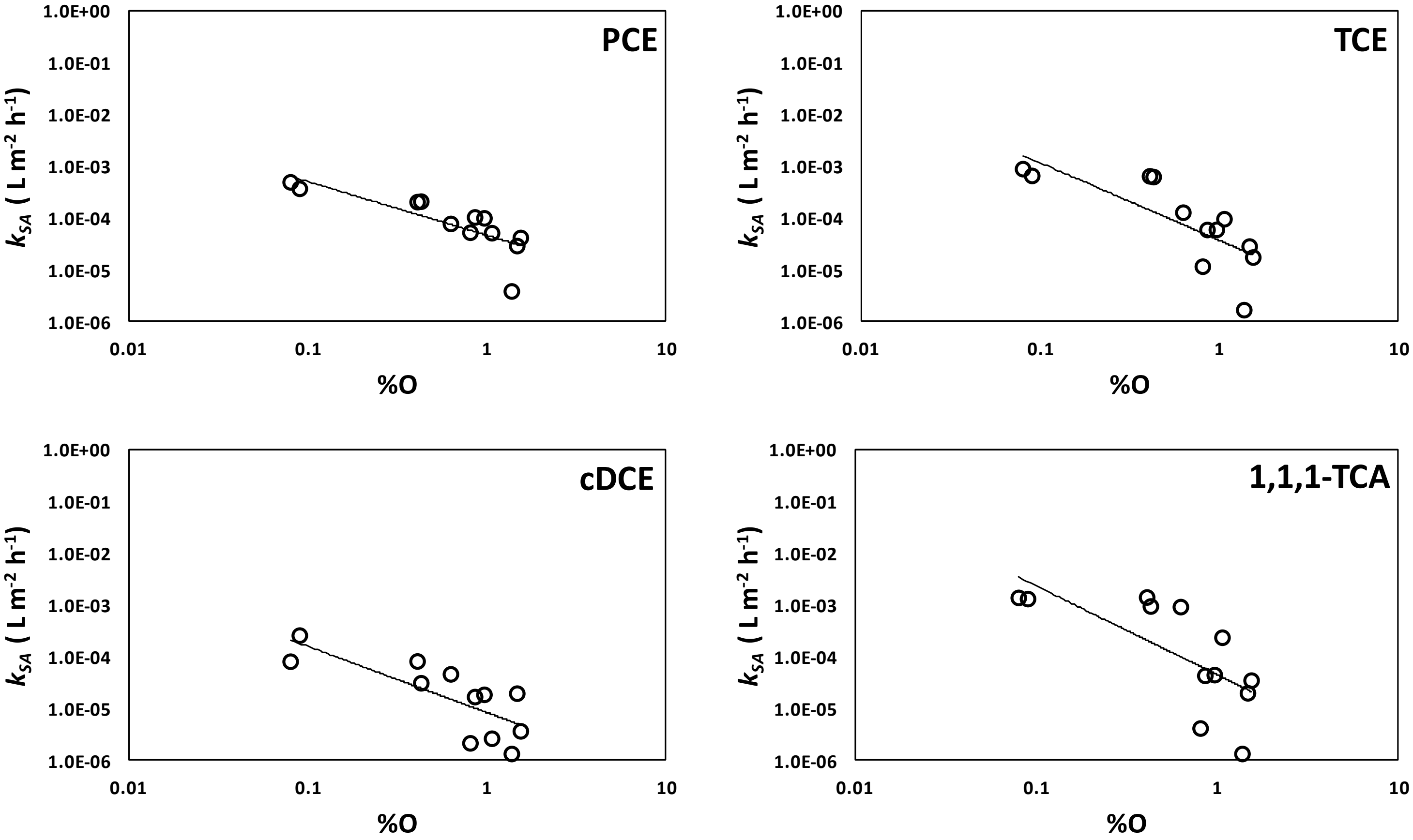

Figure 16 - Surface area normalized rate constants for the reduction of PCE, TCE, cDCE and 1,1,1-TCA plotted as a function of oxygen (% O) content.

In our study, more efficient H_2-reducing process was used to significantly reduce the amount of surface oxides which resulted in new particles (called FeH17) with approximately 1.4 times lower oxygen content (decrease from 1.48 % to 1.04 %) and 2 to 6 times higher removal rates of PCE and TCE for FeH1 and FeH9 (Figure 17). However, the resulting amount of oxygen content (1.04 %) is still higher than is acceptable for efficient reduction of CAHs.

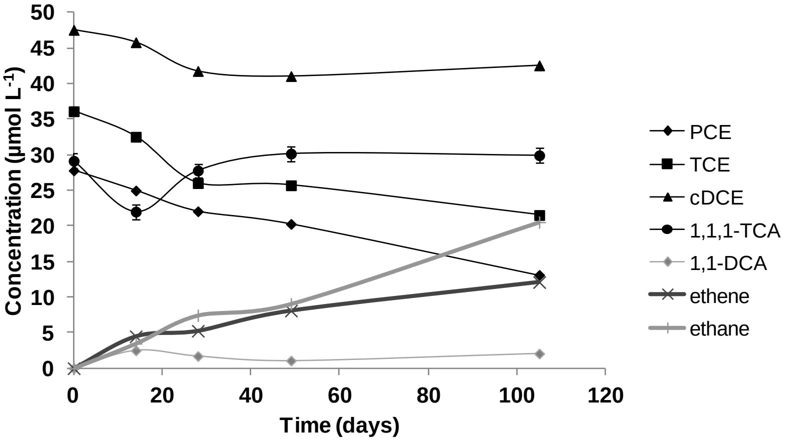

Figure 17 - Reduction of different CAHs by 50 g L^{-1} of FeH17 iron.

3.3.4. EFFECT OF SULFUR CONTENT ON CAHS DEGRADATION IN BATCH MZVI SYSTEMS

A positive impact of the sulfur content on the reactivity of ZVI particles has been reported (Butler and Hayes, 2001; Hassan, 2000). Our data do confirm this correlation to some extent, especially for TCE and 1,1,1-TCA. For instance, despite higher oxygen content, FeH13 (1.10 % S) is more reactive iron than FeH10 (0.01 % S). This observation can be explained by the fact that FeH13 has been modified with sulfur (100 times higher sulfur content than for FeH10) instead of carbon. Comparison of these two mZVIs shows that sulfur in some cases can alter particles degradation behavior.

When comparing FeH6 (0.01 % S) and FeH7 (0.83 % S), that have both been produced in a similar way and from the same raw material, the higher sulfur content did not significantly improve the iron reactivity towards selected CAHs. According to the presented data, the effect of sulfur content on iron reactivity is less pronounced than it was observed for the oxygen and carbon content.

3.3.5. COMBINED EFFECT OF CARBON, OXYGEN AND SULFUR ON CAHS DEGRADATION IN BATCH MZVI SYSTEMS

By varying simultaneously the carbon, oxygen and sulfur content of mZVI particles, a combined effect of iron particles composition on different CAHs degradation can be obtained. This is illustrated with PCE as an example in Figure 18.

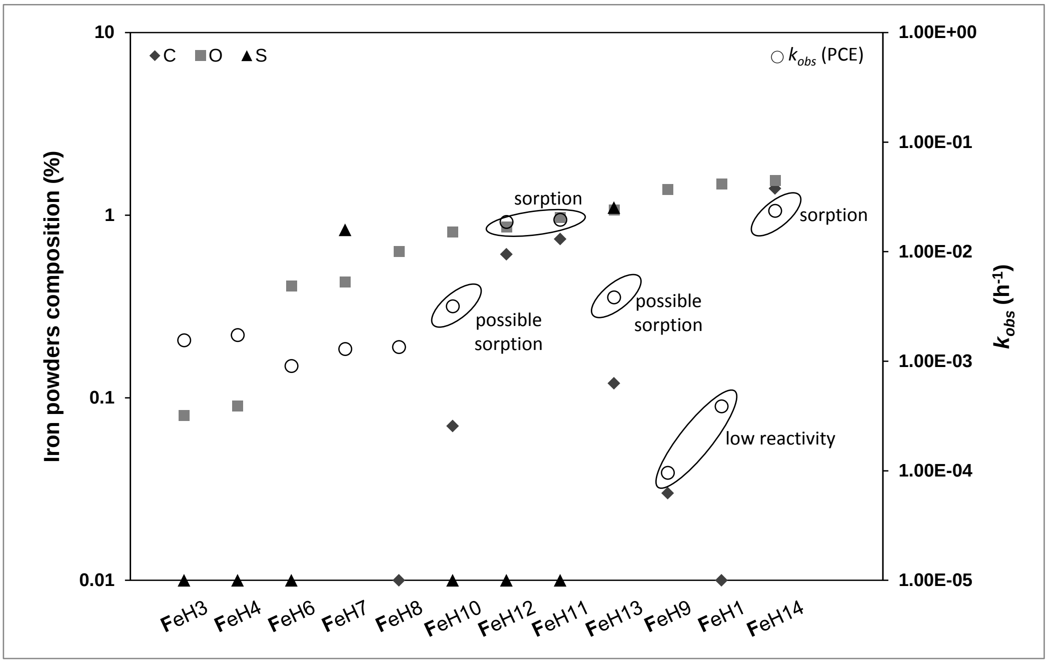

Figure 18 - Effect of iron surface composition (%) on disappearance rate of PCE (h^{-1}) by different mZVIs.

Despite having the lowest specific surface area, it is evident that FeH3 and FeH4 irons obtained a high disappearance rate of PCE as a consequence of low amounts of oxygen and carbon. In contrast, the high disappearance rate of PCE for particles with oxygen content higher than 1 % is explicable by a carbon content higher than 0.5 % and consequently by sorption of PCE (FeH11, FeH12 and FeH14). A small difference between FeH11 and FeH13 in the disappearance rate of PCE was observed. However mass balance data contributed to distinguishing between the reactivity of FeH13 and sorption properties of FeH11. As presented, the higher carbon content will negatively affect iron reactivity towards PCE and alter the removal mechanism promoting the sorption properties of the iron particles. A similar pattern was obtained for other CAHs (Figure 19).

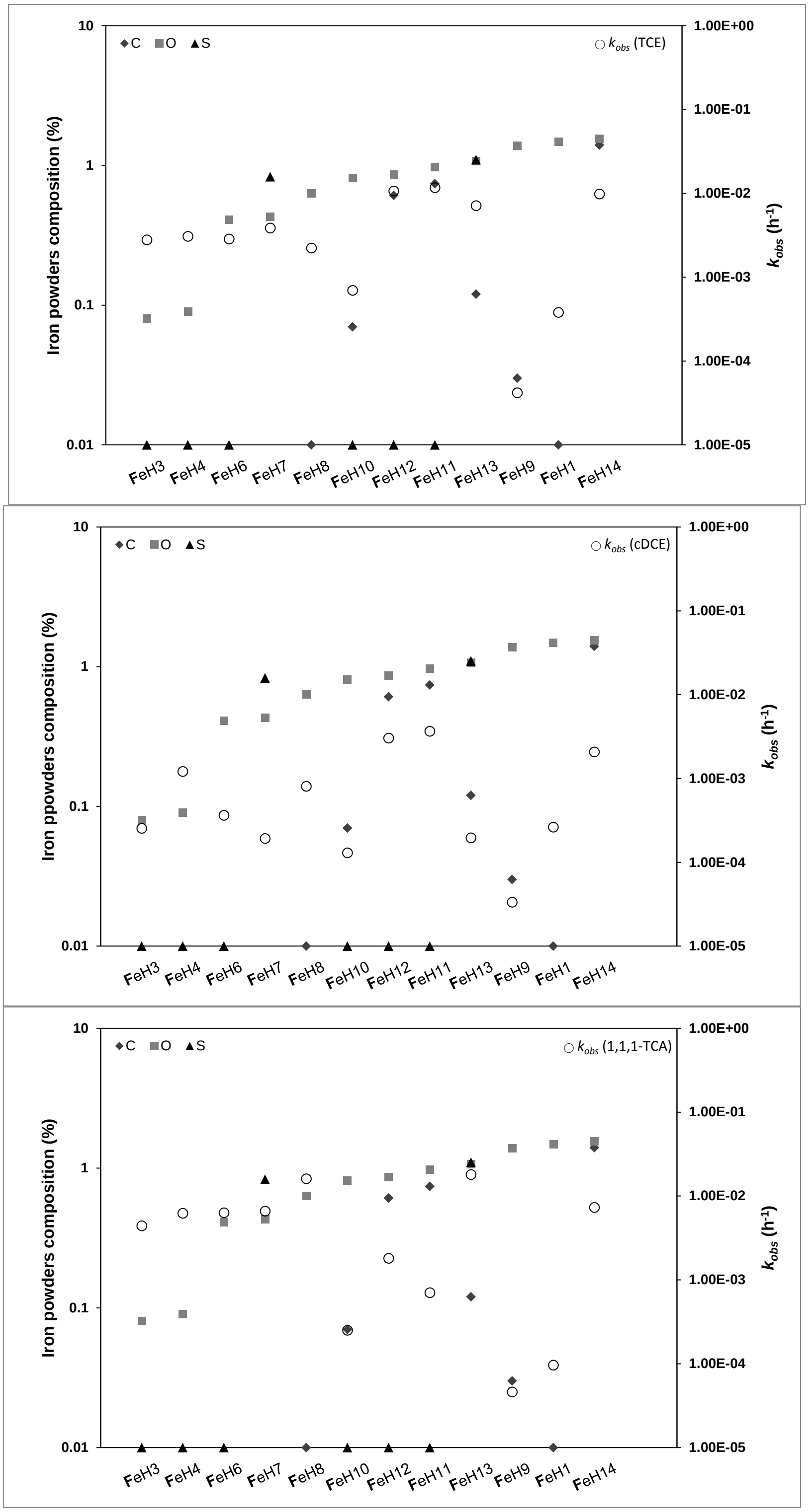

Figure 19 - Effect of iron surface composition on disappearance rate of TCE, cDCE and 1,1,1-TCA by different mZVIs.

Elemental analysis has been performed for FeH4 and FeH9 iron to investigate whether more noble metals have an influence on the reactivity of mZVI particles (Table 11).

Table 11 : Trace elements analysis for FeH4 and FeH9 iron.

Element name	FeH4 (elemental wt%)	FeH9 (elemental wt%)
Co	0.01	0.00
Cr	0.03	0.08
Cu	0.03	0.02
Mn	0.09	0.64
Mo	0.01	0.01
Ni	0.03	0.03
Sb	0.00	0.00
Si	0.01	0.15
V	0.00	0.01
Zn	0.00	0.00

FeH4 iron has been selected as an iron with high reactivity and no carbon content, while FeH9 has no or limited reactivity. In comparison to FeH4 iron, besides high oxygen, higher content of trace metals, particularly Mn (0.64 %) and Si (0.15 %) was observed for FeH9. This finding suggests that FeH4 reactivity towards CAHs was not due to the alloying of mZVI particles with noble metals that could serve as a catalyst while iron serves as an electron donor, but is more likely due to the low amount of oxygen and carbon. More detailed investigation is required to clarify the composition of the mZVI particles as an important parameter for iron reactivity.

3.4. CONCLUSION

This study shows that the composition of iron particles impacts the CAHs removal. Correlations between the reactivity data and the composition (C, O and S content) of the different tested mZVI particles indicate that:

- Sorption characteristics of iron particles are controlled by the carbon content. Carbon content higher than 0.5 % increases the sorption capacity of mZVIs.
- The carbon content can be an indicator of the surface area of mZVI particles and an important input for further development of kinetic models to describe sorption characteristics of the mZVI particles.
- The reactivity of iron particles decreases with the oxygen content in the mZVIs.
- When aiming at maximum degradation rates, the carbon and oxygen content shall not exceed 0.5 % and 1 % respectively.

- The effect of the sulfur content on reactivity of mZVI particles is less pronounced than that of carbon and oxygen.

The ability to predict the reactivity of mZVI via its composition is valuable when designing and optimizing reactive mZVI particles.

CHAPTER 4 CORROSION RATE ESTIMATIONS OF MICROSCALE ZEROVALENT IRON PARTICLES VIA DIRECT HYDROGEN PRODUCTION MEASUREMENTS

Based on: Velimirovic, M., Carniato, L., Simons, Q., Schoups, G., Seuntjens, P., Bastiaens, L. Corrosion rate estimations of microscale zerovalent iron particles via direct hydrogen production measurements. In preparation for Science of the Total Environment.

4.1. INTRODUCTION

Reductive dechlorination of chlorinated aliphatic hydrocarbons (CAHs) with zerovalent iron (ZVI) particles has been shown as the most promising technique for in-situ remediation of contaminated groundwater (Gillham and O'Hannesin, 1992, 1994; Matheson and Tratnyek, 1994). The long-term performance of ZVI remedial systems and consequently site cleanup time depends on the continued effectiveness of the iron surface to serve as an electron donor in reducing CAHs (Farrell et al., 2000). Under anaerobic conditions, ZVI mainly corrodes by the oxidative action of groundwater where one mole of hydrogen gas is generated for every mol of iron corroded (Reardon, 1995, 2005):

$$Fe^0 + H_2O \rightarrow Fe^{2+} + 2OH^- + H_2 \qquad (12).$$

As a consequence of the possible conversion of $Fe(OH)_2$ to Fe_3O_4, an additional 0.33 moles of hydrogen might be produced for every mole of iron corroded under field conditions (Reardon, 2005). The actual corrosion pathway is even more complex as the precipitates formed is strongly dependent on geochemical conditions such as groundwater composition, pH, redox potential, alkalinity and dissolved oxygen. However, estimation of the corrosion rate is important as ZVI corrosion negatively impacts the reactivity of ZVI particles (1) by forming a corrosion layer on the surface of ZVI which reduces the exchange rate of electrons between ZVI and the CAHs, and (2) by depletion of ZVI, and as such of electrons. To date, precise estimation of the longevity and long-term performance of ZVIs is challenging.

The aging behavior due to corrosion of different ZVI particles was investigated previously (Reardon, 1995, 2005; Reardon et al. 2008; Gillham, 2003; Liu et al., 2005a; Liu and Lowry, 2006). According to previous studies, granular particles the estimated life-time ranged from several years to several decades (Reardon, 1995; Farrell et al., 2000;

Klausen et al., 2003). On the other hand, nanoscale zerovalent iron (nZVI) particles had relatively shorter life-time compared to granular ZVI (He and Zhao, 2007; Noubactep et al., 2012). Expected life-time of nZVIs was just a few weeks (Liu et al., 2005a; Liu and Lowry, 2006) or up to one year for Ni/Fe nanoparticles (Schrick et al., 2002) and crystalline nZVI (Liu et al., 2005b). According to the limited data, microscale zerovalent (mZVI) particles are expected to have an intermediate life-time (Reardon, 2005; Chen et al., 2011). However, the effective life-time of ZVI particles after in-situ application is a point of discussion in many studies. The correlation of long-term performance and longevity of granular and microscale particles was investigated most of the time using column tests or via hydrogen pressure build-up in long-term batch studies (Reardon, 2005; Suk O et al., 2009). The aging rate of particularly nZVIs was estimated via direct hydrogen evolution in batch tests (Liu and Lowry, 2006; Zhuang et al., 2011).

Several models were proposed to estimate the longevity of permeable reactive barriers, where granular iron was used. Kouznetsova et al. (2007) proposed a phenomenological model where the decline in iron reactivity is a function of space and time, without describing the geochemical processes occurring in the barrier. More detailed geochemical modeling of iron deactivation was proposed by Mayer et al. (2001), Jeen et al. (2007) and Carniato et al. (2012). For nZVI, empirical rate laws describing the iron consumption due to corrosion and contaminant degradation, were developed by Liu and Lowry (2006).

Within batch degradation study reported in Chapter 2 low-cost mZVI particles were developed to treat groundwater which was polluted by different CAHs. One of the fundamental parameters for a successful application of these mZVI particles in reactive zones, besides reactivity and mobility, is long-term performance to serve as an electron donor for effective contaminant removal.

The aim of this study was to fill the knowledge gap and assess the life-time of mZVI particles via hydrogen (H_2) production measurements and calculation of corrosion rates. In a first step H_2 production was quantified for 17 different types of ZVI in a standardized batch reactors with synthetic groundwater polluted by CAHs (Chapter 2) and converted to ZVI corrosion rates. Correlations between the ZVI corrosion rate and particle sizes, specific surface areas and CAH-degradation rates were determined. Next, the impact of aquifer material and real CAH-polluted groundwater on the H_2 production rate and consequently on the corrosion of selected ZVI particles was studied. Iron corrosion rates were determine via zero-order fitting but also via numerical modeling (by TU Delft using a customized PHREEQC model, Parkhurst and Appelo, 1999) where inhibitory effects of the iron corrosion reaction products (OH^-, dissolved iron and dissolved H_2) on the corrosion rates were taken into account. Finally, life-times of the different ZVIs were estimated based on the obtained corrosion rates.

4.2. MATERIALS AND METHODS

4.2.1. ZEROVALENT IRON PARTICLES

mZVIs were supplied by Höganäs and BASF, while granular ZVI and nZVI particles by Gotthart Maier and Nanoiron/TODA, respectively (Table 5).

4.2.2. BATCH EXPERIMENTS WITH ARTIFICIAL MEDIUM

Parallel with batch degradation study reported in Chapter 2, the corrosion rate of ZVIs was determined in the same reactors via pressure and hydrogen (H_2) gas measurements. For nZVIs, samples were taken 0, 3, 6, 8 and 22 days after the start of the test, for other ZVI particles after 0, 14, 28, 49 and 105 days. Pressure build-up was measured manually using a BLAUWE LIJN® S2401-10A pressure manometer (EURO-INDEX, Netherlands). Before performing CAH-analysis, 2000 µL headspace-samples were taken directly from the batch reactors with an air-tight syringe for H_2 analyses using a gas Trace GC MPT-10286 (Interscience) equipped with a HayeSepQ column (Alltech Associates, Inc.) and a thermal conductivity detector. Calibration was based on standard gas mixtures ranging from 2 to 60 % hydrogen in a N_2-headspace taking into account the low solubility of H_2 in water.

4.2.3. BATCH EXPERIMENTS WITH CONTAMINATED AQUIFER AND GROUNDWATER

For three ZVI types, an additional set of similar experiments was set-up using natural groundwater (taken 8 m below ground surface, Table 12) and aquifer material originating from a CAHs contaminated site in Belgium (see Chapter 7). To mimic in-situ conditions after iron injection, batch tests contained 45 g of aquifer material and 25 g of real groundwater supplied with 50 g kg^{-1} of a selected granular and microscale ZVI or 5 g kg^{-1} of nanoscale ZVI, leaving an 85 ml headspace. The experiments were set-up in an anaerobic glove box (nitrogen) and consisted of 3 replicates. The vials were incubated at groundwater temperature (12 ^{0}C) on an Edmund Bühler SM 30-control shaker (125 rpm min^{-1}). Each series included a control set using the same conditions but without ZVI particles.

In time, the CAH-concentrations, pressures and hydrogen measurements were performed as described for the tests with artificial medium (Chapter 2). ORP and pH were measured using a redox/pH meter (Radiometer) at the first and last sampling point in the test conditions with mZVI. For nZVIs pH and ORP were measured 0, 6 and 22 days after the beginning of experiment.

4.2.4. CORROSION RATE AND IRON PARTICLE LIFE-TIME CALCULATIONS

Due to fluctuations in pressure build-up during the incubation period, only hydrogen production data were used for calculating iron corrosion rates using the method suggested by Liu and Lowry (2006). A zero-order model of H_2 (ml) evolution was used to calculate the amount of moles of hydrogen produced per day:

$$k = - d[H_2] / dt \qquad (13).$$

The slope of the curve (*k*) was assumed to be equal to the rate of hydrogen production per day and the corrosion rate was calculated using equation 12.

From the ideal gas low, the moles of hydrogen produced per day in the reactor, were calculated:

$$n_{H2} = PV_{H2} / (RT) \qquad (14)$$

where n_{H2} is the moles of hydrogen realized per day (mol H_2 d^{-1}), V_{H2} is the corresponding volume of H_2 realized per day (L d^{-1}), R is the ideal gas constant (8.314 J K^{-1} mol^{-1}) and T is temperature during the measurements (293.15 K). A pressure, P of 1 atm (ideal gas pressure) was used to calculate the moles of hydrogen formed per day in the reactor. Pressure build-up in the batch reactors was measured and ranged from 1 to 1.1 atm, while up to 1.3 atm was only observed for batch reactors containing nZVI particles at the last time point. The error of 10 % made by assuming 1 atm is within the uncertainty of the method.

The corrosion rate (R, mmol of Fe kg^{-1} d^{-1}) was calculated assuming that 1 mol of H_2 (g) in the reactor is produced for every mole of iron corroded with no conversion of $Fe(0H)_2$ to Fe_2O_3 (Reardon, 1995):

$$R = \text{Moles } H_2 \text{ realized per day} / M_{\text{Fe}} \qquad (15)$$

where M_{Fe} is the mass of iron in kilograms.

Finally, the corrosion rate was normalized to the specific surface area of the iron.

Assuming that iron particles will be completely consumed in the reaction with groundwater, calculated iron corrosion rates can be used to estimate life-time of iron particles, namely by dividing the iron content by the calculated corrosion rate.

4.2.5. MODELING APPROACH

For three iron types, the H_2 and the pH measurements were used to estimate the parameters of a PHREEQC (version 2) batch model (Parkhurst and Appelo, 1999) that simulates the corrosion rate in the liquid phase and the hydrogen volume in the headspace. The GAS_PHASE keyword in PHREEQC was used by TU Delft to simulate the batch system, keeping the total gas volume equal to the headspace (60 ml) and allowing hydrogen and carbon dioxide to enter in the gas phase (at the beginning of the experiment no hydrogen is present). The information about the aquifer composition and iron content were used as initial condition for the liquid phase (120 ml). The corrosion rate in the liquid phase was described using the following formula (Mayer et al., 2001) and implemented in PHREEQC using the kinetic keyword:

$$R_{IrC} = \max\left\{ k_{IrC} M_{Fe^0} \left[\left(1 - \frac{IAP_{IrC}}{K_{IrC}} \right) \right], 0 \right\} \tag{16}$$

where R_{IrC} is the actual corrosion rate (mol L^{-1} s^{-1}), k_{IrC} is the calculated corrosion rate parameter (mol g_{Fe0}^{-1} s^{-1}), M_{Fe0} is the amount of iron present in the bottle (g_{Fe0} L^{-1}), K_{IrC} is an equilibrium constant for the iron corrosion reaction and IAP is the ion activity product of iron corrosion reaction (following eq. 9, IAP is equal to $\{Fe^{2+}\}\{H_2\}\{OH^-\}^2$, where curly brackets stand for activity). Thus, the corrosion rate slows down when the IAP increases and when the mass of iron present M_{Fe0} in the liquid phase is consumed. The rate expression in eq. 16 accounts for the inhibitory effect of high pH, hydrogen and iron concentrations on the corrosion rate. Inhibitory effect of high pH concentration on batch tests has been reported for similar experiments (Liu and Lowry, 2006). This study concluded that iron corrosion rate has a first-order dependency on dissolved H^+ at pH less than 8 and a zero-order dependency at higher pH. The rate expression in eq. 16 provides a model to account for this observed shift.

Moreover, the influence of aquifer composition on the ion activity product, and therefore the corrosion rate, is also accounted for by the model, since dissolved species (dissolved iron, dissolved hydrogen and pH) are calculated from geochemical equilibrium reactions (Annex I) included in the PHREEQC database. The precipitation of carbonate minerals (such as calcite and iron hydroxycarbonate) was not modeled, even if their precipitation is likely to occur. A reasonable approximation was to assume the liquid phase in equilibrium with amorphous iron hydroxide, a mineral that certainly forms in iron/water systems. Using this approximation the average pH value was reasonably reproduced for 4 out of 6 experiments.

The corrosion rate parameter k_{IrC} and the equilibrium constant K_{IrC} were calibrated on the available hydrogen and pH measurements for each batch experiment (both with synthetic and real groundwater). The calibration was performed minimizing the following objective function:

$$\phi = \frac{\sum_{i=1}^{n} \left| \log(C_{i,meas}) - \log(C_{i,sim}) \right|}{n} \qquad (17)$$

where $C_{i,meas}$ is the measured concentration (hydrogen in the headspace and pH) , $C_{i,sim}$ is the model simulated counterpart and n is the total number of measurements (varying from a minimum of 5 to a maximum of 8). Minimization was performed using the SCEUA algorithm (Duan et al., 1992). The initial groundwater compositions and physical conditions used in the model are reported in Table 12.

Table 12 : Detailed groundwater chemistry used in batch experiments.

Field parameters	**Unit**	**Synthetic groundwater**	**Natural groundwater**
temperature	°C	12.0	12.5
pH		7.27	5.75
ORP	mV	56.2	-27.5
Conductivity	µs cm^{-1}	nm	858
Dissolved O_2	mg L^{-1}	0.31	0.59
Redox parameters	**Unit**		
$NaHCO_3$	mM	0.5	nm
$KHCO_3$	mM	0.5	nm
$CaCl_2.2H_2O$	mM	0.5	nm
$MgCl_2.6H_2O$	mM	0.5	nm
CO_3^{2-}	mg L^{-1}	nm	0.00
HCO_3^-	mg L^{-1}	nm	82.3
Dissolved Ca	mg L^{-1}	nm	34.2
Dissolved Fe	mg L^{-1}	nm	121
Dissolved Mn	mg L^{-1}	nm	0.62
Cl^-	mg L^{-1}	nm	114
SO_4^{2-}	mg L^{-1}	nm	201
CAHs	**Unit**		
Chloroethane	µg L^{-1}	0	50
1,1-dichloroethene	µg L^{-1}	0	716
Trans-dichloroethene	µg L^{-1}	7±0	78
1,1-dichloroethane	µg L^{-1}	0	8360
Cis-dichloroethene	µg L^{-1}	5644±56	2116
1,1,1-trichloroethane	µg L^{-1}	4983±191	15
trichloroethene	µg L^{-1}	5574±368	916
tetrachloroethene	µg L^{-1}	5284±288	22
Vinyl chloride	µg L^{-1}	0	21

nm – not measured

Grain size distribution of aquifer material was d_{90} = 374 µm. Aquifer material contained 111 g of total iron per kg^{-1} of dry weight, while organic matter was < 1 % of dry weight.

4.3. RESULTS AND DISCUSSION

4.3.1. H_2 PRODUCTION RATE AND ESTIMATED INITIAL CORROSION RATES OF ZVI

According to the zero-order fits of H_2 (ml) produced in the ZVI batch reactors over time (Figure 20) iron corrosion rates were calculated (Table 13). Most reactors exhibited initially a linear increase in H_2 production.

The H_2 production based corrosion rate of the examined mZVIs ranged between 0.21 ± 0.01 and 5.46 ± 0.06 mmol kg^{-1} d^{-1}, with an average of 2.10 mmol kg^{-1} d^{-1}. The lowest corrosion rate corresponds to the SM iron, which is also the least reactive towards contaminants. Highly reactive HQ iron has the highest corrosion rate (5.46 ± 0.06 mmol kg^{-1} d^{-1}), followed by FeQ2 (4.27 ± 0.03 mmol kg^{-1} d^{-1}) and FeH14 (3.08 mmol kg^{-1} d^{-1}) among other mZVI particles. The calculated corrosion rates are lower than previously reported for electrolytic irons (d_{50} < 150 µm) according to the H_2 pressure build up (Reardon et al., 2008).

For a number of ZVIs, a clearly decreased production was observed near the end of the 105 days experimental time. This is especially the case for carbonyl irons MS200, MS200+ and HQ were the corrosion rate slowed down and the H_2 content reached a plateau after 49 days. This is consistent with previously published data where plateau in H_2 production and consequently iron passivation is explained by accumulation of carbonate-containing precipitates (Nurmi and Tratnyek, 2008). In this case, only the first 4 data points were used for calculation of the initial corrosion rate, resulting in overestimated corrosion rates. Interestingly, as previously reported in Chapter 2, MS200+ is more reactive than MS200, yet its initial corrosion rate is lower. Deviations from a linear increase in H_2 evolution are also evident for FeH11 (R^2 = 0.703) and FeH12 (R^2 = 0.714). The origin of the lag phase might be a consequence of the high oxygen content of these particles (Chapter 3). This phenomenon was previously observed by Reardon (2005) and includes various processes on the iron surface and permeation of the oxide film by water and hydrogen.

The H_2 production based corrosion rate of reference granular material FeA4 was 0.36 ± 0.06 mmol kg^{-1} d^{-1}. This is consistent with reported corrosion rates from 0.1 to 0.7 mmol kg^{-1} d^{-1} for granular iron supplied by Master Builders (Reardon, 1995) and 0.3 mmol kg^{-1} d^{-1} for Connelly iron (Reardon, 2005).

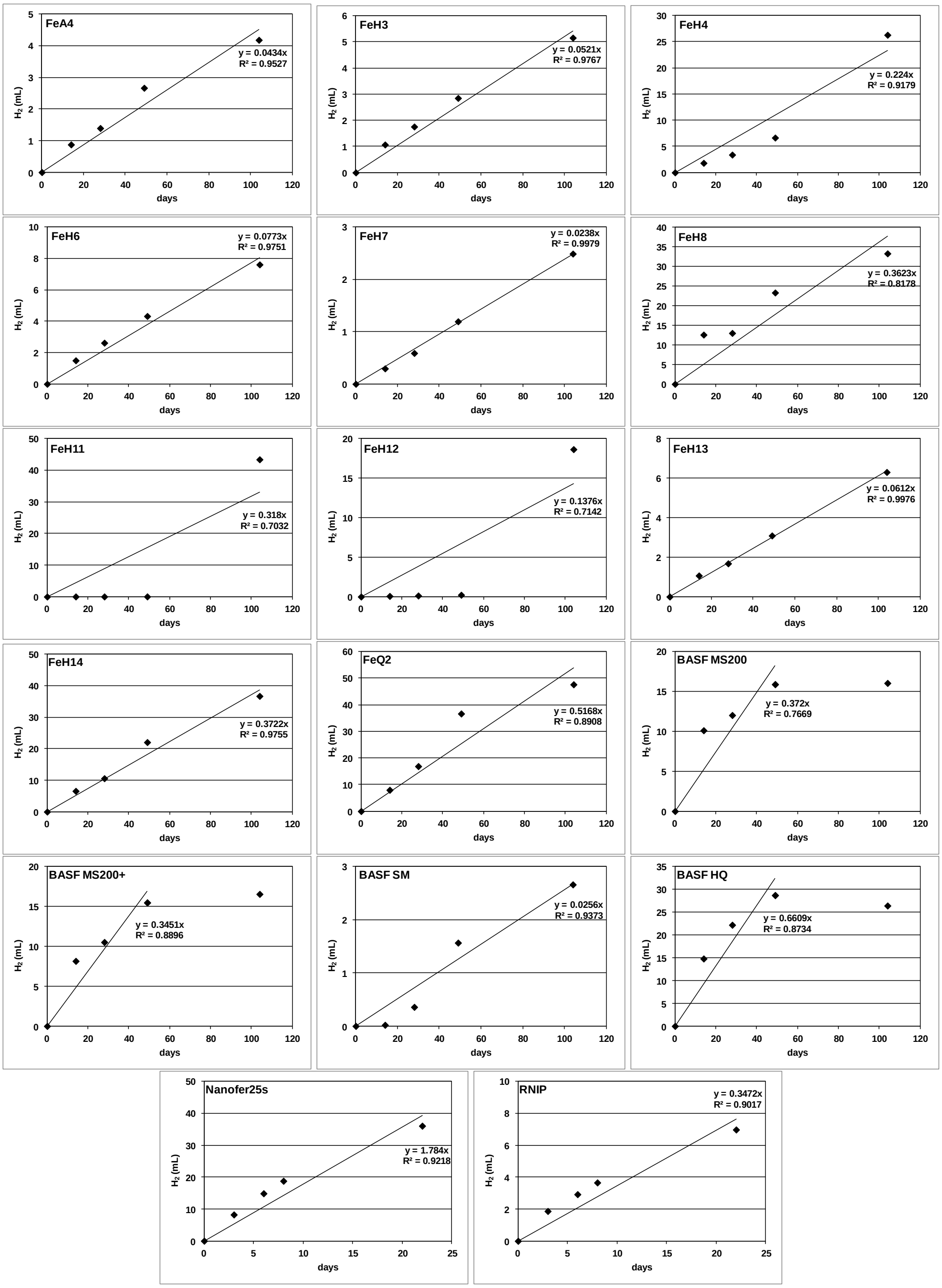

Figure 20 - A zero order fit of H_2 (ml) evolution in batch reactors for examined zerovalent iron particles.

For the nZVI Nanofer25s the highest initial corrosion rate (143 ± 4.22 mmol kg^{-1} d^{-1}) was recorded. The initial corrosion rate of nZVI RNIP was approximately 5 times lower than that of Nanofer25s. The large surface area of nZVIs particles may be one of the reasons for their fast consumption in batch reactors. Moreover, the calculated corrosion rate of nZVI corresponds to previously reported corrosion data (35.4 to 41.1 mmol kg^{-1} d^{-1}) (Zhuang et al., 2011). Finally, the initial corrosion rate of mZVI, compared to granular ZVI and nZVI, identify mZVI as prospective particles for in-situ reactive zones treatments.

4.3.2. EFFECT OF PARTICLE SIZE AND SURFACE AREA ON THE INITIAL CORROSION RATES OF ZVI

H_2 production measurements in batch reactors revealed that generally particle size influences the iron corrosion rate, which confirms findings reported by Noubactep et al. (2012). An inverse correlation was found between iron corrosion rates and ZVI particle sizes (Figure 21), although the correlation factor was relatively low (R^2=0.56).

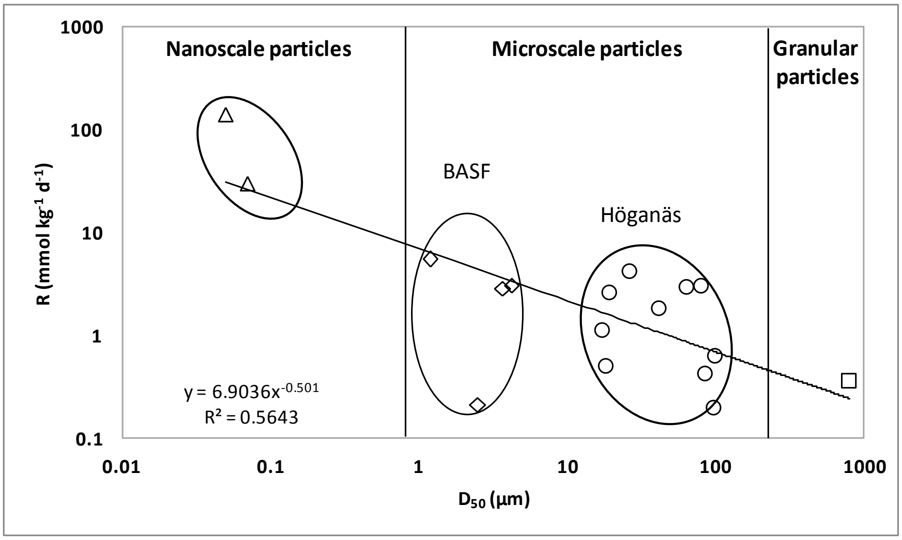

Figure 21 - Power trend line for the calculated iron corrosion rate (R) relative to particle size (D_{50}) of zerovalent iron.

Comparing to all examined ZVIs, mZVI particles supplied by Höganäs showed lower corrosion rate as a result of their larger particle size. Particles with similar size, FeH3 (D_{50} = 84 µm), FeH6 (D_{50} = 98 µm) and FeH7 (D_{50} = 96 µm), showed similar corrosion rates. Corrosion rate of BASF irons was generally in the similar range of Höganäs particles. The only exception is SM iron that showed a significant lower corrosion rate, explicable by its limited reactivity reported in Chapter 2.

Finally, corrosion rates for nZVIs are one order of magnitude higher than for mZVIs with intermediate corrosion rate (1 to 4 mmol kg^{-1} d^{-1}) as a consequence of smaller particle size.

Table 13 : Information on iron samples used in the batch study with calculated corrosion rates and iron particle life-times. All data on iron concentration and H_2 production are averages of triplicates.

Iron manufacturer	Iron name	Iron concentration [g L^{-1}]	H_2 production [ml day^{-1}]	R^2 (n)[a]	R[b] [mmol kg^{-1} d^{-1}]	R_{SA}[c] [mol m^{-2} h^{-1}]	Estimated life-time [years]
Gotthart Maier (DE)	FeA4	50.04	4.34 x 10^{-2}	0.95 (5)	0.36 ± 0.06	1.30 x 10^{-8}	137.8
Höganäs (SE)	FeH3	50.00	5.21 x 10^{-2}	0.98 (5)	0.43 ± 0.01	2.85 x 10^{-7}	113.8
	FeH4	49.98	2.24 x 10^{-1}	0.92 (5)	1.86 ± 0.29	8.21 x 10^{-7}	26.32
	FeH6	49.97	7.73 x 10^{-2}	0.97 (5)	0.64 ± 0.04	2.99 x 10^{-7}	76.76
	FeH7	49.99	2.38 x 10^{-2}	0.99 (5)	0.20 ± 0.01	6.61 x 10^{-8}	249.3
	FeH8	49.97	3.62 x 10^{-1}	0.82 (5)	3.00 ± 0.17	3.57 x 10^{-7}	16.37
	FeH11	49.64	3.18 x 10^{-1}	0.70 (5)	2.65 ± 0.27	2.75 x 10^{-8}	18.53
	FeH12	50.01	1.38 x 10^{-1}	0.71 (5)	1.14 ± 0.01	1.31 x 10^{-8}	43.14
	FeH13	49.99	6.12 x 10^{-2}	0.99 (5)	0.51 ± 0.00	1.40 x 10^{-8}	97.01
	FeH14	49.99	3.72 x 10^{-1}	0.97 (5)	3.08 ± 0.09	1.12 x 10^{-8}	15.94
	FeQ2	50.02	5.17 x 10^{-1}	0.89 (5)	4.27 ± 0.03	4.45 x 10^{-7}	11.49
BASF (DE)	BASF MS200	50.00	3.72 x 10^{-1}	0.77 (4)	3.08 ± 0.28	6.41 x 10^{-7}	15.95
	BASF MS200+	50.01	3.45 x 10^{-1}	0.89 (4)	2.85 ± 0.16	2.53 x 10^{-7}	17.20
	BASF SM	49.98	2.56 x 10^{-2}	0.94 (5)	0.21 ± 0.01	1.84 x 10^{-8}	231.6
	BASF HQ	50.01	6.61 x 10^{-1}	0.87 (4)	5.46 ± 0.06	2.78 x 10^{-7}	8.979
NANOIRON (CZ)	Nanofer25s	5.150	1.78 x 10^{0}	0.92 (5)	143 ± 4.22	2.46 x 10^{-7}	0.342
TODA (JP)	RNIP	4.740	3.47 x 10^{-1}	0.90 (5)	30.3 ± 0.28	2.41 x 10^{-8}	1.620

[a] Correlation coefficient (number of data points).

[b] Corrosion rate (average ± standard deviation).

[c] Surface area normalized corrosion rate.

A better correlation was observed between the corrosion rate of ZVI particles and their particle surface area (Figure 22). As expected, particles with higher surface area obtained the highest corrosion rate. Exceptions from the correlation analysis are particles with high carbon content (Chapter 3), and as a consequence it’s high sorption properties and limited or no reactivity. Moreover, high carbon content can affect surface area measurements as stated in Chapter 3.

As such, iron corrosion rates are a complex function of different factors like particle size, specific surface area of the particles, as well as iron composition.

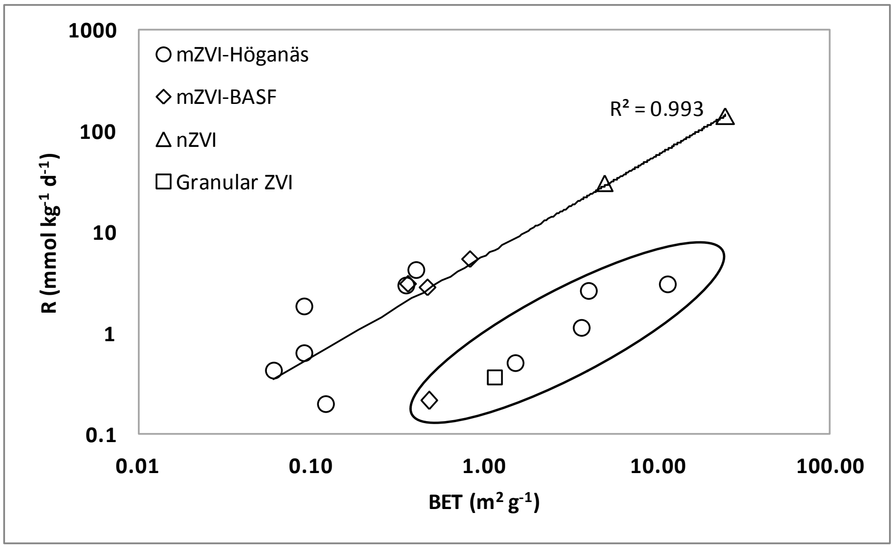

Figure 22 - Correlation between effect of BET surface area (m^2 g^{-1}) and calculated iron corrosion rate (R). The linear log-log relationship (R_2 = 0.993) was observed between 11 of 17 particles. Particles excluded from the correlation analysis (black color ellipse).

4.3.3. CORRELATION BETWEEN INITIAL IRON CORROSION RATES AND CAH DEGRADATION RATES

In our study, for all examined ZVIs, previously presented surface area normalized degradation rate coefficients (k_{SA}) for PCE, TCE, cDCE and 1,1,1-TCA were plotted as a function of surface area normalized iron corrosion rates (R_{SA}, Table 13), as shown in Figure 23.

A significant effect ($p<0.05$) of surface normalized iron corrosion rates on surface area normalized degradation rates is observed, using a one-way analysis of variance (ANOVA).

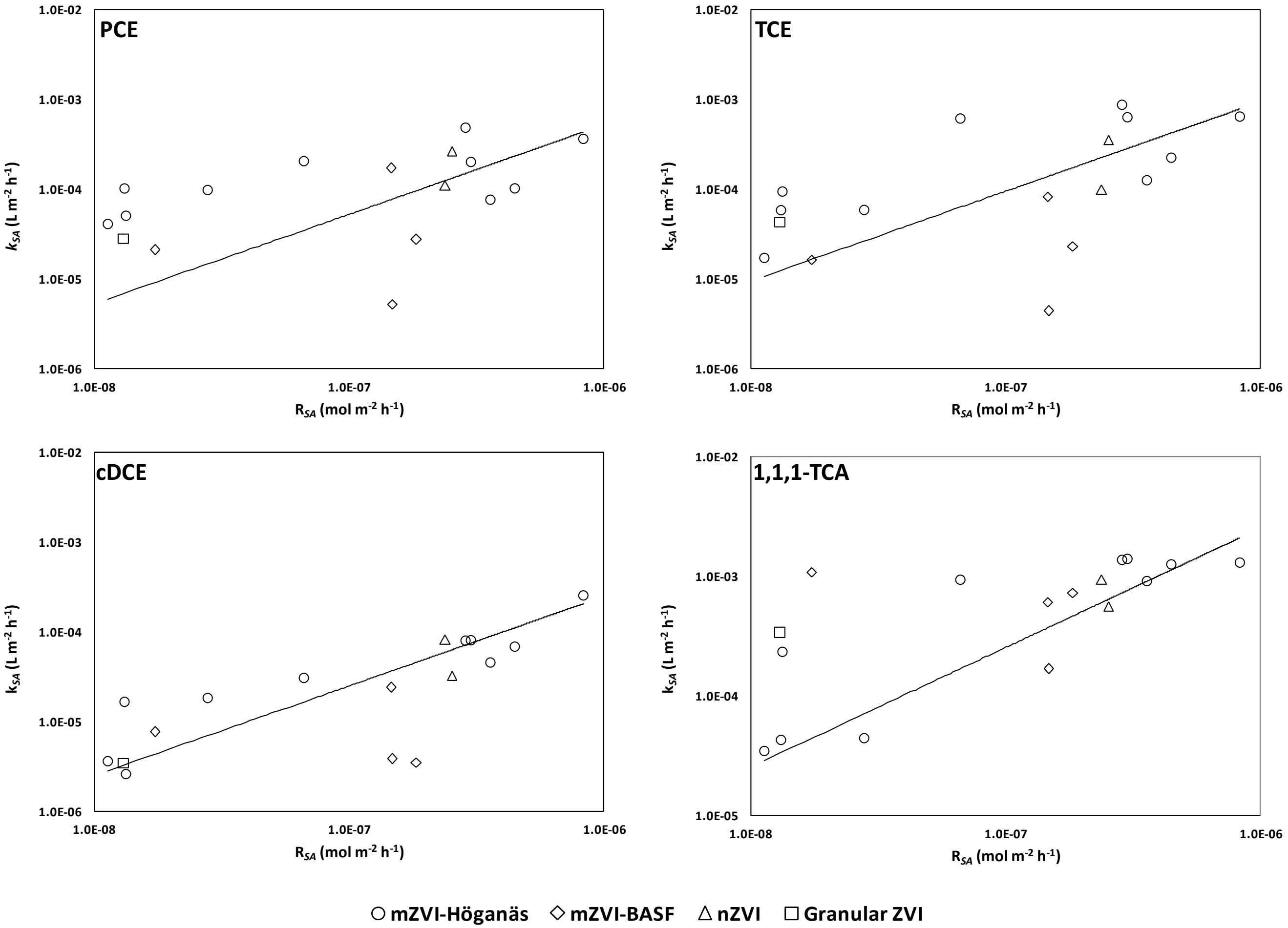

Figure 23 - Surface normalized degradation rate coefficient (k_{SA}) plotted as a function of surface area normalized iron corrosion rate (R_{SA}).

FeH3 and FeH4 particles with the highest k_{SA} coefficients are among the particles with the highest R_{SA} values, namely 2.85 x 10^{-7} and 8.26 x 10^{-7} mol m^{-2} h^{-1}, respectively. Exceptions of this correlation are BASF irons as the corrosion rate slowed down due to the possible iron passivation (Nurmi and Tratnyek, 2008). This observation is generally consistent with other studies where in some cases the degradation rate constants were found to be dependent on the iron corrosion rate (Jiao et al., 2009; Liu and Lowry, 2006). The normalized corrosion rates for nZVIs are in the same order of magnitude as most mZVIs.

4.3.4. IMPACT OF AQUIFER ON H_2 PRODUCTION AND INITIAL CORROSION RATES

In the presence of aquifer material and real groundwater H_2 production based iron corrosion rates were determined for three selected ZVIs. FeH4 and BASF HQ were selected as representative reactive mZVIs, while Nanofer25s as nZVI with the highest reactivity and the fastest corrosion rate in the aquifer free conditions. Figure 24 shows the H_2 evolution measured in aquifer batch reactors supplied with FeH4, BASF HQ and Nanofer25s in similar conditions.

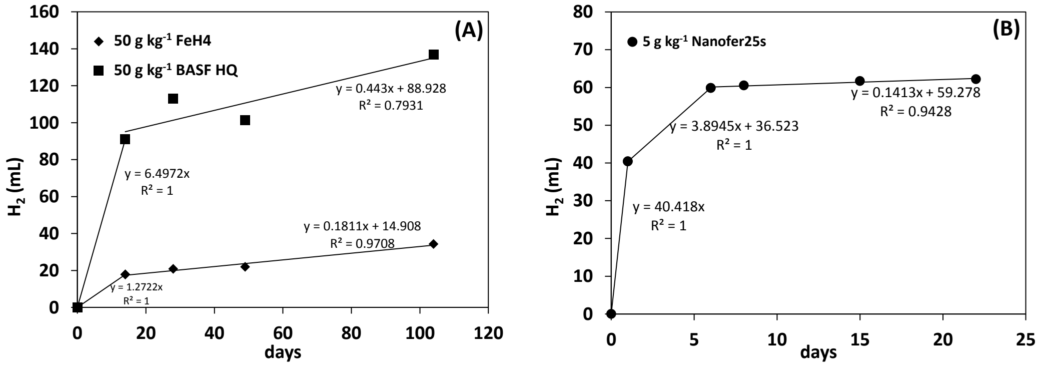

Figure 24 - H_2 evolution rate measured in batch reactors containing aquifer material and microscale ZVIs (FeH4 and BASF HQ, each loaded at a dose of 50 g kg^{-1}) (A) and H_2 evolution rate measured in batch reactors containing aquifer material and 5 g kg^{-1} of Nanofer25s (B).

H_2 evolution data were plotted as a function of time and it is shown that after 14 days H_2 concentrations exhibited a linear increase. Resulting corrosion rates calculated using a zero-order approximation for FeH4 and HQ iron were 10.5 and 54.1 mmol kg^{-1} d^{-1}, respectively. Afterwards, the corrosion rate of particles dropped approximately one order of magnitude. A three-step H2 production was observed for Nanofer25s with a corresponding initial corrosion rate of 3.44 x 10^3 mmol kg^{-1} d^{-1}. The next six days, the calculated corrosion rate was 10 times lower (3.31 x 10^2 mmol kg^{-1} d^{-1}). Finally, a plateau was observed, suggesting that no further significant corrosion was ongoing. The initial corrosion rates of particles in batch degradation tests with aquifer materials were 6 to 24 times higher than the condition with artificially CAH-polluted groundwater as a consequence of initially low pH in the slurry (pH = 5.11). For TCE and cDCE, present both in the test with synthetic groundwater and real aquifer system, faster degradation rates were observed in the natural environment, explicable by the lower pH (Liu and Lowry, 2006).

4.3.5. IRON CORROSION RATES DETERMINED VIA NUMERICAL MODELING

A tool to predict corrosion rate of the iron particles under different conditions was developed by TU Delft. A limitation of the zero-order model is its inability to describe the observed plateau in the H_2 content observed for some batch experiments (see Figure 25). The model proposed with eq. 16 is able to adapt the iron corrosion rate as the liquid phase becomes saturated with hydrogen, iron and OH^- and aims reproducing the observed plateau in the H_2 content.

The comparison between the measured and simulated pH and hydrogen productions with synthetic and real groundwater is shown in Figure 25.

The observed higher hydrogen production in batch reactors with lower pH (real groundwater) is in agreement with the formulation of the corrosion rate proposed in eq. 16.

From the hydrogen measurements it can be seen that the hydrogen production slows down at later time, except for the last measurements of the FeH4 synthetic groundwater batch experiment (Figure 25 (a)) and FeH4 real groundwater batch experiment (Figure 25 (b)). As the liquid phase becomes saturated with the products of the iron corrosion reaction (dissolved hydrogen, iron and OH^-), the iron corrosion rate slows down. This gave a good fit of the hydrogen measurements in the headspace for the first measurements of the FeH4 test with real groundwater (Figure 25 (b)) and for BASF HQ iron (Figure 25 (c) and Figure 25 (d)) and Nanofer25s with real groundwater. For the BASF HQ iron with synthetic groundwater the rate model proposed with eq. 16 fits the hydrogen measurements much better than the zero-order model. Adapting the value of the equilibrium constant allows the model to behave as a zero-order model (high equilibrium constant, (Figure 25 (a) and 22 (e)) or as a saturation model (low equilibrium constant).

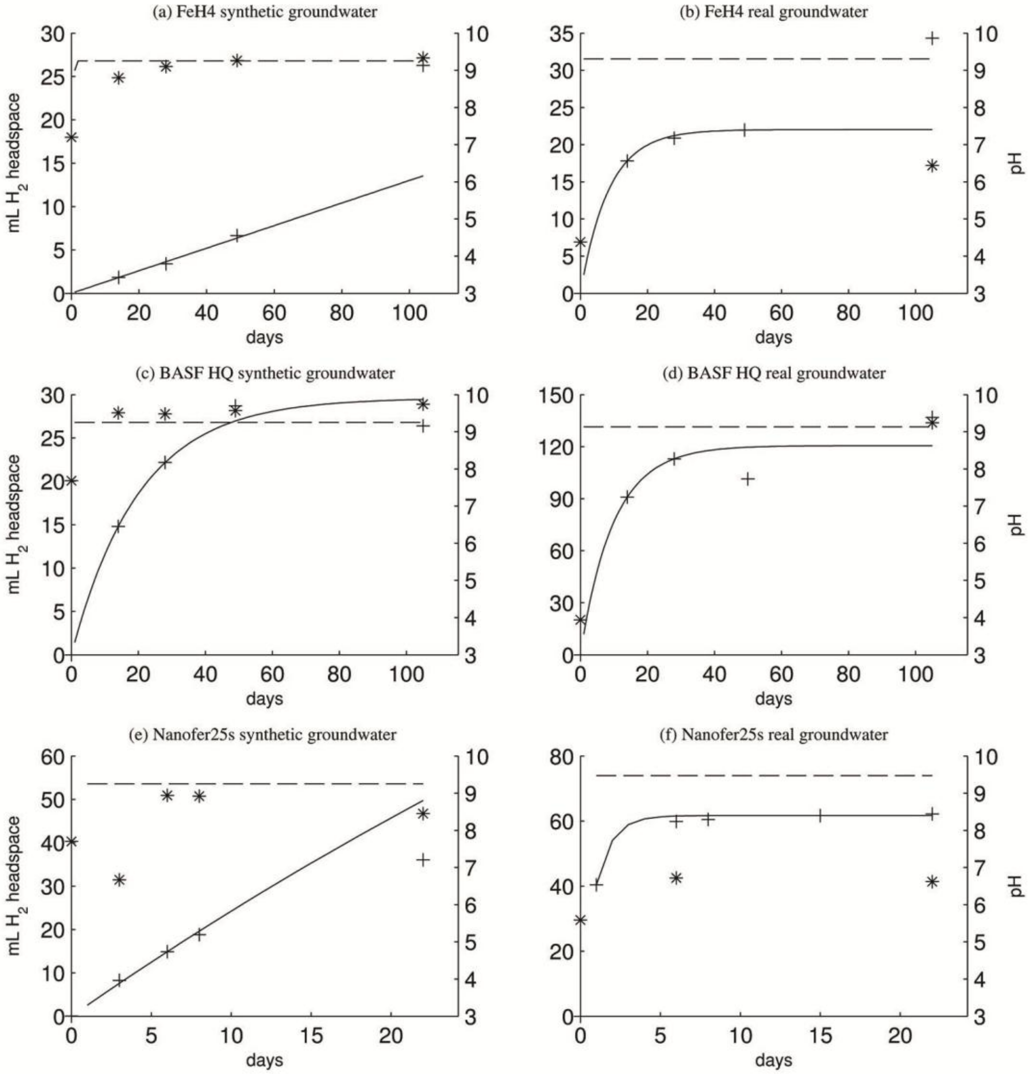

Figure 25 - Simulated hydrogen volumes in the headspace (solid line) and pH in the liquid phase (dashed line) for three types of iron (FeH4, BASF HQ and Nanofer25S). Measured hydrogen volumes are shown with the cross marker while measured pH with asterisks.

The observed higher hydrogen production in batch reactors with lower pH (real groundwater) is in agreement with the formulation of the corrosion rate proposed in eq. 16.

The simplified geochemistry used in the model, here simulated using the equilibrium reactions of the PHREEQC database and assuming the liquid phase in equilibrium with amorphous iron hydroxide, did not allow the reproduction of pH dynamics but only the prediction of a constant pH value. This constant value agrees reasonably with the pH measurements of the FeH4 batch experiment with synthetic groundwater (Figure 25 (a)) and BASF HQ with synthetic groundwater and real groundwater (Figure 25 (c) and 22 (d)). However, the pH values measured at the end of the tests 22 (b) and 22 (f) were largely overestimated by model simulations. Even considering the liquid phase in equilibrium also with magnetite (which releases acidity), the pH did not decrease below 8.6. These low pH measurements can only be reproduced with a zero corrosion rate, which is not plausible based on the hydrogen measurements. It is hypothesized that in the experiments performed with real groundwater the soil matrix was able to buffer the pH increase due to the cation exchange capacity. As can be seen from Figure 25 the initial pH values in the real groundwater batch reactors is much lower than those in the synthetic groundwater batch reactors. For BASF HQ the initial groundwater pH was 4.38, which indicates a strongly acid soil. While corrosion proceeds part of the OH^- released could be compensated by H^+ releases previously sorbed in the soil. Detailed soil composition and inorganic were not included in the model.

Is interesting to note that in Figure 25 (b) and 22 (c) the hydrogen production reach a plateau despite the low pHs during the experiment. This suggests again that eq. 16 is appropriate to model corrosion reaction because can also account for the effect of hydrogen and dissolved iron on the iron corrosion rate, despite that, passivation layer was not included.

In Table 14, the calibrated corrosion rate parameters and the iron corrosion equilibrium constants are reported.

Table 14 : Estimated corrosion rates by fitting iron corrosion rates and hydrogen inhibitory terms (eq. 13) to hydrogen and pH measurements.

	Synthetic groundwater		**Natural groundwater**	
Iron type	Corrosion rate [mmol kg^{-1} d^{-1}]	Equilibrium constant [mol L^{-1}]	Corrosion rate [mmol kg^{-1} d^{-1}]	Equilibrium constant [mol L^{-1}]
FeH4	1.1	9.18×10^{-14}	29.2	1.20×10^{-18}
BASF HQ	12.6	2.29×10^{-18}	139.1	6.59×10^{-18}
Nanofer25S	213.8	3.39×10^{-12}	1675.6	3.37×10^{-18}

The estimated iron corrosion equilibrium constants differ widely in the batch experiments performed with synthetic groundwater. These equilibrium constants accounts for the inhibitory effects of the iron corrosion products and these estimates might be influenced by the precipitation reactions not accounted for the model. The measurement of the inorganic concentrations in the liquid phase (e.g. iron and calcium concentrations) might support a detailed mineral precipitation model and might give a less variable estimation of equilibrium constants for the same iron type.

As expected, the higher hydrogen production observed for the batch experiments performed with real groundwater gave an estimate of higher corrosion rates, which can be attributed to the higher groundwater buffer capacity in the experiments performed with real groundwater and soil material.

4.3.6. TRANSLATION OF CORROSION RATES INTO LIFE-TIMES OF ZVIS

The initial corrosion rates reported in Table 13 were extrapolated to life-time of studied ZVI particles. The estimation was obtained by dividing the iron mass present in the batch tests by the estimated initial corrosion rate of the particles assuming no passivation occurs. This can be considered as a worst case scenario for estimated life-time of ZVIs, as corrosion rates slow down over time due to the formation of passivating precipitates.

The extrapolated life-time under aquifer free conditions according to the initial corrosion rate of reference granular material FeA4 was 137.8 years. The shortest life-time within mZVIs was estimated for highly reactive HQ (8.98 years), followed by FeQ2 (11.49 years) and FeH14 (15.94 years). Estimated life-time of FeH4 iron further studied in the presence of aquifer and real groundwater was 26.32 years. Clear iron passivation was observed for MS200, MS200+ and HQ (Figure 20), and the extrapolated life-time of particles was 15.95, 17.20 and 8.98 years, respectively. The shortest life-time among all examined ZVIs was reported for Nanofer25s (0.34 years) and RNIP (1.62 years). The estimated life-time of Nanofer25s corresponds to previously reported life-time of 8 to 80 days (Liu and Lowry, 2006; Reardon et al., 2008).

As reported, in the presence of aquifer and real groundwater initial corrosion rate was higher than for the tests with artificial groundwater polluted by CAHs. The same can be extrapolated for life-time. Considering only the initial corrosion rate (Figure 24), before passivation occurs, estimated life-time of FeH4, HQ and Nanofer25s was 4.66, 0.91 and 0.01 years, respectively. However, taking into account the corrosion rate of the second passivation phase, after the initial high corrosion phase, the estimated life-time of FeH4, HQ and Nanofer25s increased till 33.13, 13.51 and 0.15 years, respectively. This is significantly higher than estimated for the initial corrosion rate. However, the real life-time of particles have to be further studied. Last passivation phase of Nanofer25s was omitted as no significant production of H_2 was observed.

Finally, presented data on extrapolated life-times of particles can serve as a starting point for future research.

4.4. CONCLUSION

This study was performed (1) to determine the corrosion rates for mZVI particles in batch reactors and (2) to extrapolate the results in time to estimate worst case life-times of mZVI under field conditions.

The obtained results suggest that the initial corrosion rate of ZVIs depends on particle properties (the particle size, specific surface area of the particle, particle composition), as well as on environmental factors (pH, buffer capacity). Using a zero-order model, initial corrosion rates of ZVIs in liquid medium were calculated, which is probably an overestimation of the real corrosion rate of ZVI particles. On the other hand, via numerical modeling inhibitory effects of the iron corrosion reaction products can be taken into account. To allow more accurate prediction of the corrosion rate of ZVI in liquid medium, iron speciation within the passivating corrosion layer on the ZVI particle should be investigated more in detail.

In contrast to aquifer-free conditions, higher initial iron corrosion rates were estimated for the batches performed with aquifer and real groundwater, where low pH levels were measured during the experiments. Low pH levels might be maintained by the soil buffer capacity and can promote iron corrosion. In contrary, limited buffer capacity will lead to the increase in pH and lead to the precipitation of ferrous hydroxide. Summarizing this experiments as a worst case scenario, under field conditions the estimated life-time of mZVIs using only initially high corrosion rates was 0.9-4.7 years for mZVIs and only 0.01 years for nZVI. When using corrosion rates from a later experimental phase, estimated life-time of mZVIs was 13.5-33.1 years, and 0.15 years for nZVI. Reality is expected to be in between the two scenarios.

Other factors that might be determinant for the estimation of the particle life-time includes the precipitation of carbonate minerals, which have a direct effect on pH and might hamper the electron transfer due to the formation of a mineral cover around the particles. For that reason, future research is needed to assess the life-time of iron particles in real in-situ conditions incorporating the precipitation of carbonate minerals and corrosion layers formation in the iron corrosion model.

CHAPTER 5 REACTIVITY RECOVERY OF GUAR GUM STABILIZED MICROSCALE ZEROVALENT IRON PARTICLES BY MEANS OF ENZYMATIC BREAKDOWN AND RINSING

Based on: Velimirovic, M., Chen, H., Simons, Q., Bastiaens, L. Reactivity recovery of guar gum coupled mZVI by means of enzymatic breakdown and rinsing. Journal of Contaminant Hydrology 142-143 (2012) 1-10.

5.1. INTRODUCTION

Chlorinated aliphatic hydrocarbons (CAHs) such as tetrachlorethene (PCE), trichloroethene (TCE), and 1,1,1-trichloroethane (1,1,1-TCA) represent the most frequently detected groundwater contaminants in industrialized countries (Prommer et al., 2008; Westrick et al., 1984). *Cis*-dichloroethene (cDCE), vinyl chloride (VC) and 1,1-dichloroethane (1,1-DCA) are often present in ground water as degradation products. In order to remediate such pollutants, the use of zerovalent iron (ZVI) as a nontoxic material has been shown to be a promising technique for in-situ degradation of CAHs via abiotic reductive dehalogenation based on pseudo-first-order kinetics (Gillham and O'Hannesin, 1992, 1994; Matheson and Tratnyek, 1994). Initially, granular ZVI particles were used to construct reactive barriers in the subsurface by digging and refilling a trench (Gillham and O'Hannesin, 1992). Recently, there has been growing interest in finer ZVI particles (micro- and nanoscale) because of their higher reactivity and potential to be injected in the subsurface as slurry. The injection of solid particles in the subsurface, however, is much more challenging than initially expected, due to (1) aggregation of especially nano-sized ZVI particles (nZVI) resulting in filtration of the particles in the porous medium making them less mobile and less reactive (Kanel et al., 2007; Phenrat et al., 2009; Saleh et al., 2007; Schrick et al., 2004) and (2) sedimentation of mainly microscale zerovalent iron (mZVI) particles in the slurry reservoir, tubing and injection wells prior to and during injection caused by the high density and size of particles (Elimelech et al., 1995; Vecchia et al., 2009). Numerous research groups have carried out investigations on stability and dispersion of nanoparticles (Comba and Sethi, 2009; He and Zhao, 2007; He et al., 2009; Tosco et al. 2012; Vecchia et al., 2009; Wang and Zhou, 2010). They mainly involve laboratory scale tests, although in recent years the number of field applications has increased (Klaine et al., 2008; Varadhi et al., 2005; Zhang, 2003). To increase injectability of nZVI into the subsurface and its reactivity at the same time, surface modification of nZVIs is necessary. Modifiers used so far for increasing the colloidal stability and preventing nanoscale particle agglomeration include different polymers like guar gum (Tiraferri et al., 2008; Tiraferri and Sethi, 2009), xanthan gum (Comba and Sethi, 2009; Vecchia et al., 2009), carboxymethyl cellulose (He et al., 2007), and starch (He and Zhao, 2005). Modified nZVI particles can be directly injected in the field, making this technology very promising for the future (He et al., 2010; Zhang, 2003).

The primary focus of the current study is the reactivity of microscale zerovalent iron particles towards CAHs. In comparison with nanoscale (nZVI), mZVI particles are less expensive, have a longer life-time and pose less risk for human health (Lee et al., 2008). However, mZVI particles are less reactive than suspended nZVIs. In order to facilitate their transport in the subsurface and prevent sedimentation of mZVIs during the injection process, the use of stabilizing agents is necessary as shown by laboratory (Cantrell et al. 1997; Comba and Braun, 2012; Oostrom et al., 2007; Vecchia et al., 2009) and field studies (Truex et al., 2011). For effective transport of mZVIs xanthan gum and guar gum were introduced as favorable polymers due to their shear thinning properties making the suspension viscous enough to keep particles in suspension for a relatively long period and to move it through porous media (Cantrell et al. 1997; Comba and Braun, 2012).

In the current study, to stabilize mZVI particles, guar gum was chosen as a green, low cost stabilizing polymer with biodegradation properties (Singh et al., 2005). Once guar gum stabilized mZVI is injected into the subsurface, degradation of guar gum is needed as its viscosity (1) may create a hydraulic barrier by plugging intergranular channels and (2) may inhibit the contact between contaminants and the reactive surface area of the iron particles affecting CAHs degradation rates. To reduce viscosity once iron has been emplaced in the aquifer, the use of enzymes is a possibility (Imeson, 2009). In terms of field application, guar gum has already been used in groundwater remediation as a shoring fluid for the emplacement of permeable reactive barriers, where subsequently enzymes were injected for its breakdown (Day et al., 1999; Di Molfetta and Sethi, 2006; Gavaskar, 1999; Gu et al., 1988; U.S. EPA, 1999; Yang and McCarty, 2000; Zolla et al., 2009). After guar gum breakdown, TCE reduction was observed in a zerovalent iron barrier (U.S. EPA, 1999). Navon et al. (1998) showed that the guar gum used to stabilize trenches for the implementation of the granular zerovalent iron barrier decreased the reactivity of the barrier significantly towards TCE, especially with non-acid washed ZVI. In addition, initial column tests using granular iron stabilized by guar gum suggested that guar gum may be the cause of the reduced ZVI reactivity towards CAHs, which seems to return over time (Focht et al., 2001). Guar gum has been reported as a good dispersing agent for nZVI particles (Tiraferri et al., 2008; Tiraferri and Sethi, 2009) but a limited amount of detailed information is available about its impact on mZVI reactivity. Guar gum has been presented as a biopolymer capable of increasing the colloidal stability of the microscale iron slurries during the column experiments (Comba and Braun, 2012). To our knowledge, the current study is the first on the impact of guar gum on the reactivity of mZVI particles with proposed measures for reactivity recovery by means of enzymatic breakdown and intensive rinsing.

The objective of this study is to investigate the impact of guar gum as a stabilizer on the CAH removal capacity of mZVI particles. Sedimentation tests were performed to evaluate guar gum as a promising stabilizer for mZVI particle stabilization. The interaction mechanism between guar gum and mZVI was discussed, including contaminant diffusion effects and guar gum adsorption on the iron surface that may affect iron reactivity and the degradation of CAHs. Subsequently, batch experiments were performed to determine the impact of different guar gum concentrations on the reactivity of mZVI and to evaluate the impact of enzymatic breakdown of guar gum and the impact of rinsing on reactivity recovery of guar gum coupled mZVI.

5.2. MATERIALS AND METHODS

5.2.1. MEDIA

Same procedure described in Chapter 2.2.1 was applied to prepare artificial groundwater in this study.

5.2.2. MICRO-IRON PARTICLES

The reactive micron sized zerovalent iron particles used in this study were obtained from Höganäs (Sweden). Characteristics of the particles are given in Table 15.

Table 15 : Characteristics of studied mZVI.

Sample	PSD[a] D_{10}, D_{50}, D_{90} (µm)	Carbon content (%)	Oxygen content (%)	Sulfur content (%)	BET[b] ($m^2\ kg^{-1}$)
mZVI	22, 41, 62	0.00	0.09	0.01	94

[a] Particle Size Distribution;
[b] BET : Specific Surface Area according to Brunauer-Emmett-Teller (Single point measurement) - analysis was conducted by Höganäs.

5.2.3. SEDIMENTATION TEST

Guar gum (Apcol 150) purchased from Apex Resources (USA) was used for the initial screening of mZVI colloidal stability. This biopolymer consists of (1 → 4)-linked β-D-mannopyranose units with α-D galactopyranose units connected to the mannose backbone through (1 → 6) glycosidic linkages (Figure 26). The polymannose chain is randomly substituted with galactose units at a mannose-to-galactose ratio of 1.8–1.0 (Painter et al. 1979; Whistler and Hymowitz, 1979). Each unit contains nine hydroxyl groups, available for hydrogen bonding with other molecules (Mackenzie et al., 1980). Sedimentation experiments were prepared in 15 ml IWAKI conical centrifuge tubes with tapered bottoms for iron suspension (50 g L^{-1}) of non-stabilized material and iron suspension (50 g L^{-1}) stabilized by guar gum (6 g L^{-1}) (Sun et al., 2007). The tubes were shaken for 1 minute, and during the subsequent static observation phase digital photos were taken at different times to estimate visually the sedimentation rate of the suspensions (Tiraferri et al., 2008).

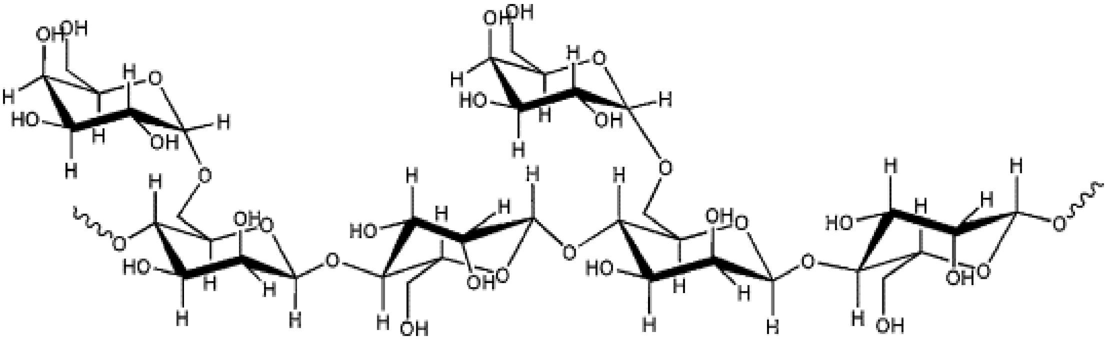

Figure 26 – The monomeric structure of guar gum (Wang et al., 2010).

5.2.4. SET UP OF EXPERIMENTAL BATCHES AND GAS CHROMATOGRAPHY (GC) METHODS

CAHs degradation experiments with mZVI in the absence and presence of guar gum as stabilizer were performed in 160 ml glass vials with butyl/PFTE grey septum. The vials were filled in an anaerobic chamber (nitrogen) and contained 50 g L^{-1} of mZVI and 0 g L^{-1}, 2 g L^{-1}, 4 g L^{-1} or 6 g L^{-1} of guar gum (Apcol 150) and 100 ml anaerobic simulated groundwater, leaving a 60 ml headspace. The experiments were set up with 4 replicates and the vials were incubated at groundwater temperature (12 ^{0}C) on an Edmund Bühler SM 30-control shaker (125 rpm min^{-1}). After 42 days, for each experimental condition two of the four vials were sacrificed for complete degradation of guar gum by adding 4 mg L^{-1} (final concentration) commercially available enzyme LEB-H™ (Rantec Corporation, USA) with maximum activity at pH 7-8, > 80% of maximal activity at pH 10. In the next step groundwater flow in the field was simulated. The guar gum breakdown fragments were removed by replacing the liquid phase in the batches (1 to 6 times) with new artificial groundwater and guar gum degradation products were removed. At the end new artificially contaminated groundwater was added in the vials. Each test series included a control set in the absence of mZVI particles and guar gum, a poisoned control (formaldehyde with final concentration of 0.4% in the batch system) and a reference set with guar gum to examine CAH-removal via biodegradation or leakage. The effect of guar gum on CAH-equilibrium during the analyses was found to be negligible (< 5 %).

The concentration of CAHs and their breakdown products were determined via headspace measurements as described in chapter 2. At each time point mass balances were made on molar basis (PCE + TCE + cDCE + VC + 1,1,1-TCA + 1,1-DCA + acetylene + ethene + ethane) to determine whether sorption occurred. Redox potential (ORP) and pH were measured using a redox/pH meter (Radiometer).

5.2.5. GUAR GUM VISCOSITY MEASUREMENTS

The viscosity of the guar gum suspensions was determined using the Haake Mars rheometer (Thermo Electron Corporation). In a preliminary test, a suspension containing 6 g L^{-1} of guar gum and 100 ml of deionized water was supplied with 4 mg L^{-1} of previously prepared LEB-H^{TM} enzyme and was continuously shaken at 12^0C. The viscosity of the suspension was measured before and 2 hours after adding enzymes. To determine the guar gum concentration after iron rinsing in batch degradation experiments, simulated groundwater samples were filtrated with a 0.45 µm membrane filter and phenol–sulfuric acid tests were conducted using colorimetric method (Dubois et al., 1956). The absorbance measurements were performed using a Spectronic Genesys 6 UV–Vis spectrophotometer (Thermo Electron Corporation) with the maximum absorbance for guar gum occurring at λ_{max} = 490 nm.

5.2.6. CHARACTERIZATION OF GUAR GUM STABILIZED MZVI

To avoid further particle oxidation after the batch study, iron samples were prepared by drying at room temperature under N_2 environment and directly analyzed by SEM and FTIR.

The morphology of the reacted non-stabilized mZVI stabilized and intensively rinsed mZVI particles was studied by means of scanning electron microscopy (SEM, Jeol JSM-6340-F) at 5-20 keV electron beam energy. Electron beam energy of 20 keV was used for guar gum stabilized mZVI particles. For surface morphology, particles were mounted on SEM stubs using double-sided carbon tape. Elemental information was obtained from the chosen region with EDS in conjunction with SEM.

The characteristics of guar gum stabilized mZVI were investigated using Fourier Transform Infrared (FTIR) spectroscopy. Three types of samples: (1) mZVI; (2) guar gum coupled mZVI; and (3) intensively rinsed mZVI were recorded in contact with diamond crystal using Thermo Nicolet Nexus Model operating in the range 6000-650 cm^{-1}.

5.2.7. DETERMINATION OF CAH DEGRADATION RATES

The first-order rate equation was used to determine kinetic parameters related to CAH degradation rates (Johnson et al., 1996). Further, the observed first-order rate coefficients (k_{obs}) were normalized to the total surface area of mZVI in solution (k_{SA}, L m^{-2} h^{-1}). Mass transfer resistance at the vapor/liquid interface was not considered as these phases are assumed to be in equilibrium with each other (Burris et al., 1996).

5.3. RESULTS AND DISCUSSION

5.3.1. RELATIVE STABILITY OF GUAR GUM STABILIZED MICROSCALE PARTICLES

Sedimentation experiments performed with mZVI, clearly showed an improved stabilization of mZVI after addition of guar gum (Figure 27). In tubes containing only microscale particles, sedimentation occurred within 1 min. Particles stabilized by guar gum remained in suspension for a few hours, which is the minimum needed during the injection phase (Tiraferri et al., 2008; Tosco and Sethi, 2010). The difference can be explained by the high viscosity of the guar gum solution hindering sedimentation of mZVI. High polymer concentration and its ability to form a gel structure at a larger length scale was also used to avoid sedimentation of highly concentrated nZVIs (Comba and Sethi, 2009). These results confirm that guar gum is a suitable polymer for enhancing stability of the mZVI particles in suspension. Also better mobility of microscale iron particles in guar gum solution was confirmed by a 1D column study by Comba and Braun (2012). Similar results were obtained for mZVI stabilized by xanthan gum which has been more extensively studied as an mZVI stabilizer (Tiraferri et al., 2008, Tosco and Sethi, 2010), but which is more difficult to biodegrade (Cadmus et al., 1982; Hou et al., 1986).

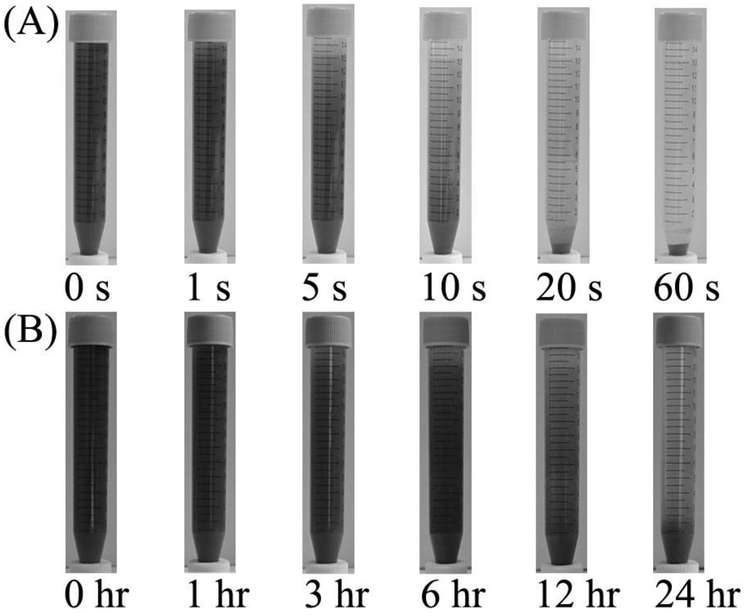

Figure 27 - Qualitative sedimentation experiment with (A) non-stabilized mZVI (50 g L^{-1}) and (B) mZVI (50 g L-1) stabilized by guar gum (6 g L^{-1}).

5.3.2. ENZYMATIC BREAKDOWN OF GUAR GUM

The high viscosity of guar gum solutions may reduce iron reactivity by coating of the iron surface. Therefore, viscosity reduction once iron is injected in the aquifer, may have a positive impact on the iron reactivity. Enzymes have been reported to reduce the viscosity of guar gum by breaking the chemical bonds of the guar gum and forming soluble oligosaccharides (Imeson, 2009).

The viscosity of a guar gum solution before and after using a commercial enzyme (LEB-H^{TM}) for breakdown was measured as a function of the shear rate (Figure 28). A high viscosity of the guar gum solution was measured before addition of enzymes, while afterwards the viscosity reduced significantly. This indicates that the selected enzyme degraded the guar gum efficiently and is suitable for use in our study.

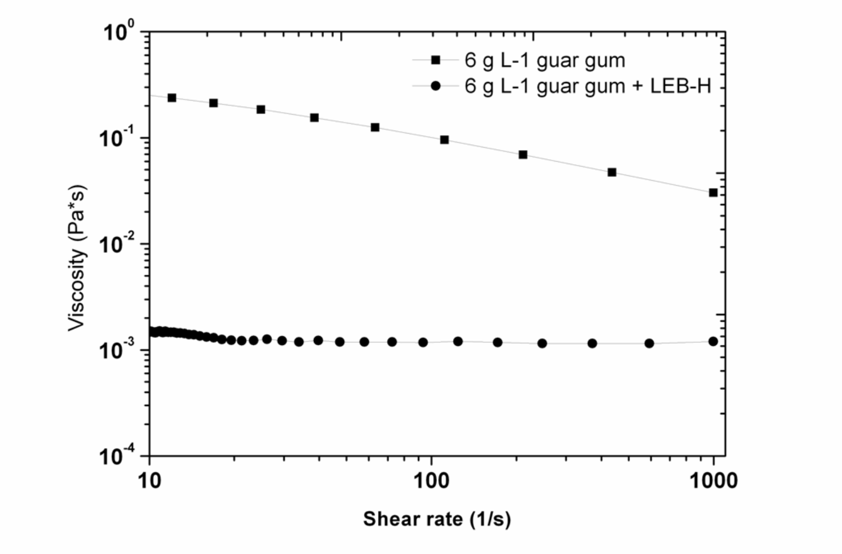

Figure 28 - Viscosity as a function of shear rate for the guar gum suspension before and after breakdown by enzymes.

5.3.3. REMOVAL KINETICS OF DIFFERENT CAHS BY NON-STABILIZED MZVI

Batch degradation experiments were performed to evaluate degradation of PCE, TCE, cDCE and 1,1,1-TCA by non-stabilized mZVI (Figure 29). The calculated surface area normalized reaction rate constants (k_{SA}) for PCE, TCE, cDCE and 1,1,1-TCA are summarized in Figure 30.

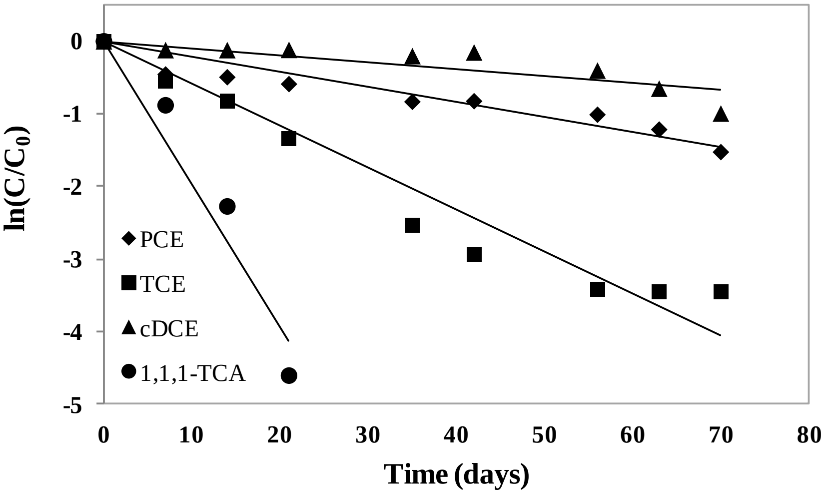

Figure 29 - PCE, TCE, cDCE and 1,1,1-TCA degradation by mZVI (50 g L^{-1}).

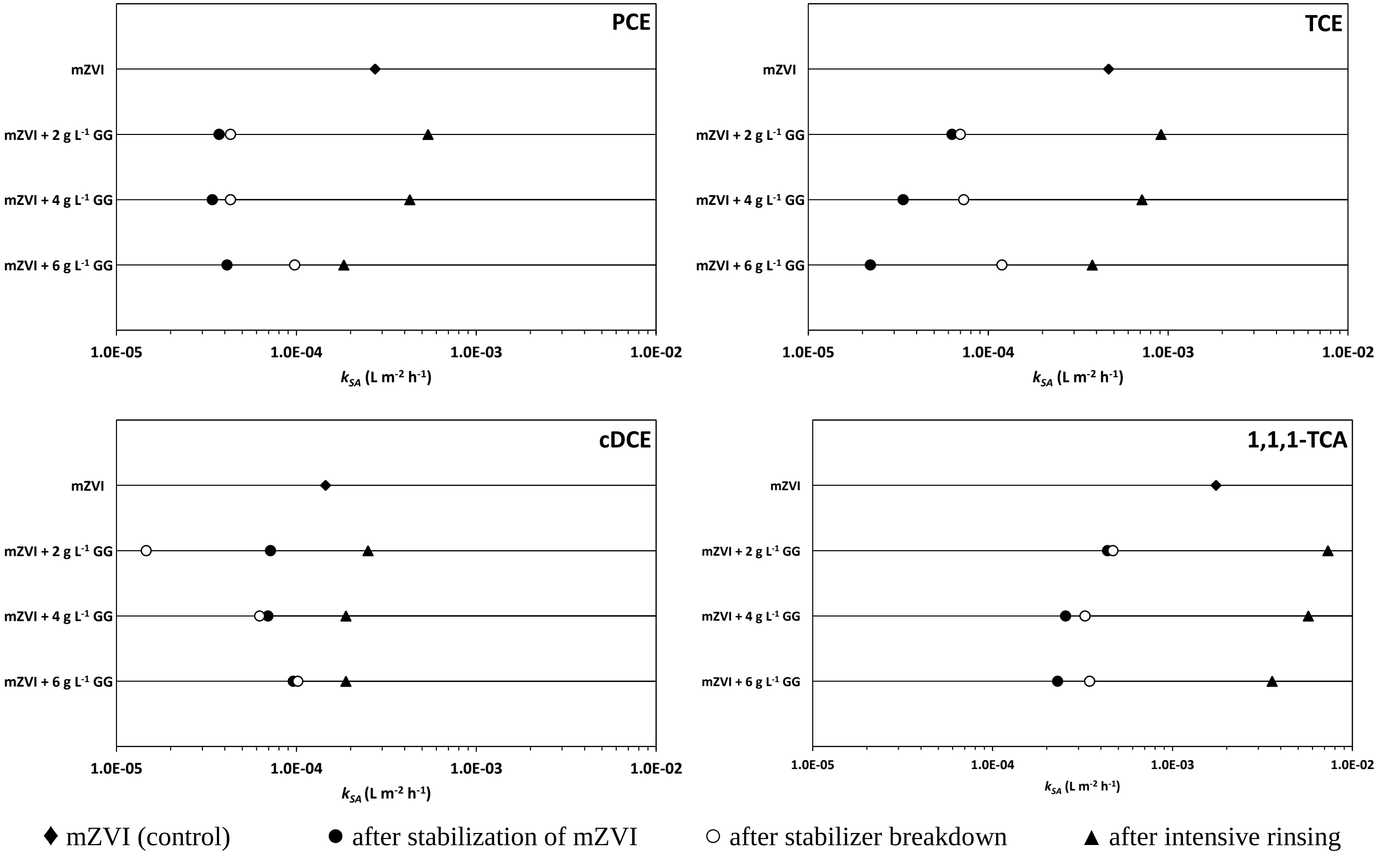

Figure 30 - Comparison of k_{SA} (L m^{-2} h^{-1}) data obtained from batch tests for mZVI (black solid diamonds), mZVI stabilized by different guar gum concentrations before (black circles) and after (open circles) guar gum enzymatic breakdown. Black solid triangles indicate mZVI kinetics after intensive rinsing. The standard deviations were too small to be illustrated.

k_{SA} values of non-stabilized mZVI for PCE, TCE, cDCE and 1,1,1-TCA were 2.74 x 10^{-4}, 4.67 x 10^{-4}, 1.45 x 10^{-4} and 1.745 x 10^{-3} L m^{-2} h^{-1} respectively, which is in the same order of magnitude as rates previously reported in the literature for ZVI (10^{-4} – 10^{-2} L m^{-2} h^{-1}) (Johnson et al., 1996). The results indicate that, without guar gum, the examined mZVI degraded the provided CAHs efficiently. According to the observed data, the order of reactivity among chloroethenes is TCE > PCE > cDCE. This agrees with a study by VanStone et al. (2004) that reported two different orderings in the relative reactivity of chloroethenes depending on the iron type used in experiments (VanStone et al., 2004). cDCE concentrations were found to be higher when PCE and TCE degradation started, suggesting that part of PCE and TCE degradation follows the hydrogenolysis pathway (Arnold and Roberts, 2000). 1,1,1-TCA degraded faster than the examined chlorinated ethenes. This might be due to differences in bond strength between ethenes and ethanes (sp2 > sp3) (Scherer et al., 1998). More specifically, the carbon-to-carbon double bond (611 kJ mol^{-1}) is stronger than a single covalent bond (347 kJ mol^{-1}) (Wade, 2006) and the energy required to break a double bond is higher than for a single bond. The final degradation products were 1,1-DCA, ethene (reactive intermediate mainly transformed to ethane) and ethane, which is in line with the reported degradation pathways (Arnold and Roberts, 2000; Liu et al., 2005). VC as intermediate product did not increase significantly. During the batch experiments drastic decreases in ORP (from +275 mV to -485 mV) and elevated pH were observed, as expected (Figure 31). The pH increase from near neutral to approximately pH 10 is due to proton consumption by reductive dechlorination and anaerobic corrosion (Dries et al., 2005).

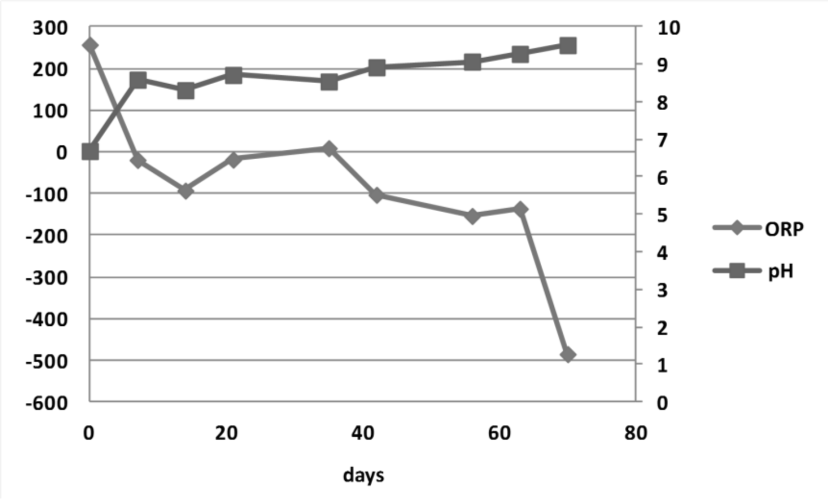

Figure 31 - Change of pH and ORP values over time (days).

5.3.4. REMOVAL KINETICS OF DIFFERENT CAHS BY GUAR GUM STABILIZED MZVI

Despite successful stabilization of mZVI particles, strong adsorption of guar gum chains to the surface of iron particles and limited diffusion of the contaminants before adding the enzymes might inhibit CAH degradation rates. To examine the CAH degradation efficiency of guar gum stabilized mZVI, lab scale CAH degradation experiments were performed with three different guar gum concentrations (Table 16). As shown in Figure 30, all examined guar gum concentrations show a clear negative impact on the reactivity of mZVI, which is in line with observations described for granular zerovalent iron particles (Focht et al., 2001). Guar gum improved the stability of mZVI, but seems to alter the surface of the mZVI resulting in decreased degradation rates of all tested CAHs compared to original non-stabilized mZVI. Because cDCE (k_{ow} = 1.86) is much more hydrophilic than PCE (k_{ow} = 2.88), TCE (k_{ow} = 2.53) and 1,1,1-TCA (k_{ow} = 2.49), the cDCE availability is less affected by partition into guar gum resulting in less affected cDCE remediation by coupled mZVI (Mackay et al., 2003). For other compounds, degradation rates were more negatively affected by using guar gum as iron stabilizer due to hydrophobicity of the PCE, TCE and 1,1,1-TCA.

Radial diffusion tests for dextrin blue in different guar gum concentrations (2, 4 and 6 g L^{-1}) were performed by measuring the diameter of the diffusion zone. Dextrin blue diffused from the spot where it was initially placed into the guar gum (Figure 32), with the fastest diffusion for the lowest guar gum concentration (2 g L^{-1} of GG).

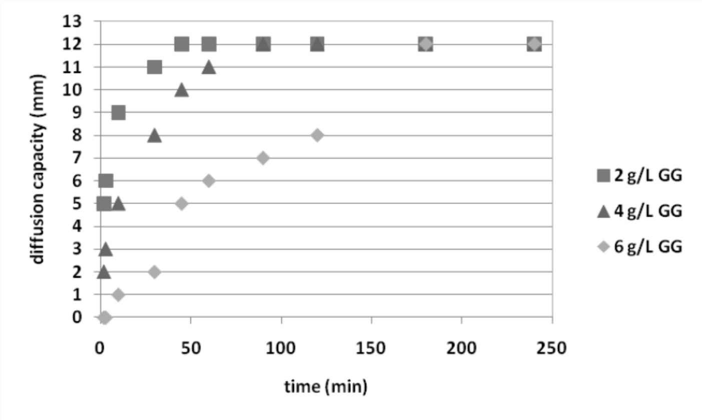

Figure 32 - Results of radial diffusion test for dextrin blue in different guar gum concentrations. Tube open from the both sides (Ø 8 mm) was placed in the middle of the plate (Ø 8 cm) containing 5 mm thick guar gum solution in different concentrations (2, 4 and 6 g L-1). To determine guar gum diffusion rate tube was filled with 500 µL of dextrin blue solution. Tube was removed from the plate, while dextrin blue suspension started to diffuse from the spot where was placed into the guar gum. Radial diffusion was observed measuring the diameter of the dextrin blue diffusion zone.

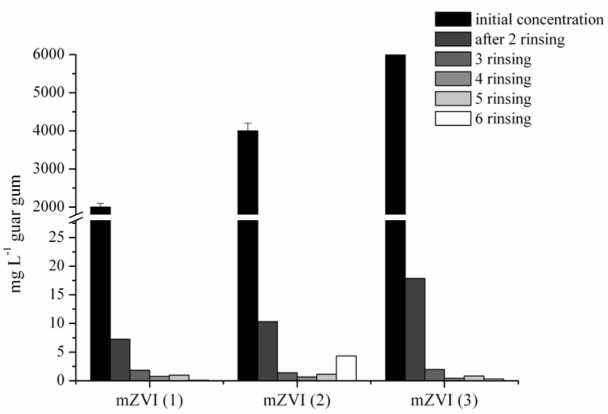

Figure 33 - Guar gum (GG) concentration after guar gum breakdown and during flushing of guar gum lower molecular weight products from the batch systems (1) mZVI + 2g L^{-1} GG; (2) mZVI + 4g L^{-1} GG; (3) mZVI + 6g L^{-1} GG.

The correlation between the guar gum concentration and decreasing degradation rates might be explained by the polymeric network that hindered pollutant migration towards the ZVI due to the high guar gum concentration. The increase of final degradation products such as ethene and ethane, was significantly lower than for non-stabilized mZVI. In contrast with PCE, TCE and cDCE, relatively rapid 1,1,1-TCA reduction and 1,1-DCA formation by guar gum coupled mZVI was observed. Mass recoveries were calculated (89 – 98 %) and no indications for adsorption of 1,1,1-TCA on the guar gum were obtained. This could be explained by parallel pathways involving reductive *α*-elimination and coupling, in competition with hydrogenolysis (Fennelly and Roberts, 1998), which seems to be less sensitive to the presence of higher guar gum concentrations than *β*-elimination (Arnold and Roberts, 2000).

To investigate whether breakdown of the polysaccharide guar gum to soluble oligosaccharides would restore the reactivity of the mZVIs, the enzyme LEB-H^{TM} was added in two of the four vials for guar gum degradation. The main assumption was that the reactivity of mZVI could be improved by increasing the accessibility of the mZVI by guar gum breakdown. However, the reactivity of mZVI towards the CAH mixture remained limited (Figure 30), although some improvements could be observed especially for the highest guar gum concentration towards PCE and TCE. Also, first-order rate linearity increases with degradation of guar gum which can be seen in Table 16. In the next step, the guar gum breakdown fragments were removed by replacing the liquid phase in the batches with new simulated groundwater, polluted by selected CAHs (1 batch volume). This mimics to a certain extent the groundwater flow through an in-situ injection area. After one flushing event, only the reactivity of mZVI stabilized with 2 g L^{-1} of guar gum increased, but not drastically (results not shown). A more intensive iron rinsing (up to 6 batch volumes) was included to decrease further the concentration of remaining guar gum breakdown fragments. Figure 33 shows that the guar gum concentration in batch systems decreased rapidly during the rinsing process.

After intensive rinsing process, a significantly enhanced reactivity of mZVI could be observed (Figure 30). The degradation rates of PCE, TCE, cDCE and 1,1,1-TCA were significantly faster than the ones calculated for the guar gum stabilized mZVI and in the same order of magnitude of the rates determined for mZVI before stabilization. Similar trends were obtained for other types of mZVIs (results not shown). The results clearly indicate that the reactivity of stabilized mZVI particles could be restored completely, except for PCE and TCE degraded by iron particles stabilized by 6 g L^{-1} of guar gum. This can be explained by (1) low amount of guar gum remaining as a coupling layer on the mZVI, and by (2) the higher hydrophobicity of these two compound compared to cDCE and 1,1,1-TCA. Even slightly faster degradation rates were observed for mZVI than before stabilization especially for iron stabilized by 2 g L^{-1} and 4 g L^{-1}. After guar gum breakdown, acetic acid was detected in high concentrations, up to 10 g L^{-1}. The associated decreased pH (from pH 9.4 to pH 8.5) may have stimulated the dissolution of the iron oxide layer, resulting in an improved reactivity. A similar effect was reported before for a ZVI - polyhydroxybutyrate (PHB) column system. The effluent pH observed for ZVI column was 7.5-8, while for ZVI – PHB column system was 6.2-6.3 (Baric et al., 2012).

The significantly reduced reactivity of stabilized mZVI could be explained by guar gum adsorption blocking available iron reactive sites responsible for the reductive dechlorination. Recently, the negative effect of adsorbed polyelectrolyte coatings on nZVI particles reactivity towards TCE has been reported, and was explained by a combination of direct blocking of reactive surface sites and decreased TCE concentrations near the nZVI surface (Phenrat et al., 2009). In our study, compared to 6 g L^{-1} of guar gum, lower guar gum concentrations (2 and 4 g L^{-1}) had generally less impact on mZVI reactivity after guar gum enzymatic breakdown and intensive rinsing. Possible explanations for this observation are the reaction of ZVI with hydroxyl functional groups of the guar gum or strong sorption of guar gum on the iron surface preventing contact between mZVI and the pollutant. The same explanations were proposed for nZVI particles immobilized in alginate bead (Kim et al., 2010). The correlation between increasing guar gum concentration and decreasing TCE degradation rates was also observed for FePd nanoscale particles (Sakulchaicharoen et al., 2010). The same research group reported effective complexation between guar gum and FePd nanoscale particles.

Table 16 : Summary of the results for PCE, TCE, cDCE and 1,1,1-TCA degradation by mZVI (50 g L^{-1}) in different conditions.

	PCE (5 mg L^{-1})[a]			TCE (5 mg L^{-1})			cDCE (5 mg L^{-1})			1,1,1-TCA (5 mg L^{-1})		
	k_{ob}[b]	SD*	R^2 (n)[c]	k_{ob}	SD	R^2 (n)	k_{ob}	SD	R^2 (n)	k_{ob}	SD	R^2 (n)
50 g L^{-1} mZVI	1.29x10^{-3}	5.19x10^{-5}	0.76 (11)	2.20x10^{-3}	3.81x10^{-5}	0.85 (4)	2.84x10^{-4}	5.30x10^{-5}	0.76 (11)	8.22x10^{-3}	1.94x10^{-4}	0.94 (4)
Stabilized mZVI (1)[d]	1.75x10^{-4}	1.18x10^{-5}	0.55 (13)	2.96x10^{-4}	5.90x10^{-6}	0.76 (13)	3.38x10^{-4}	5.90x10^{-6}	0.22 (13)	2.05x10^{-3}	3.54x10^{-5}	0.92 (13)
mZVI (1) after enzymes addition	2.02x10^{-4}	6.18x10^{-5}	0.78 (3)	3.29x10^{-4}	4.71x10^{-5}	0.89 (3)	6.88x10^{-5}	6.88x10^{-8}	0.58 (3)	2.19x10^{-3}	2.06x10^{-5}	0.99 (3)
Rinsed mZVI (1)	2.54x10^{-3}	3.15x10^{-4}	0.98 (4)	4.30x10^{-3}	7.37x10^{-5}	0.76 (4)	1.18x10^{-3}	1.45x10^{-4}	0.99 (4)	3.44x10^{-2}	2.34x10^{-3}	1.00 (4)
Stabilized mZVI (2)[e]	1.60x10^{-4}	8.82x10^{-6}	0.27 (13)	1.58x10^{-4}	5.88x10^{-6}	0.68 (13)	3.27x10^{-4}	2.65x10^{-5}	0.53 (6)	1.20x10^{-3}	1.02x10^{-4}	0.95 (13)
mZVI (2) after enzymes addition	2.02x10^{-4}	2.65x10^{-5}	0.55 (3)	3.44x10^{-4}	1.47x10^{-5}	0.71 (3)	2.94x10^{-4}	2.65x10^{-5}	0.62 (3)	1.54x10^{-3}	1.15x10^{-4}	0.97 (3)
Rinsed mZVI (2)	2.01x10^{-3}	1.09x1$^{0-4}$	0.97 (4)	3.37x10^{-3}	1.59x10^{-4}	0.99 (4)	8.88x10^{-4}	7.08x10^{-5}	0.99 (4)	2.68x10^{-2}	6.69x10^{-4}	1.00 (4)
Stabilized mZVI (3)[f]	1.94x10^{-4}	1.48x10^{-5}	0.26 (13)	1.04x10^{-4}	1.04x10^{-7}	0.36 (13)	4.52x10^{-4}	7.95x10^{-5}	0.76 (6)	1.08x10^{-3}	7.36x10^{-5}	0.92 (13)
mZVI (3) after enzymes addition	4.60x10^{-4}	4.42x10^{-5}	0.76 (3)	5.60x10^{-4}	2.65x10^{-5}	0.85 (3)	4.79x10^{-4}	4.12x10^{-5}	0.87 (3)	1.63x10^{-3}	4.13x10^{-5}	0.97 (3)
Rinsed mZVI (3)	8.65x10^{-4}	3.50x10^{-5}	0.89 (4)	1.78x10^{-3}	6.14x10^{-5}	0.98 (4)	8.88x10^{-4}	7.08x10^{-5}	0.99 (4)	1.69x10^{-2}	3.38x10^{-3}	1.00 (4)

[a] Initial concentration or concentration range; [b] k_{ob} the first order decay constant (h^{-1}); [c] *n*, number of data points; [d] *(1)* 50g L^{-1} mZVI + 2g L^{-1} GG; [e] *(2)* 50g L^{-1} mZVI + 4g L^{-1} GG; [f] *(3)* 50g L^{-1} mZVI + 6g L^{-1} GG; * standard deviation.

5.3.5. ADSORPTION MECHANISM OF GUAR GUM STABILIZED MZVI

The surface morphology and composition of reacted non-stabilized mZVI and guar gum stabilized mZVI material were compared to explain the effect of the guar gum on mZVI reactivity. EDS mapped images of non-stabilized mZVI (Figure 34) and stabilized mZVI (Figure 35) from the batch degradation test, show that in contrast to non-stabilized mZVI, a lot of carbon was present on most of the stabilized iron grains. This carbon can be associated with thick polymer coatings, being guar gum sorbed onto the mZVI and blocking reactive iron spots. The restoration of the mZVI reactivity after treatment by enzymes and intensive rinsing, was also indicated by SEM-EDS by less carbon on the iron grains, similar to reacted non-stabilized mZVI. Chloride was observed only in reacted non stabilized mZVI (Figure 34 (D)).

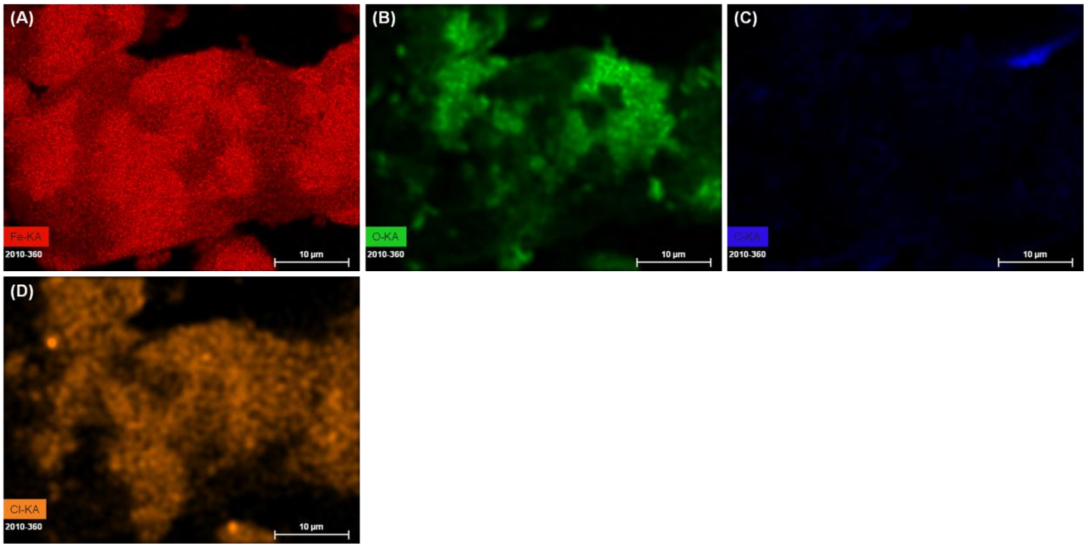

Figure 34 - The SEM-EDS elemental maps (scale 10 µm) of Fe Kα (A), O Kα (B), C Kα (C) and Cl Kα (D) collected from the reacted non-stabilized mZVI.

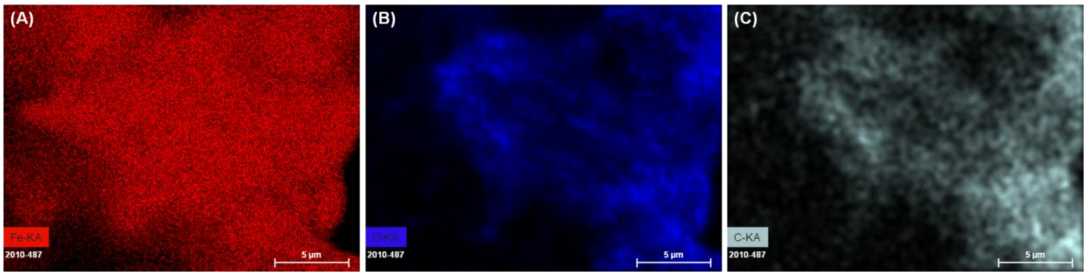

Figure 35 - The SEM-EDS elemental maps (scale = 5 µm) of Fe Kα (A), O Kα (B) and C Kα (C) collected from stabilized mZVI.

The interaction mechanism between various polysaccharides (e.g. starch, dextrin, guar gum and carboxymethyl cellulose) and mineral surfaces has been studied widely (Laskowski et al., 2007; Lin et al., 2010; Liu et al., 2000; Liu and Laskowski, 1989; Ma and Pawlik, 2007; Rath et al., 2001). To further explain the stabilization mechanisms and adsorption configuration between mZVI and guar gum in this particular case, a FTIR study was carried out. Before the FTIR study, the pH-values measured in the batch systems decreased with increasing guar gum concentrations. For non-stabilized mZVI, pH 9.75 was recorded, while in the presence of 2, 4 and 6 g L^{-1} guar gum, pH 9.41, pH 8.24 and pH 7.04 were measured, respectively. The observed pH-shift can be explained by surface interaction between guar gum and iron-hydroxylated species formed during iron reaction with water (Liu et al., 2000). The infrared spectra of non-stabilized mZVI, guar gum stabilized mZVI and only guar gum shown in Figure 36 could be used to explain the stabilization mechanism and the negative impact of guar gum on iron reactivity.

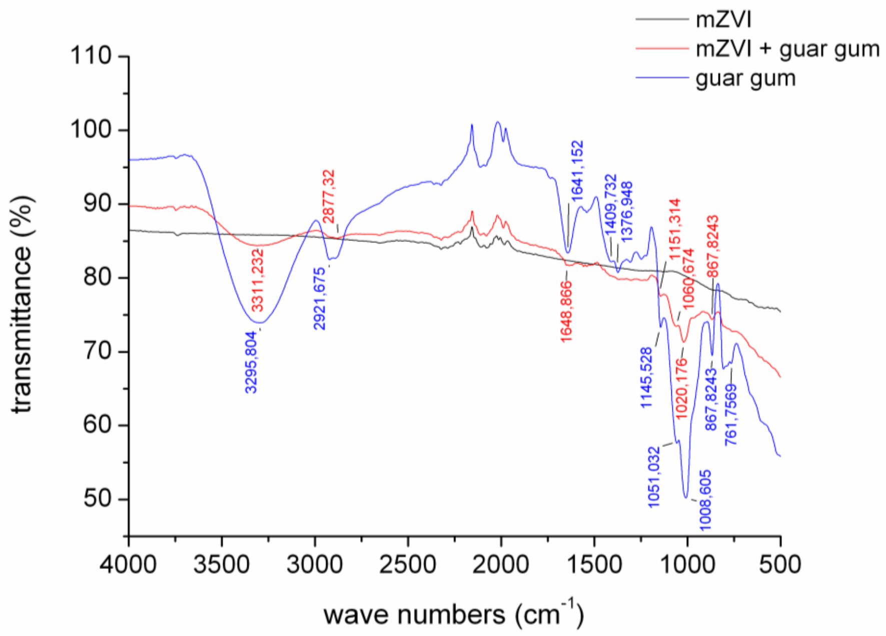

Figure 36 - FTIR spectra of the non-stabilized mZVI, guar gum stabilized mZVI and guar gum powder as a reference.

Non-stabilized mZVI infrared spectra show no apparent IR signal, as observed by other researchers as well (Lin et al., 2010). Similar bands for guar gum observed in this study have been reported by other researches (Liu and Laskowski, 1989). Iron coupled with guar gum spectra reveal a few differences compared to the guar gum, pointing towards intermolecular interactions between guar gum and iron. Table

17 shows characteristic peak assignments for guar gum and guar gum coupled iron.

Table 17 : Characteristic IR frequencies of guar gum Apcol (150) and guar gum coupled mZVI.

Wave number (cm^{-1})	**Wave number (cm^{-1})**	**Peak assignment**
Guar gum	**Coupled mZVI**	
3296	3311	O-H stretching vibration
2921	2877	C-H stretching of CH_2 group
1641	1649	Ring stretching
1377, 1410		Symmetrical deformations of CH_2 group
1146, 1051	1151, 1061	C-OH and primary alcoholic CH_2OH stretching mode
1009	1020	- CH_2 twisting vibration
868	868	Galactose and mannose
761		(1-4), (1-6) linkage of mannose

The shift of the broad band at 3296 to 3311 cm^{-1} assigned to the hydrogen-bonded hydroxyl groups for guar gum and coupled mZVI, respectively, may imply an interaction of the mZVI via hydrogen bonding. The band shift from 1008 cm^{-1} to 1020 cm^{-1} and the band shift from 2921 cm^{-1} to lower wave numbers after iron coating indicates a possible deformation of the $–CH_2$ group connected to the hydroxyl group. Due to interaction of the iron and hydroxyl groups of the guar gum, the bands at 1146 and 1051 cm^{-1} appear slightly altered after adsorption. Further, the band at 868 cm^{-1} appears at almost the same wave numbers after adsorption of guar gum, confirming the adsorption between mZVI and guar gum with no change in the sugar structures. Significantly reduced intensity of band at 761 cm^{-1} might be influenced by mZVI presence as a large part of the mixture in the coupled case. After iron stabilization with guar gum, the manifested spectral changes indicated guar gum adsorption onto the mZVI. In addition, the results point towards intermolecular interaction with possible hydrogen bonding between mZVI and guar gum (Laskowski et al., 2007; Ma and Pawlik, 2007). The adsorbed guar gum might affect the particle surface reactivity by inhibiting: (1) diffusion of CAHs to reactive sites (Kortunov et al., 2005), (2) adsorption of CAH to these reactive sites, and/or (3) surface reaction at specific active sites due to possible intermolecular interaction between iron and guar gum and/or competition of guar gum with CAHs for surface sites (Phenrat et al., 2009; Tratnyek et al., 2001).

5.4. CONCLUSIONS AND PERSPECTIVES

In order to improve the mobility of mZVI particles during an injection, the use of stabilizers such as guar gum is necessary. This study, however, proves that, initially, guar gum negatively impacts ZVI reactivity. As intensive rinsing was found to be necessary to recover the mZVI reactivity, the degradation of guar gum and removal of guar gum degradation products must be considered for in-situ applications. The guar gum break down can be realized by the addition of commercial enzymes, and groundwater flow can dilute and remove the guar gum degradation fragments. However, these processes require time and result in temporarily sub-optimal mZVI reactivity. The duration of this period depends on site conditions (e.g. groundwater flow, velocity) and should be taken into consideration when judging the performance of the mZVI reactive zone. After removal of the guar gum, the mZVI has been shown to functioning at least as good as non-stabilized material, which confirms the compatibility of guar gum and ZVI (Focht et al., 2001; Navon et al., 1998). In addition, the guar gum degradation products may be expected to serve as electron donors for potentially present CAH-degrading microorganisms and in this way stimulate CAH-biodegradation (Phillips et al., 2003; Truex et al., 2011). Overall, this study suggests that guar gum stabilized mZVI particles might be considered as potentially effective for the in-situ treatment of CAHs because the inactivation of stabilized mZVI is temporary.

CHAPTER 6 GUAR GUM COUPLED MZVI FOR IN-SITU TREATMENT OF CAHS: CONTINUOUS-FLOW COLUMN STUDY

Based on: Velimirovic, M., Simons, Q., Bastiaens, L. Guar gum coupled mZVI for in-situ treatment of CAHs: continuous-flow column study. Submitted to Journal of Hazardous Materials.

6.1. INTRODUCTION

Two decades after Gillham and O'Hannesin (1992) introduced the zerovalent iron (ZVI) particles as a new concept to efficiently treat groundwater contaminated with chlorinated aliphatic hydrocarbons (CAHs), permeable reactive barriers (PRBs) are a common technology for in-situ remediation of CAHs. PRBs are constructed in the subsurface by digging and refilling a trench using granular ZVI (Gillham and O'Hannesin, 1992; 1994), which is technically and economically possible for limited depths (Day et al., 1999). To reduce the cost of PRB installation and expand the application area of ZVI, researchers focused more recently on micro- and nanoscale ZVI particles. These particles have higher reactivity towards different CAHs and the potential to be injected in the deep subsurface (> 10-20 m) as slurry creating in-situ reactive zones (RZ). However, estimated life-times of several weeks for nanoscale zerovalent iron (nZVI) particles (He and Zhao, 2007; Noubactep et al., 2012) as well as fast aggregation and filtration in the porous medium with reduced radius of influence (Schrick et al., 2004; Kanel et al., 2007; Saleh et al., 2007; Phenrat et al., 2009; Tiraferri and Sethi, 2009), indicate that injection of nZVI slurry is more challenging than initially expected. On the other hand, microscale zerovalent iron (mZVI) particles have longer life times (Reardon, 2005; Chen et al., 2011), they are less expensive and pose less risk for human health than nZVI particles (Lee et al., 2008). Nevertheless, sedimentation of mZVI particles in the slurry reservoir, tubing and injection wells prior to and during injection, which is a consequence of the high density and size of particles (Elimelech et al., 1995; Vecchia et al., 2009), is crucial when designing mZVI reactive zones.

To prevent sedimentation of mZVI particles during the injection period, the use of shear thinning fluids may offer a solution to transport mZVI particles through porous media (Cantrell et al. 1997; Oostrom et al., 2007; Vecchia et al., 2009; Truex et al., 2011; Xue and Sethi, 2012). Comba and Braun (2012) reported guar gum as a polymer suitable to keep mZVI particles in suspension. Guar gum is a common biopolymer for stabilizing trenches during the soil excavation and construction of a treatment walls (Navon et al., 1998; Di Molfetta and Sethi 2006), but inactivation of ZVI reactivity by guar gum has been reported (Navon et al., 1998). In Chapter 5 detailed batch degradation study provided that guar gum negatively impacts the reactivity of mZVI in liquid medium. However, once guar gum was degraded and breakdown products removed, full recovery of the mZVI reactivity was obtained (Velimirovic et al., 2012).

Here the results of a column test that was performed under in-situ conditions to evaluate the impact of guar gum on the degradation efficiency of mZVI particles in the presence of aquifer material and under continuous groundwater flow conditions are reported. Special attention was given to (1) the duration of the inactivation period for guar gum stabilized mZVI particles, and (2) the ability of naturally present microorganisms to degrade the guar gum to soluble oligosaccharides, as a substitute for commercial enzymes used in our previous study. In addition, the impact of mZVI and guar gum on the naturally present soil bacterial community was examined via microbial analyses performed at the end of the experiment using 16S rRNA genes based molecular techniques.

6.2. MATERIALS AND METHODS

6.2.1. MICRO IRON PARTICLES

The reactive mZVI particles used in this study were obtained from Höganäs (Sweden). Characteristics of the particles are given in Table 18. Guar gum HV7000 (Rantec Corporation, USA) was used as mZVI stabilizer.

Table 18 : Characteristic of studied mZVI.

Sample	PSD[a] D_{10}, D_{50}, D_{90} (µm)	Carbon content (%)	Oxygen content (%)	Sulfur content (%)	Nitrogen content (%)	BET[b] ($m^2\ kg^{-1}$)
mZVI	24, 56, 69	0.02	1.10	0.00	0.02	57

[a]Particle Size Distribution;
[b]BET : Specific Surface Area according to Brunauer-Emmett-Teller (Single point measurement) - analysis was conducted by Höganäs.

6.2.2. COLUMN TEST

The one dimensional column test set up is shown in Figure 37.

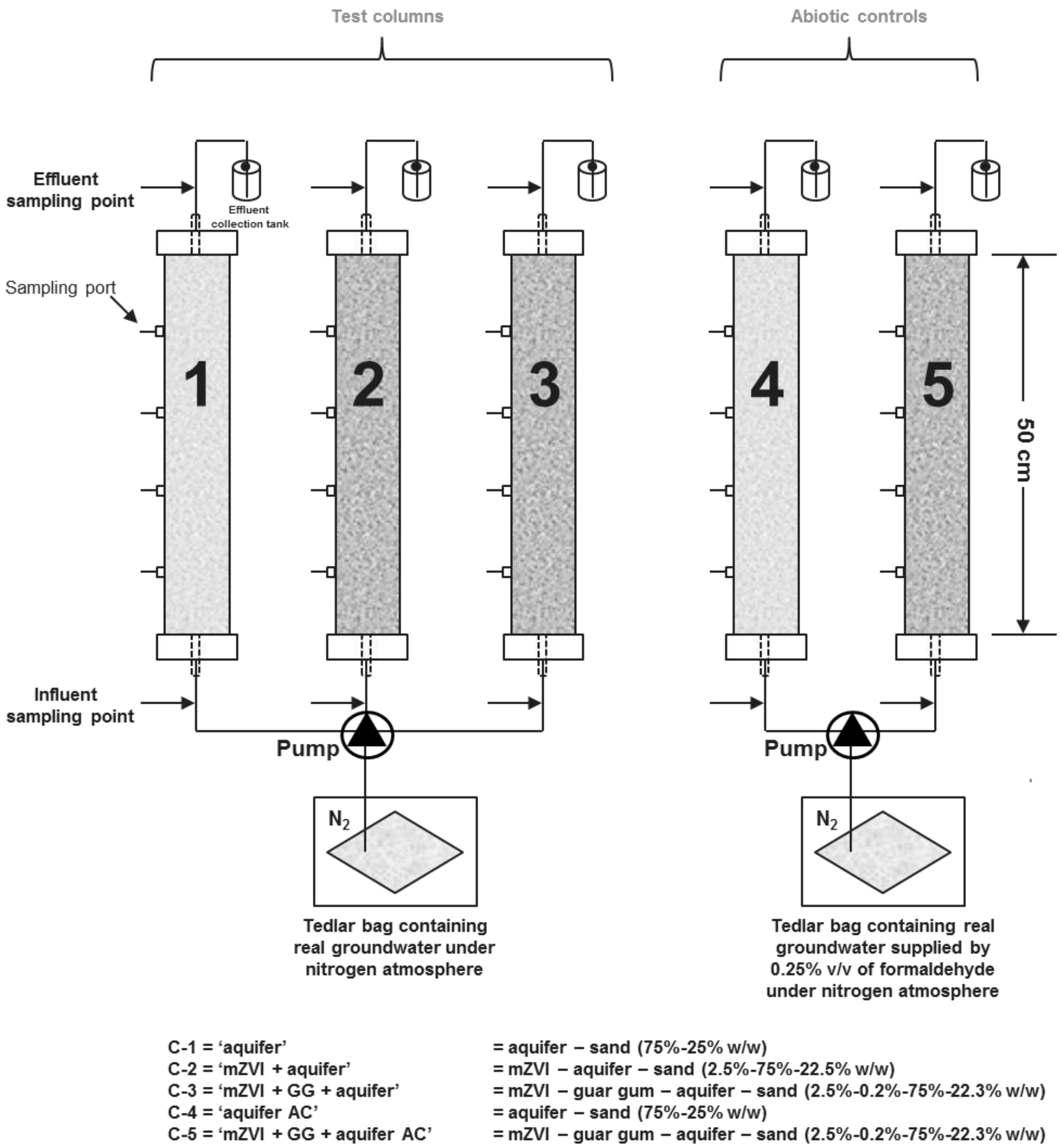

Figure 37 - Schematic overview of the laboratory continuous flow column test set up. All columns were operated under anaerobic conditions. C- 4 and C-5 were included as abiotic controls (AC). GG = guar gum.

Five flow-through plexiglas columns (height, 50 cm; inside diameter, 4 cm) were set-up under anaerobic conditions with representative CAHs-contaminated groundwater and aquifer material (8 m bgs) from a real contaminated site in Belgium. Detailed groundwater chemistry and aquifer contamination are presented in Table 19 and Table 20 respectively.

Table 19 : Groundwater chemistry applied to column study.

Field parameters	**Unit**	
temperature	°C	12.5 ± 0.1
pH		5.75 ± 0.02
ORP	mV	-56 ± 10
Conductivity	μs cm^{-1}	858 ± 0
Dissolved O	mg L^{-1}	0.59 ± 0.07
Redox parameters	**Unit**	
CO_3^{2-}	mg L^{-1}	0.00
HCO_3^-	mg L^{-1}	82.3
Dissolved Ca	mg L^{-1}	34.2
Dissolved Fe	mg L^{-1}	121
Dissolved Mn	mg L^{-1}	0.62
Cl^-	mg L^{-1}	114
SO_4^{2-}	mg L^{-1}	201
CAHs	**Unit**	
Chloroethane	μg L^{-1}	30 ± 9
1,1-dichloroethene	μg L^{-1}	310 ± 17
Trans-dichloroethene	μg L^{-1}	42 ± 1
1,1-dichloroethane	μg L^{-1}	6047 ± 382
Cis-dichloroethene	μg L^{-1}	1806 ± 639
1,1,1-trichloroethane	μg L^{-1}	15 ± 3
trichloroethene	μg L^{-1}	344 ± 109
tetrachloroethene	μg L^{-1}	17 ± 13
Vinyl chloride	μg L^{-1}	7 ± 2

Table 20 : Contamination of soil applied to column study.

CAHs	**Unit***	
Chloroethane	μg kg^{-1}	28 ± 2
1,1-dichloroethene	μg kg^{-1}	12 ± 5
Trans-dichloroethene	μg kg^{-1}	3 ± 0
1,1-dichloroethane	μg kg^{-1}	158 ± 17
Cis-dichloroethene	μg kg^{-1}	13 ± 8
1,1,1-trichloroethane	μg kg^{-1}	1 ± 1
trichloroethene	μg kg^{-1}	15 ± 0
tetrachloroethene	μg kg^{-1}	2 ± 1
Vinyl chloride	μg kg^{-1}	BDL

* μg per kg of dry aquifer material
BDL – below detection limit

The aquifer was mixed with filter sand (1-2 mm, considered nonreactive, 25 % w/w) to increase the conductivity of the medium. The first column (C-1) was completely filled with the aquifer/sand mixture without mZVI to investigate the biodegradation potential of aquifer material from site. Column 2 (C-2) contained the same filling material amended with 25 g kg^{-1} of mZVI to investigate the reactivity of non-stabilized mZVI. To compare reactivity of non-stabilized and guar gum stabilized mZVI, Column 3 (C-3) was amended with 25 g kg^{-1} of mZVI as well as 2 g kg^{-1}

of guar gum. Column 4 (C-4) and 5 (C-5) were poisoned by addition of 0.25 % v/v of formaldehyde to the feed (Van Nooten et al., 2008) and served as abiotic controls (AC) of C-1 and C-3.

The columns were fed with the real groundwater mainly polluted by 1,1-DCA (5.4 ± 0.9 mg L^{-1}), TCE (0.5 ± 0.1 mg L^{-1}), cDCE (0.9 ± 0.4 mg L^{-1}) and 1,1-DCE (0.7 ± 0.4 mg L^{-1}). The groundwater was continuously pumped (Watson Marlov 205s peristaltic pump) in an upward flow through the columns with an average total flow rate of 18.18 ± 2.67 mL day^{-1}, corresponding to an initial pore water velocity of 4.38 ± 1.82 cm day^{-1}. Pore volume and porosity were based on weight and volume measurements. Characteristics of every column individually are given in Table 21. The columns were operated at temperature of 12°C.

Table 21 : Characteristics of the columns used for CAHs remediation.

Characteristic	C-1	C-2	C-3	C-4	C-5
Solid weight (g)	1121	1051	862	1034	871
Iron concentration(g kg^{-1})	-	25	25	-	25
Guar gum concentration (g kg^{-1})	-	-	2	-	2
Pore volume (mL)	224	143	213	292	253
Flow velocity (ml day^{-1})	20.8	20.9	18.0	16.5	14.7
Effective velocity (cm day^{-1})	4.64	7.31	4.23	2.83	2.91
Porosity	0.08	0.05	0.08	0.11	0.09

To avoid accidental microbial contamination, columns and columns parts were sterilized by autoclaving before start of experiment.

During operation, influent and effluent of the columns were sampled every two weeks for measurements of CAHs concentrations and their breakdown products. 5 mL of liquid samples was directly collected by connecting 12 mL vials (previously capped and flushed with nitrogen) to a sampling port allowing the samples to spontaneously flow into the vials. In addition, after 4, 5 and 6 months of operation, liquid samples were taken at intermediate sampling points located at every 10 cm along the column, to determine CAHs concentrations and their breakdown products. pH and ORP were measured in effluent samples after 4, 5 and 6 months of column operation.

After 5 months of column operation 100 µL of effluent samples were withdrawn for adenosine tri-phosphate (ATP) analysis as an indicator for viable biomass estimation in groundwater (Eydal and Pedersen, 2007; Hammes et al., 2010; Vital et al., 2012).

6.2.3. COLUMN DISMANTLING

After more than 6 months of operation (corresponding to 15 ± 5 pore volumes), the columns were dismantled in an anaerobic glove box (Jacomex, France). Column filling was vertically divided into ten sections of 5 cm length, beginning at the influent side of the column. For selected column sections (0-5 cm, 20-25cm and 40-45cm) composite subsamples of approximately 2 g were taken for DNA based microbial analyses. For guar gum analysis, approximately 5 g of homogenized sample was taken from selected selections (0-10 cm, 10-20 cm, 20-30cm, 30-40 cm and 40-50 cm) and extracted with 15 mL of anaerobic deionized water for one week. To quantify the remaining iron in solid samples, approximately 5 g of homogenized sample was taken from the same compartments.

6.2.4. CHEMICAL ANALYSIS

The concentrations of CAHs, intermediate- and end-products were determined via direct headspace measurements using a Varian GC-FID as reported in Chapter 2. An external calibration standard was prepared in the 12 mL vial with the same water/headspace volume ratio as samples. Redox potential (ORP) and pH were measured using a PHM62 electrode (Radiometer, Copenhagen) and PH535 electrode (WTW), respectively.

Guar gum concentration in effluent samples, as well as column fillings, was determined by the phenol–sulfuric acid tests using colorimetric method (Dubois et al., 1956). The absorbance measurements were performed using a Spectronic Genesys 6 UV–Vis spectrophotometer (Thermo Electron Corporation) with the maximum absorbance for guar gum occurring at λ_{max} = 490 nm.

To quantify remaining iron in solid samples, approximately 5 g of sample was mixed with 5 g of 1 M HCl. After one month of incubation, the hydrogen (H_2) gas produced was quantified as reported in Chapter 4. The amount of iron retained in column was calculated assuming that 1 mol of H_2 is produced for 1 mol of iron (Reardon, 1995).

6.2.5. CALCULATION OF RATE COEFFICIENTS

The pseudo-first-order model was applied to describe the reductive dechlorination of CAHs by mZVI and guar gum stabilized mZVI. The degradation rates were calculated by fitting the experimental breakthrough curves using the linear regression method. Residence times were calculated using porosity and water flow, while dispersion was neglected.

6.2.6. MICROBIAL CHARACTERIZATION

Adenosine tri-phosphate (ATP) analysis as an indicator for viable biomass was measured using the BacTiter-Glo™ reagent (G8231; Promega Corporation, Dübendorf, CH) and Luminoskan Ascent Microplate Luminometer (Thermo Labsystems). The BacTiter-Glo™ reagent was prepared according to the manufacturers' procedures and stored as previously described by Hammes et al. (2010). ATP reagent was warmed to 38°C, while 100 µL of effluent sample was transferred directly into the white wall multiwell plate; then 100µL BacTiter-Glo™ reagent was added and mixed properly with the sample. After 1 minute of incubation at room temperature luminescence was recorded as relative light units (RLU) with an integration time of 10 seconds. Calibration curve was made in the same way with a known ATP standard (Promega) ranging between 10-6 M to 10-12 M ATP including blank.

DNA was extracted from the aquifer/sand/(mZVI)samples as described by Hendrickx et al. (2005). Population dynamics was quantified using real time quantitative PCR (qPCR) with different group specific primer sets, targeting total bacteria (Muyzer et al., 1993; Smits et al., 2004), *Dehalococcoides* spp. (He et al., 2003; Sung et al., 2006)*, SRB* (Geets et al., 2005) and *Geobacter* (Holmes et al., 2002). Primers and probes were synthesized by Operon Biotechnologies GmbH (Cologne, Germany). All qPCR runs were performed on the Westburg Rotor-Gene 3000 (Corbett Research, Sydney, Australia) and the data were analyzed using the quantification analysis with the built-in software.

6.3. RESULTS AND DISCUSSION

6.3.1. CAHS DEGRADATION IN CONTINUOUS FLOW COLUMN SYSTEMS WITHOUT GUAR GUM

The timely evolutions of TCE, cDCE, 1,1-DCE and 1,1-DCA influent and effluent concentrations (Figure 38) indicate during the conditioning phase (week 1-7) some retardation of TCE, cDCE, 1,1-DCE and 1,1-DCA in columns (C-1 and C-4), explicable by sorption onto the aquifer solids. Once 3 pore volumes (PV) were pumped through the column (week 5-7), retardation of contaminants decreased and the columns were considered close to steady-state condition (60 – 82 % of contaminants were recovered from the influent sample). No CAH-biodegradation in the aquifer was observed as C-4 (AC) showed a similar pattern as C-1 (only "aquifer"). Additionally, no significant production of VC, ethene and ethane was observed in comparison with influent concentrations.

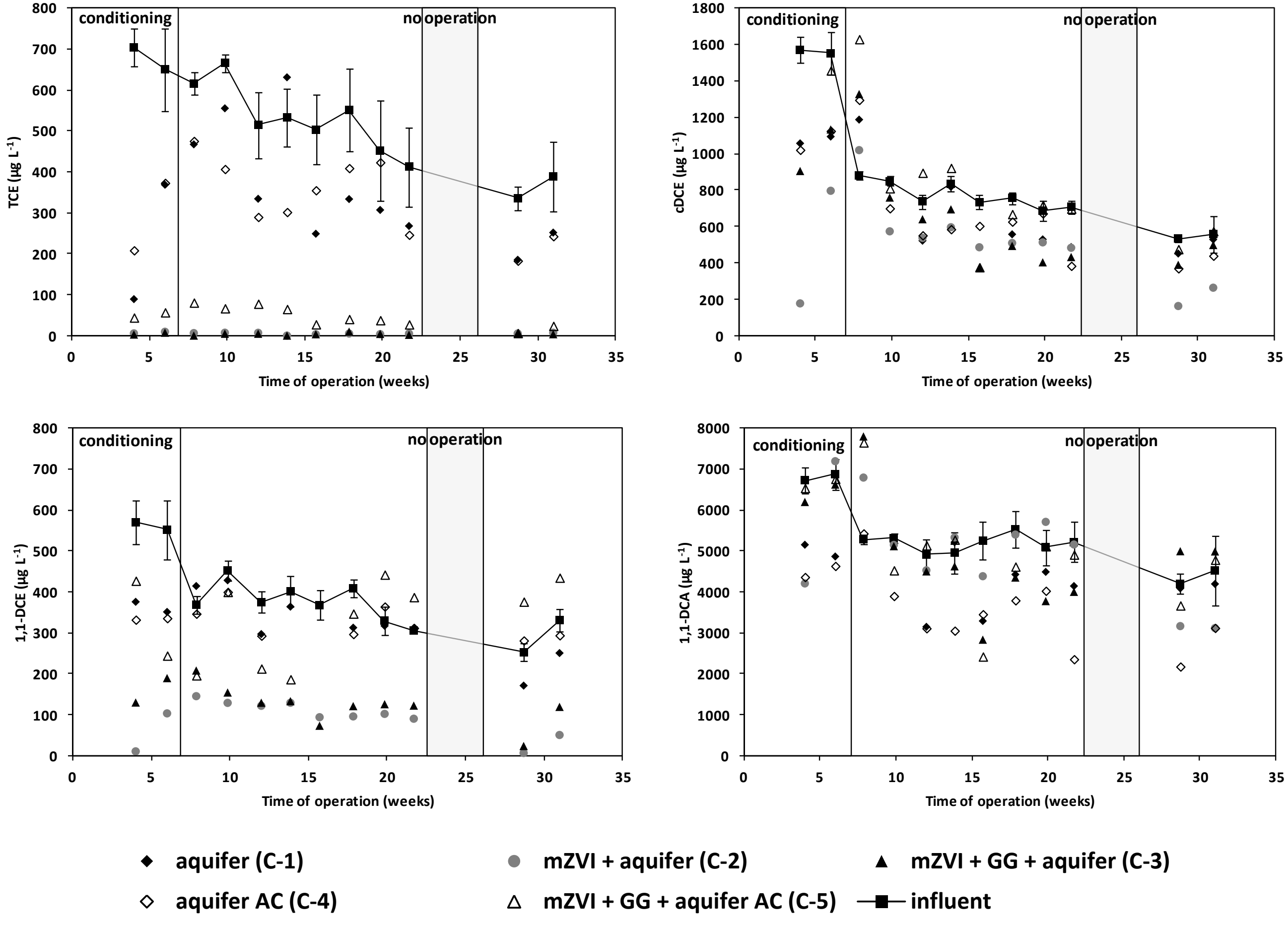

Figure 38 - Measured concentrations of TCE, cDCE, 1,1-DCE and 1,1-DCA in effluent samples of columns containing aquifer material (C-1), non-stabilized mZVI (C-2) and guar gum stabilized mZVI (C-3). Two abiotic controls were included: aquifer material (C-4) and guar gum stabilized mZVI (C-5). Average influent concentrations were also included for comparison.

In the presence of non-stabilized mZVI (C-2), the average removal of TCE was 100 %. cDCE, 1,1-DCE and 1,1-DCA effluent concentrations decreased 37, 76 and 8 %, respectively, compared to the influent. High efficiencies in TCE and 1,1-DCE removal might be explained by significantly lower concentrations present in the groundwater than for cDCE and 1,1-DCA. The main degradation products observed were ethene and ethane (Figure 39), while significant concentrations of VC and CA have not been observed. During passage of the water through column C-2, the average ORP decreased slightly from -56 ± 10 mV to -85 ± 28 mV, while the average pH value increased slightly from pH 5.75 ± 0.02 to pH 6.16 ± 0.57. These trends are explicable by anaerobic corrosion of the present mZVI (Shi et al., 2011). The pH change, however, is less pronounced than previously observed in the batch degradation experiments (Velimirovic et al., 2012). The buffering properties of the aquifer material in the columns and the continuous operation mode are possible explanations. The presented results show that the tested non-stabilized mZVI is highly efficient in reducing TCE and 1,1-DCE in aquifers under continuous flow conditions and can be used as a reactive material for in-situ applications. However, to prevent sedimentation of mZVI particles during the injection, stabilizing agents are necessary (Cantrell et al. 1997; Oostrom et al., 2007; Vecchia et al., 2009; Truex et al., 2011; Xue and Sethi, 2012).

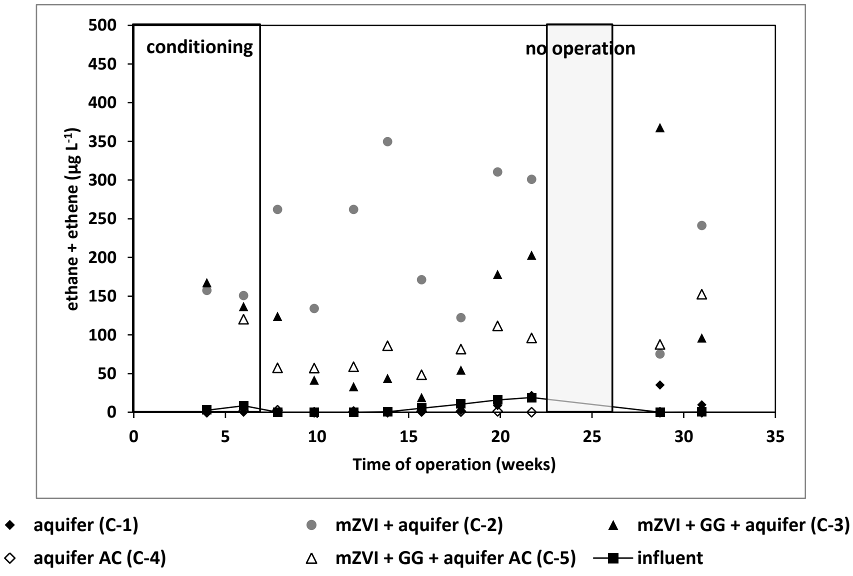

Figure 39 - Sum of ethene and ethane (µg L^{-1}) as end degradation products in continuous flow column experiments containing aquifer material (C-1), non-stabilized mZVI (C-2) and guar gum stabilized mZVI (C-3). Two abiotic controls were included: aquifer material (C-4) and guar gum stabilized mZVI (C-5). Average influent concentrations were also included for comparison.

6.3.2. CAHS REDUCTION BY GUAR GUM STABILIZED MZVI IN CONTINUOUS FLOW COLUMN SYSTEMS

The effect of guar gum (GG) on mZVI reactivity was examined by comparing the results of C-2 (non-stabilized mZVI), C-3 (GG-mZVI) and C-5 (GG-mZVI, abiotic control).

Guar gum concentrations measured in effluent samples of the columns revealed guar gum removal from both C-3 and C-5 (Figure 40) which is a crucial step for reactivity regeneration of GG-mZVI. Four weeks (1.5 PVs) after start-up, the guar gum concentration decreased significantly in the effluent of C-3, but not in the effluents of the abiotic control C-5, pointing towards biodegradation of guar gum in C-3. At that time, the effluent samplings for CAHs analyses were started.

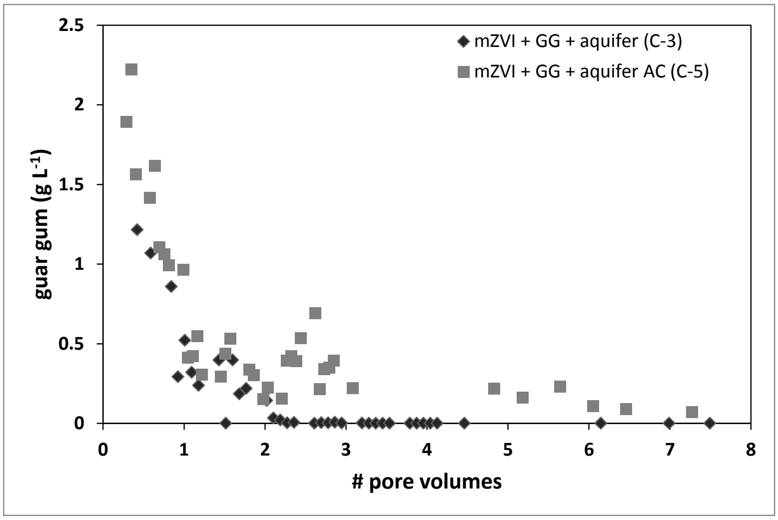

Figure 40 - Difference between guar gum (GG) concentration in effluent samples for the continuous column flow systems amended with guar gum stabilized mZVI (C-3) and its abiotic control (C-5) as a function of number of pore volumes pumped through the column.

The columns simulate a 50 cm wide in-situ reactive system with a groundwater flow velocity of approximately 10 m year^{-1}. According to data from a previously reported batch degradation study, where minimal 3 pore volumes were estimated to be required for full reactivity recovery of GG-mZVI (Chapter 5), a reduced reactivity period of approximately 2 months can be predicted for the column test. Data from the first CAH-measurements on (1.5 months after start) showed already that the TCE removal efficiency of GG-mZVI (C-3) was comparable to the non-stabilized mZVI (C-2) after conditioning phase (Figure 38).

The average efficiency of TCE removal in the columns was high (99 - 100%). On the other hand, for 1,1-DCE, 1,1-DCA and especially cDCE, a reduced removal was observed in C-3. At the end of the conditioning phase (2 months), the difference between C-2 and C-3 nearly disappeared. For cDCE, 1,1-DCE and 1,1-DCA, an average concentration decrease of 20, 67 and 8 % respectively was observed. An increase of final degradation products such as ethene and ethane was observed (Figure 39). However, significantly lower concentrations were observed for GG-mZVI and GG-mZVI (AC) compared to mZVI. The same was previously reported in batch tests (Velimirovic et al., 2012). ORP (-115 ± 33 mV) and pH (6.69 ± 0.08) values in the effluent of GG-mZVI amended column were similar to the column amended by non-stabilized mZVI.

To compare the reactivity of non-stabilized mZVI and GG-mZVI in more detail, TCE, cDCE, 1,1-DCE and 1,1-DCA concentration profiles along the columns were recorded. The results obtained after 4 months of operation (10 PV) are presented in Figure 41.

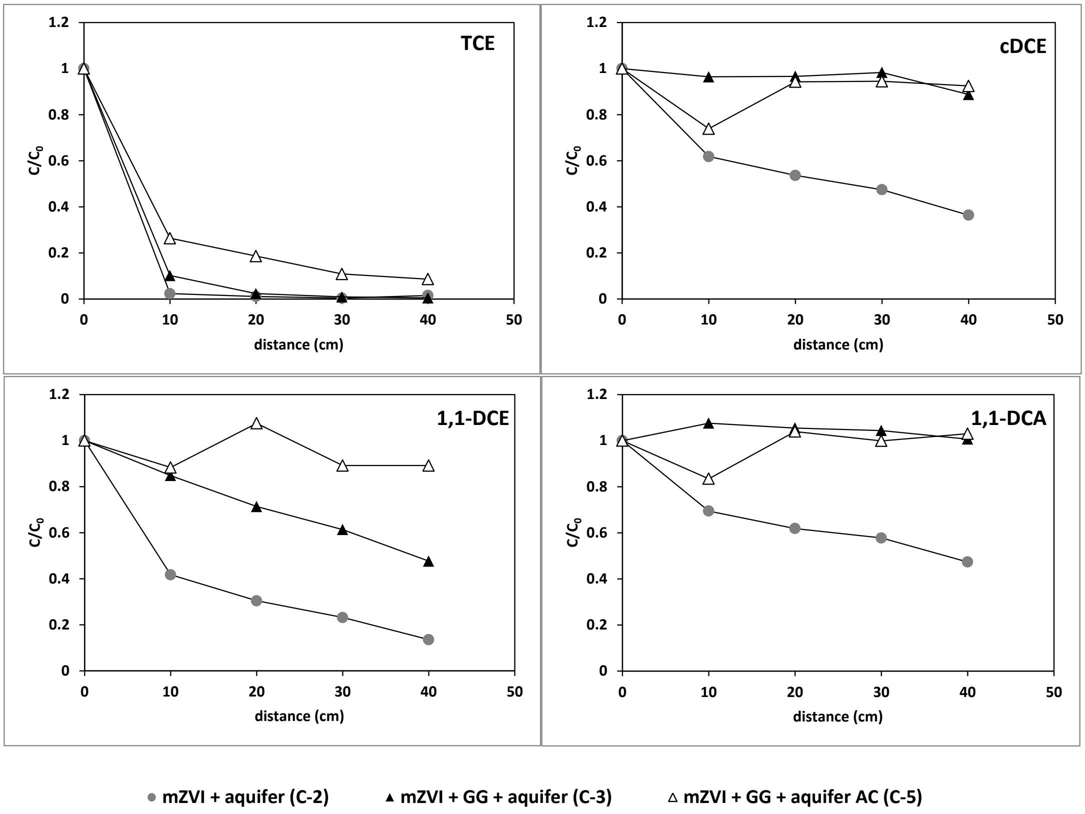

Figure 41 - Breakthrough curves for TCE, cDCE, 1,1-DCE and 1,1-DCA dechlorination using non-stabilized mZVI (C-2), GG-mZVI (C-3) and GG-mZVI - abiotic control (C-5) after 4 months of operation.

Table 22 : Summary of the results for TCE, cDCE, 1,1-DCE and 1,1-DCA disappearance rate constants with half life time of the selected chlorinated compounds in continuous flow column systems after 4, 5 and 6 months of operation.

	TCE **(0.5 ± 0.1 mg L^{-1})[a]**		**cDCE** **(0.9 ± 0.4 mg L^{-1})**		**1,1DCE** **(0.7 ± 0.4 mg L^{-1})**		**1,1-DCA** **(5.4 ± 0.9 mg L^{-1})**	
	k_{ob}[b]	$t_{1/2}$[c]	k_{ob}	$t_{1/2}$	k_{ob}	$t_{1/2}$	k_{ob}	$t_{1/2}$
After 4 months of operation								
mZVI + aquifer (C-2)	2.75 x 10^{0}	0.25	4.84 x 10^{-2}	14.3	1.15 x 10^{-1}	6.02	3.62 x 10^{-2}	19.2
mZVI + GG + aquifer (C-3)	9.62 x 10^{-1}	0.72	1.08 x 10^{-2}	64.2	3.64 x 10^{-2}	19.0	3.80 x 10^{-3}	183*
mZVI + GG + aquifer AC (C-5)	3.89 x 10^{-1}	1.78	1.57 x 10^{-3}	442*	1.82 x 10^{-2}	38.1	3.87 x 10^{-3}	179*
After 5 months of operation								
mZVI + aquifer (C-2)	2.60 x 10^{0}	0.27	5.69 x 10^{-2}	12.2	2.25 x 10^{-1}	3.08	3.02 x 10^{-2}	22.9
mZVI + GG + aquifer (C-3)	8.20 x 10^{-1}	0.85	1.02 x 10^{-2}	68.2	1.10 x 10^{-1}	6.30	4.36 x 10^{-2}	15.9
mZVI + GG + aquifer AC (C-5)	2.38 x 10^{-1}	2.92	1.63 x 10^{-3}	426*	3.46 x 10^{-2}	20.1	2.90 x 10^{-3}	239*
After 6 months of operation								
mZVI + aquifer (C-2)	2.51 x 10^{0}	0.28	7.37 x 10^{-2}	9.41	2.44 x 10^{-1}	2.84	5.52 x 10^{-2}	12.5
mZVI + GG + aquifer (C-3)	1.15 x 10^{0}	0.60	4.57 x 10^{-3}	152	5.77x 10^{-3}	120	ND*	ND*
mZVI + GG + aquifer AC (C-5)	7.82 x 10^{-1}	0.89	1.63 x 10^{-3}	426*	ND*	ND*	ND*	ND*

[a] Initial concentration or concentration range;

[b] k_{ob} the first order rate constant (day^{-1});

[c] $t_{1/2}$ half-life time (day);

[*] No degradation.

Guar gum has a slightly negative impact on the TCE removal by mZVI. Similar results were obtained after 5 months of operation. After 6 months, TCE-removal by GG-mZVI and mZVI was similar again. After 6 months of operation, however, the reactivity of GG-mZVI (abiotic control) was improved compared to the TCE-removal obtained after 4 and 5 months. This can be explained by the intensive rinsing process resulting in lower concentration of the guar gum present as a coupling layer on the mZVI (Velimirovic et al., 2012).

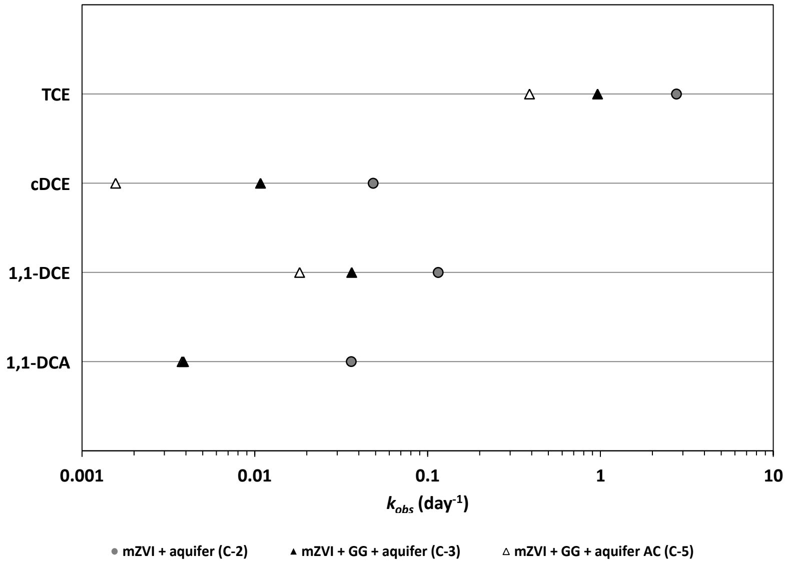

Figure 42 - Comparison of k_{obs} (day^{-1}) data obtained from continuous flow column study for non-stabilized mZVI (C-2), guar gum stabilized mZVI (C-3) and guar gum stabilized mZVI - abiotic control (C-5). Data reflecting situation after 4 months of operation.

Pseudo-first-order rate disappearance constants (k_{obs}) with calculated half life time ($t_{1/2}$) were used to compare reactivity of mZVI in C-2 and C-3, taking into account residence times calculated for each column separately (Table 22, Figure 42). The data presented in Figure 42, reflecting the condition after 4 months of operation, provides evidence that k_{obs} of TCE, cDCE and 1,1-DCE were 3 to 4 times lower for GG-mZVI than for non-stabilized mZVI. Even lower k_{obs} were obtained for the abiotic control. Comparable data were obtained after 5 months of the columns operation. Finally, after 6 months of operation, TCE disappearance rate was in the same order of magnitude for non-stabilized and GG-mZVI. Calculated $t_{1/2}$ < 1 day^{-1} for mZVI, GG-mZVI and GG-mZVI (AC) indicate that mZVI reactivity towards TCE in the field application of the reactive zone is not significantly affected by guar gum. Similarly, Tratnyek et al. (2001) concluded that decreased TCE reduction rates, due to competition for reactive surface sites by adsorbed natural organic matter, does not significantly impact the performance of iron permeable reactive barriers. However, the performance of mZVI towards cDCE and 1,1-DCA is significantly affected by guar gum and might be explained by the direct blocking of reactive surface sites (Phenrat et al., 2009) which possibly has a larger impact on the lower degrading CAH-compounds like cDCE and 1,1-DCA in comparison with TCE or by significantly higher concentrations present in the groundwater.

In the abiotic control C-5 a clearly reduced reactivity of GG-mZVI was observed (Figure 38 and Figure 41). k_{obs} of TCE and 1,1-DCE were 6-7 times slower than for the non-stabilized particles, while no degradation of cDCE and 1,1-DCA was observed. These findings indicate that soil microorganisms do have a function in degrading guar gum and the subsequent removal of the guar gum degradation products by the groundwater flow (intensive rinsing), both required to reactivate the guar gum stabilized mZVI particles. This hypothesis is supported by the guar gum concentrations analyzed at the effluent of the columns (Figure 40). After 2 PVs, guar gum was no longer detected in the effluent of guar gum stabilized mZVI, while the effluent of the corresponding abiotic control still contained guar gum. This is explicable by the absence of active soil microorganisms. However, after 6 PVs almost no guar gum was detected in the effluent samples of the abiotic control, while no full recovery of the mZVI reactivity was realized at that moment. One explanation might be that the rinsing process as described earlier for batch degradation tests (Chapter 5) was still insufficient, leaving guar gum remains in the system as a coupling layer on the mZVI. Quantification of the remaining guar gum concentrations on the aquifer samples at the end of the experiment (Figure 43) supports this hypothesis, as significantly more (4-7 times) guar gum remained in the C-5 (GG-mZVI, abiotic control) as compared to test C-3 (GG-mZVI).

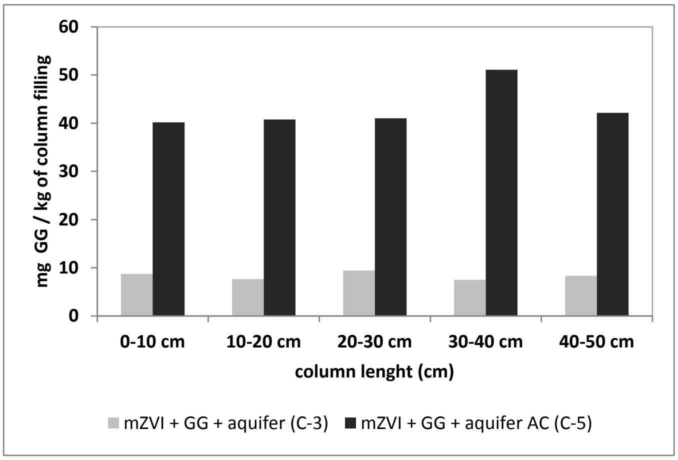

Figure 43 - Difference between guar gum (GG) concentration in columns amended with guar gum stabilized mZVI (C-3) and guar gum stabilized mZVI - abiotic control (C-5).

These data prove that the soil microbial community degrades guar gum and therefore, indirectly, regenerates the reactivity of the guar gum stabilized mZVI particles. However, the rinsing process is not fully effective under simulated in-situ conditions as it was in the batch experiments where even slightly faster disappearance rate constants were observed.

6.3.3. EFFECT OF MZVI AND GUAR GUM STABILIZED MZVI ON THE SOIL MICROBIAL POPULATION

The column test was also conducted to evaluate the effect of mZVI and guar gum stabilized mZVI on the naturally present microbial population.

ATP analysis was performed on effluent samples taken after 5 months of operation, to determine the activity of total bacterial population under the different conditions (Figure 44). In the effluents of the abiotic controls (C-4 and C-5), the total ATP concentrations were below the detection limit, showing the absence of bacterial activity. Interestingly, similar microbial activity was observed for the C-1 with aquifer material (1.66×10^{-1} ng mL^{-1}) and C-2 with mZVI (1.98×10^{-1} ng mL^{-1}). These data imply that there is no negative impact of the selected mZVI on total microbial activity present in aquifer material. Finally, the highest concentration of total ATP (4.86×10^{0} ng mL^{-1}) was observed in the effluent samples for C-3 (GG-mZVI), suggesting a positive impact of GG-mZVI on the microbial activity in the column.

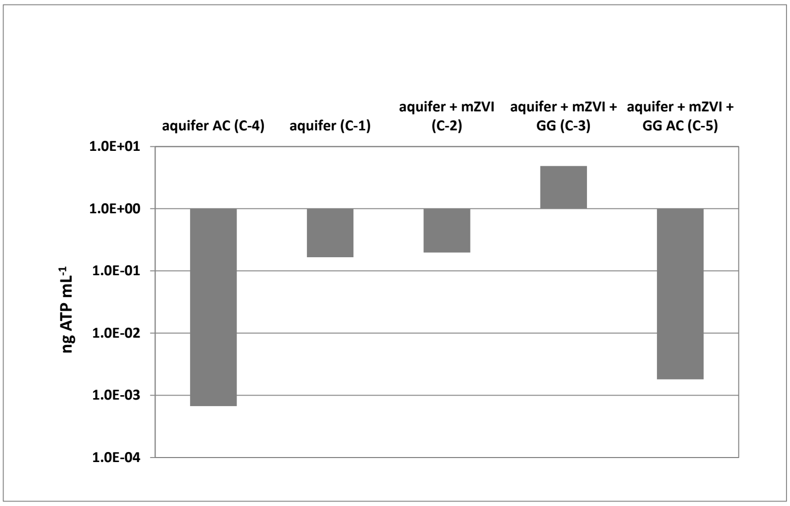

Figure 44 - ATP concentrations as an indicator for viable biomass in effluent samples. Abiotic controls were below method detection limit (MDL = 1×10^{-2} ng ATP mL^{-1}) indicating on no viable biomass.

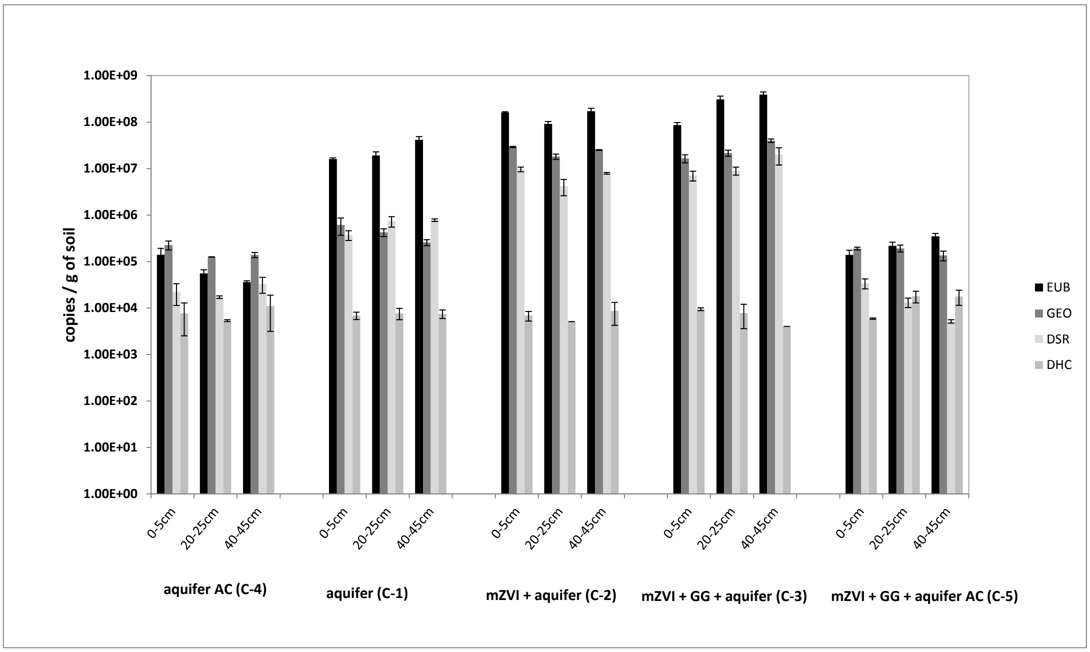

Figure 45 - Dynamic of the total bacterial community, *Dehalococcoides* (DHC), *Geobacter* and *Desulforeducers* on DNA level for aquifer samples collected in column study.

Results of qPCR analysis targeting different bacterial groups in aquifer samples collected from different horizontal column sections, are presented in Figure 45. *Eubacteria* could be detected in all sections of the aquifer column (C-1), as well as in columns amended by mZVI (C-2) and GG-mZVI (C-3). Lower numbers of *Eubacteria* were detected for both abiotic controls (C-4, C-5), as expected. Compared to the column (C-1), a clear increase in *Eubacteria* community was observed in C-2, suggesting that mZVI after in-situ application does not negatively affect the total amount of bacteria on the long term. Even a slightly higher number of *Eubacteria* was detected in the downstream part C-3, confirming the conclusions based on ATP analyses, namely a positive impact of guar gum on the bacterial community. *Geobacter* and *Desulforeducers* species were detected in all aquifer samples with the highest values in C-2 and C-3, and the lowest ones in the abiotic controls (C-4, C-5). These results are consistent with the study of Gu et al. (2002) where biomass increases in and in the surroundings of the ZVI barrier were reported and were explained by microbial consumption of residual byproducts of the guar gum which was used during trench excavation. Moreover, Van Nooten et al., 2007 reported that the presence of carbon sources can make the aquifer material a favorable environment for the growth of microorganisms.

Finally, *Dehalococcoides* spp. were found to be present in the aquifer samples, but in very low numbers that are insufficient for supporting the biodegradation of high concentrations of CAHs. In the effluent, the ethane and ethane concentrations were not higher compared to the influent (Figure 39).

No significant biodegradation was also observed in batch reactors with aquifer material collected from the site either, nor in reactors supplied by guar gum furthermore discussed in Chapter 7. Additionally, low pH values measured in the influent samples might also be a reason for the low number of *Dehalococcoides* detected in samples. Optimal pH range of near neutral was reported for dechlorination activity of *Dehalococcoides* (Gerritse et al. 1999; Suyama et al. 2001).

6.3.4. IMPACT OF GUAR GUM ON THE LIFE-TIME OF MZVIS UNDER IN-SITU CONDITIONS

To evaluate the impact of guar gum on the iron consumption and iron corrosion, both influencing the life-time of mZVI, the remaining concentrations of mZVI in the column fillings were determined after 6 months of continuous operation (Figure 46).

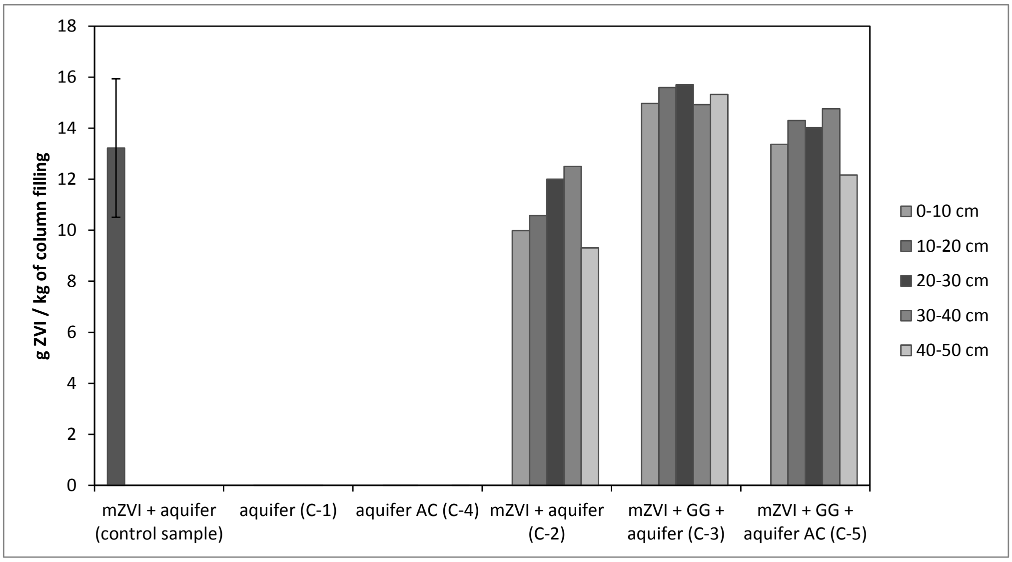

Figure 46 - ZVI concentration along the columns after column dismantling.

Before start up, columns contained 13 ± 2.7 g of ZVI per kg of column filling. After more than 6 months of operation the average ZVI concentration in C-2 (mZVI) was 11 ± 1.3 g of ZVI per kg of column filling. Compared to the initial concentration, approximately 70 to 80%

of ZVI remained in the column suggesting that ZVI will possibly be consumed after 2-3 years. This is 4-6 times longer than initially presented for nZVIs used for in-situ applications (Liu and Lowry, 2006). A higher remaining concentration of ZVI was detected in C-3 (GG-mZVI), predicting a life-time of 13 years. The presence of guar gum slightly reduced the reactivity of iron, but also slowed down the iron corrosion rate which prolongs the life time of the reactive zone. The reduced corrosion rate can be explained by the reduced accessibility of guar gum coupled mZVI particles.

6.4. CONCLUSION

Results of our column study demonstrate that under conditions that are closer to the real in-situ environment, guar gum may affect the performance of mZVI in the reactive zone, but in a slightly different way than was previously observed in batch degradation experiments (Chapter 5). The ability of the soil microbial population to degrade guar gum without addition of commercial enzymes, was confirmed. The reduced reactivity of GG-mZVI as compared to mZVI was also confirmed, but was found to be less pronounced under continuous flow conditions. On the other hand, to gain full reactivity recovery of guar gum stabilized mZVIs, more time was needed as the guar gum degradation by microorganisms requires some time and the removal of guar gum and its breakdown products was slower under in-situ conditions than predicted via the batch test. The coupling of guar gum with mZVI which is responsible for the latter finding, was hypothesized to be also responsible for the observed reduced corrosion rate of GG-mZVI, and consequently the longer life-time of the particles.

Importantly, mZVI and GG-mZVI did not significantly affect the activity and/or the amount of the total bacterial community, even when induced bacterial growth and activity was observed, which may be considered a strong point for in-situ applications.

In conclusion, GG-mZVI particles were shown to have good potential for the in-situ treatment of CAHs.

CHAPTER 7 FIELD ASSESSMENT OF GUAR GUM STABILIZED MICROSCALE ZEROVALENT IRON PARTICLES FOR IN-SITU REMEDIATION OF CAHs

7.1. INTRODUCTION

Zerovalent iron (ZVI) particles are used for in-situ remediation of chlorinated aliphatic hydrocarbons present in groundwater. While granular ZVI is mainly used as filling material for trenches to create permeable reactive barriers (PRBs), microscale (mZVI) and nanoscale (nZVI) ZVI particles also have the potential to be injected in the subsurface as water-based slurries, close to the source of contamination and/or in a contaminant plume, creating so-called reactive zones. A major advantage of reactive zones is that they can be installed in a less invasive and more flexible way (at deeper levels, underneath buildings), and generally decrease the costs required for the excavation of deep trenches. Here, we report on a mZVI injection in the field at pilot scale that was performed with a direct push delivery method.

mZVI particles can be delivered in the subsurface via injection wells or direct-push methods creating preferential flow paths (Suthersan, 1999; Christiansen et al., 2010). Homogenous distribution of iron via permeation delivery is only possible in highly permeable aquifers when sufficiently small particles (nanoscale or lower microscale) are injected at low pressures. Conversely, when applying higher pressures and flow rates, preferential flow paths will be induced resulting in an inhomogeneous distribution of the iron particles after injection. Controlled delivery of reagents in the subsurface is a challenge under most in-situ conditions.

Earlier in this work, the efficiency of mZVI for CAH-removal has been described (Chapter 2), but stabilizers were found necessary to prevent sedimentation of the mZVIs (Chapter 5). Guar gum stabilized mZVI, however, has a temporarily negative impact on the mZVI reactivity towards CAHs. Degradation of the guar gum and subsequent removal of its break-down products were necessary to reactivate mZVI in batch systems (Chapter 5), and to improve reactivity of mZVI in in-situ simulated continuous systems (Chapter 6).

These findings do have implications for field scale applications of the stabilized mZVI technology as well as for reactive barriers where guar gum is used as a trenching slurry, because a temporary inactivation of the ZVI will occur. Based on lab-scale column studies, the duration of the mZVI inactivation period, was found to be relatively limited when compared to the duration time of the treatment.

While laboratory studies reported in Chapter 5 and Chapter 6 have already provided detailed insights into processes occurring considering reactivity of stabilized mZVI particles, the knowledge from field studies is limited. Nevertheless, sedimentation of mZVI particles in the injection fluid and temporarily inactivation should be considered when up scaling the technology to the field scale. For that reason, a pilot-scale field study was performed. A highly concentrated guar gum stabilized mZVI slurry, previously tested for reactivity in Chapter 5, was injected into an aquifer at a CAH-contaminated site (Site V, Belgium).

The pilot test was aimed at demonstrating the injection characteristics of the mZVI particles (reported in detail by Luna, 2013) and at determining the vertical and horizontal distribution of mZVI particles in the subsurface after injection what is elaborated in this study. Finally, this study covers the efficiency of mZVI in reducing contaminant fluxes such as 1,1,1-TCA, 1,1-DCA, TCA and cDCE was examined after mZVI delivery. In order to distinguish between a reduction in concentration due to mixing with the injected fluid and a reduction due to degradation, specific stable isotope analyses (CSIA) were conducted.

7.2. MATERIALS AND METHODS

7.2.1. TEST SITE DESCRIPTION

The Site V is an industrial site (Flanders, Belgium) where former painting and coating activities resulted in CAH-contamination of the groundwater.

A field investigation was conducted to characterize the site and the contaminant source (Figure 47).

The hydro-geological schematization (Figure 48) of the site shows a shallow sandy aquifer (0 to 3 m bgs), a fine clayey-sandy aquitard (3 to 8 m bgs) and a deep sandy aquifer (8 to 20 m bgs) with grain size distribution of d_{10} = 52 µm and d_{90} = 374 µm. The layer of 8-10 m bgs was the target of the pilot test. The water table was approximately 2 m bgs.

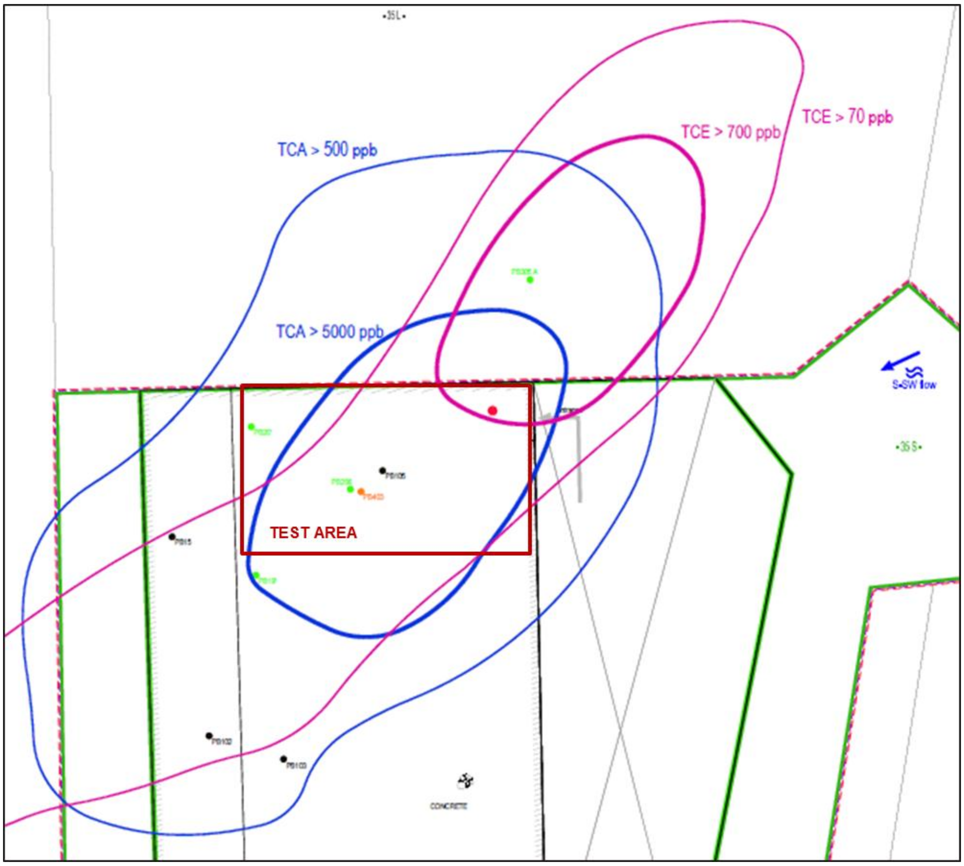

Figure 47 - A detailed map of the Site V with contaminants contours.

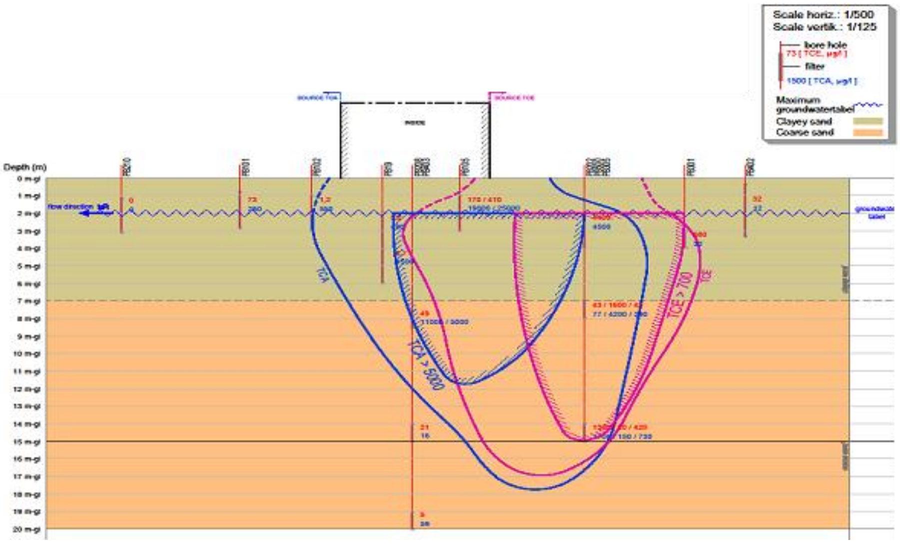

Figure 48 - Hydro-geological conceptual model of the test area at Site V.

The groundwater flow is preferentially toward the south-southwest with estimated flow velocity of 10 m year^{-1}. An average hydraulic conductivity of 8.2 x 10^{-5} m s^{-1} was calculated based on pumping test and slug test data. The hydraulic gradient ranges from 9.0 x 10^{-4} to 2.5 x 10^{-3}, while effective porosity estimated on grain size distribution data is approximately 18 %.

With respect to pollution, in particular chlorinated ethanes (1,1,1-TCA) and chlorinated ethenes (TCE) were detected. The 1,1,1-TCA plume reaches the depth of 13.5 m bgs, while TCE plume reaches 15.5 m bgs. According to the monitoring campaign obtained one week before the injection test was performed, the dominant pollutant is 1,1,1-TCA (4-6 mg L^{-1} at 4.5 m bgs) and its associated daughter product 1,1-DCA (2-11 mg L^{-1} at 8-9.5 m bgs). The highest concentration of TCE (< 1 mg L^{-1}) was at 4.5 m bgs, while for its associated daughter product cDCE (1.5 – 4 mg L^{-1}) was at 9 m bgs. 1,1-DCE (3-5 mg L^{-1}) was also present in shallow layer.

7.2.2. LAB-SCALE TESTS PRIOR TO THE FIELD TEST

To examine the CAH-biodegradation potential at Site V, small scale batch experiments under anaerobic conditions were performed. Batch tests were prepared (triplicates) in a 160 mL glass vials capped with butyl/PFTE grey septum containing 30 g of soil and 70 g of groundwater collected from the Site V before the injection was performed. Besides a control without additional electron donor, two test conditions were set-up with sodium lactate (0.2 g kg^{-1}) and guar gum (2 g kg^{-1}), respectively, as potential carbon source. Additionally, one of four batch reactor containing sodium lactate and guar gum was supplemented by formaldehyde (0.4 % v/v) and served as a abiotic controls. The batch reactors were incubated (shaking) at groundwater temperature (12°C). Analyses were performed at different time points: at the beginning, and after 2, 4, 16, 34 and 47 weeks. Concentrations of CAHs, ethene, ethane and acetylene were determined via headspace measurements as described in Chapter 2.

7.2.3. FIELD-SCALE INJECTION TEST

Before the field injection of mZVI particles (Table 18), five multilevel detection systems (MLDS) comprising groundwater sampling points, temperature sensors and detectors for the magnetic susceptibility (Buchau et al., 2010; de Boer, 2012; Li et al., 2012) were installed within 2.5 m of radius around the planned injection point. The position of the MLDS was 0.5, 1, 1.5, 2 and 2.5 m from planned injection spot in different directions as indicated in Figure 49. Every MLDS consisted of 7 groundwater sampling ports at different depths (approximately 4.5, 8, 8.5, 9, 9.5, 10 and 10.5 m bgs) that were used to evaluate contaminant concentration. For MLDS5, the groundwater sampling port at 4.5 m bgs was not available due to the damage during the MLDS installation.

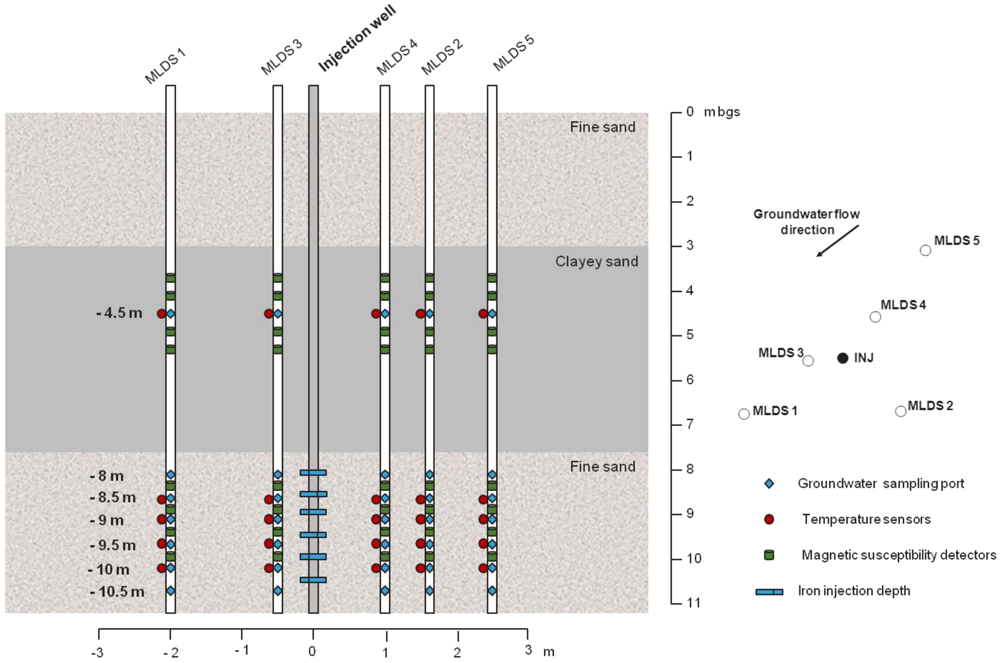

Figure 49 - Monitoring wells location with indicated depth of groundwater sampling ports, temperature sensors and magnetic susceptibility detectors.

According to the sedimentation tests and rheological measurements performed by Politecnico di Torino (Luna, 2013), a guar gum concentration of 4.5-5 g L^{-1} was needed for stabilization of 120 g L^{-1} of mZVI with sedimentation half time of 3 h. In the field approximately 70 g L^{-1} of mZVI was stabilized by ~7.2 g L^{-1} of guar gum.

The pilot test set up is shown in Figure 50. The day before the injection, 1.5 m^3 of guar gum (Rantec Corporation, USA) solution was prepared by dispersing 360 g of guar gum powder into 50 L of warm water (about 50 °C) and subsequently mixed with high shear rate mixing device (Collomix CX 200 hand mixer). Afterwards, the guar gum solution was transferred to cubitainer for the transport to the field site. To avoid sedimentation, mZVI was mixed with the guar gum solution just before the injection.

The guar gum stabilized mZVI was introduced in the subsurface via direct push (Geoprobe, 7822T) at high pressures (GS2000 dual piston pump) with average flow rate of 8.6 L min^{-1}. At 1 single spot 1.5 m^3 of mZVI slurry was injected bottom up at 5 different depths between 10.5 to 8.5 m bgs (Table 23). For every injection interval, approximately 20 kg of mZVI was dispersed into 300 L of previously prepared guar gum solution and recirculated for 10 minutes before injection. To understand phenomena occurring in the subsurface during the injection, a pressure transducer (Delta Ohm) was connected at the top of the tubing of the Geoprobe injection probe by Politecnico di Torino and logged the evolution of the injection pressure over time during iron injection.

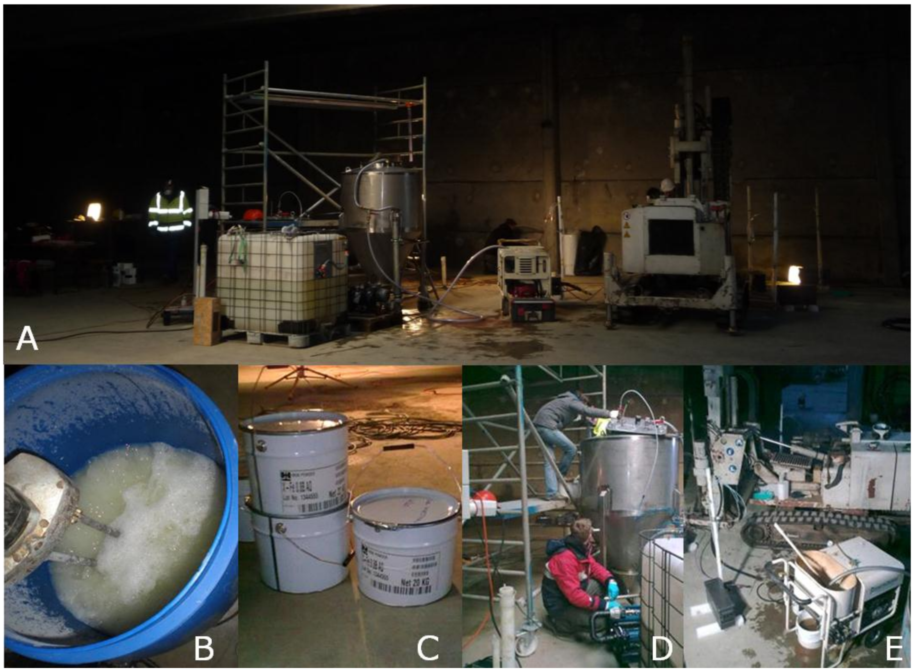

Figure 50 - Iron injection set up. (A) injection area, (B) guar gum preparation, (C) mZVI, (D) mixing of guar gum and mZVI, (E) Geoprobe injection.

Table 23 : Bottom-up injection at the Site V.

Injection #	Depth (m bgs)	Volume (L) of guar gum solution	Amount of mZVI (kg)	Average flow rate (L min^{-1})
1	10.5	300	19.6	8.69
2	10.0	300	22.0	9.63
3	9.5	300	20.6	8.93
4	9.0	300	21.2	8.40
5	8.5	300	21.2	7.45

Enzymes were used to induce fast guar gum degradation after the injection (Chapter 5). For this reason, commercially available enzyme

(LEB-H, Rantec) was directly dosed into the pump tank at the end of each injection. Two weeks after injection, an extraction well (filter 8-11 m bgs) was installed near the injection point and 4 m^3 of groundwater was extracted to remove potentially remaining guar gum from the system and simultaneously pull contaminated groundwater into the created reactive zone.

After injection, two different soil core samplings were organized to evaluate the distribution of mZVI in the subsurface. Two weeks after the injection core samples were taken at three spots (CS1-CS3), while 22 weeks after the injection 4 additional soils cores were sampled in the shallow aquifer (CS4-CS7) as detailed in Figure 51.

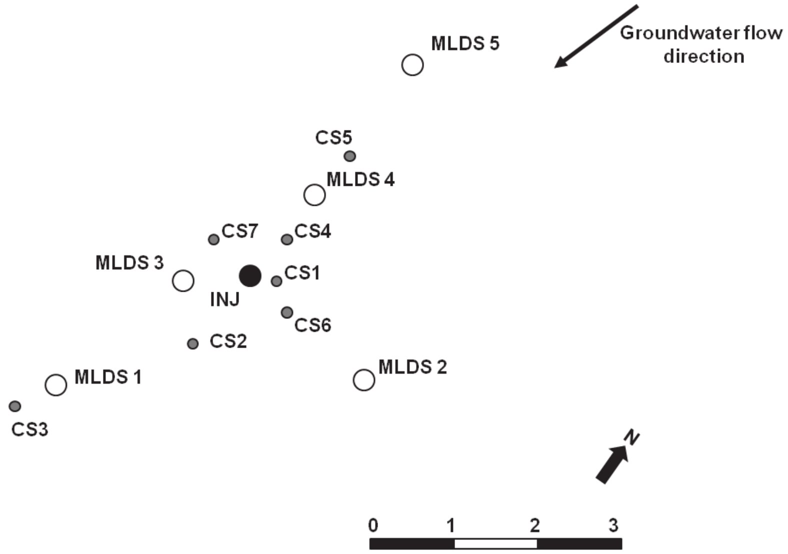

Figure 51 - Location of soil cores extracted for evaluation of guar gum stabilized mZVI distribution: CS1 (0 – 11 m bgs); CS2-3 (4.5 – 11 m bgs) and CS4-7 (1 – 6 m bgs).

The presence of mZVI was evaluated visually and via hydrogen measurements. For the latter, aliquots of soil samples (5 g) were amended with 5 g of 1 M HCl. The generated hydrogen (H_2) gas was directly analyzed and converted to ZVI concentrations as described in Chapter 4.

7.2.4. GROUNDWATER SAMPLING AND ANALYSIS

To monitor the performance of the created mZVI reactive zone, groundwater samples were collected every five weeks. Groundwater samples were collected by connecting the Teflon tubing of the MLDS and conventional wells, with a peristaltic pump. Field parameters were measured in a flow-through cell by a portable Multi 340i (WTW, Germany) equipped with pH and temperature electrode SenTix41, conductivity measuring cell TetraCon® 325 and Liq-Glass ORP electrode (Hamilton- Nevada, USA). Samples for CAHs analysis were collected in 30 mL vials (headspace free) capped with butyl/PFTE grey septa and stored at 12°C. Within 48 hours, the concentrations of CAHs, intermediate- and end-products were determined via direct headspace measurements using a Varian GC-FID. Guar gum present in groundwater samples was quantified as described in Chapter 5. To characterize the geochemistry of the groundwater, several groundwater samples were taken from monitoring wells for analysis of chloride, sulfate, nitrate, nitrite, dissolved and total iron.

Additionally, groundwater samples for compounds specific isotope analysis (CSIA) were collected from the MLDSs (at 3 different depths 4.5, 9 and 10.5 m bgs) directly into 40 mL vials and capped with sealing cap. Groundwater from non-layered wells (injection point and control wells outside of the test area) was transferred in 1 L or 0.5 L glass bottles. Sodium hydroxide pellets were used for sample preservation.

7.2.5. COMPOUND SPECIFIC ISOTOPE ANALYSES (CSIA)

Gas chromatography combustion isotope ratio mass spectrometry (GC-C-IRMS) was applied to determine the stable carbon isotope composition of CAHs. All samples were measured in duplicates. Isotope analysis was done via (i) accumulation by a purge-and-trap unit (Teledyne Tekmar); (ii) transfer to a gas chromatograph split injector at -100°C ; (iii) injection at a split ratio of 1:7 to 1:100 to a capillary column (VOCOL 60 m x 0.25 mm ID or DB624 60 m × 0.25 mm ID × 1.4 µm FD); (iv) separation of compounds in GC by specific temperature shifts (TRACE GC Ultra, Thermo Fisher Scientific); (v) combustion of CAH to CO_2-molecules; (vi) transfer and further separation of $^{12}CO_2$ vs. $^{13}CO_2$ in an isotope ratio mass spectrometer (Thermo Finnegan MAT 253).
Isotope ratios are reported as $\delta^{13}C$ values ‰ relative to the international standard V-PDB (Vienna Pee Dee Belemnite) according to:

$$\delta^{13}C = [(R_{sample} - R_{standard}) / R_{standard}] * 1000 \qquad (19)$$

where R_{sample} and $R_{standard}$ are the $^{13}C/^{12}C$-ratios of the sample and an international standard, respectively.

Depending on the level of CAH-concentrations, variable injection split ratios and volumes were applied. Isotope values were retrieved by automatic and occasionally also manual peak integration. Authentic laboratory standards were used for identification of CAHs and to improve the accuracy of the isotope analyses by linear correction of isotope values.

The analytical uncertainty of isotope analyses in an identical sample given by the standard deviation (sd) of the replicate measurements generally is ±0.5 ‰ (Sherwood Lollar et al., 2007). However, field samples comprised additional variability arising from the sampling procedure. Isotope measurements regarded for interpretation had a mean standard deviation of ±0.46 ‰ (n = 341) with 37 values ranging in between ±1.0 ‰ and ±3.0 ‰; values with higher sd were excluded.

7.2.6. REACTIVITY OF USED MZVI MATERIAL

A batch degradation experiment was conducted to investigate the reactivity of mZVI after field injection for comparison with unreacted mZVI. The mZVI containing soil samples was taken two weeks after injection and stored for 2 months at 12°C under anaerobic conditions prior to the test. The experiment was carried out in 160 mL vials, each containing 5 g of aquifer material from which 0.04 g of iron and 100 mL of polluted groundwater from the Site V collected before injection. Vials filled with aquifer material without iron and polluted groundwater were used as a control. For comparison, laboratory batch degradation experiments with unreacted mZVI (100 g L^{-1}) were performed in parallel for artificial groundwater (Chapter 2) polluted by TCE, cDCE, and 1,1-DCE separately at initial concentration of 10 mg L^{-1}. Headspace analyses were regularly performed (start, after 7, 14, 35 and 70 days) as previously described in Chapter 2. Pseudo-first-order rate constants (k_{obs}, h^{-1}) and specific surface area normalized rate constants (k_{SA}, L m^{-2} h^{-1}) were calculated as previously described (Chapter 2).

7.3. RESULTS AND DISCUSSION

7.3.1. BIODEGRADATION POTENTIAL OF SITE

The presence of a CAHs biodegradation potential at Site V was assessed via batch degradation experiments. After 47 weeks of incubation under in-situ conditions, TCE, cDCE and 1,1-DCA concentration decreases observed for reactors with only aquifer material (Figure 52) were limited and comparable with the abiotic control. Similar results were obtained for reactors supplied by guar gum and lactate as extra electron donors (Figure 52). No production of vinyl chloride and methane as potential biodegradation products was observed. Average mass recoveries of 87 % suggested on possible removal of TCE, cDCE and 1,1-DCA by sorption to the aquifer material. This is concluded as the abiotic controls showed similar trend. Additionally, losses of present pollutants are possible during the headspace measurements. Finally, measured pH of 4.92 is the reason of no active CAH-biodegradation in the aquifer material.

Concentrations of chloride, sulfate, nitrate, nitrite, dissolved and total iron did not change after injection as compared to the pre-injection situation confirming no active CAH-biodegradation.

The absence of an active biodegradation potential at the Site V was also concluded from the long-term column test described in Chapter 6.

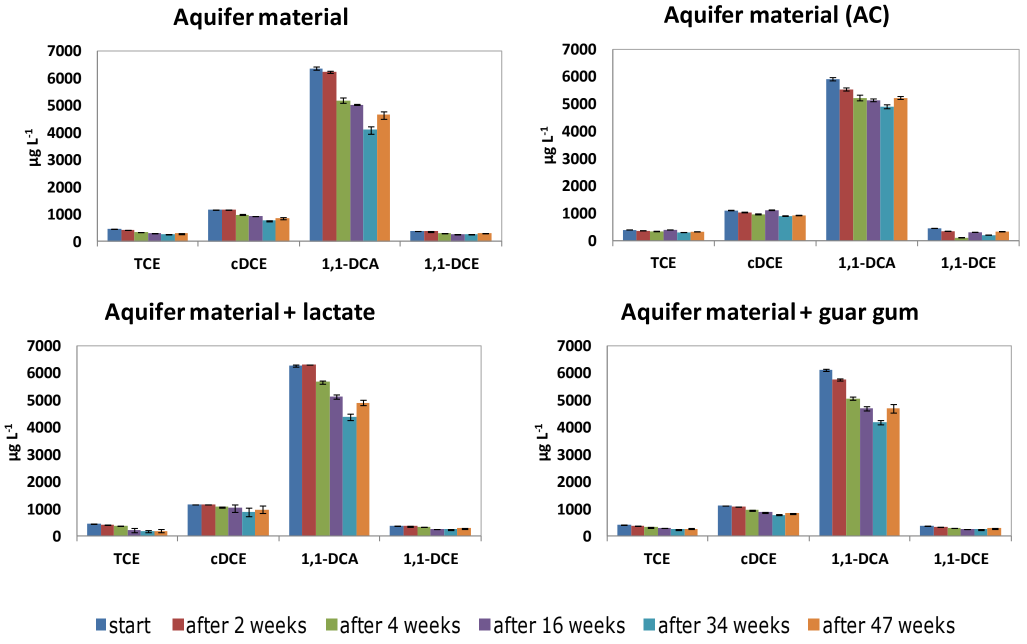

Figure 52 - TCE, cDCE, 1,1-DCA and 1,1-DCE change over time in batches containing only aquifer material and supplemented with lactate or guar gum.

7.3.2. DISTRIBUTION OF MZVI PARTICLES IN THE SUBSURFACE AFTER INJECTION

Results on field parameters (pH, ORP and conductivity) recorded during the monitoring phase before and after iron injection (Annex II) provide an indication of the distribution of the mZVI in the subsurface. ORP decreased significantly from 89 to -343 mV one day after injection in the MLDS4 (1 m from injection point) at depth 4.5 m bgs (Figure 53). For MLDS3 ORP decrease from 101 mV to -56 mV was recorded 14 days after injection. Similar results were obtained by Truex et al. (2010) where ORP decreased significantly at the wells within the ZVI delivery zone. For other wells no significant change in ORP and conductivity was observed. The electrical conductivity in the MLDS4 decreased from 1013 to 6 µS cm^{-1} one day after injection due to the guar gum stabilized mZVI delivery (Figure 53).

A significant pH change one day after injection was not observed due to the possible buffering capacity of the aquifer as previously described in column study (Chapter 6). However, pH data revealed an increase over time for MLDS4 and MLDS3 from 5.3-5.4 at the beginning of experiment to 6.4-6.5 at the end of monitoring campaign. Moreover, the low pH data (5.4-6.5) may explain the absence of an active microbial reductive dechlorination at the site as the optimum pH range (6.8-7.6) was not achieved (Zhuang and Pavlostathis, 1995). A pH increase to 7.3-8.5 was observed for MLDS1 after 25 and 30 weeks of injection, as well as increase to 6.8-7.1 for MLDS2 (deeper layers) 2 weeks after injection, which implies potentially the presence of iron.

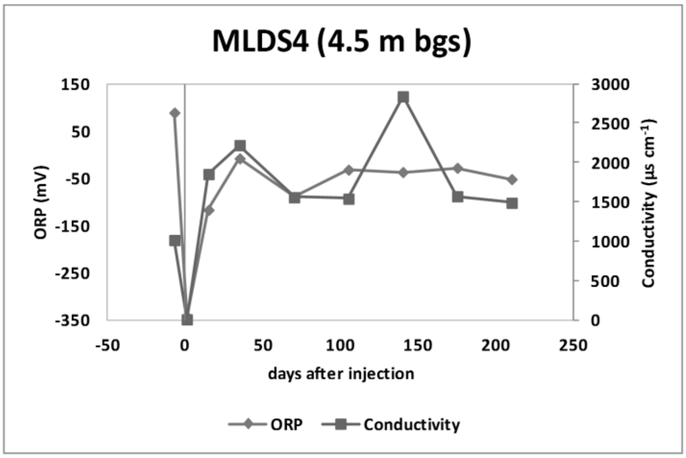

Figure 53 - ORP and conductivity data over time for MLDS4 at 4.5 m bgs.

Vertical distributions of mZVI in all core samples as determined via acid digestion are presented in Figure 54. The mZVI concentrations reached a maximum radial distance from the injection well of 2.5 m (CS3) at the depth 8 m bgs (3.2 mg ZVI per kg of aquifer) what was hypothesized considering the site geology and injection characteristics. However, the highest mZVI concentration was detected 0.5 m from injection point (CS4) in the direction of MLDS4 at the depth 3.1 m (4.1 g ZVI per kg of aquifer) and 4.5 m (7.7 g ZVI per kg of aquifer) indirectly showing on preferential flow paths occurred in the direction of monitoring wells installed before injection. Visual observations confirmed this data. Next to the injection point (CS1) at a depth of 3.1 m, also high mZVI concentrations were detected (4.2 g ZVI per kg of aquifer). From the presence of iron at different depths around the injection point, it can be concluded that preferential flow paths were created and that the iron is heterogeneously distributed and mainly present in shallow zone.

Guar gum concentrations were also measured in the monitoring wells 1 day after injection to give indirect evidence on iron distribution (Figure 55).

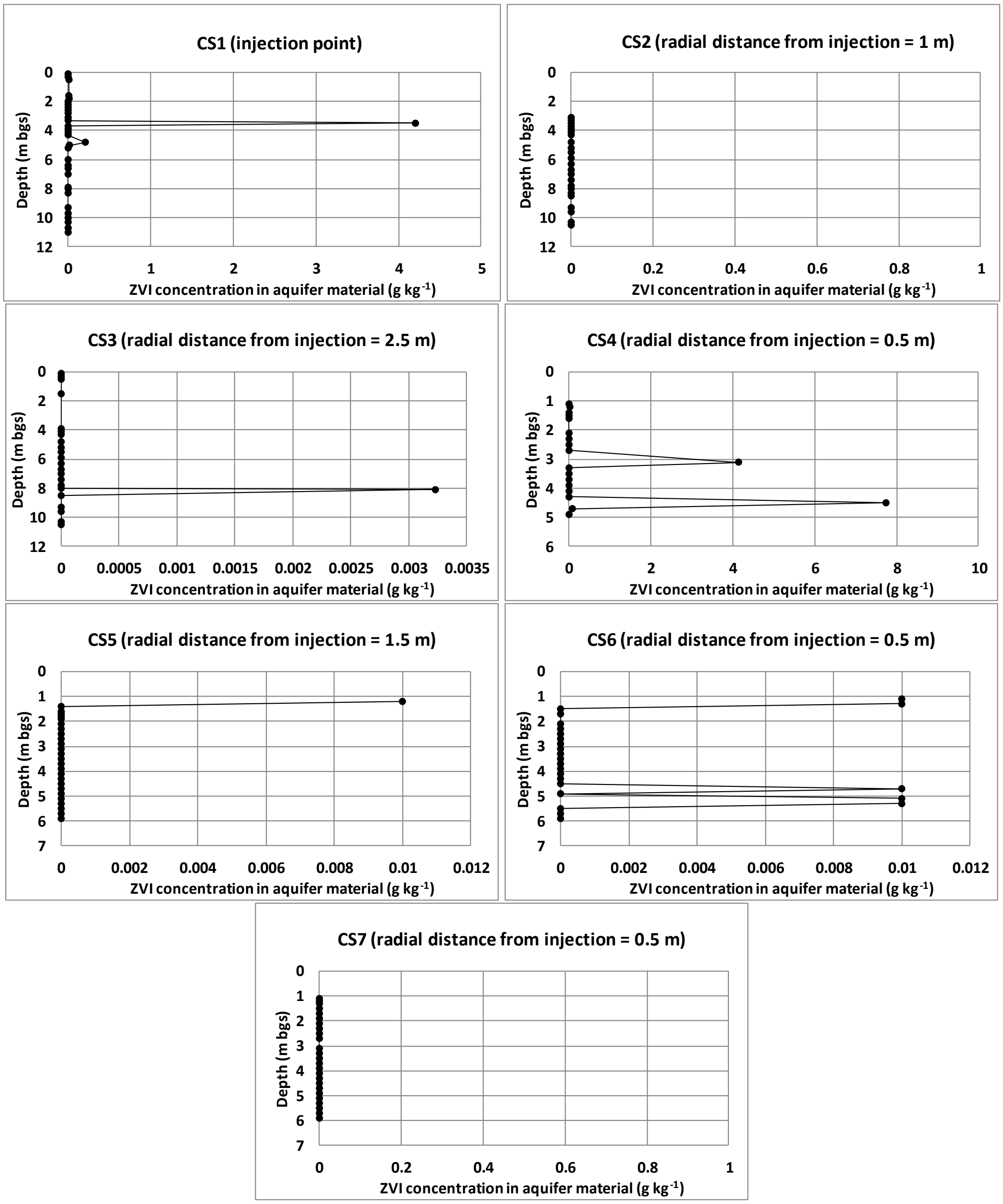

Figure 54 - Distribution of mZVI material in aquifer determined via acid digestion from core samples extracted after mZVI injection. Note that scale for each plot might be different.

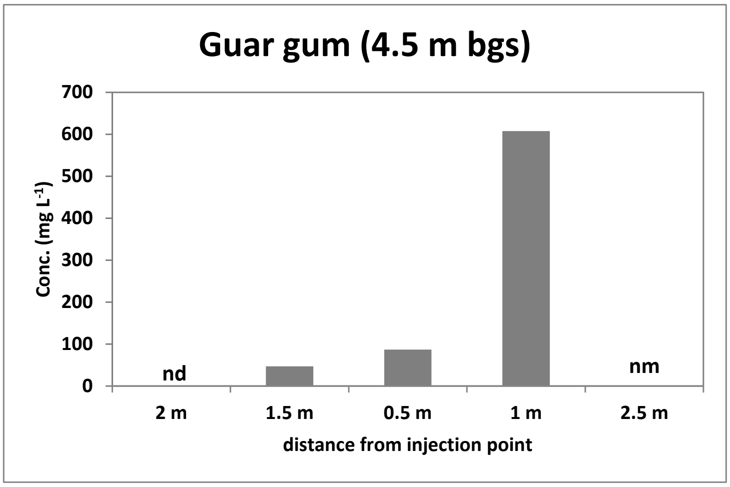

Figure 55 - Guar gum detection in monitoring wells at 4.5 m bgs one day after iron injection.

Guar gum was detected in groundwater collected from the shallow layer (4.5 m bgs) with highest concentration of 608 mg L^{-1} observed in MLDS4 (1 m from injection point). Lower concentrations of guar gum in groundwater samples were in MLDS3 and MLDS2 at 4.5 m bgs. In the deeper layers guar gum concentrations were below detection limits indicating that no major amount of injection fluids reached the desired depth. After the groundwater extraction step, the guar gum concentration in MLDS4 (4.5 m bgs) dropped to 45 mg L^{-1} while it was below detection limits for other wells.

The presented data indicate a clear heterogeneous distribution of mZVI around the injection spot. Preferential flow paths were clearly generated during injection, as also was concluded from the recorded injection pressure data (Luna, 2013). Moreover, mZVI and guar gum data revealed that the most of the slurry preferentially flew towards the shallow layers of the aquifer system as possible upwelling along the injection well or MLDS occurred.

7.3.3. IMPACT OF THE INJECTED MZVI ON CAHS CONCENTRATIONS

An overview of the CAH-concentrations measured in time in the different wells/sampling points is given in Annex III. Generally, the injection of guar gum stabilized mZVI slurry resulted in a significant reduction of 1,1,1-TCA and TCE in the area where mZVI was detected.

One day after the mZVI injection, 1,1,1-TCA concentrations at MLDS4 (4.5 m bgs) decreased significantly (Figure 56). Similar results were obtained for TCE and 1,1-DCE. This may be caused by dilution, dislocation of contaminant to greater depths or degradation by the injected mZVI particles. For other compounds no significant change in concentration was observed, which points towards degradation of the above mentioned compounds. Nevertheless, a significant reduction of the total CAHs concentration (75-80%) in MLDS4 (4.5 m bgs) was observed in the first 35 days of monitoring.

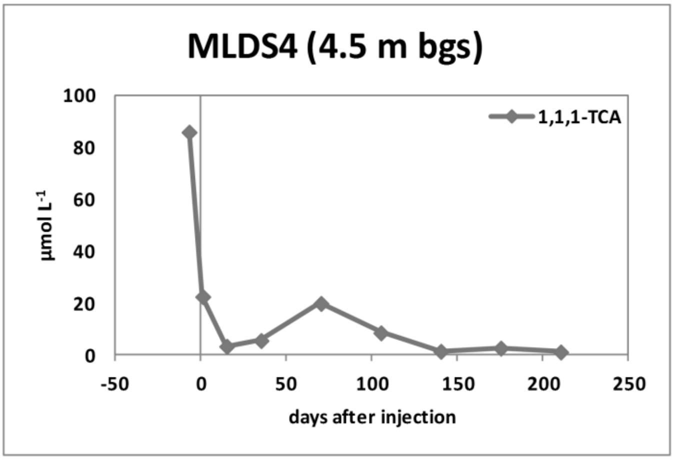

Figure 56 - Changes in concentration of 1,1,1-TCA in groundwater over time in the MLDS4 at 4.5 m bgs.

To distinguish between degradation and dilution of CAHs in the test area, carbon stable isotope analyses were performed. On the one hand, fourteen days after the injection, approximately 4 m^3 of groundwater were extracted to pull "fresh" contaminated groundwater into the reactive zone and avoid dilution of pollutants. CSIA analyses performed on the different fractions of the extracted groundwater revealed constant values ($\delta^{13}C$) for the pollutants, indicating that no major degradation processes were induced (Figure 57). However, there was one exception. 1,1,1-TCA exhibited a clear isotope enrichment ($\delta^{13}C$) in the first three samples (≤ 1.3 m^3) pointing towards degradation induced in the close vicinity of the injection well (Figure 57). Similar observations were made for the measured pollutant concentrations. At the beginning of the extraction (≤ 1 m^3), 1,1,1-TCA concentration exhibited 3.2 µmol L^{-1}. Later, 1,1,1-TCA concentration increased up to 10.8 µmol L^{-1}, whereas no change for other pollutants was observed.

On the other hand, samples extracted from the different wells and samplings points were also analyzed on carbon stable isotopes to evaluate the success of injected guar gum stabilized mZVI. Pre-injection isotope measurements are available for 2 deeper spots, at 9 m bgs (MLDS2 and MLDS5) and at 10 m bgs (MLDS3), which is the depth the reactive zone was envisioned. Figure 58 shows CSIA results for the zone (4.5 m bgs) where the main part of the mZVI was actually situated. The $\delta^{13}C$ mean values measured after the extraction step are compared with baseline measurements. As no pre-injection isotope values were measured at 4.5 m bgs, the most consistent isotope value measured during the pilot test at 4.5 m bgs (being MLDS2, at 1.5 m from injection point) was used as baseline.

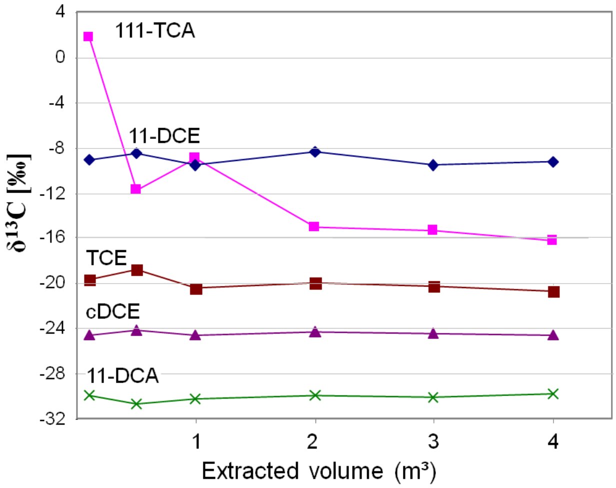

Figure 57 - Carbon isotope values of five contaminants in extracted groundwater from a pilot test field 14 days after guar gum stabilized mZVI injection.

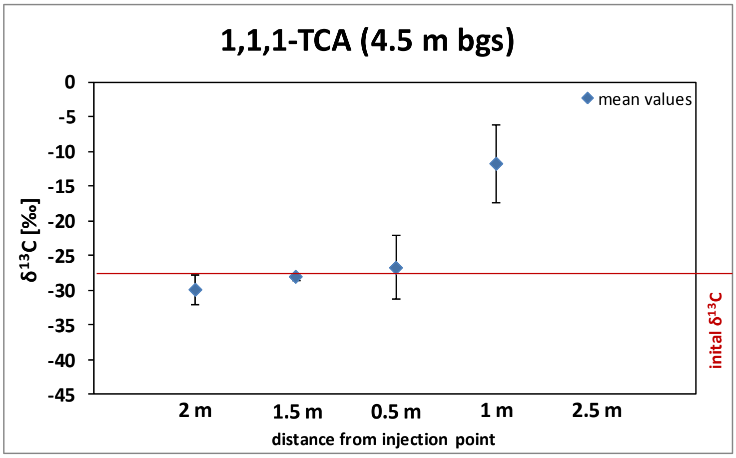

Figure 58 - $\delta^{13}C$ (‰) mean values of 1,1,1-TCA in the monitoring wells (MLDS1 – MLDS5) at 4.5 m bgs.

All collected CSIA data for TCE, cDCE, 1,1-DCE, 1,1,1-TCA and 1,1-DCA are presented in Annex IV. No significant change in carbon isotope values was observed at 9 m bgs despite iron injection at that depth. However, iron distribution data show that particles were mainly delivered to more shallow depths where changes were noticed. $\delta^{13}C$ mean values indicate a clearly stimulated degradation of contaminants at 4.5 m bgs. Strong enrichment of 1,1,1-TCA in close vicinity of the injection well (MLDS4) at 4.5 m bgs was observed. Isotopic evidence supports reaction of delivered mZVI with 1,1,1-TCA in this well. Interestingly, some enrichment of TCE and 1,1-DCE was also observed in this well. $\delta^{13}C$ mean values at 1 m and less explicitly at 2.5 m from injection well at 10 m bgs indicate on possible degradation of 1,1,1-TCA at this depth as well. No significant changes of present CAHs were observed for other wells. This supports the data presented in Chapter 5 and 6, where in contrast with PCE, TCE and cDCE, removal of 1,1,1-TCA was less affected by guar gum used to stabilize mZVI. Elsner et al. (2010) reported that only full-scale applications allow detecting enhanced transformations of CAHs such as TCE as the iron is distributed more evenly due to the multiple loads in more injection wells.

7.3.4. REACTIVITY OF USED mZVI IN THE SUBSURFACE

The reactivity of mZVI present in the reactive zone (2 months after injection, referred to as 'used mZVI') was evaluated in batch degradation tests (Figure 59) and compared to the reactivity of original unreacted material.

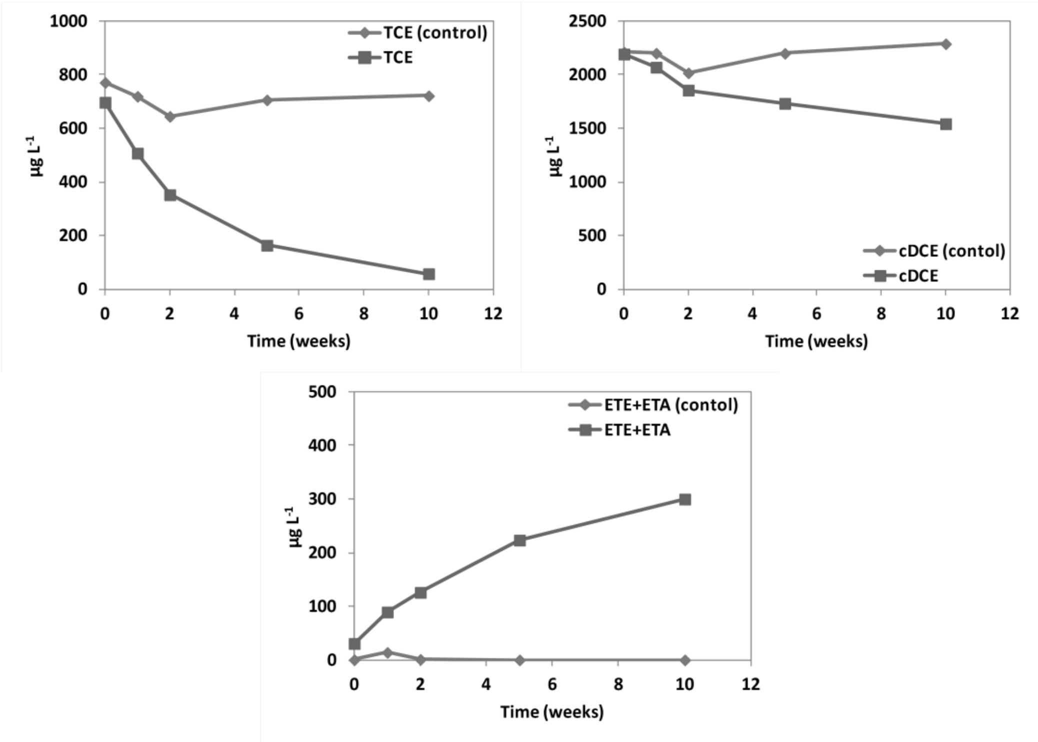

Figure 59 - Reduction of TCE and cDCE in the presence of used mZVI extracted from core samples after injection with production of ethene (ETE) and ethane (ETA) under laboratory conditions. Control conditions without mZVI are also presented.

A clear degradation of TCE and cDCE was obtained in the soil samples with the used mZVI, while no degradation occurred in the control without mZVI. Increases in ethene and ethane as end products confirm that CAHs were degraded by the injected mZVI. Acetylene was also detected evidencing that *β*-elimination pathway was included.

k_{obs} and k_{SA} for transformation of TCE and cDCE and 1,1-DCE by used mZVI and unreacted mZVI are shown in Figure 60. The calculated k_{obs} data for unreacted mZVI are about one order of magnitude higher than for used mZVI from the reactive zone. This was expected as a lower amount of mZVI was calculated to be present in batch reactors containing used mZVI. On the other hand, surface normalized data (k_{SA}) revealed a significantly higher reactivity of the reacted material. Much higher starting pollutant concentrations in the batch reactors containing unreacted mZVI might be the reason of this observation. Moreover, significantly higher reactivity of the used iron material might be due to the lower pH of 6.90 as a consequence of the lower iron concentration present in batch reactors compared to the batch reactors with unreacted mZVI where pH increase to 8.19 was evident.

Although the comparison of the reactivity data from the unreacted and used mZVI needs careful interpretation, the results show that guar gum stabilized mZVI that has been injected in the field is reactive (reactivated) within 2 months after the injection.

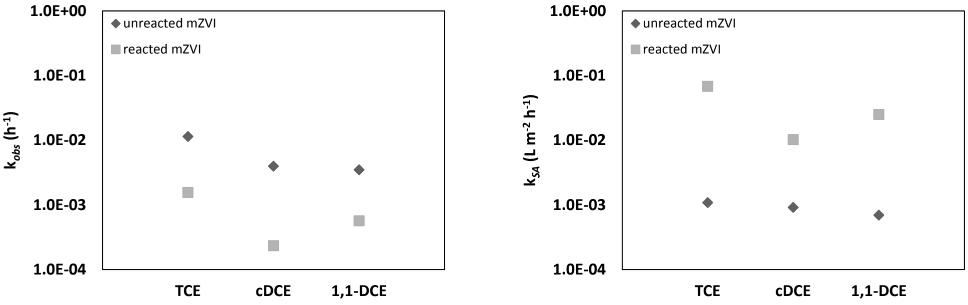

Figure 60 - k_{obs} and k_{SA} data for reduction of TCE, cDCE and 1,1-DCE by unreacted and used mZVI.

7.4. CONCLUSION

The presented field test demonstrated that the use of guar gum stabilized mZVI slurries in the field is possible. Firstly, it was shown that guar gum stabilized mZVI slurry can be relatively easily prepared at a pilot scale in the field, and with the appropriate equipment, full scale preparation is predicted to be feasible. Next, via direct push techniques, the slurry was found injectable in the subsurface. A controlled delivery of the product in the subsurface, on the other hand, is a challenge. Preferential flow paths of the injected iron slurry were created when applying high pressures of approximately 80 bars for clay and 60 bars for sand (Luna, 2013) and average flow rates of 8.6 L min^{-1} and large injection volumes per interval (300 L). Consequently, a heterogeneous distribution of the iron particles was obtained. While the deeper layer (8-10.5 m bgs) was targeted, a significant part of the mZVI flowed upward in the shallow zone (4.5 m bgs) due to created preferential paths during high pressure and flow injection. More specifically, the data point towards a preferential flow near MLDS4 located 1 m from the injection point. Maximum observed delivery distance of mZVI particles from the injection point is 2.5 m at 8 m bgs.

A significant abiotic degradation of 1,1,1-TCA was proven to occur in the zone where the highest ZVI concentration was actually delivered (4.5 m bgs). Faster reduction of 1,1,1-TCA by used guar gum stabilized mZVI as compared to reduction of chlorinated ethenes (TCE, cDCE, 1,1-DCE) confirmed the results presented in Chapter 5.

Finally, batch tests data with used mZVI from injection zone, prove that guar gum stabilized mZVI is reactive within 2 months after the injection.

In conclusion, despite the fact that guar gum stabilized mZVI particles were delivered at a different depth than intended, delivered mZVI can degrade 1,1,1-TCA in the field. Further demonstration of this technology in zones with different CAH-pollutants and with more controlled delivery of the reagents has been performed within the Aquarehab project.

CHAPTER 8 GENERAL CONCLUSIONS AND PERSPECTIVES

From early 90s, introduced by Gillham and O'Hannesin at the University of Waterloo, the use of ZVI particles as nontoxic materials is extensively studied for abiotic removal of many chlorinated aliphatic hydrocarbons (CAHs), heavy metals, pesticides etc. It is now widely accepted that granular ZVIs are used for in-situ remediation of different CAHs (plume treatment) by creating PRBs. On the other hand, PRBs are not suitable for the contaminant source treatment. As an alternative to granular ZVI particles, nZVI particles were introduced as highly reactive towards CAHs, resulting in the development of fine ZVI injection technologies for contaminant plume treatment as well as contaminant treatment close to the source zone. Conversely, fast consumption of nZVIs in reaction with water as well as agglomeration properties during the injection remains a challenge for further research and the uncertainty related to costs and risks associated with nZVI may hamper its use in groundwater remediation.

The aim of the described research was to evaluate injectable mZVI particles as a substitution to nZVI particles for in-situ reactive zone treatment of CAHs. In contrast to nZVI particles, the mZVI particles are less reactive, they do have an expected longer life-time and are less expensive, more available and easier to handle. Moreover, the reactivity of mZVI particles is expected to be higher than the granular ZVIs. However, a key challenge will be to deploy the mZVI particles in the subsurface because sedimentation during the injection is concern.

In essence, this study focused on the main concerns raised for using mZVI particles for in-situ treatment of CAHs being: (1) the reactivity and consequently life-time of mZVI particles as compared to the granular ZVIs and nZVIs, (2) the stability of mZVI particles in the suspension, (3) the distribution of mZVI particles in the subsurface after injection, (4) the efficiency of mZVI particles after in-situ application in reducing CAHs and (5) the impact of mZVIs on soil microbial community.

8.1. GENERAL CONCLUSIONS

8.1.1. MZVI PARTICLES HAVE POTENTIAL TO REMEDIATE CAHS IN GROUNDWATER

Major statements driven by studding the mZVI particles reactivity towards different CAHs are:

1. **Reactivity of mZVIs is suitable for in-situ remediation and comparable to nZVIs when calculated per surface area.**
2. **Reactivity of mZVI is influenced by surface composition.**
3. **Corrosion rate and consequently life-time is affected by particle size.**

In this study, newly developed mZVI particles (16-168 µm) were presented as an alternative to highly reactive nZVI particles. To evaluate the reactivity of mZVI particles and compare it to commercially available nZVIs and/or mZVIs, a lab-scale experimental study was conducted under consistent test conditions. Highly effective remediation of PCE, TCE, cDCE and 1,1,1-TCA was observed for nZVIs, but also for a number of newly developed mZVIs. However, up to now, comparing data from different independent literature sources was not very successful, as quantitative relations between iron reactivity and different experimental conditions could not be made. To compare reactivity of different mZVIs, the observed (k_{obs}) and mass-normalized (k_M) pseudo-first-order degradation rate constants, as well as specific surface area-normalized reaction rate constants (k_{SA}) were used. For this evaluation under consistent experimental conditions for all examined iron based materials, k_{SA} data obtained in Chapter 2 indicate that the degradation rate by the mZVI particles is equivalent to the nZVI particles and in certain cases even higher. On the other hand, based on the k_M data the higher concentration of mZVI particles is needed to obtain the degradation kinetic as fast as it is for nZVIs. However, 10 times higher concentration of mZVI particles can efficiently cope with the pollutants, but only in the longer time scale. In respect to the cost-efficiency of the injecting technology, even 10 times higher required concentrations of mZVI particles predicted for in-situ injection would be 20 times lower in cost than commercially available nZVIs (see below). This leads to the conclusion that mZVI particles can potentially be used for efficient remediation of different CAHs. The data provided in Chapter 2 suggests that the reactivity of biogenic iron sulfides as a supplement to mZVIs needs more attention. This is of interest as FeS formation under sulfur- and iron-reducing conditions has been previously reported in PRBs constructed with ZVIs.

In Chapter 2 it was shown that the performance of the mZVIs could be partially explained by the surface area of the particles. However, it was still unclear what codetermined the reaction rate. For that reason, a quantitative relationship between mZVI reactivity and its composition was made (Chapter 3). The chemical composition of the mZVI particles was found to significantly enhance or inhibit CAHs degradation kinetics. This observation clearly indicates the importance of iron composition during the production process besides particle size. Reactivity of mZVI particles was correlated with O-content recommending that the surface oxides from the iron particles should be removed in a pretreatment step before their use for in-situ applications. Particles reactivity and/or sorption properties can be maintained during the production process. Given recommendations on the composition of mZVI particles will help in further development of mZVIs and predicting its efficiency. This might be further extrapolated for granular ZVIs and nZVIs as well. Finally, it is evident that the iron composition might further indicate on the reactive sites on the iron surface. To characterize the "reaction" sites surface sensitive techniques such as X-ray Photoelectron Spectroscopy (XPS-ESCA) or Temperature- Programmed Desorption Mass Spectroscopy might be useful.

The long-term performance of mZVI particles to serve as an electron donor in effective reduction of CAHs and consequently site cleanup time is important (Farell et al., 2000). In other words, knowing the corrosion rate of the particles, the time interval between injections can be estimated and technology costs can be reduced considerably. Many studies were conducted to answer on this question (Reardon, 1995, 2005; Gillham, 2003; Liu et al., 2005a; Liu and Lowry, 2006). However, iron longevity after in-situ application cannot be confirmed with certainty. In Chapter 4, corrosion rates of the particles were obtained by measuring the evolution of hydrogen gas as a consequence of anaerobic corrosion of iron during batch degradation tests. As expected, the nZVI particles have higher corrosion rate than the mZVIs. Here, particle size does have an impact on iron corrosion rate. Additionally, laboratory experiments under in-situ equivalent conditions showed that the reactivity of the mZVI particles can be maintained for at least 6 months. In contrast, expected life-time of nZVIs after in-situ application is just a few weeks (Liu et al., 2005a; Liu and Lowry, 2006; He and Zhao, 2007). For that reason use of mZVI particles for in-situ application is highlighted. In contrast to the boosting effect of nZVI after in-situ application, mZVI particles will possibly maintain CAHs degradation longer, directly by chemical reduction, or indirectly releasing the H_2 as a potential electron donor for potentially present CAH-degrading microorganisms. Predicted life-times based on initial corrosion rates of 0.91 years for commercially available to 4.66 years for Höganäs mZVIs and only 0.01 years for nZVIs is of significant importance for in-situ application of mZVIs. The relevance of modeling mZVI particles life-time after in-situ application is very high as the corrosion products inhibit the iron corrosion rate and consequently reduction rate constants.

Presented batch scale laboratory studies clearly indicate that mZVI particles can be applicable for effective remediation of CAHs and therefore it is imperative to confirm this under in-situ conditions as well.

8.1.2. STABILIZERS IMPROVE THE APPLICABILITY OF MZVI FOR IN-SITU REMEDIATION

Major statements obtained by studding the applicability of mZVI for in-situ remediation of CAHs are:

1. **Guar gum reversibly decreases the reactivity of mZVI.**
2. **Enzymes and rinsing can restore the efficiency of guar gum stabilized mZVI.**
3. **Under natural conditions guar gum can be biologically degraded improving the reactivity of the mZVI.**
4. **There is no negative impact of mZVI particles on soil micro-organisms.**
5. **Guar gum stabilized mZVI is able to degrade pollutants in the subsurface, as was shown for 1,1,1-TCA.**
6. **The delivery of the mZVI at desired spot in the subsurface is a major challenge.**
7. **Heterogeneous distribution of the mZVI in the field as a consequence of preferential flow paths necessitates a dense monitoring network to prove that the technology actually works in field conditions.**

Field scale applications have been performed all over the world to explain processes ongoing during and after injection of mostly nZVI particles. Success of the application depends on particles properties as well as the injection technology. Application of mZVI particles for in-situ remediation is less examined, as mZVI particles cannot be injected as water slurries due to the sedimentation properties. On the other hand, considering longevity properties and overall costs, mZVI particles might be more favored for in-situ application. Fast sedimentation of mZVI particles in water can be hindered by use of stabilizing agents such as green polymers (Comba and Sethi 2009; Dalla Vecchia et al. 2009, Tiraferri and Sethi, 2008), more particularly guar gum (Comba and Braun, 2012; Xue and Sethi, 2012). Using highly viscous fluids created from guar gum, mZVI particles can be easily applied in the field by different technologies. Injection technologies of guar gum stabilized mZVI particles have been discussed more in detail by Luna (2013) as the mobility of particles, and as a consequence transport distance in porous medium is controlled by particle size, grain-size distribution, aquifer permeability, injection rate, iron concentration and the properties of the suspension. Shortly, for the new developed mZVI particles high pressure injection is the most suitable injection technology as these particles do have larger particle size comparing to the nZVIs. Consequently, slurry viscosity has to be high to obtain satisfactory stability during injection of guar gum stabilized mZVI particles.

Figure 61 illustrates the knowledge gained in Chapter 5 regarding the impact of green polymer guar gum on the reactivity of mZVI particles towards different CAHs that has been raised as a main question. Guar gum has a positive impact on mZVI stability, but decreased the reactivity of the particles towards CAHs up to 8 times due to the intermolecular hydrogen bonding between mZVI and the guar gum. Higher guar gum concentration used for stabilization of particles will have more impact on the reactivity than a lower concentration. Interestingly, addition of commercially available enzymes resulted in the cleavage of the polysaccharide guar gum into lower molecular fragments, but not in improved reactivity as expected. To recover reactivity of guar gum coupled mZVI particles, intensive rinsing of the iron particles is necessary to remove the guar gum degradation fragments. This study shows that CAHs can be treated efficiently by guar gum stabilized mZVI after reactivation by means of enzymatic breakdown and rinsing and in-situ use of guar gum stabilized mZVI particles for environmental cleanup would be possible.

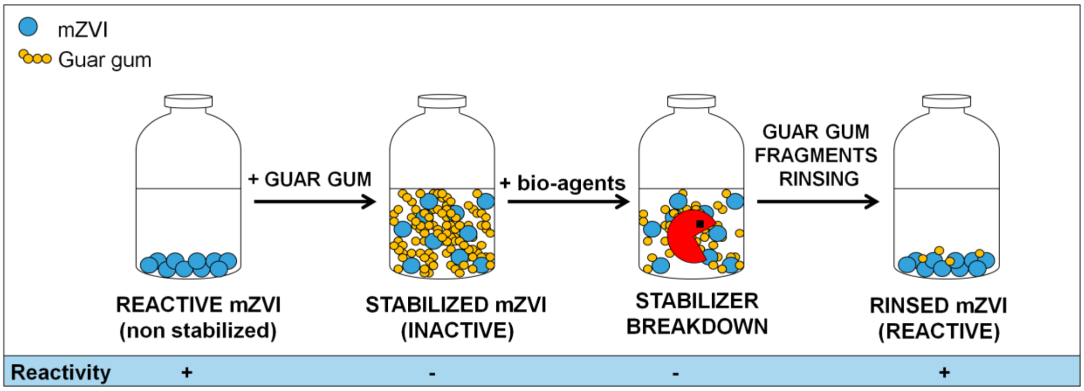

Figure 61 - The reactivity recovery of guar gum coupled mZVI after intensive rinsing of the iron particles.

To confirm results obtained in the batch study and evaluate whether the inactivation of the mZVI by the guar gum is relevant under in-situ conditions a column study was performed (Chapter 6). A slightly reduced activity of the guar gum stabilized mZVI has been observed in the columns. Instead of using commercially available enzymes, it was hypothesized that soil microorganisms can induce guar gum degradation. Our study confirms that soil microorganisms can degrade guar gum and that subsequent removal of the guar gum degradation products by the groundwater flow (flushing effect) can reactivate the mZVI. Most importantly, temporary decreased mZVI reactivity due to guar gum, has only a very limited impact on the performance of in-situ reactive zone. The presence of guar gum slightly reduced the reactivity of iron, but also slowed down the iron corrosion rate which prolongs the life time of reactive zone.

nZVIs are mostly used in the United States for the remediation of polluted groundwater (Klaine et al., 2008). Several pilot scale studies were introduced in Europe as well, with three full scale applications (Mueller et al. 2012). However, legislation in some countries across Europe raise questions regarding use of nZVI for in-situ applications as nZVIs are concerned to be exotoxic after injection and with possible impact on human health (Kirschling et al., 2010). For that reason impact of mZVI on a bacterial community was studied in Chapter 6. DNA-based qPCR analysis revealed that mZVI did not significantly affect total bacterial community, while guar gum stabilized mZVI particles even induce bacterial growth after application. This should be considered as a strong point for using mZVI particles in-situ.

The first field demonstration on mZVIs emplacement was reported by Tuex et al. (2011). 2 μm mZVI particles were effectively distributed through an injection well using shear thinning fluid containing the commercial polymer. mZVI particles developed in the current PhD study are with particle size of approximately 50 μm. Based on the batch and column results, as well as the study on transport properties of guar gum stabilized mZVI presented by Xue and Sethi (2012) and Luna (2013) the field test was designed as described in Chapter 7. The pilot scale field test was performed in order to demonstrate distribution of guar gum stabilized mZVI particles creating an in-situ reactive zone within the aquifer of relatively low permeability and effective remediation of CAHs. Pressure data together with direct ZVI identification confirmed that guar gum stabilized mZVI particles can be injected via direct push technology and distributed within the aquifer creating preferential flow paths. Here, more attention was given to the iron reactivity and evidence was collected for an induced remediation of CAHs in the close vicinity of spots where the iron was distributed. For that reason not only contaminants concentrations were measured during monitoring campaigns, also a specific stable isotope analysis was conducted. Specific stable isotope analysis yielded information on the success of the remediation action, while it was not possible to clearly distinguish the microbial degradation from abiotic degradation in the field as a consequence of heterogeneous distribution of iron and limited specific stable isotope data.

8.2. FUTURE PERSPECTIVES

This study clearly proves the potential of mZVI to degrade CAHs in the subsurface. A further optimization of mZVI injection technology is required in order to make it more accessible to policy makers, consultants and site owners.

Injection methods have to be optimized to distribute mZVI particles less heterogeneous in the aquifer where pollution is present. Confirmation methods on mZVI distribution in the subsurface are also required. One of the methods for proof of iron distribution after injection is soil cores sampling. Visual observations of core samples might qualitatively confirm the iron distribution, while H_2 measurements can determine ZVI concentration (Chapter 6 and 7) present in soil. Moreover, magnetic susceptibility measurements (Luna, 2013) can be performed in order to additionally confirm H_2 measurements.

Predicting the mZVI life-time after in-situ application will consequently lead to the effectiveness of reactive zone for contaminants degradation. Based on our findings, mZVI life-time will significantly depend on the pH in the aquifer environment. Despite the invested effort, more work is needed to further model mZVI corrosion rates and consequently life-time after in-situ application. Therefore, it would be interesting to perform tests on soil buffering capacity to evaluate the impact of aquifer material on mZVI corrosion rate, and consequently improve the proposed model. Moreover, investigating the precipitation of carbonate minerals and corrosion layers formation with iron speciation would lead to the improved iron corrosion model.

Another area of investigation that can widen the in-situ application of proposed mZVI particles is their reactivity towards other different pollutants than the ones studied here. Lab scale batch degradation experiments reported in Chapter 2 can be adapted for this application.

Furthermore, the use of mZVI particles can be combined with the biodegradation potential of contaminated sites. Hydrogen gas formed during the anaerobic corrosion of the mZVI in the aquifer might support microbial degradation downstream extending the radius of influence. The impact of mZVI and guar gum stabilized mZVI on soil microorganisms needs to be investigated further including not only on DNA, but also on RNA level.

In general, this research provides detailed information on mZVI particles reactivity from the laboratory scale studies to the field application. mZVI particles will have a great potential for in-situ treatment of CAHs and most probably inorganic anions and metals. However, predicting the fate of the mZVI particles after injection in the aquifer will remain challenging. For that reason research should focus more on the field test verifications. Compound specific isotope analysis (CSIA) may be used to evaluate reductive dechlorination using ZVI in PRBs (Vanstone et al., 2005). Added value of this type of analysis would be to evaluate abiotic degradation of contaminants, as well as biotic. In this study, stable carbon isotope analysis confirmed the pollutant removal process. However, a combined approach of CAHs data and CAHs concentrations may be the best option for proving reaction induced weather by iron or biodegradation in the field.

New field tests within the Aquarehab project will be performed in order to implement lessons learned from this study and to further optimize guar gum stabilized mZVIs for in-situ treatment of CAHs. The direct push technique used in this study to inject guar gum stabilized mZVI created preferential flow paths. Therefore, a pulsed injection will be employed to minimize heterogeneous distribution of the particles. “Top->down” injection with high pressures and injection rates with reduced volume of the slurry will replace the “bottom->up” procedure applied here. As the preferential flow paths cannot be predicted, several injection points close to each other at different depths will possibly be sufficient to create a reactive zone required for contaminant plume remediation.

The economic sustainability of the technology is essential for future development. Apart from cost reductions, price is approximately 100 € per kg for commercially nano-sized (Nanoiron, CZ) to 30 € per kg for commercially micro-sized (BASF, DE), mZVI particles have a higher socio-economical acceptability at least in Europe. The price of Höganäs particles, introduced in this study, is approximately 5 € per kg. However, this price might be further influenced by mZVI production process (particle size and composition) and amount of iron required for application. Moreover, cost of guar gum is approximately 10 € per kg (Rantec Corporation, USA). More research is needed to evaluate the economic effects of the technology proposed in this study.

The cost of the technology will also depend on the type and quantity of the contaminants, as well as their distribution in the subsurface. Based on the reaction kinetics shown in the Chapter 1, one kg of mZVI is required to reduce one kg of CAHs. However, future application studies need to be obtained to estimate exact mZVI concentration required for successful remediation of contaminants according to the different legislations.

BIBLIOGRAPHY

Agrawal, A., Tratnyek, P.G., 1996. Reduction of nitro aromatic compounds by zero-valent iron metal. Environ. Sci. Technol. 30, 153-160.
Arnold, W.A., Roberts, A.L. 2000. Pathways and kinetics of chlorinated ethylene and chlorinated acetylene reaction with Fe(0) particles. *Environ. Sci.* Technol. 34 (9), 1794-1805.

Baric, M., Majone, M., Beccari, M., Petrangeli Papini, M. 2012. Coupling of polyhydroxybutyrate (PHB) and zero valent iron (ZVI) for enhanced treatment of chlorinated ethanes in permeable reactive barriers (PRBs). Chem. Eng. J. 195-196, 22-30.

Barnes, R.J., Riba, O., Gardner, M.N., Scott, T.B., Jackman, S.A., Thompson, I.P. 2010. Optimization of nano-scale nickel/iron particles for the reduction of high concentration chlorinated aliphatic hydrocarbon solutions, Chemosphere. 79, 448-454.

Bastiaens, L., Vos, J., Gemoets, J., Diels, L., Van Gestel, G. 2005. Nanoiron: a new technology for in-situ remediation of VOCl contaminated groundwater. In L. Bastiaens (Ed), Proceedings of 2nd International PRB/RZ-symposium, Antwerp, November 14-16. ISBN 90587007x, p133-137.

Bayer, P., Finkel, M. 2005. Modeling of sequential groundwater treatment with zerovalent iron and granular activated carbon. J. Contam. Hydrol. 78, 129–146.

Bennett, P., He, F., Zhao, D., Aiken, B., Feldman, L. 2010. In situ testing of metallic iron nanoparticle mobility and reactivity in a shallow granular aquifer. J. Contam. Hydrol. 30, 116(1-4), 35-46.

Buchau, A., de Boer, C.V., Klaas N. 2010. Inductive detection and concentration measurement of nano sized zero valent iron in the subsurface. IET Sci. Meas. Technol. 4, 289-297.

Burris, D.R., Allen-King, R.M., Manoranjan, V.S., Campbell, T.J., Loraine, G.A., Deng, B., 1998. Chlorinated ethene reduction by cast iron: sorption and mass transfer. J. Environ. Eng., 1012–1019.

Burris, D.R., Campbell, T.J., Manoranjan, V.S., 1995. Sorption of trichloroethylene and tetrachloroethlyene in a batch reactive metallic iron-water system. Environ. Sci. Technol. 29, 2850–2855.

Burris, D.R., Delcomyn, C.A., Smith, M.H., Roberts, A.L. 1999. Reductive dechlorination of tetrachloroethylene and trichloroethylene catalyzed by Vitamin B12 in homogeneous and heterogeneous systems. Environ. Sci. Technol. 30, 3047-3052.

Butler, E.C., Hayes, K.F. 2000. Kinetics of the transformation of halogenated aliphatic compounds by iron sulfide. Environ. Sci. Technol. 34, 422–429.

Butler, E.C., Hayes, K.F. 2001. Factors influencing rates and products in the transformation of trichloroethylene by iron sulfide and iron metal. Environ. Sci. Technol. 35, 3884-3891.

Cadmus, M.C., Jackson, L.K., Burton, K.A., Platiner, R.D., Slodki, M.E. 1982. Biodegradation of xanthan gum by Bacillus sp. Appl. Environ. Microbiol. 44, 5–11.

Cantrell, K. J., Kaplan, D. I., Gilmore, T. J. 1997. Injection of colloidal Fe-0 particles in sand with shear-thinning fluids. J. Environ. Eng-Asce. 123, 786-791.

Carniato, L., Schoups, G., Seuntjens, P., Van Nooten, T., Simons, Q., Bastiaens, L. 2012 Predicting longevity of iron permeable reactive barriers using multiple iron deactivation models. J. Contam. Hydrol. 142–143, 93–108.

Chang, P.R., Pantaleoni, A.D., Shenk, D.J., 2010. Jet-Assisted Injection of Nano-scale, Zero-valent Iron to Treat TCE in a Deep Alluvial Aquifer Proceedings of the Seventh International Conference on Remediation of Chlorinated and Recalcitrant Compounds, Monterey, CA.

Chen, K.-F., Li, S., Zhang, W.-X. 2011. Renewable hydrogen generation by bimetallic zerovalent iron nanoparticles. Chem. Eng. J. 170, 562–567.

Cheng, S.F., Wu, S.C. 2000. The enhancement methods for the degradation of TCE by zero-valent metals. Chemosphere 41, 1263–1270.

Cho, Y., Choi, S.I. 20120. Degradation of PCE, TCE and 1,1,1-TCA by nanosized FePd bimetallic particles under various experimental conditions. Chemosphere 81, 940–945.

Christiansen, C.M., Damgaard, I., Broholm, M., Kessler, T., Klint, K.E., Nilsson, B., and Bjerg, P.L. 2010. Comparison of Delivery Methods for Enhanced In Situ Remediation in Clay Till. Ground Water Monit. R. 30, 107-122.

Comba, S., Braun, J. 2012. An empirical model to predict the distribution of iron micro-particles around an injection well in a sandy aquifer. J. Contam. Hydrol. 132, 1–11.

Comba, S., Di Molfetta, A., Sethi, R.A. 2011. Comparison Between Field Applications of Nano-, Micro-, and Millimetric Zero-Valent Iron for the Remediation of Contaminated Aquifers. Water Air Soil Pollut. 215, 595–607.

Comba, S., Sethi, R. 2009. Stabilisation of highly concentrated suspensions of iron nanoparticles using shear-thinning gels of xanthan gum. Wat. Res. 43 (15), 3717-3726.

Day, S.R., O'Hannesin, S.F., Marsden, L. 1999. Geotechnical techniques for the construction of reactive barriers, J. Hazard. Mater. 67, 285–297.

De Boer, C. 2012. Transport of Nano Sized Zero Valent Iron Colloids during Injection into the Subsurface. PhD Thesis. Institut für Wasser- und Umweltsystemmodellierung der Universität Stuttgart.

Deng, B., Buris, D.R., Campbell, T.J., 1999. Reduction of vinyl chloride in metallic iron–water system Environ. Sci. Technol. 33, 2651–2656.

Deng, B., Campbell, T.J., Burris, D.R. 1997. Hydrocarbon formation in metallic iron/water systems. Environ. Sci. Technol. 31, 1185–1190.

Di Molfetta, A., Sethi, R. 2006. Clamshell excavation of a permeable reactive barrier. Environ. Geol. 50 (3), 361-369.

Doherty, R.E. 2000a. A history of the production and use of carbon tetrachloride, tetrachloroethylene, trichloroethylene and 1,1,1-trichloroethane in the United States: part 1 – historical background; carbon tetrachloride and tetrachloroethylene. Environ. Forensics. 1, 69–81.

Doherty, R.E. 2000b. A history of the production and use of carbon tetrachloride, tetrachloroethylene, trichloroethylene and 1,1,1-trichloroethane in the United States: part 2 – trichloroethylene and 1,1,1-trichloroethane. Environ. Forensics 1, 83–93.

Dries, J., Bastiaens, L., Springael, D., Agathos, S.N., Diels, L. 2005. Combined removal of chlorinated ethenes and heavy metals by zerovalent iron in batch and continuous flow column systems. Environ. Sci. Technol. 39, 8460-8465.

Duan, Q., Sorooshian, S., Gupta, V. 1992. Effective and efficient global optimization for conceptual rainfall-runoff models. Water Resour. Res. 28, 1015-1031.

Dubois, M., Gilles, K.A., Hamilton, J.K., Rebers, P.A., Smith, F. 1956. Colorimetric method for determination of sugars and related substances. Anal. Chem. 28, 350–356.

Ebert, M., Kober, R., Parbs, A., Plagentz, V., Schafer, D., Dahmke, A. 2006. Assessing degradation rates of chlorinated ethylenes in column experiments with commercial iron materials used in permeable reactive barriers. Environ. Sci. Technol. 40, 2004-2010.

EEA, Progress in management of contaminated sites (CSI 015) - Assessment published Aug 2007. http://www.eea.europa.eu/data-and-maps/indicators/progress-in-management-of-contaminated-sites/progress-in-management-of-contaminated-1. Accessed on 3rd of January, 2013.

Elimelech, M., Gregory, J., Jia, X., Williams, R.A. 1995. Particle deposition and aggregation: measurement, modeling and simulation, first ed. Butterworth-Heinemann, Oxford.

Elliott D., Zhang, W. 2001. Field assessment of nanoparticles for groundwater treatment. Environ. Sci. Technol. 35, 4922–4926.

Elsner, M., Lacrampe Couloume, G., Mancini, S., Burns, L., Sherwood Lollar, B. 2010. Carbon Isotope Analysis to Evaluate Nanoscale Fe(O) Treatment at a Chlorohydrocarbon Contaminated Site. Ground Water Monit. R. 30, 79-95.

Eydal, H.S.C., Pedersen, K. 2007. Use of an ATP assay to determine viable microbial biomass in Fennoscandian Shield groundwater from depths of 3–1000 m. J. Microbiol. Methods. 70, 363-373.

Farrell, J., Kason, M., Melitas, N., Li, T. 2000. Investigation of the longterm performance of zero-valent iron for reductive dechlorination of trichloroethylene. Environ. Sci. Technol. 34, 514-521.

Fennelly, J.P., Roberts, A.L. 1998. Reaction of 1,1,1-trichloroethane with zero-valent metals and bimetallic reductants. Environ. Sci. Technol. 32, 1980-1988.

Focht, R.M., Vogan, J.L., Krug, T.A. 2001. Biopolymer construction techniques for installation of permeable reactive barriers containing granular iron for groundwater remediation. Natl. Meet., Am. Chem. Soc., Div. Environ. Chem. 41 (1), PEACF 2, 1120-1125.

Gander, J.W., Parkin, G.F., Scherer, M.M. 2002. Kinetics of 1,1,1-trichloroethane transformation by iron sulfide and 1 methanogenic consortium. Environ. Sci. Technol. 36, 4540–4546.

Gavaskar, A.R., 1999. Design and construction techniques for permeable reactive barriers. J. Hazard. Mater. 68, 41-71.

Gavaskar, A.R., 1999. Design and construction techniques for permeable reactive barriers. J. Hazard. Mater. 68, 41-71.

Gavaskar, A.R., Tatar, L., Condit, W. 2005. Cost And Performance Report Nanoscale Zero-Valent Iron Technologies For Source Remediation. http://www.dtic.mil/dtic/tr/fulltext/u2/a446916.pdf

Geets, J., Vanbroekhoven, K., Borremans, B., Vangronsveld, J., van der Lelie, D., Diels, L. 2005. Molecular monitoring of SRB community structure and dynamics in batch experiments to examine the applicability of in situ precipitation of heavy metals for groundwater remediation. J. Soils Sediments. 5, 149-163.

Gerritse, J., Drzyzga, O., Kloetstra, G., Keijmel, M., Wiersum, L.P., Hutson, R., Collins, M.D., Gottschal, J.S. 1999. Influence of different electron donors and acceptors on dehalorespiration of tetrachloroethene by Desulfitobacterium frappieri TCE1. Appl. Environ. Microbiol. 65, 5212-5221.

Gillham, R.A. 2003. Discussion of nano-scale iron for dehalogenation. Ground Water Monit. R. 23, 6-8.

Gillham, R.W., O’Hannesin, S.F. 1994. Enhanced degradation of halogenated aliphatics by zerovalent iron. Ground Water. 32, 958–971.

Gillham, R.W., O'Hannesin, S.F. *1992.* Metal-catalysed abiotic degradation of halogenated organic compounds. Proceedings of IAH Conference Modern Trends in Hydrogeology, Hamilton, Ontario, Canada, May 10-14*.*

Gu, B., Watson, D., Goldberg, W., Bogle, M.A., Allred, D. 1988. Reactive barriers for the retention and removal of uranium, technicium, and nitrate in groundwater. RTDF Permeable Reactive Barriers Action Team Meeting, Beaverton, Oregon, April 15.

Gu, B., Watson, D.B., Wu, L., Phillips, D.H., White, D.C., Zhou, J. 2002. Microbial characteristics in a zero-valent iron reactive barrier. Environ. Monit. Assess. 77, 293-309.

Hammes, F., F. Goldschmidt, M. Vital, Y. Wang, and T. Egli. 2010 Measurement and interpretation of microbial adenosine triphosphate (ATP) in aquatic environments. Water Res. 44, 39153923.

Hara, J., Ito, H., Suto, K., Inoue, C., Chida, T. 2005. Kinetics of trichloroethene dechlorination with iron powder. Water Res. 39, 1165–1173.

Hassan, S.M., 2000. Reduction of halogenated hydrocarbons in aqueous media: I. Involvement of sulfur in iron catalysis. Chemosphere. 40, 1357-1363.
He, F., Zhang, M., Qian, T., Zhao, D. 2009. Transport of carboxymethyl cellulose stabilized iron nanoparticles in porous media: Column experiments and modeling. J. Colloid. Interface Sci. 334, 96-102.

He, F., Zhao, D. 2005. Preparation and characterization of a new class of starch-stabilized bimetallic nanoparticles for degradation of chlorinated hydrocarbons in water. Environ. Sci. Technol. 39, 3314-3320.

He, F., Zhao, D. 2007. Manipulating the size and dispersibility of zerovalent iron nanoparticles by use of carboxymethyl cellulose stabilizers. Environ. Sci. Technol. 41, 6216-6221.

He, F., Zhao, D., Liu, J., Roberts, C.B. 2007. Stabilization of Fe–Pd nanoparticles with sodium carboxymethyl cellulose for enhanced transport and dechlorination of trichloroethylene in soil and groundwater. Ind. Eng. Chem. Res. 46, 29-34.

He, F., Zhao, D., Paul, C. 2010. Field assessment of carboxymethyl cellulose stabilized iron nanoparticles for in situ destruction of chlorinated solvents in source zones. Water Res. 44 (7), 2360–2370.

He, J., Ritalahti, K.M., Aiello, M.R., Löffler, F.E. 2003. Complete detoxification of vinyl chloride by an anaerobic enrichment culture and identification of the reductively dechlorinating population as a Dehalococcoides species. Appl Environ Microbiol. 69, 996–1003.

He, Y.T., Wilson, J.T., Wilkin, R. 2010. Impact of iron sulfide transformation on trichloroethylene degradation. Geochim. Cosmochim. Ac. 74, 2025-2039.

Hendrickx, B., Dejonghe, W., Boënne, W., Brennerova, M., Cernik, M., Lederer, T., Bucheli-Witschel, M., Bastiaens, L., Verstraete, W., Top, E.M., Diels, L., Springael, D. 2005. Dynamics of an oligotrophic bacterial aquifer community during contact with a groundwater plume contaminated with benzene, toluene, ethylbenzene, and xylenes: An in situ mesocosm study. Appl. Environ. Microbiol. 71, 3815–3825.

Henschler, D. 1994. Toxicity of organochlorine compounds: effect of introduction of chlorine into organic molecules. Angew. Chem. Int. Ed. 33, 1920–1935.

Holmes, D.E., Finneran, K.T., O'Neil, R.A., Lovley, D.R. 2002. Enrichment of members of the family Geobacteraceae associated with stimulation of dissimilatory metal reduction in uranium contaminated aquifer sediments. Appl. Environ. Microbiol. 68, 2300–2306.

Hou, C.T., Barnabe, N., Greaney, K. 1986. Purification and properties of a novel xanthan depolymerase from salt-tolerant bacterial culture, HD1. Appl. Environ. Microbiol. 52, 37–44.

Imeson, A., 2009. Food Stabilisers, Thickeners and Gelling Agents, first ed. Wiley-Blackwell, Hoboken.

Jeen, S.-W., Mayer, K.U., Gillham, R.W., Blowes, D.W. 2007. Reactive Transport Modeling of Trichloroethene Treatment with Declining Reactivity of Iron. Environ. Sci. Technol. 41, 1432-1438.

Jeffers, P.M., Ward, L.M., Woytowitch, L.M., Wolfe, N.L. 1989. Homogeneous hydrolysis rate constants for selected chlorinated methanes, ethanes, ethenes, and propanes. Environ. Sci. Technol. 23, 965–969.

Jeong, H.Y., Kim, H., Hayes, K.F. 2007. Reductive Dechlorination Pathways of Tetrachloroethylene and Trichloroethylene and Their Products by Mackinawite (FeS) in the Presence of Metals. Environ. Sci. Technol. 41, 7736-7743.

Jiao, Y., Qiu, C., Huang, L. Wu, K., Ma, H., Chen, S., Ma, L., Wu, D. 2009. Reductive dechlorination of carbon tetrachloride by zero-valent iron and related iron corrosion. Appl. Catal. B-Environ. 91, 434–440.

Johnson, T.L., Scherer, M.M., Tratnyek, P.G. 1996. Kinetics of halogenated organic compound degradation by iron metal. Environ. Sci. Technol. 30, 2634-2640.

Jung, L.C, Lo, S.L., 2005. Effects of iron surface pretreatment on sorption and reduction kinetics of trichloroethylene in a closed batch system. Water Res. 39, 1037–1046.

Kanel, S.R., Nepal, D., Manning, B., Choi, H. 2007. Transport of surface-modified iron nanoparticle in porous media and application to arsenic(III) remediation. J. Nanopart. Res. 9 (5), 725–735.

Karn, B., Kuiken, T., Otto, M. 2009. Nanotechnology and in Situ Remediation: A Review of the Benefits and Potential Risks. Environ. Health Perspect. 117, 1823-1831.

Kavanaugh, M.C., Rao, P.S.C. 2003. The DNAPL remediation challenge: Is there a case for source depletion? EPA expert panel.

Kim, H., Hong, H.-J., Jung, J, Kim, S.-H., Yang, J.-W. 2010. Degradation of trichloroethylene (TCE) by nanoscale zero-valent iron (nZVI) immobilized in alginate bead. J. Hazard. Mater. 176, 1038–1043.

Klaine, S.J., Alvarez, P.J.J., Batley, G.E., Fernandes, T.F., Handy, R.D., Lyon, D.Y., Mahendra, S., McLaughlin, M.J., Lead, J.R. 2008. Nanomaterials in the environment: Behaviour, fate, bioavailability, and effects. Environ. Toxicol. Chem. 27, 1825–1851.

Klausen, J., Vikesland, P.J., Kohn, T., Burris, D.R., Ball, W.P., Roberts, A.L. 2003. Longevity of granular iron in groundwater treatment processes: solution composition effects on reduction of organohalides and nitroaromatic compounds. Environ. Sci. Technol. 37, 1208-1218.

Kohn, T., Livi, K.J.T., Roberts, A.L., Vikesland, P.J. 2005. Longevity of granular iron in groundwater treatment processes: corrosion product development. Environ. Sci. Technol. 39, 2867-2879.

Kortunov, P., Vasenkov, S., Kärger, J., Elia, M.F., Perez, M., Stöcker, M., Papadopoulos, G.K., Theodorou, D., Drescher, B., McElhiney, G., Bernauer, B., Krystl, V., Kocirik, M., Zikanova, A., Jirglova, H., Berger, C., Glaser, R., Weitkamp, J., Hansen, E.W. 2005. Diffusion in fluid catalytic cracking catalysts on various displacement scales and its role in catalytic performance. Chem. Mater. 17, 2466-2474.

Kouznetsova, I., Bayer, P., Ebert, M., Finkel, M. 2007. Modelling the long-term performance of zero-valent iron using a spatio-temporal approach for iron aging. J. Contam. Hydrol. 90, 58-80.

Lai, K.C.K., Lo, I.M.C., Kjeldsen, P. 2005. Remediation of Chlorinated Aliphatic Hydrocarbons in Groundwater using Fe^0 PRB. in: G.A. Boshoff, B.D. Bone (Eds.), Permeable Reactive Barriers, IAHS press, Wallingford, 2005, pp. 12-22.

Laskowski, J.S., Liu, Q., O'Connor, C.T. 2007. Current understanding of the mechanism of polysaccharide adsorption at the mineral/aqueous solution interface. Int. J. Miner. Process. 87, 59-68.

Lee, C., Kim, J.Y., Lee, W.I., Nelson, K.L., Yoon, J., Sedlak, D.L. 2008. Bactericidal effect of zerovalent iron nanoparticles on Escherichia coli. Environ. Sci. Technol. 42, 4927-4933.

Lee, W., Batchelor, B. 2002. Abiotic reductive dechlorination of chlorinated ethylenes by iron-bearing soil minerals. 2. Green rust. Environ. Sci. Technol. 36, 5348-5354.

Li, H., de Boer, C.V., Buchau, A., Klaas N., Rucker, W.M., Hermes, H. 2012. Development of an inductive concentration measurement sensor of nano sized zero valent iron. 9th International Multi-Conference on Systems, Signals and Devices.

Li, H., Zhou, Q., Wu, Y., Fu, J., Wang, T., Jiang, G. 2009. Effects of waterborne nano-iron on medaka (*Oryzias latipes*): antioxidant enzymatic activity, lipid peroxidation and histopathology. Ecotoxicol. Environ. Saf. 72, 684–692.

Li, X.-Q., Elliott, D.W., Zhang, W.-X. 2006. Zero-Valent Iron Nanoparticles for Abatement of Environmental Pollutants: Materials and Engineering Aspects. Crit. Rev. Solid State Mater. Sci. 31, 111–122.

Liang, L., Korte, N., Gu, B., Puls, R., Reeter, C. 2000. Geochemical and microbial reactions affecting the long-term performance of in situ 'iron barriers'. Adv. Environ. Res. 4, 273-286.

Lien H.-L., Zhang, W.-X. 2001. Complete dechlorination of chlorinated ethenes with nanoparticles. Colloid. Surface. A 191, 97–105.

Lin, C.J., Lo, S.-L. 2005. Effects of iron surface pretreatment on sorption and reduction kinetics of trichloroethylene in a closed batch system. Wat. Res. 39, 1037–1046.

Lin, Y.H., Tseng, H.H, Wey, M.Y., Lin, M.D. 2010. Characteristics of two types of stabilized nano zero-valent iron and transport in porous media. Sci. Total. Environ. 408 (10), 2260-2267.

Liu, Q., Laskowski, J.S. 1989. The interactions between dextrin and metal hydroxides in aqueous solutions. J. Colloid. Interf. Sci. 130, 101-111.

Liu, Q., Zhang, Y., Laskowski, J.S. 2000. The adsorption of polysaccharides onto mineral surfaces: an acid/base interaction. Int. J. Miner. Process. 60, 229–245.

Liu, Y., Choi, H., Dionysiou, D., Lowry, G.V. 2005. Trichloroethene hydrodechlorination in water by highly disordered monometallic nanoiron. Chem. Mater. 17, 5315-5322.

Liu, Y., Lowry, G.V. Effect of Particle Age (Fe0 Content) and Solution pH On NZVI Reactivity: H_2 Evolution and TCE Dechlorination. Environ. Sci. Technol. 2006, 40, 6085-6090.

Liu, Y., Majetich, S.A., Tilton, R.D., Sholl, D.S., Lowry, G.V. 2005. TCE dechlorination rates, pathways, and efficiency of nanoscale iron particles with different properties. Environ. Sci. Technol. 39, 1338-1345.

Lookman, R., Bastiaens, L., Borremans, B., Maesen, M., Gemoets, J., Diels, L. 2004. Batch test study on the dechlorination of 1,1,1-trichloroethane in contaminated aquifer material by zero-valent iron. J. Contam. Hydrol. 74, 133–144.

Luna, M. 2013. Injection of zerovalent iron particles: from laboratory scale to field application. PhD Thesis. Dipartimento di Ingegneria dell'Ambiente, del Territorio e delle Infrastrutture – DIATI. Politecnico di Torino.

Ma, C., Wu, Y. 2008. Dechlorination of perchloroethylene using zerovalent metal and microbial community. Environ. Geol. 55, 47–54.

Ma, X., Pawlik, M. 2007. Role of background ions in guar gum adsorption on oxide minerals and kaolinite. J. Colloid. Interf. Sci. 313, 440–448.

Mace, C. 2006. Controlling groundwater VOCs: do nanoscale ZVI particles have any advantages over microscale ZVI or BNP. Pollut. Eng. 38, 24–27.

Mackay, D., Shiu, W.Y., Ma, K.C. 1993. Illustrated Handbook of Physical-Chemical Properties and Environmental Fate for Organic Chemicals. Lewis Publishers, Chelsea, MI, USA.

Mackenzie, J.M.W., 1980. Guar-based reagents. EGMJ.

Matheson, I.J., Tratnyek, P.G. 1994. Reductive dehalogenation of chlorinated methanes by iron metal. Environ. Sci. Technol. 28, 2045-2053.

Mayer, K.U., Blowes, D.W., Frind, E.O. 2001. Reactive transport modeling of an in situ reactive barrier for the treatment of hexavalent chromium and trichloroethylene in groundwater. Water Resour. Res. 37, 3091–3103.

McCarty, P.L. 1997. Biotic and Abiotic Transformations of Chlorinated Solvents in Groundwater, In Proceedings of the Symposium on Natural Attenuation of Chlorinated Organics in Groundwater. United States Environmental Protection Agency, Washington D.C., EPA/540/R-97/504.

Miehr, R., Tratnyek, P.G., Bandstra, J.Z., Scherer, M.M., Alowitz, M., Bylaska, E.J. 2004. The diversity of contaminant reduction reactions by zero-valent iron: role of the reductate. Environ. Sci. Technol. 38, 139-147.

Moore, K., Forsberg, B., Baer, D., Arnold, W., Penn, R., 2011. Zero-Valent Iron: Impact of Anions Present during Synthesis on Subsequent Nanoparticle Reactivity. J. Environ. Eng. 137 (10), 889–896.

Mueller, N.C., Braun, J. Bruns, J., Černík, M., Rissing, P. Rickerby, D., Nowack, B. 2012. Application of nanoscale zero valent iron (NZVI) for groundwater remediation in Europe. Environ. Sci. Pollut. Res. 19, 550–558.

Muyzer, G., De Waal, E.C., Uitterlinden, A. 1993. Profiling of complex microbial populations using denaturing gradient gel electrophoresis analysis of polymerase chain reaction-amplified genes coding for 16S rRNA. Appl. Environ. Microbiol. 59, 695-700.

Navon, D., Loehr, R.C., Liljestrand, H.M., Daniel, D.E. 1998. Impact of biodegradable trenching slurry on iron treatment wall performance. Water Sci. Technol. 38 (7), 49–53.

North Wind Inc., 2010. EHC Case Study. http://environmental.fmc.com/media/resources/FMC_EHC_Case_Study-TCE-Atlas_Missle_Site-Windsor,CO.pdf

Noubactep, C., Caré, S. 2010. On nanoscale metallic iron for groundwater remediation. J. Hazard. Mater. 182, 923-927.

Noubactep, C., Caré, S., Crane, R.A. 2012. Nanoscale metallic iron for environmental remediation: prospects and limitations. Water Air Soil Poll. 223, 1363-1382.

Nurmi, J., Tratnyek, P., 2008. Electrochemical studies of packed iron powder electrodes: Effect of common constituents of natural waters on corrosion potential. Corros. Sci. 50, 144-154.

Nurmi, J., Tratnyek, P., Sarathy, V., Baer, D., Amonette, J, Pecher, K., Wang, C., Linehan, J., Watson, D., Penn, R., 2005. Driessen, M. Characterization and properties of Metallic Iron Nanoparticles: Spectroscopy, Electrochemistry and Kinetics. Environ. Sci. Technol. 39, 1221-1230.

Ohfuji, H., Rickard, D. 2006. High resolution transmission electron microscopic study of synthetic nanocrystalline mackinawite. Earth and Planetary Sc. Lett. 241, 227–233

Olson, M.R., Sale, T.C., Shackelford, C.D., Bozzini, C., Skeean, J. 2012. Chlorinated Solvent Source-Zone Remediation via ZVI-Clay Soil Mixing: 1-Year Results. Ground. Water. Monit. R. 32, 63-74.

Odziemkowski, M.S., Schuhmacher, T.T., Gillham, R.W., Reardon, E.J. 1998. Mechanisms of oxide film formation on iron in simulating groundwater solutions: raman spectroscopic studies. Corros. Sci. 40, 371-389.

Oostrom, M., Wietsma, T.W., Covert, M.A., Vermeul, V.R., 2007. Zero-valent iron emplacement in permeable porous media using polymer additions. Ground. Water Monit. R. 27, 122–130.

OVAM, 2009. Vlaams Reglement rond bodemsanering en bodembescherming - Vlarebo. Openbare Vlaamse Afvalstoffenmaatschappij. D/2005/5024/44.

Painter, T.J., Gonzalez, J.J., Hemmer, P.C. 1979. The distribution of D-galactose residues in guaran and locust-bean gum. Carbohydr. Res. 69, 217.

Pankow, J.F., Cherry, J.A. 1996. Dense chlorinated solvents and other DNAPLs in Groundwater. Waterloo Press, pp. 522.

Parkhurst, D.L., Appelo, C.A.J. 1999. User's guide to PHREEQC (Version 2) - a computer program for speciation, batch-reaction, one-dimensional transport, and inverse geochemical calculations. U.S. Geological Survey, Water-Resources Investigations Report 99-4259.

Phenrat, T., Liu, Y., Tilton, R.D., Lowry, G.V. 2009. Adsorbed polyelectrolyte coatings decrease Fe^0 nanoparticle reactivity with TCE in water: conceptual model and mechanisms. Environ. Sci. Technol. 43 (5), 1507–1514.

Phenrat, T., Saleh, N., Sirk, K., Tilton, R.D,, Lowry, G.V. 2007. Aggregation and sedimentation of aqueous nanoscale zerovalent iron dispersions. Environ. Sci. Technol. 41. 284–290.

Phillips, D.H., Watson, D.B., Roh, Y., Gu, B. 2003. Mineralogical characteristics and transformations during long-term operation of a zerovalent iron reactive barrier. J. Environ. Qual. 32, 2033-2045.

Postgate, J.R. 19984. The J’ulphate-Reducing Bacteria, Cambridge University Press, Cambridge.

Prokop G., Schamann, M., Edelgaard, I. 2000. Management of contaminated sites in Western Europe, Topic Report No. 13/199, European Environment Agency.

Prommer, H., Aziz, L.H., Bolano, N., Taubals, H., Schuth, C. 2008. Modeling of geochemical and isotopic changes in a column experiment for degradation of TCE by zerovalent iron. J. Contam. Hydrol. 97, 13-26.

Quinn, J., Geiger, C., Clausen, C., Brooks, K., Coon, C. 2005. Field Demonstration of DNAPL Dehalogenation Using Emulsified Zero-Valent Iron. Environ. Sci. Technol. 39, 1309-1318.

Rath, R.K., Subramanian S., Sivanandam, V., Pradeep, T. 2001. Studies in the interaction of guar gum with chalcopyrite. Can. Metall. Q. 40 (1), 01-12.

Reardon, E. J. 1995. Anaerobic corrosion of granular iron: Measurement and interpretation of hydrogen evolution rates. Environ. Sci. Technol. 29, 2936-2945.

Reardon, E.J. 2005. Styles of Corrosion and Inorganic Control on Hydrogen Pressure Buildup. Environ. Sci. Technol. 39, 7311-7317.

Reardon, E.J., Fagan, R., Vogan, J.L. 2008. Przepiora, A. Anaerobic Corrosion Reaction Kinetics of Nano-sized Iron. Environ. Sci. Technol. 42, 2420-2426.

Roh, Y., Lee, S.Y., Elless, M.P. 2000. Characterization of corrosion products in the permeable reactive barriers. Environ. Geol. 40, 184-194.

Roberts, A.L., Totten, L.A., Arnold, W.A., Burris, D.R., Campbell, T.J. 1996. Reductive elimination of chlorinated ethylenes by zero-valent metals. Environ. Sci. Technol. 30, 2654–2659.

Sakulchaicharoen, N., O'Carroll, D.M., Herrera, J.E. 2010. Enhanced stability and dechlorination activity of pre-synthesis stabilized nanoscale FePd particles. J. Contam. Hydrol. 118, 117–127.

Saleh, N., Sirk, K., Liu, Y., Phenrat, T., Dufour, B., Matyjaszewski, K., Tilton, R.D., Lowry, G.V. 2007. Surface modification enhance nanoiron transport and NAPL targeting in saturated porous media. Environ. Eng. Sci. 24 (1), 45-57.

Schafer, D., Kober, R., Dahmke, A. 2003. Competing TCE and cis-DCE degradation kinetics by zero-valent iron-experimental results and numerical simulation. J. Contam. Hydrol. 65, 183-202.

Scherer, M.M., Balko, B.A., Gallagher, D.A., Tratnyek, P.G. 1998. Correlation analysis of rate constants for dechlorination by zero-valent iron. *Environ. Sci. Technol. 32*(19), 3026-3033.

Scherer, M.M., Westall, J.C., Ziomek-Moroz, M., Tratnyek P.G. 1997. Kinetics of carbon tetrachloride reduction at an oxide-free iron electrode Environ. Sci. Technol., 31, 2385–2391.

Schrick, B., Blough, J.L., Jones, A.D., Mallouk, T.E. 2002. Hydrodechlorination of trichloroethylene to hydrocarbons using bimetallic nickle-iron nanoparticles. Chem. Mat. 14, 5140-5147.

Schrick, B., Hydutsky, B.W., Blough, J.L., Mallouk, T.E. 2004. Delivery Vehicles for Zerovalent Metal Nanoparticles in Soil and Groundwater. C*hem. Mater.* 16 (11), 2187–2193.

Sherwood Lollar, B., Hirschorn, S.K., Chartrand, M.M.G., Lacrampe-Couloume G. 2007. An approach for assessing total instrumental uncertainty in compound specific carbon isotope analysis: implications for environmental remediation studies. Anal. Chem. 79, 3469–3475.

Shi, Z., Nurmi, J.T., Tratnyek, P.G. 2011. Effects of Nano Zero-Valent Iron on Oxidation-Reduction Potential. Environ. Sci. Technol., 45, 1586-1592.

Singh, V., Tiwari, A., Tripathi, D.N., Sanghi, R. 2005. Poly(acrylonitrile) grafted ipomoea seed-gums: A renewable reservoir to industrial gums. Biomacromolecules. 6, 453–456.

Smits, T.H.M., Devenoges, C., Szynalski, K., Maillard, J., Holliger, C. 2004. Development of a real-time PCR method for quantification of the three genera Dehalobacter, Dehalococcoides, and Desulfitobacterium in microbial communities. J. Microbiol. Methods. 57, 369–378.

Song, H., Carraway, E.R. 2005. Reduction of chlorinated ethanes by nanosized zero-valent iron: Kinetics, pathways, and effects of reaction conditions. Environ. Sci. Technol. 39, 6237-6245.

Sprinkle, C., Ewing, D., Strong, M., Owens, D., Ventura, B.,. Smith, L. 2004. Pilot-Testing Four Treatment Technologies For Chlorinated Solvents In Low - Permeability Formations. 4th International Conf. On Remediation of Chlorinated and Recalcitrant Compounds, Monterey, CA. pages 5B-06.Battelle Press.

Squillace, P.J., Moran, M.J., Price, C.V. 2004. Vocs in shallow groundwater in new residential/commercial areas of the united states. Environ. Sci. Technol. 38, 5327–5338.

Su, C., Puls, R.W. 1999. Kinetics of trichloroethene reduction by zerovalent iron and tin: pretreatment effect, apparent activation energy, and intermediate products. Environ. Sci. Technol. 33, 163–168.

Suk O.J., Jeen, S.-W., Gillham, R. W., Gui, L. 2009. Effects of initial iron corrosion rate on long-term performance of iron permeable reactive barriers: column experiments and numerical simulation. J. Contam. Hydrol. 103, 145-156.

Sun, Y.P., Li, X-Q, Zhang, W-X., Wang, H.P. 2007. A method for the preparation of stable dispersion of zero-valent iron nanoparticles. Colloid. Surface. A. 60–66.

Sung, Y., Ritalahti, K.M, Apkarian, R.P., Löffler, F.E. 2006. Quantitative PCR confirms purity of strain GT, a novel trichloroethene-to-ethene-respiring Dehalococcoides isolate. Appl Environ Microbiol. 72, 1980–1987.

Suthersan, S.S. 1999. Hydraulic and pneumatic fracturing. Chapter 9 in Remediation Engineering Design Concepts. Lewis Publishers, USA.

Suyama, A., Yamashita, M., Yoshino, S., Furukawa, K. 2001. Isolation and characterization of Desulfitobacterium sp. strain Y51 capable of efficient dehalogenation of tetrachlorethene and polychloroethanes. Biosci. Biotechnol. Biochem. 65, 1474-1481.

Tiraferri, A., Chen, K.L., Sethi, R., Elimelech, M. 2008. Reduced aggregation and sedimentation of zerovalent iron nanoparticles in the presence of guar gum. J. Colloid Interf. Sci. 324, 71-79.

Tiraferri, A., Sethi, R. 2009. Enhanced transport of zerovalent iron nanoparticles in saturated porous media by guar gum. J. Nanopart. Res. 11 (3), 635-645.

Tobiszewski, M., Namieśnik, J. 2012. Abiotic degradation of chlorinated ethanes and ethenes in water. Environ. Sci. Pollut. Res. Int. 19(6), 1994–2006.

Tosco, T., Bosch, J., Meckenstock, R., Sethi, R. 2012. Transport of ferrihydrite nanoparticles in saturated porous media: role of ionic strength and flow rate. Environ. Sci. Technol. 46, 4008-4015.

Tosco, T., Sethi, R., 2010. Transport of Non-Newtonian Suspensions of Highly Concentrated Micro- And Nanoscale Iron Particles in Porous Media: A Modeling Approach. Environ. Sci. Technol. 44, 9062–9068.

Tratnyek, P.G., Johnson, T.L., Scherer, M.M., Eykholt, G.R. 1997. Remediating groundwater with zero-valent metals: Kinetic considerations in barrier design. Ground Wat. Monitor. Remed. 17, 108-114.

Tratnyek, P.G., Scherer, M.M., Deng, B., Hu, S. 2001. Effects of natural organic matter, anthropogenic surfactants, and model quinones on the reduction of contaminants by zero-valent iron. Water Res. 35, 4435-4443.

Truex, M.J., Vermeul, V.R., Mendoza, D.P., Fritz, B.G., Mackley, R.D., Oostrom, M., Wietsma, T.W., Macbeth, T. 2011. Injection of Zero-Valent Iron into an Unconfined Aquifer Using Shear-Thinning Fluids. Ground Water Monit. R. 31 (1), 50-58.

Uludag-Demirer, S., Bowers, A.R., 2003. Effects of Surface Oxidation and Oxygen on the Removal of Trichloroethylene From the Gas Phase Using Elemental Iron. Water Air Soil Pollut. 142, 1-4.
US EPA, 1999. Field Applications of In Situ Remediation Technologies: Permeable Reactive Barriers. EPA 542-R-99-002. Office of Solid Waste and Emergency Response Technology Innovation: Washington, DC.

US EPA. 2001. Cost Analysis for Selected Groundwater Cleanup Projects: Pump and Treat Systems and Permeable Reactive Barriers. US EPA 542-R-00-01.

US EPA. 2003a. The DNAPL Remediation Challenge: Is There a Case for Source Depletion? EPA/600/R-03/143.

US EPA. 2003b. Cost and Performance Summary Report In Situ Chemical Reduction at the Marshall Space Flight Center, Source Area 2, Huntsville, Alabama.

US EPA. 2006. In situ Thermal Treatment of Chlorinated Solvents: Fundamentals and Field Applications. EPA 542-R-04-010.

Van Nooten, T., Lieben, F., Dries, J., Pirard, E., Springael, D., Bastiaens, L. 2007. Impact of Microbial Activities on the Mineralogy and Performance of Column-Scale Permeable Reactive Iron Barriers Operated under Two Different Redox Conditions. *Environ. Sci. Technol. 41,* 5724–5730.

Van Nooten, T., Springael, D., Bastiaens, L. 2008. Design of a multifunctional permeable reactive barrier for the treatment of landfill leachate contamination: laboratory column evaluation. Environ. Sci. Technol. 42, 8890–8895.

Van Nooten, T., Springael, D., Bastiaens, L. 2010. Microbial Community Characterization in a Pilot-Scale Permeable Reactive Iron Barrier. Environ. Eng. Sci. 27, 287-292.

VanStone, N.A., Focht, R., Mabury, S., Sherwood Lollar, B. 2004. Effect of iron type on kinetics and carbon isotopic enrichment of chlorinated ethylenes during abiotic reduction on Fe(0). Ground Water. 42 (2), 268-276.

VanStone, N., Przepiora, A., Vogan, J., Lacrampe-Couloume, G., Powers, B., Perez, E., Mabury, S., Sherwood Lollar, B. 2005. Monitoring trichloroethene remediation at an iron permeable reactive barrier using stable carbon isotopic analysis. J. Contam. Hydrol. 78, 313-25.

Varadhi, S. N., Gill, H.S., Apoldo, L.J., Liao, K., Blackman, R.A., Wittman, W.K. 2005. Full-scale nanoiron injection for treatment of groundwater contaminated with chlorinated hydrocarbons. Proceedings of Natural Gas Technologies 2005 Conference, Orlando, Florida, January 30 – February 2.

Vecchia, E.D., Luna, M., Sethi, R. 2009. Transport in Porous Media of Highly Concentrated Iron Micro- and Nanoparticles in the Presence of Xanthan Gum. *Environ. Sci. Technol.* 43 (23), 8942-8947.

Velimirovic, M., Chen, H., Simons, Q., Bastiaens, L. 2012. Reactivity recovery of guar gum coupled mZVI by means of enzymatic breakdown and rinsing J. Contam. Hydrol. 142-143, 1-10.

Velimirovic, M., Larsson, P.-O., Simons, Q., Bastiaens L. 2013. Reactivity screening of microscale zerovalent irons and iron sulfides towards different CAHs under standardized experimental conditions. J. Hazard. Mater. 252-253, 204-212.

Vital, M., Dignum, M., Magic-Knezev, A., Ross, P., Rietveld, L., Hammes, F. 2012. Flow cytometry and adenosine tri-phosphate analysis: Alternative possibilities to evaluate major bacteriological changes in drinking water treatment and distribution systems. Water Res. 44, 4665-4676.

Wade, L.G., 2006. Organic Chemistry (Sixth Ed.). Pearson Prentice Hall. pp. 279.
Wang C., Zhang, W. 1997. Nanoscale metal particles for dechlorination of PCE and PCBs. Environ. Sci. Technol. 31, 2154–2156.

Wang, W., Zhou, M., 2010. Degradation of trichloroethylene using solvent-responsive polymer coated Fe nanoparticles. Colloid. Surface. A. 369 (1), 232-239.

Water Framework Directive 2000/60/EC, 2000, 1-73.

Westrick, J.J., Mello, J.W., Thomas, R.F., 1984. The ground water supply survey. J. Amer. Water Works Assoc. 76, 52-59.

Whistler, R.L., Hymowitz, T., 1979. Guar: Agronomy, production, industrial use and nutrition. Purdue University Press, West Lafayette, IN, USA.

Wolery, T.J., Daveler, S.A., 1992. EQ6, A Computer Program for Reaction Path Modeling of Aqueous Geochemical Systems: Theoretical Manual, User's Guide, and Related Documentation (Version 7.0). E1.28: UCRL-MA-110662Pt4, Lawrence Livermore National Laboratory, Livermore, CA.

Wüst, W. F., Köber, R., Schlicker, O., Dahmke, A., 1999. Combined zero and first-order kinetic model of the degradation of trichloroethene and *cis*-dichloroethene with commercial iron. Environ. Sci. Technol. 33, 4304–4309.
Xu, Y., Zhang, W. 2000. Subcolloidal Fe/Ag particles for reductive dehalogenation of chlorinated benzenes. Ind. Eng. Chem. Res. 39, 2238–2244.

Xue, D., Sethi, R. 2012. Viscoelastic gels of guar and xanthan gum mixtures provide long-term stabilization of iron micro- and nanoparticles. J. Nanopart. Res. 14: 1239.

Yang, Y., McCarty, P.L., 2000. Biologically enhanced dissolution of tetrachloroethene DNAPL. *Environ*. *Sci*. Technol. 34 (14), 2979-2984.

Yin, Y., Allen, H.E. 1999 Technology evaluation report: In situ chemical treatment. http://clu-in.org/download/toolkit/inchem.pdf

Zhang, W. 2003. Nanoscale iron particles for environmental remediation: An overview. J. Nanopart Res. 5, 323–332.

Zhang, W., Elliott, D. 2006. Applications of iron nanoparticles for groundwater remediation. Remediation Journal, 16(2), 7-21.

Zhang, W., Wang, C.B., Lien, H.L. 1998. Treatment of chlorinated organic contaminants with nanoscale bimetallic particles. Catal. Today. 40, 387–395.

Zhuang, P., Pavlostathis., S.G. 1995. Effect of Temperature, pH and Electron Donor on the Reductive Dechlorination of Chloroalkenes. Chemosphere. 31, 3537-3548.

Zhuang, Y., Ahn, S., Seyfferth, A.L., Masue-Slowey, Y., Fendorf, S., Luthy, R.G. 2011. Dehalogenation of Polybrominated Diphenyl Ethers and Polychlorinated Biphenyl by Bimetallic, Impregnated, and Nanoscale Zerovalent Iron. Environ. Sci. Technol. 45, 4896–4903.

Zolla, V., Freyria, F.S., Sethi, R., Di Molfetta, A. 2009. Hydrogeochemical and biological processes affecting the long-term performance of an iron-based permeable reactive barrier. J. Environ. Qual., 38 (3), 897-908.

ANNEX I INITIAL CONSTANTS USED BY PHREEQC

Speciation reactions and equilibrium constants (note that Fe^{3+} is included in the speciation database)

Equilibrium reaction	**Log K**
H_2O ---> $OH^- + H^+$	-14.000
$2H_2O$ ---> $O_2 + 4H^+ + 4e^-$	-86.080
$2H^+ + 2e^-$ ---> H_2	-3.15
$CO_3^{2-} + H^+$ ---> HCO_3^-	10.329
$CO_3^{2-} + 2H^+$ ---> $CO_2 + H_2O$	16.681
$Ca^{2+} + H_2O$ ---> $CaOH^+ + H^+$	-12.780
$Ca^{2+} + CO_3^{2-}$ ---> $CaCO_3$	3.224
$Ca^{2+} + CO_3^{2-} + H^+$ ---> $CaHCO_3^+$	11.435
$Na^+ + H_2O$ ---> $NaOH + H^+$	-14.180
$Na^+ + CO_3^{2-}$ ---> $NaCO_3^-$	1.270
$Na^+ + HCO_3^-$ ---> $NaHCO_3$	-0.250
$Fe^{2+} + H_2O$ ---> $FeOH^+ + H^+$	-9.500
$Fe^{2+} + 2H_2O$ ---> $Fe(OH)_2 + 2H^+$	-20.570
$Fe^{2+} + 3H_2O$ ---> $Fe(OH)_3^- + 3H^+$	-31.000
$Fe^{2+} + Cl^-$ ---> $FeCl^+$	0.140
$Fe^{2+} + CO_3^{2-}$ ---> $FeCO_3$	4.380
$Fe^{2+} + HCO_3^-$ ---> $FeHCO_3^-$	2.000
Fe^{2+} ---> $Fe^{3+} + e^-$	-13.020
$Fe^{3+} + H_2O$ ---> $FeOH^{2+} + H^+$	-2.190
$Fe^{3+} + 2H_2O$ ---> $Fe(OH)^{2+} + 2H^+$	-5.670
$Fe^{3+} + 3H_2O$ ---> $Fe(OH)_3 + 3H^+$	-12.560
$Fe^{3+} + 4H_2O$ ---> $Fe(OH)_4^- + 4H^+$	-21.60
$2Fe^{3+} + 2H_2O$ ---> $Fe_2(OH)_2^{4+} + 2H^+$	-2.950
$3Fe^{3+} + 4H_2O$ ---> $Fe_3(OH)_4^{5+} + 4H^+$	-6.300
$Fe^{3+} + Cl^-$ ---> $FeCl^{2+}$	1.480
$Fe^{3+} + 2Cl^-$ ---> $FeCl^{2+}$	2.130
$Fe^{3+} + 3Cl^-$ ---> $FeCl_3$	1.130

Iron corrosion reaction stoichiometry

Reaction	**Stoichiometry**
Anaerobic iron corrosion	$Fe^0 + 2H_2O \rightarrow Fe^{2+} + 2OH^- + H_2$
K_{IrC} reported in Mayer et al 2001 **1.6596E-12**	

Minerals and liquid-gas equilibriums and equilibrium constants

Mineral phase	**log K**
H_2 (g) ---> H_2 (aq)	-3.150[a]
CO_2 (g) ---> CO_2 (aq)	-1.468[a]
$Fe(OH)_2$ (am) ---> Fe^{2+} $2H_2O$ - $2H^+$	13.905[b]

[a] From PHREEQC database (Parkhurst and Appelo, 1999).
[b] From EQ/6 database (Wolery and Daveler, 1992).

ANNEX II FIELD PARAMETERS DATA (CHAPTER 7)

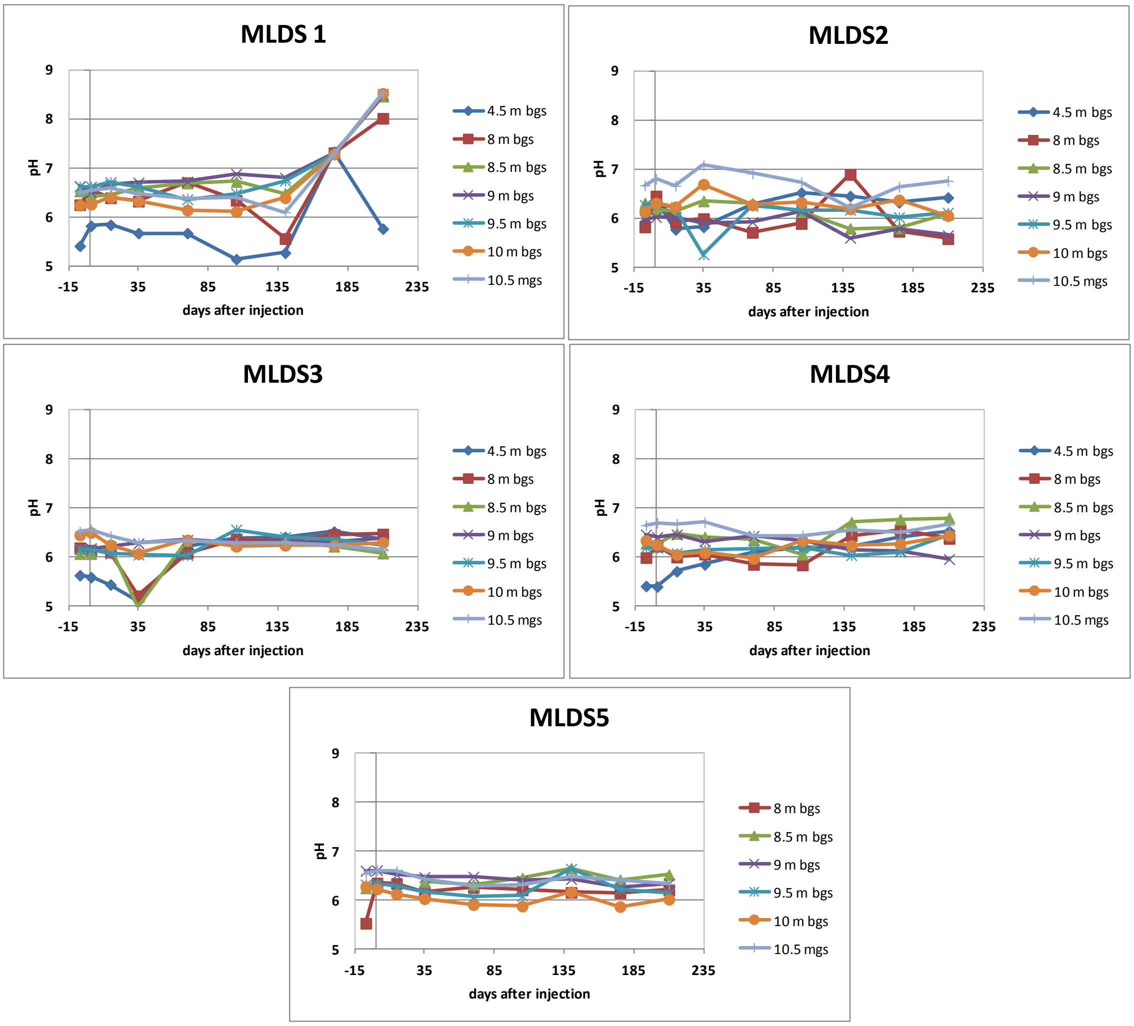

pH values measured over time.

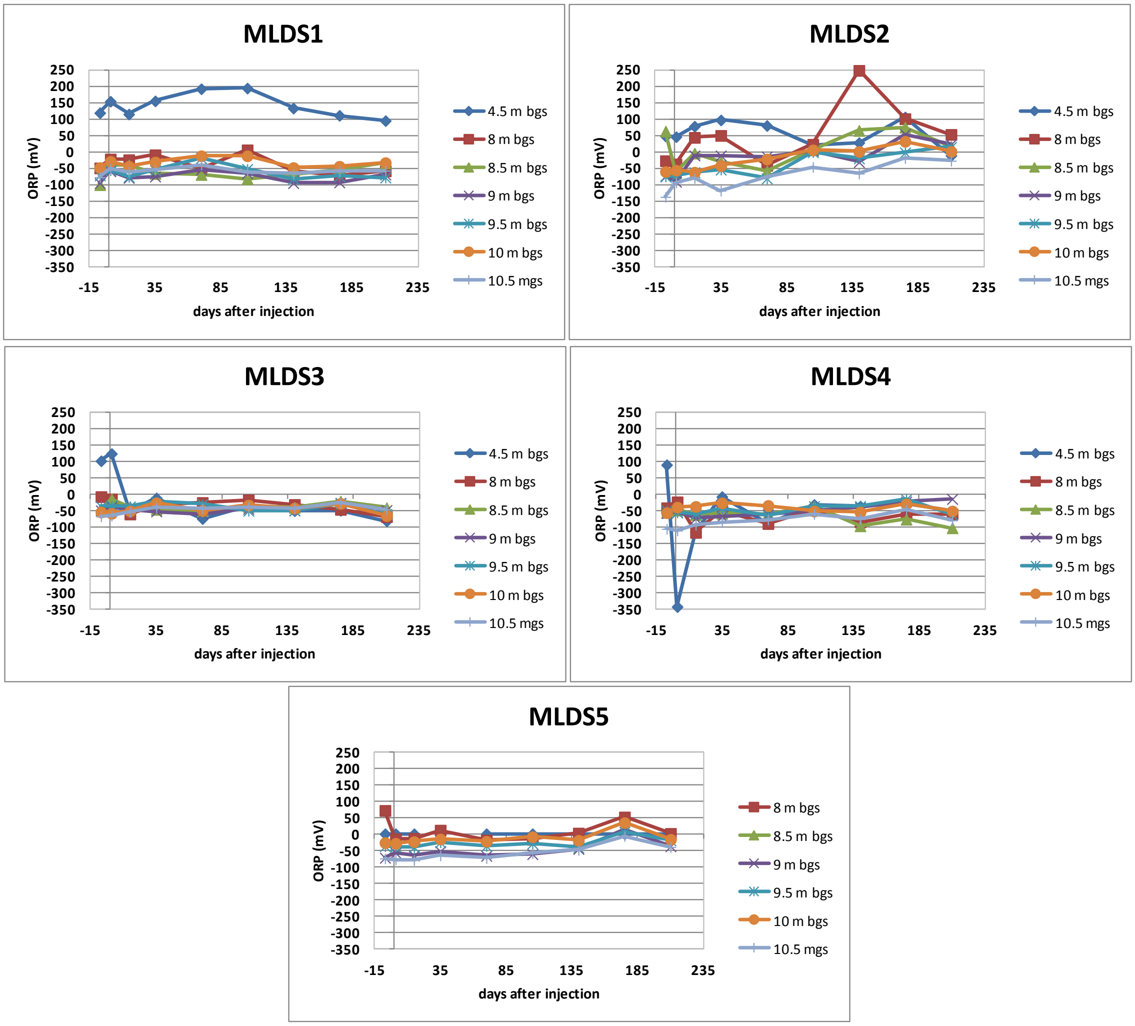

ORP values measured in groundwater over time.

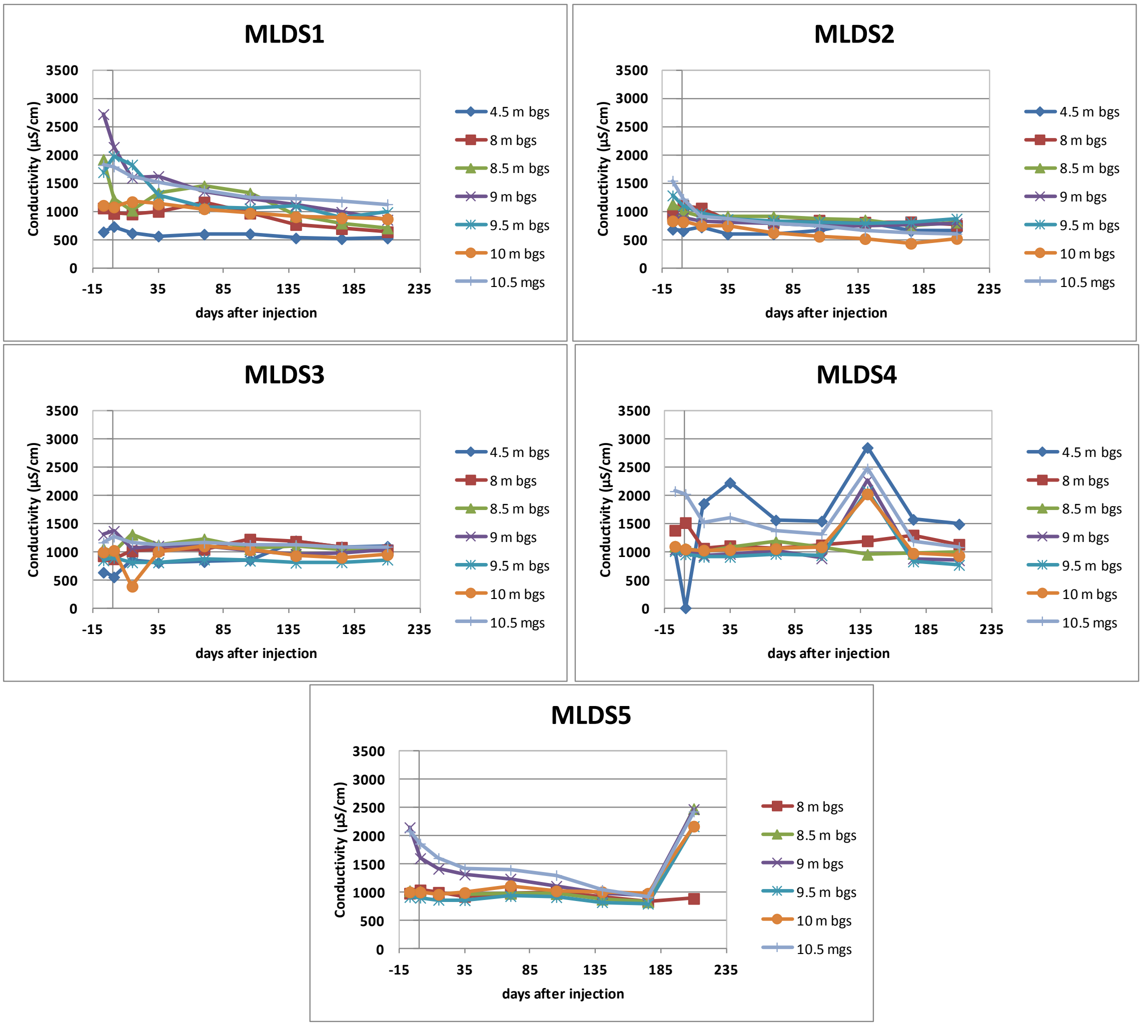

Electrical conductivity (EC) measured in groundwater over time.

ANNEX III FIELD MONITORING DATA (CHAPTER 7)

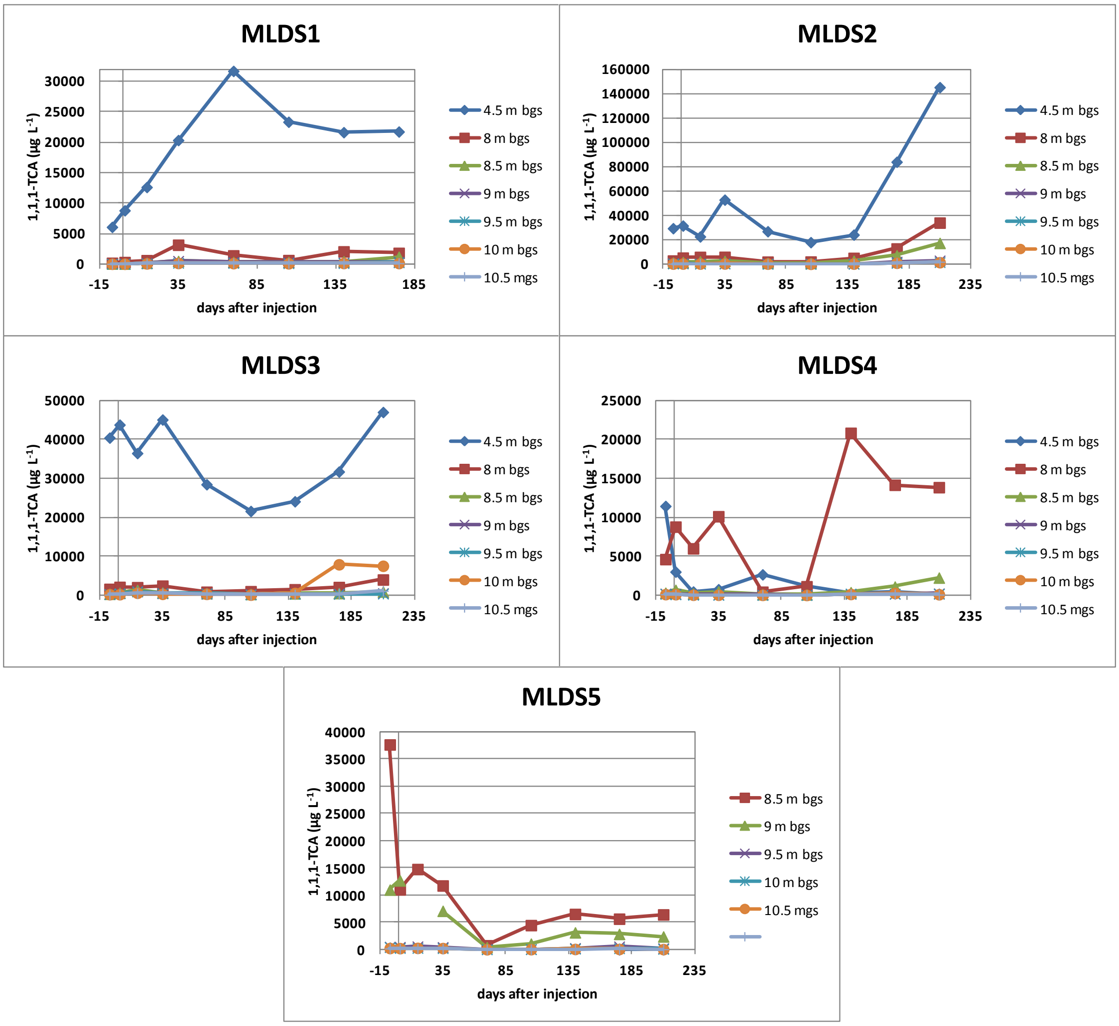

1,1,1-TCA concentrations over time. Note that the scale of each plot may be different.

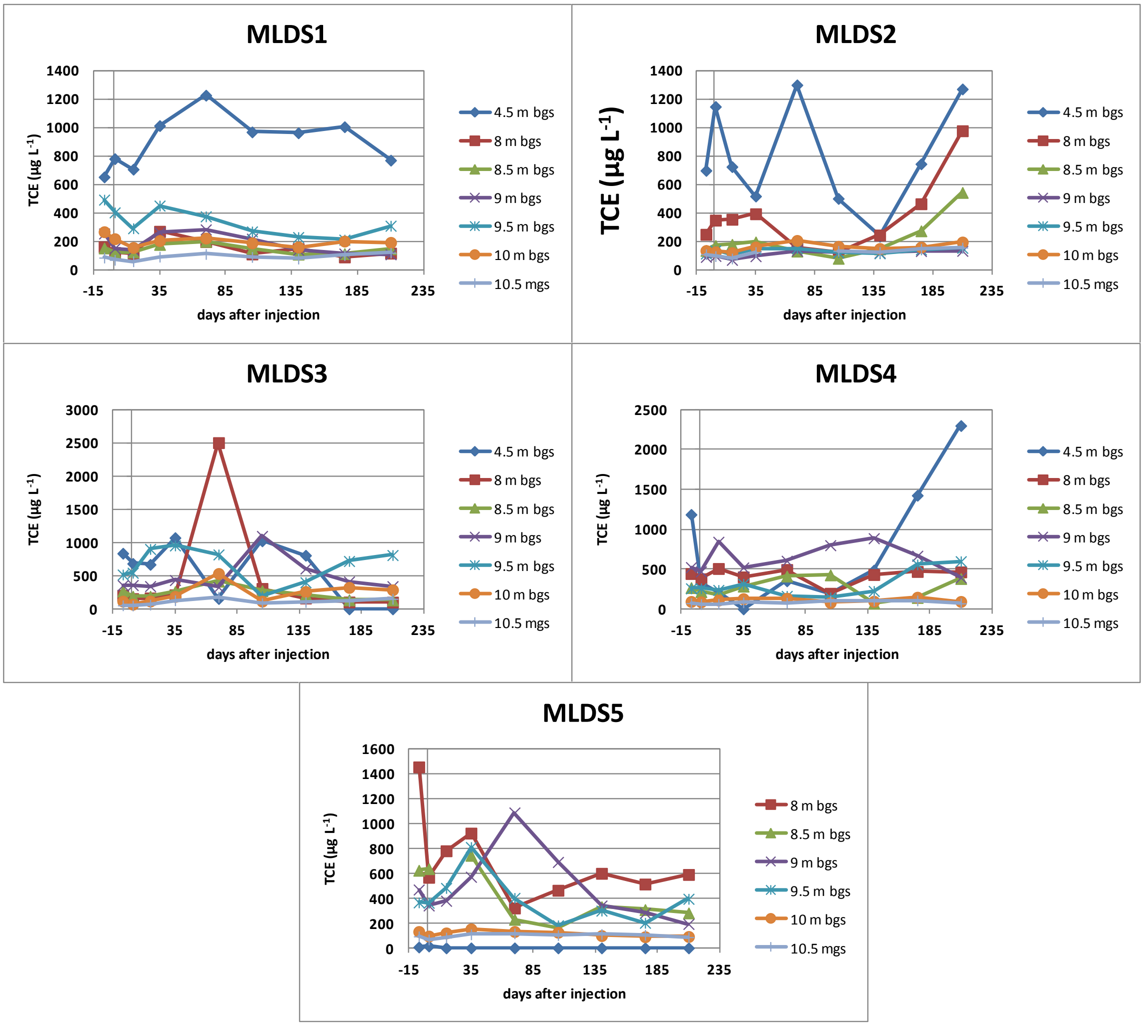

TCE concentrations over time. Note that the scale of each plot may be different.

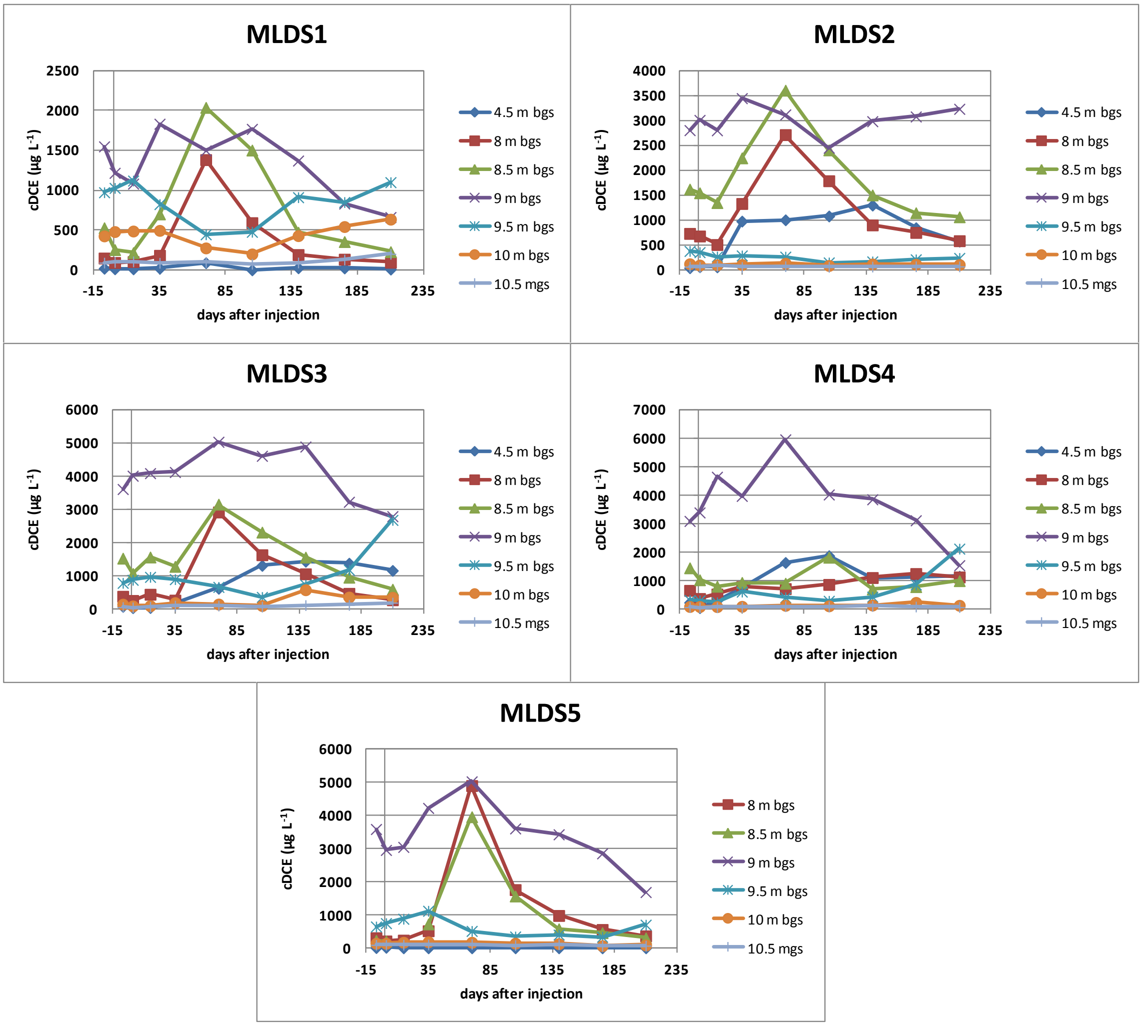
MLDS1

MLDS2

MLDS3

MLDS4

MLDS5

cDCE concentrations over time. Note that the scale of each plot may be different.

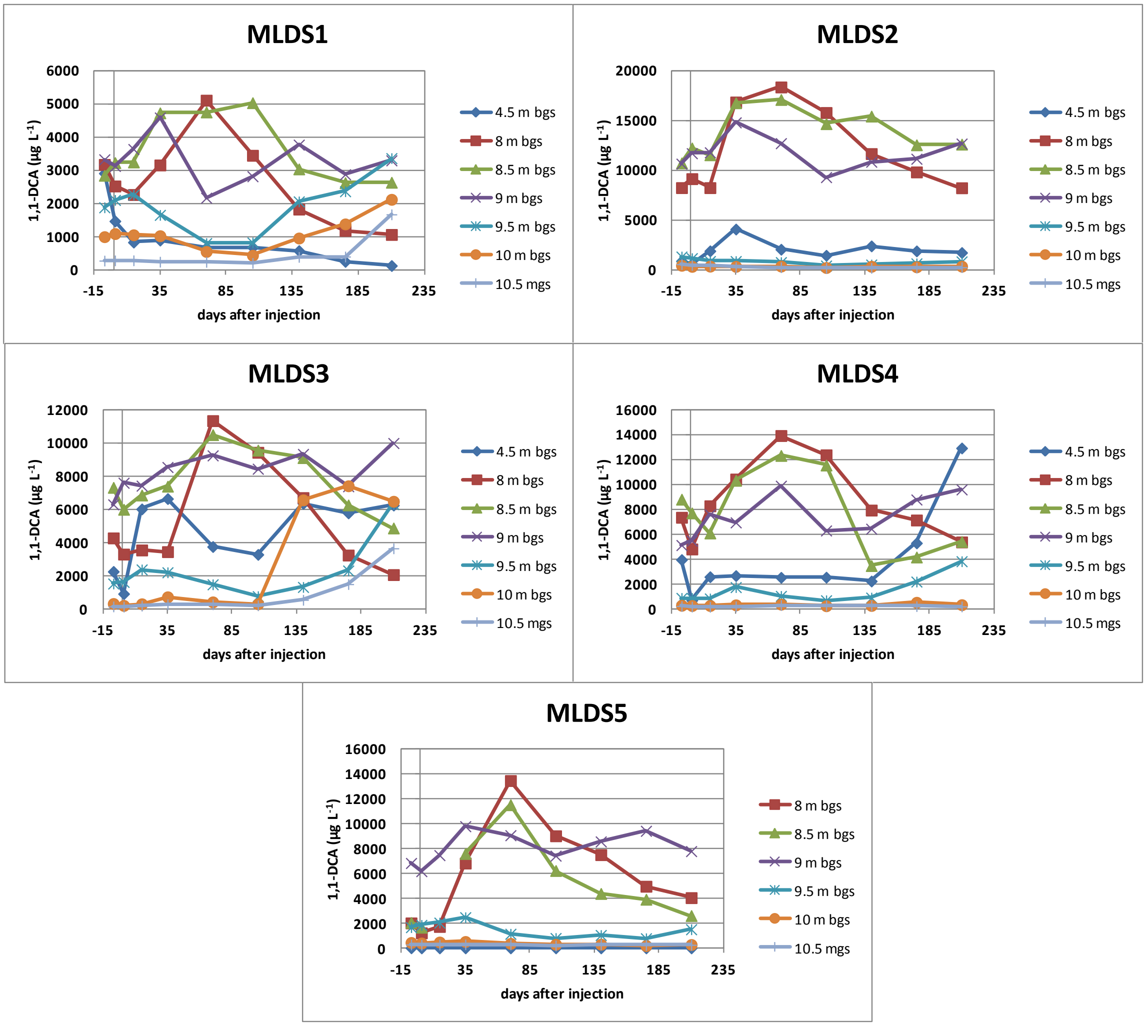
MLDS1

MLDS2

MLDS3

MLDS4

MLDS5

1,1-DCA concentrations over time. Note that the scale of each plot may be different.

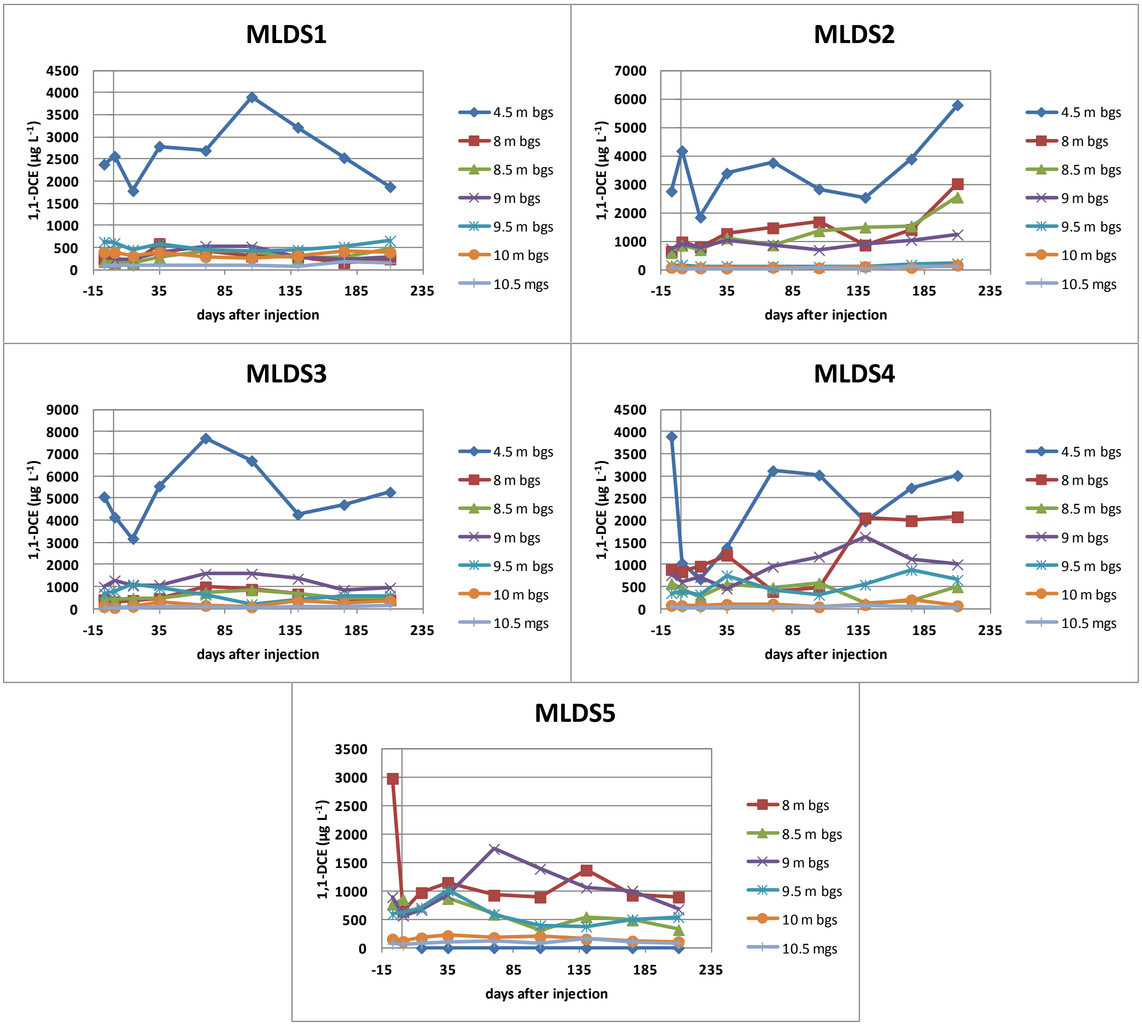

1,1-DCE concentrations over time. Note that the scale of each plot may be different.

ANNEX IV CSIA FILED DATA (CHAPTER 7)

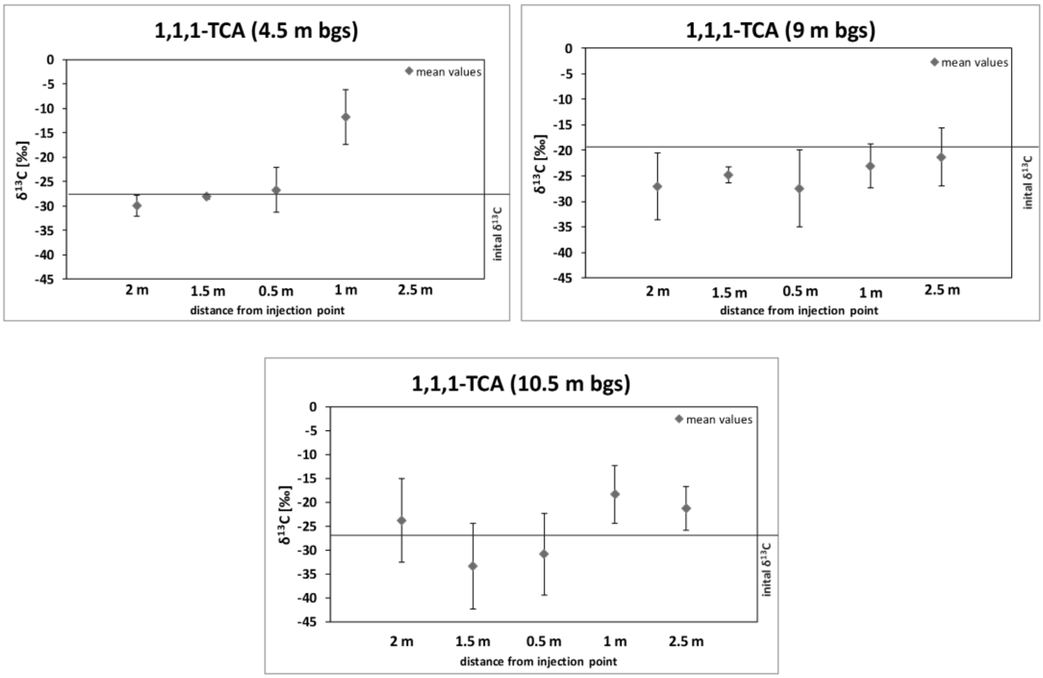

1,1,1-TCA (4.5 m bgs)

1,1,1-TCA (9 m bgs)

1,1,1-TCA (10.5 m bgs)

δ^{13}C (‰) mean values of 1,1,1-TCA in the monitoring wells (MLDS1 – MLDS5) at different depths (4.5, 9 and 10.5 m bgs).

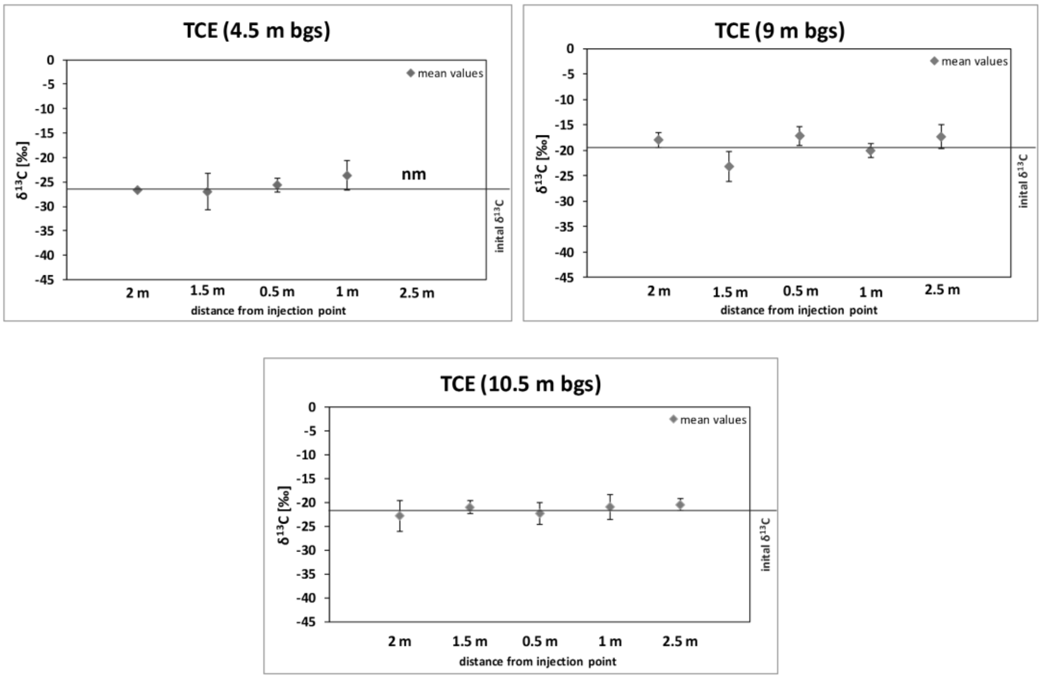

$\delta^{13}C$ (‰) mean values of TCE in the monitoring wells (MLDS1 – MLDS5) at different depths (4.5, 9 and 10.5 m bgs).

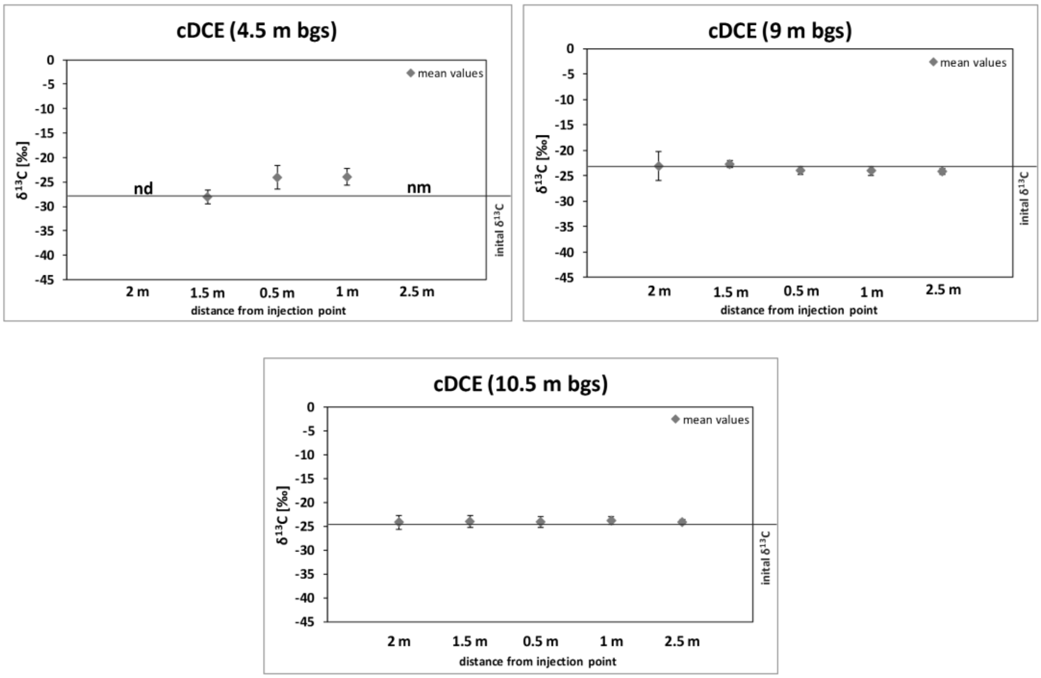

$\delta^{13}C$ (‰) mean values of cDCE in the monitoring wells (MLDS1 – MLDS5) at different depths (4.5, 9 and 10.5 m bgs).

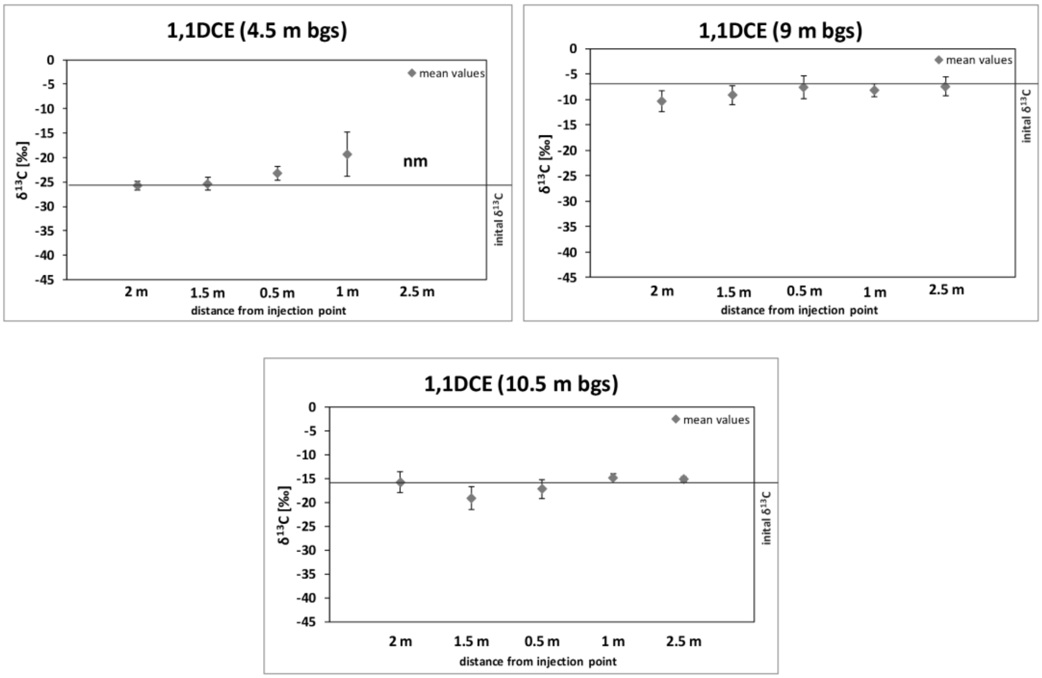

$\delta^{13}C$ (‰) mean values of 1,1-DCE in the monitoring wells (MLDS1 – MLDS5) at different depths (4.5, 9 and 10.5 m bgs).

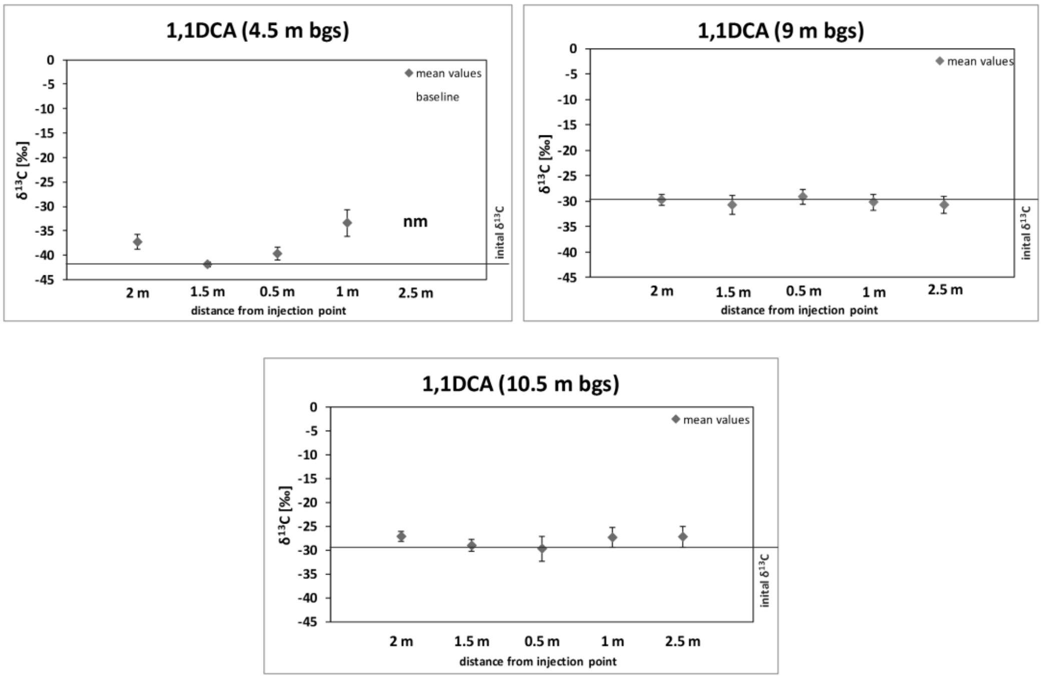

$\delta^{13}C$ (‰) mean values of 1,1-DCA in the monitoring wells (MLDS1 – MLDS5) at different depths (4.5, 9 and 10.5 m bgs).